DOCTOR OF SCIENCES

Chemistry and physics of plasma polymerization probed by mass spectrometry

Gillon, Xavier

Award date:
2014

Awarding institution:
University of Namur

UNIVERSITÉ DE NAMUR

Science Faculty

Research Center in Physics of
Matter and Radiation - LISE

Chemistry and physics of plasma polymerization probed by mass spectrometry

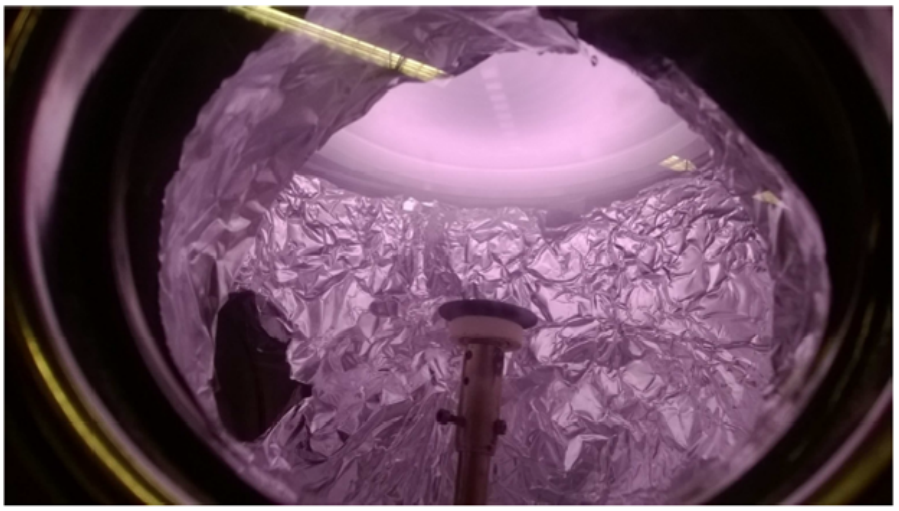

Xavier Gillon

Thèse présentée en vue
de l'obtention du titre de
docteur en science

Juin 2014

Jury members:
Pr Achim von Keudell
Pr François Reniers
Pr Rony Snijders
Pr Jean-Jacques Pireaux
Pr Laurent Houssiau (supervisor)

Rempart de la Vierge, 13
B - 5000 Namur (Belgium)

Printed in Belgium
ISBN : 978-2-87037-859-5
Dépôt légal: D/2014/1881/50

Abstract

To completely refashion our well-known glasses, metals and semiconductors, the deposition techniques using plasma have many advantages. The deposited coatings are indeed tightly adherent to its substrate, covers it completely and can have a large diversity of tunable properties. Among plasma treatment, plasma polymerization produces thin films of plastic, or polymeric, material.

The present work investigated the low-pressure plasma polymerization in a radio-frequency reactor with planar inductive power coupling. The monomers studied were styrene (C_8H_8), benzene (C_6H_6), ethylene (C_2H_4) and acetylene (C_2H_2), which are pure hydrocarbons, but also methyl methacrylate ($C_5H_8O_2$ - MMA) which contains oxygen. The neutral by-products of their plasmas were investigated by mass spectrometry (MS) downstream of the discharge. In the case of styrene and MMA, the elemental composition of the plasma-deposited polymers was measured by X-Ray Photoeletron Spectroscopy (XPS) and the deposition rate by contact profilometry. The main results of the thesis are the following.

- A systematic approach based on low electron impact energy and Threshold Ionization Mass Spectrometry (TIMS) allowed an extensive species identification of the by-products. To explain the many new species detected, light-weighted carbon containing radicals with low hydrogen content are proposed as intermediates of reaction. In the case of MMA, the dominating species suggested that oxygen containing radicals are not likely to participate to recombination reactions.
- The partial pressures of the dominant species were quantified by MS in the discharges of styrene, benzene, ethylene and acetylene. Varying the plasma power revealed a systematic and large content of hydrogen and acetylene in the discharge. Effects due to hydrogen were proposed to explain the lower depletion of ethylene compared to the three other monomers.
- Surface characterization of the plasma deposited styrene film revealed an abrupt increase of the deposition rate. The simultaneous occurrence of two phenomena is discussed with the specific planar inductive geometry: a non-linear increase of the coupling efficiency (E-to-H transition) and a sudden pressure drop.
- Finally, the study of the MMA discharge pressure has led to the discovery of a method to quantify for the first time the partial flows of plasma pumped by a nitrogen trap. The result is important, giving access to the production rates of the plasma effluents.

In summary, the present work has developed a complete methodology to detect and quantify the neutral by-products of plasma polymerization. Its application allowed a deeper insight into the plasma chemistry of hydrocarbons and oxygen containing monomers. It opens the way to correlate this chemistry with the thin plasma polymer films.

Remerciements

As it is the most read part by the people close to you, the acknowledgments are written in French. The only exception will be for the Jury Members, to which I address my gratitude for the lecture of the thesis and the crucial comments based on recent research.

Tout d'abord, mes remerciements vont bien sûr au laboratoire.

- Au Professeur Houssiau, promoteur de cette thèse, Laurent, je voudrais te remercier pour l'enthousiasme dont tu as fait part pour ma thèse, pour tes relectures et surtout pour la simplicité de notre relation.
- Au Professeur Pireaux, Monsieur Jean-Jacques, merci pour votre bienveillance toujours présente et votre sens de la gestion qui fait vivre le laboratoire.
- Au Docteur Louette, Pierre, merci pour tous les coups de main et les discussions sur la vie.
- Au Docteur Ghijsens, Jacques, merci pour les énigmes et le sens du règlement, qui aura malgré tout toléré un petit dépassement.
- Au Baron Comes, Frédéric, merci pour les coups de mains aussi et les bonnes tranches de rire dans la salle des machines.

Le laboratoire, c'est aussi Alex, mon cher soupirant collègue de bureau, depuis seulement deux ans, mais qui dès mes débuts m'a emmené voir le monde, avec la Californie, San Fransisco et sa Gai Pride...! Merci du fond du coeur vraiment, puisque plus que tous, ton aide m'a été très précieuse. Je n'oublie pas les heures de travaux forcés que je te dois.

Parmi les contributeurs à ce travail que je dois le plus remercier, il y également Laurent (Nittler cette fois), dont les coups de mains, les horaires et le sens pratique sont d'une aide inestimable. Alors Laurent, à toi aussi, merci du fond du coeur. Je n'oublie pas les prosternations que je me dois d'accomplir quotidiennement devant ton effigie.

Pour une thèse en tant qu'assistant, six années et allongées d'une dans mon cas, le laboratoire, cela a été également beaucoup de rencontres et en dehors du laboratoire bien plus encore. On

en retiendra tous les actuels et anciens du laboratoire (Yan, Céline, Mac, Michal, Nico, Bastien, Sami, Jérémy, Vincent, Ludovic, Olivier, Hubert, Mathilde, Audrey, Neyda, Zhiling, Marwane, Karim, Marie), l'équipe des Supers Joggueurs (Annick, Dan, Alex, Audrey, Fransesca, Céline G et Céline N), les rendez-vous des As du Pokers, les dîners à la salle café avec le LPS et les soirées doctorants...

Au rayon plus personnel, Gaëlle, merci pour tout ce que tu as enduré à travers cette épreuve qui a tout autant été la tienne. Merci pour tous les sacrifices, ton soutien et tes attentions. Maman, merci pour les services de dernières minutes, toujours présente pour cela. Et merci à toute la famille pour son soutien en général. Merci aux amis pour les bons moments passés et les discussions qui font avancer.

Ce qui fait mémoire dans toute aventure, c'est sans nul doute ses anecdotes et la présente thèse n'en a pas été exempte...! Comment ne pas évoquer la belle arabesque décrite par-dessus le guidon, chemin faisant en direction du bureau, à une heure incongrue, typique des déréglés horlogiques dont j'ai fait activement partie ? A un mois de la remise du premier manuscrit, la rédaction a pris une dimension intéressante. En effet, affublé d'un plâtre au coude gauche et d'une attèle au coude droit, les réactions ont été diverses : rires ou consternations. Au quotidien, manger est devenu synonyme de spaghetti sur table et se gratter le visage s'est transformé en "je frotte mon visage sur les chambranles de portes". Au rayon scientifique, c'est plutôt une jauge de pression qui a été au rendez-vous. Ce genre de petit appareil, très anodin dans un laboratoire de recherche, a eu le don de mettre du suspense. En effet, quand vous découvrez après 5 ans et demi de thèse et à 4 mois de la fin, que la jauge utilisée à chaque expérience depuis les débuts comportent de "petites erreurs de mesure de 400% ", vous criez à la joie...!

Pour terminer, l'aventure de la thèse, c'est aussi une expérience en soi: le challenge de la construction de la connaissance, ses forces et ses défauts; les voyages à l'étranger qui font découvrir des centres de recherches à la pointe et d'autres cultures; le dépassement de soi et le sacrifice sur l'autel de la connaissance; le questionnement sur l'utilité et sur l'avenir... Mais ce qui fait surtout la thèse, avouons-le, c'est que cela fait du bien quand cela s'arrête ...!

Contents

Introduction

New materials are at the center of the technical and technological development of our civilization. Metal alloys dominated complete periods throughout history, from the Bronze Age to the Steel Age. Glass, paper, dyes and cement brought deep changes in construction, art and knowledge. And today, how many objects and devices in everyday life are not made of plastics or semiconductors?

One of the current pillars towards creation of new materials is thin film. Covering substrates, the tiny amounts of matter completely refashion our well-known glasses, metals and semiconductors: their surfaces are now able to produce light, to transform sun light into energy, to withstand wear, corrosion and oxidation, to conduct electricity in microprocessors or to be inserted inside bodies without rejection. When made of the same atoms than living matter – like carbon, oxygen, nitrogen... – thin films may become flexible and are named "polymer" or "organic". They are found in textile coatings, biomaterials, membranes, biological sensors or even electronic papers.

Reaching the delicate nanoscale, the narrow coatings need to be tightly adherent to their substrate, to cover it completely and to be homogeneous. These challenges are successfully met by deposition processes using plasma. This ionized gas is effectively able to reach every corner of a rough surface, to strongly bond film and substrate, and to produce coatings without pinholes.

Not surprisingly, plasma polymerization delivers... polymer thin film, but, contrary to the conventional wet chemical industry, in a one-step and greener process, being solventless. The plasma activation of organic vapors succeeds in creating an exceptionally wide range of singular and unique polymers unattainable by any other available techniques. This method is effectively able to tune the chemical composition, thickness, morphology and stability of the deposited layer. It is controlled by varying the plasma parameters such as the reactor geometry, the organic vapor pressure, its flow rate or even the plasma power...

The plasma polymerization technique, used now for more than 50 years, should be well understood. It would be true without its intrinsic complexity. Plasmas are effectively highly complex, being a mixture of ions, electrons, neutral species, with some of them excited, other in ground state, undergoing dissociation or, on the contrary, recombination. Despite all this, a significant knowledge has been built now, reaching even modeling and prediction of species densities and energies. However, this is only true for plasma of molecules small and easier to handle, like methane or acetylene. Important research is still required for larger molecules. The present work is in line with this overall objective of unraveling an additional piece of plasma polymerization.

Choice of the materials

Polymers are built from numerous identical small units called monomers. These units are the building blocks of the polymerization. Two of them were chosen to carry out the present study: styrene and methyl methacrylate (MMA). They respectively produce the well-known polystyrene (PS) and poly(methyl methacrylate) (PMMA).

Styrene and MMA are model compounds, found in conventional polymerization as well as in plasma polymerization. Within polymer materials, PS is one of the most used. In Europe, it belongs to the recycled plastics (Number 6). Its usual shapes can go from yogurt containers, CD packaging to insulator and protective foam packaging if expanded. PMMA is more appreciated for its glassy and transparent properties. One of its well-known trade names is “Plexiglas”. It has composed the transparent nose of a bombardier as soon as the 1930s, and nowadays is used for intraocular lenses, transparent sculptures or large aquarium windows, among many other applications.

It is then not unexpected to observe that characterization of plasma deposited PS films is already largely reported, regarding composition, deposition rate, morphology, biocompatibility (see Section 4.1)... Without studying the species present in the plasma, several pioneering works attempted to model the deposition rate of styrene plasma polymerization [47, 49, 50, 52]. Surprisingly, the studies on the styrene plasma diagnostics and chemistry are scarce [62, 111, 113, 116, 117], although it is an important step to understand the deposition.

Similarly, plasma deposited PMMA has previously been extensively studied in regard to composition, deposition rate or morphology (see Section 4.2.2)... The studies on the

plasma-phase lead to proposition of reaction mechanisms and even to quantification of the products partial pressures (Section 4.2.3).

Contributions of the present thesis

The scientific strength of the Laboratoire Interdisciplinaire de Spectroscopie Electronique (LISE) rests upon its expertise in surface characterization, within the Research Centre in Physics of Matter and Radiation (PMR) in Namur. The thesis was then originally oriented towards the characterization of the plasma deposited polymers. In parallel, two plasma diagnostic techniques had to be developed: Mass spectrometry (MS) and Optical Emission Spectroscopy (OES).

As the work and the bibliography progressed, the more original and fruitful results were revealed to lie in the plasma characterization. Firstly, it brought a distinct improvement to control the process itself: total pressure and partial pressure measurements, injection of gases and vapors, plasma reproducibility. Secondly, for styrene plasma, three new unstable species – C, C_2 and C_6H_6* – were detected by OES by Dr Li, being a partner of the present work [118]. In addition, 45 new stable species were detected by MS, which constitutes one of the strong results of the present work [224]. For the MMA plasma, our group published the first OES spectrum and unstable species identification – CO*, O_2*, H*, C* and H_2O* [118]. By MS, the present work detected 38 new stable species.

In addition, species were identified by MS in the plasma of three other hydrocarbons, themselves produced in significant amount in the styrene plasma: acetylene, ethylene and benzene. The comparison of the species between the four investigated plasmas revealed shared trends. If occurring in the gas phase, the effluents in hydrocarbon plasma effectively seem to be dominantly produced via recombination with small intermediates, containing one or two carbon atoms and with a low hydrogen contents [224]. More surprisingly, the MMA plasma seems to follow similar paths, with no dominant oxygen intermediates, despite the starting monomer contains two of these atoms.

In the present work, the pressure quantification of the dominating species in unsaturated hydrocarbon plasma was also shown to be possible, even for such large monomers like styrene, containing eight carbon atoms. In addition, the investigation of the exhaust pumping rate of gas mixtures when using cold trap led to a potential striking discovery for the field. Indeed, the quantification of the effluent production rates are very different from what could be expected from the pressure quantification.

Regarding surface characterization, the deposition rate and the chemical composition were measured for the plasma deposited polystyrene and polymethyl methacrylate films. For polystyrene, an unusual discontinuous increase of the deposition rate has been observed just before reaching saturation with power. Concomitantly, the discharge revealed two sudden changes: a strong pressure drop and an intense enhancement of its light emission. The latter was linked to the well known E-to-H mode transition in inductive plasma, recently applied in polymerizing plasma [178]. The former led to discuss the expansion of the plasma volume and the consequent change of the polymer deposition distribution in the reactor [80]. Furthermore, to our knowledge, the current work reports for the first time such discussions for planar coil geometry.

Outline of the thesis

Several aspects of the thesis constitute new expertise for the laboratory, like the plasma polymerization mechanisms and the electron ionization in gas-phase mass spectrometry. Therefore significant state of the art chapters are devoted to describe their respective theories (Chapter 2 and 3), after a proper introduction of the concept of plasma (Chapter 1). The thesis will continue with the state of the art in the characterization of the styrene and MMA plasma and of their related plasma deposited polymer films (Chapter 4). The experimental setup and the characterization techniques will be described in Chapter 5. Then the different results will be exposed, in the following order:

- Surface characterization of the plasma deposited PS and its correlation with the discharge pressure and the light emission (Chapter 6),
- Species identification in unsaturated hydrocarbons plasmas (Chapter 7),
- Pressure quantification in unsaturated hydrocarbon plasmas (Chapter 8),
- Species identification in MMA plasma (Chapter 9), and finally
- Film characterization of the plasma deposited PMMA and its correlation with the discharge pressure (Chapter 10).

Finally, the conclusions and the perspective will be drawn in Chapter 11.

Chapter 1

Plasma

While it is an important part of our daily lives, plasma is not a very well-known state of matter. As it makes up 99% of our visible universe it deserves a proper introduction...

Plasma is an ionized gas, a distinct fourth state of matter. As the temperature increases, the matter transforms from solid, to liquid, to gas and finally to plasma. "Ionized" means that at least one electron has been removed from some atoms or molecules of the gas. Plasma thus contains free charges – electron and ions – which make it conductive. However, it is usually electrically neutral, meaning that the positive charges compensate the negative charges.

The definition of plasma covers a wide range of phenomena, natural or man-made. Examples of highly ionized plasmas are the sun and more generally the stars. Weakly ionized plasmas are closer to us: neon lighting, plasma TV screens, flames. Even if not always the case, plasmas usually emit light, as is the case for lightning or the beautiful aurora borealis.

Historically, the term plasma was first introduced by Irving Langmuir in 1928 [1] due to similarity with the blood plasma . The diversity of the plasma components – electron, ions and neutrals – are, like in blood, strongly interacting with each other.

The technological applications using directly the light emitting property of plasmas are e.g. fluorescent lamps or plasma screens. Moreover, plasma systems or plasma treated materials are widely used in surface and coating technologies, in microelectronics or food packaging. More recently, the plasma has been established as nanotechnology with the production and the modification of nanotube and graphene or the formation of nanoparticles by dusty plasmas. It is also applied to environmental issues with hydrogen production and fuel conversion. Finally, plasma applications are well established in health issues with large production of potable water

by ozone-plasma processing and with the very promising development in medicine for surface and devices sterilization or direct treatment of skin diseases.

The plasma used in the present study is a non-thermal one, ignited at low-pressure, radio-frequency and with an inductive coupling. This first chapter aims at defining these different characteristics, which will require the description of macroscopic and microscopic features of plasmas, useful for the present work. Before that, the investigated plasma must firstly be located among all existing plasmas.

1.1 Low-pressure non-thermal plasmas

1.1.1 Classification among plasmas

A possible classification of plasmas can be based on the electron density and on the electron temperature. Such classification is depicted on Figure 1.1. The x axis is the electron density which ranges from 10^0 (or 1) to 10^{24} electrons per cm^3. The sun core can reach an electron density of 10^{33} cm^{-3} as indicated by the right arrow. This scale does not take into account the total pressure or density. A same electron density could be achieved for a gas with lower pressure and a higher ionization degree, than another gas with higher pressure and lower ionization degree. The y axis is the mean energy of the electron in eV. It is a measure of the electron temperature, with 1 eV corresponding to around 10^4 K. The electron temperature ranges from 0.01 eV up to 100 keV. It corresponds to temperatures from 100 K up to a billion of K.

Figure 1.1 reveals the very large diversity of conditions of ionized gases, being natural plasmas – sun core, lightning, solar corona, interplanetary nebula and aurora borealis – or man-made plasmas – thermonuclear fusion, glow discharge, neon lighting, high-pressure (HP) arcs and spatial thruster.

Plasmas of practical use in industries and laboratories are generally weakly ionized gas. Their electron temperature usually ranges from 1 to 20 eV and their electron densities from 10^8 to 10^{16} cm^{-3}. Among them, low-pressure non-thermal (LPNT) plasma occupies a place of choice, together with atmospheric plasma. On Figure 1.1, it is situated at the intersection of the dashed lines, indicating the 10^{10} cm^{-3} electron density and the 3 eV electron temperature. Low-pressure means a range of pressure from 10^{-3} to 10 mbar, corresponding to a molecule density range from 10^{14} to 10^{18} cm^{-3}. As plasma is electrically neutral, the positive ion density compensates the electron and negative ion density. Considering the above mentioned electron and molecule densities, the ionization degree is then effectively weak, lying between 10^{-7} to 10^{-4}

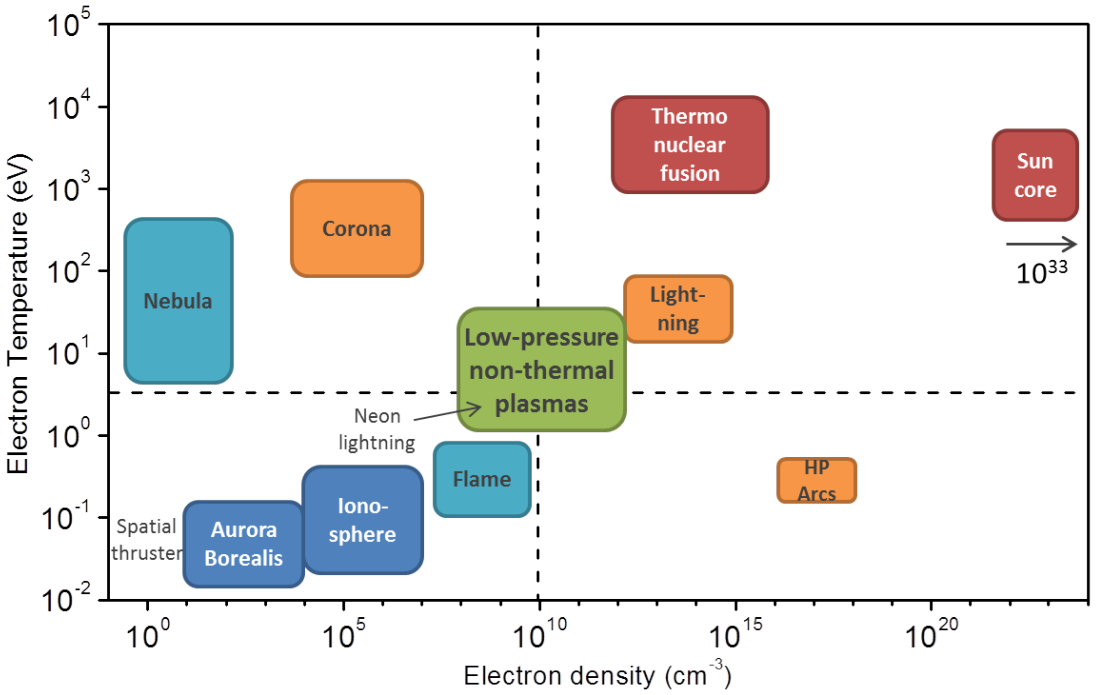

Figure 1.1: Classification of plasmas depending on their electron temperature and their electron density.

for LPNT plasmas. Non-thermal refers to the fact that these plasmas are not in thermodynamic equilibrium. Concretely, it means that all the particles composing the system are not in thermal equilibrium and do not have the same temperature. It is further explained hereafter.

1.1.2 Thermodynamic equilibrium

A volume of space containing particles is at thermodynamic equilibrium when all the processes and their reverse reactions compensate each other. This concept of compensation is called micro-reversibility. If it is respected, the plasma is called thermal or "hot". A unique temperature parameter then determines many processes in the hot plasma, from the velocity distribution of particles, to their electronic states distribution or the ionization/recombination equilibrium. In nature, stars are examples of such plasmas which are in thermodynamic equilibrium, at least locally. Man-made, thermal plasmas will potentially play an uttermost role in future energy production by controlled thermonuclear fusion. On the other hand, many other types of plasma are not in thermodynamic equilibrium and are called non-thermal or "cold". LPNT plasmas produced in laboratories belong to this category. As they emit light, radiation emission is then not compensated by reabsorption of light quanta and the micro-reversibility condition is not respected. In this case, a unique temperature cannot be defined for all particles

forming the system. For many laboratory plasmas, the electrons have a very high temperature compared to the one of the remaining species, like ions and neutrals. Furthermore, different temperatures can be observed within the different degrees of freedom of a species. For instance, vibrational temperature of a species can differ from its rotational temperature. In the worst case, the distribution of states like the velocity is not even thermalized: they do not follow a Maxwell-Boltzmann distribution and a temperature cannot be determined. Cold plasmas are typical for this lack of "thermalisation", which is actually due to an insufficient exchange of energy between all the particles. The too low density of gas (even including atmospheric plasmas) and of electrons of the weakly ionized cold plasmas is generally responsible for it. In contrast, hot plasmas are obtained at high pressure and with a high degree of ionization.

1.1.3 Ignition of the laboratory plasmas

In laboratory plasmas, the continuous loss of energy toward the outside environment, via radiations and walls absorption processes, must continuously be compensated by an external feed of energy. It is usually provided by an electric field. Applied to the gas, it creates a "gas discharge" or "electrical discharge". The ignition occurs as follows. At normal conditions, gases are already very weakly ionized, i.e. they contain a certain amount of ions and electrons due to cosmic ray ionization or when they undergo friction against solid matter. For instance, the charge density is around 10^2 cm^{-3} in the usual atmosphere, but the wind in a forest, at sea or in the mountains can increase the natural ionization degree up 10^3 ions/cm^3. When an electric field is applied across such gas, it will accelerate the present free charges, especially the electrons as they are much lighter than the ions. If they acquire sufficient energy, they can ionize a neutral molecule during a collision. The ionization is accompanied by the production of a new electron and a new ion. The new electron can in turn be accelerated and ionize another molecule. The phenomenon amplifies and creates an avalanche, increasing the ionization degree. A steady-state is maintained when the loss of electrical charges (due to the recombination in the plasma and charge flux to the plasma boundaries) is compensated by the charge production through ionization and secondary electron emission from the plasma boundaries.

1.2 Radio-frequency inductively-coupled plasmas

1.2.1 Applied frequency

Historically, the first studied LPNT plasmas were ignited in electric discharge tubes. Two powered electrodes, inserted in a glass tube, provided the necessary electric field. The tube could be filled with various gases or evacuated. The first experiments were dealing with electrodes at constant potentials, creating the so-called direct-current (DC) discharges, to which the "glow discharge" belongs [2]. The produced plasmas revealed several features. Firstly, they were highly non-uniform, with zones between the electrodes obviously emitting different light intensities: Faraday, cathode and anode dark spaces providing no visible light; negative glow and positive column with light emission [3]. Secondly, space regions bore net charge density, either positive or negative, especially close to the electrodes. Besides, positive ions are constantly collected by the anode and electrons and negative ions at the cathode. Thus continuous charge compensation is required for the metallic electrodes, which must stay conductive, without deposition of a dielectric layer. Therefore, it is not possible to use DC plasma for the deposition of dielectric materials.

In a second step, a system of electrodes with alternating potentials was investigated. Among them, radio-frequency (RF) discharges are operated at frequencies in the kHz and the MHz range. This is a smaller range than the one usually considered in the RF engineering domain, which also encompasses the GHz range [4]. But in plasma systems, these latter frequencies are rather exclusively termed as micro-wave frequencies. To avoid interference with radio communication systems, specific frequencies were assigned for operation of the industrial RF discharges; between those, 13.6 MHz is used most often. RF plasmas generally offer the following advantages in comparison to DC discharges [2, 5]: (a) they are more spatially uniform, (b) they can operate in depositing discharges with a variety of electrodes – metallic, dielectric or a combination of both –, (c) the ion losses are reduced, having too little time to reach the electrodes, (d) their ionization mechanism is more efficient (the electrons can gain energy during the whole RF period), and thereby (e) they can also operate at lower pressures. These characteristics make RF-plasmas the most common choice for e.g. the microelectronic industry [5].

1.2.2 Type of electrode coupling

The electric field generation can be provided by electrodes at different electrical potentials. The electrodes can be either in the vacuum system or outside as shown on Figure 1.2a and

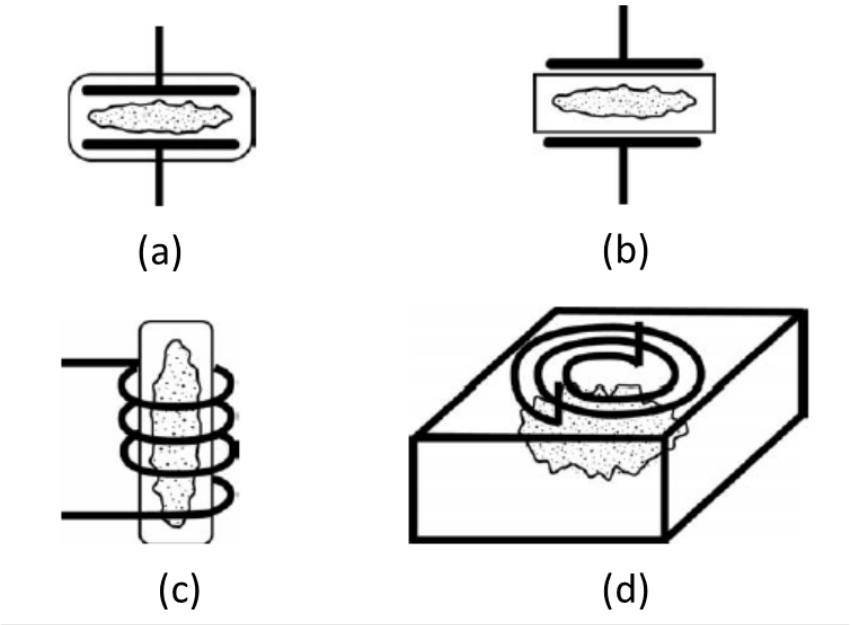

Figure 1.2: Different geometries of CCP and ICP (taken from reference [2]).

b, respectively. Reactors of this kind produce discharges referred to as capacitively-coupled plasma (CCP). Another electric field production is via alternative currents in coils, leading to the so-called inductively-coupled plasma (ICP). The coil geometry can be either helical or planar as shown on Figure 1.2c and d, respectively.

In the case of an ICP, the magnetic field is the "primary" field and, being alternative, produces an electric field, according to the Maxwell-Faraday law of induction: $\nabla \times E = -\partial B/\partial t$. The electric field is then usually lower than capacitively coupled plasma (CCP) discharge, where the electric field is primary [2]. In addition, the low-pressure ICP discharges operate at electron densities of 10^{11}–10^{12} cm^{-3}, exceeding those in CCP by more than one order of magnitude in the same conditions [2].

1.2.3 E/H transition in ICP

The transmission of the power emitted from the plasma source to the plasma may have two regimes in the case of ICP reactor, called capacitive or inductive coupling, denoted as "E" or "H" regime respectively. It mainly depends on the electron density achievable at equilibrium: either a low density or a high density, respectively. The explanation is covered in reference textbooks [6], that we will resume here with as much simplicity as possible.

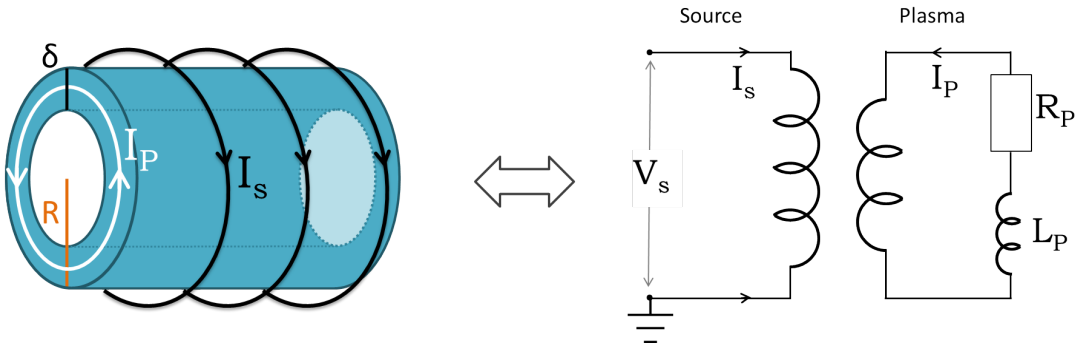

Figure 1.3: (left) Schematic diagram of the power absorption zone of a helical ICP reactor, limited to the skin depth, δ. (right) Equivalent circuit of the source-plasma coupling.

The helical coil geometry is generally more easy to understand [7]. In that case, the conductive plasma volume is a cylinder, around which the coil is wrapped (see Figure 1.3). The alternating source current, I_S, passing through the coil, generates electromagnetic fields in the plasma. The field penetration is limited to the so-called "skin depth", δ, due to shielding currents induced in the conductive plasma. These currents opposed the source current and their average value within the skin depth is the plasma current, I_P. Hence the plasma is modeled by a coil coupled to the source coil in the equivalent circuit of a transformer, as shown on Figure 1.3. R_P is simply a resistance modeling the power loss of the plasma when currents are present. L_P is the plasma inductance, determining the phase shift between the applied external field and the internal induced current, caused by the electron inertia. At equilibrium (constant electron density), the plasma is a closed circuit, as no net gain or loss of charges occur. This is the simplest picture of the inductive coupling, valid at sufficiently high electron density: the electric power is transmitted to the plasma by inducing current in it. The primary source of the coupling being a magnetic field, the regime is denoted as "H" mode.

Now, for unsufficient electron density, the induced currents are too low to efficiently transfer power. At least, sufficiently to counter balance the power loss of the plasma, leading to extinction. However, at low electron density, the skin depth is much larger and the fields penetrate far into the plasma. To generate the source current, a voltage, V_S, is applied at the source coil ends, as shown on Figure 1.3 (right). Considering one coil end grounded (which is often the case), the potential of the other can be large (1000 V) and distributes deeply into the low-density plasma volume, approximated as grounded [7]. It occurs all along the coil wire but the voltage regularly decreases when approaching the grounded end. Therefore an electric field is applied (with decreasing amplitude, approaching the grounded end) and electrons can gain energy: power is

transmitted. As it is similar to the effect of a charged electrode, this is called capacitive coupling. The primary source of the coupling being an electric field, the regime is denoted as "E" mode.

At high electron density, the source voltage of the coil is also present, but penetrates the plasma within a shallow skin depth. The voltage drop occurs then on a very short distance and geometrically a large part of it is concentrated in the thickness of the quartz window. The effective voltage can then be very low values as low as 10 V [7].

E-to-H transition

There is a threshold value for the current source I_S below which no inductive discharge can be sustained. The discharge formed below the threshold is in E mode and has a low light emission and a low electron density [8]. Increasing the current source and thus the applied power to the threshold value, the transition to the H mode is accompanied by a large non-linear increase both of light emission and electron density, which can reach two orders of magnitudes [8, 9].

The key concept to understand the non-linear increase of n_e with the source power is a linear increase of the coupling power with n_e within a limited n_e range at the onset of the H mode [8]. At the fixed applied power of transition: a slight increase of n_e raises the power coupling; the absorbed power is larger and allows a higher ionization rate, which increases the electron density; in turn the power coupling is higher... This positive feedback loop continues as long as the coupling increase is linear with the electron density. The deviation from linear dependence is due to the appearance of the skin effect [8]. By limiting the field penetration in the plasma, it reduces the plasma volume able to absorb power.

1.3 Plasma definition

The definition of plasma is actually more restrictive than simply an ionized gas. Three additional criteria must apply [10, 11]:

- Sufficiently high density of charged particles: each charge must influence several other particles to ensure a collective behavior of the charges.
- Quasi-neutrality: the positive ion density ni must approximately balance the electron density n_e. This is respected if the size of the ionized gas is markedly larger than the one of the electric shielding distance called the "Debye length", defined below.
- The plasma frequency (or Langmuir frequency) must be higher than the electron-neutral frequency, both defined below as well. The plasma frequency gives the oscillation period

of the electrons in the plasma. It then constitutes the typical timescale of reactivity of the electrons to ensure the above mentioned quasi-neutrality when a local net charge density occurs. This timescale must be lower than the time between two collisions for the electrons.

1.3.1 Debye length

The Debye length λ_D gives the characteristic plasma size scale required for shielding of an internal electric field – due to the plasma free charges – or an external one [2]. In other words, it indicates the scale of plasma quasi-neutrality: above λ_D, $n_i \approx n_e$; below it, the densities can differ. Its defining formula is:

$$\lambda_D = \sqrt{\frac{\epsilon_0 \; k_B \; T_e}{e^2 \; n_e}} \tag{1.1}$$

where ϵ_0 is the vacuum dielectric permittivity, k_B is the Boltzmann constant, T_e the electron temperature, and e the electron charge. A convenient formula is given by [2, 3]:

$$\lambda_D(\text{cm}) = 742 \; \sqrt{\frac{T_e(\text{eV})}{(n_e(\text{cm}^{-3})}} \tag{1.2}$$

For a typical electron temperature Te of 3 eV and electron density of 10^{10} cm^{-3}, the Debye length is $\approx$ 0.1 mm.

1.3.2 Plasma frequency / Langmuir frequency

The typical time of plasma response to an external field is given by the oscillation frequency of the electrons in the plasma (or in metal):

$$\omega_p(rads^{-1}) = \sqrt{\frac{n_e e^2}{\epsilon_0 m_e}} \tag{1.3}$$

where m_e is the electron mass. It is very close to the initial definition of Langmuir in 1928 [1]. A more convenient formula is:

$$\omega_p(Hz) = 5.65 \; .10^4 \sqrt{n_e(\text{cm}^{-3})} \tag{1.4}$$

For the above mentioned typical electron density of 10^{10} cm^{-3}, this gives: $\omega_p = 5$ GHz. For alternative electric fields with frequencies markedly above this value (microwave frequencies), the electrons will not follow the applied field. However, microwave discharges in the GHz range

are possible. It is due to their usually higher electron density [2], at around 10^{13} cm^{-3}, elevating the plasma frequency to around 200 GHz.

1.3.3 Sheath and plasma potential

Although plasma is quasi-neutral in general ($n_e \approx n_i$), close to the walls, thin layer regions are observed to be positively charged. They are called "sheaths". Their formation is due to the fact that electrons can move much faster than ions. The electrons can then reach surfaces much faster and create a negative potential (negative self-bias). The result is a positively charged plasma layer in the vicinity of the surface of a thickness of several Debye lengths [12]. In addition the plasma bulk is then slightly depleted of electrons and develops a positive potential. The difference of potential between the plasma bulk and the walls is called plasma sheath or plasma potential. It can reach 10 to 50 V, depending on the kind of plasma and conditions. Its value is obtained when the flux of the electrons, repelled by the negative surface, equals the flux of ions reaching the surface; the net current through the sheath is then zero.

1.4 Physical quantities in cold plasmas

1.4.1 Temperatures

As LPNT plasmas are not in thermodynamic equilibrium, a single temperature cannot be defined. Most notably, because of their lower mass, electrons are easily accelerated to energies which are sufficient to ionize the gas particles. Typical values of electron energies ranges from 0.5 to 10 eV, corresponding to electron temperatures (T_e) in the range of 10^4 to 10^5 K. On the other hand, the ions undergo a significant amount of cooling due to numerous collisions with other molecules or ions. Therefore, the ion temperature (T_i) is approximately the same as the room temperature (T_{room}) as well as the neutral particle temperature (T_g, with subscript "g" for gas). So the particle temperatures follow the relation: $T_e >> T_i \approx T_g \approx T_{room}$.

1.4.2 Energy distribution

In the case of NTLP plasmas, the electron energy distribution function (EEDF) generally differs from a maxwellian distribution due to electron-neutral inelastic collisions [2]. Instead, the EEDF is better described by a Druyvesteyn distribution, established for weakly ionized gas. A typical Druyvesteyn EEDF is compared with a maxwellian one on Figure 1.4, while having both the

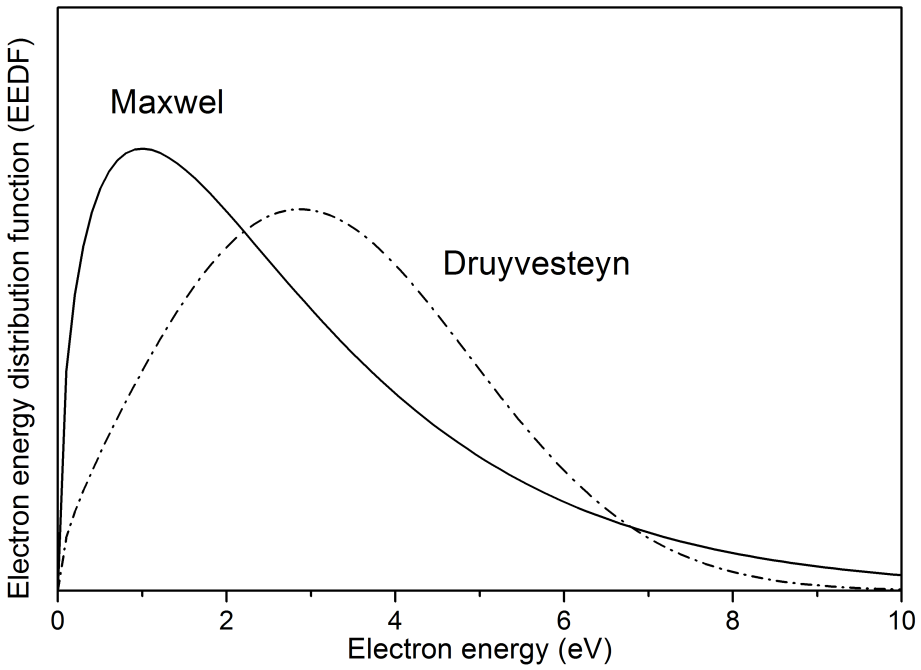

Figure 1.4: Typical Druvesteyn electron energy distribution of LPNT plasma.

same mean electron energy of 4 eV. The former can be seen to decrease faster at high energies than the latter. For the Druyvesteyn EEDF, it can be observed that a small number of electrons have relatively high energies ($> 8\ eV$) while the bulk of the electrons belongs to the low electron energy range ($<$ 8 eV). Since the ionization energies of usual gases and hydrocarbons (8 – 15 eV [13]) belong to the tail region of the electron energy distribution, there is a low degree of ionization in the cold plasmas.

It is worth noticing that the range of electron energy between 3 and 5 eV is high enough to dissociate many chemical σ bonds involved in organic compounds. While they may vary from molecule to molecule, dissociation energy of typical bonds are indicated in Table 1.1. The creation of free radical species is then greatly promoted as the number of electrons able to dissociate is large. Higher energies are usually required for the dissociation of unsaturated bonds and the formation of multiple free radicals. Accordingly, original or plasma-generated unsaturated bonds will have a better "survival rate" under plasma conditions, in comparison to σ bonds.

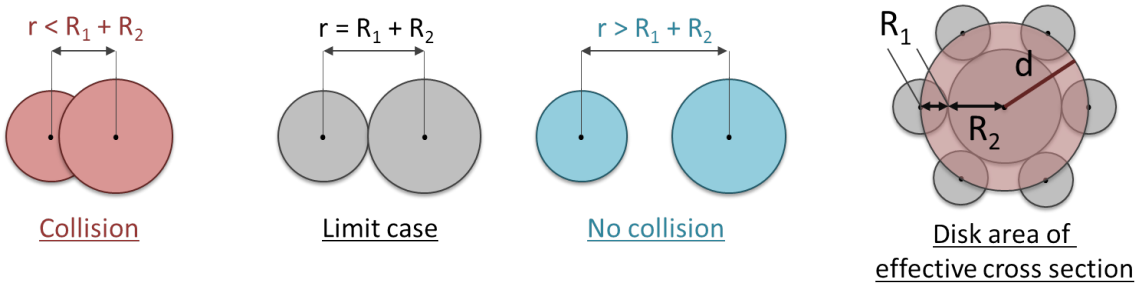

Figure 1.5: The three schemes on the left show that a collision requires that the inter-center distance r must be lower than the sum of the projectile radii. The top right schemes shows that the effective surface area of collision or cross section is a disk.

Bond	Dissociation energy (eV)	Bond	Dissociation energy (eV)
C-C	3.6	C-O	3.7
C=C	6.4 / 7.4	C=O	7.8
C≡C	9.9	O-H	4.8
C-H	4.3 / 5.7	O-O	1.5
H-H	4.5	O=O	5.1

Table 1.1: Typical bond energies involving C, O and H atoms [3, 14].

1.4.3 Cross section

The probability of occurrence of a collision reaction is generally expressed in terms of the cross section, σ. For two classical hard spheres colliding, it is the effective area of collision, expressed in square meters. The bigger the projectiles are, the larger the cross section is and the more probable the collision is. It can be simply established from considering two colliding hard spherical projectiles, with radii R_1 and R_2. The three left schemes on Figure 1.5 show that the occurrence of the collision requires that r, the distance between the two projectile centers, must be lower than d, the sum of the projectile radii: $r < d = R_1 + R_2$. The right scheme demonstrates that the (geometric) cross section is the disk area calculated with the interaction radius d: $\sigma_{geo} = \pi\, d^2$.

During elastic collisions, the internal energies of the colliding particles do not change and the total kinetic energy is conserved. All other collisions, which induce internal energy variation, are inelastic. Either the kinetic energy is transformed into internal energy or the reverse is possible for collisions with excited atoms or molecules.

The geometric cross section gives rather accurate actual cross sections for elastic collisions of projectiles which do not interact at long distance like in neutral-neutral, electron-neutral or ion-neutral collisions. For microscopic projectiles able to interact at long distance, like charges, the interaction radius and the cross section can exceed the corresponding geometric sizes. In contrast, very unlikely reactions between two colliding reactants have a cross section below the geometric one. Besides, the collision of two same projectiles can lead to different reactions. The electron impact on a neutral can be just elastic or lead to the inelastic vibrational excitation, electronic excitation or ionization. The ratio of one of the inelastic reaction cross sections to the corresponding elastic cross section at the same energy is sometimes called the probability of the elementary process [2].

In addition, cross sections usually vary with the relative kinetic energy of the two collision partners. This is shown on Figure 1.6, in the energy range of interest in LPNT plasma. The cross sections are indicated for different possible reactions during the collision of electron with acetylene molecule, HC≡CH. Three vibrational excitations were chosen, simply referred to by a number. The three electronic excitations of acetylene were simply marked by their energy level on the figure. The two remaining cross sections are the elastic one in open circle and the ionization one in filled circle, with threshold energy of 11.4 eV. No cross section of dissociation could be found, as is the case with dehydrogenation. The cross sections were obtained via an access to the Hayashi database [15] (among others) proposed by the BOLsig+ "Electron Boltzmann equation solver" website [16].

In addition to the energy dependence of the cross sections, Error! Reference source not found. reveals that the elastic collision dominates in the shown energy range. The elastic cross section reaches 2.10^{-19} m^2, which corresponds to an interaction radius of 2.5 Å. This is very close to the acetylene molecular radius of 3.8 Å [13]. At 16 eV, the ionization cross section is equal to 1.10^{-20} m^2, which corresponds to a geometrical interaction radius of only 0.6 Å.

1.4.4 Mean free path

The mean free path is the mean distance a particle travels between two successive collisions. It is a physical quantity of importance, as for the electrons it indicates how long they will be accelerated before losing energy in the next collision. In general, for a particle A colliding with a partner particle B, it is defined as:

$$\lambda_A = 1/(n_B \sigma_A B) \tag{1.5}$$

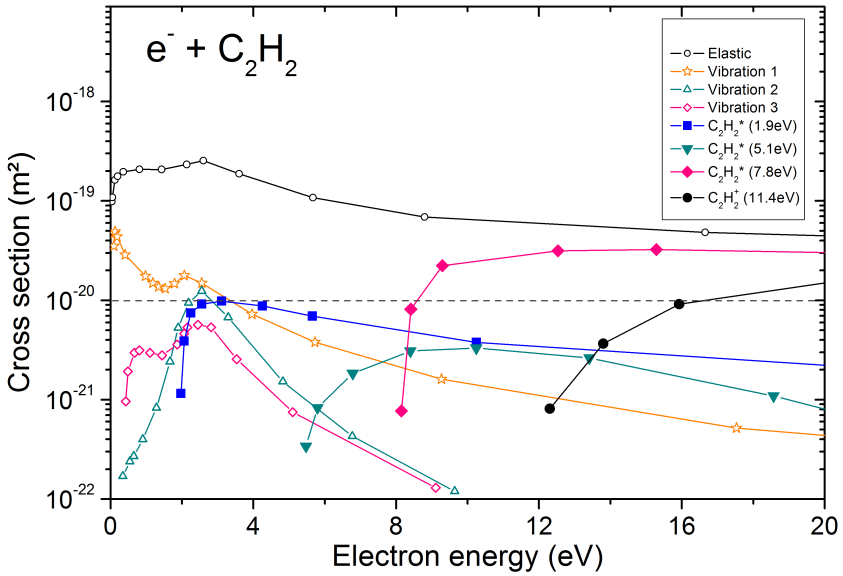

Figure 1.6: Energy dependence of the cross sections of different reactions due to the electron-acetylene collision [15].

Where n_B is the density or concentration of B and $\sigma_A B$ is the cross section of the considered reaction A+B, which can be the elastic one or one of the inelastic. It is important to note that, as the LPNT plasmas are weakly ionized, the neutral species are the dominant collision partners for all the species. In the case of the above mentioned reaction between electron (with subscript "e" below) and acetylene (subscript a), and taking an acetylene pressure of 6.7 Pa ($n_a = 1.6.10^{15}$ cm^{-3}), two different mean free paths of the electron would be at 4 eV:

- $\lambda_e^{el} = 0.3$ cm for the elastic collision with $\sigma = 1.10^{-19}$ m^2
- $\lambda_a^{inel} = 6.2$ cm for the electronic excitation of acetylene (1.9 eV) with $\sigma = 1.10^{-20}$ m^2

1.4.5 Collision frequency and reaction rate

The collision frequency of the particle A with the collision partner B, f_A, is obtained by dividing their relative velocity v by the mean free path of A:

$$f_A = v n_B \sigma \tag{1.6}$$

As there is not a unique relative velocity v but rather a velocity distribution $F(v)$, the collision frequency must be averaged taking into account the velocity dependence of the cross section:

$$f_A = n_B \int v\ \sigma(v)\ F(v)\ dv = n_B < v\sigma > \tag{1.7}$$

where "$< >$" denotes a weighted average value.

The number of reactions occurring per unit of time and per unit of volume, known as the reaction rate R_{A+B}, is calculated by multiplying the frequency of collision of the particle A with its density n_A:

$$R_{A+B} = < v\sigma > n_A \, n_B \tag{1.8}$$

The average factor is therefore the reaction rate coefficient or the constant rate: $k = < v\sigma >$.

Chapter 2

Plasma polymerization

While electric discharges underwent extensive development in the 1920s [1, 17, 18], investigations on electric discharge in hydrocarbon vapors really started in the 1930s [19]. These early studies were mainly focused on the gas phase reactions. The formation of thin solid polymer-like films on the electrodes and the reactor walls were mentioned but not of main concern [3, 19]. The description of the chemical, physical and electrical properties of such products weren't initiated until the 1950s [20] and rocketed in the 1960s [21, 22]. Naturally, the first works mostly started with the most widespread DC capacitively coupled plasmas or glow discharges. The formation of the polymer-like products were then termed "glow discharge polymerization" [21, 23]. However, since it is carried out in many other discharge reactors, the name "Plasma polymerization" covers a wider field and must be considered the appropriate term. Considerable efforts to explain the process have been given in the 1970s [23, 24]. A key step in the field is the comprehensive and unified presentation of plasma polymerization, in the book of Yasuda, published in 1985, with impressive considerations brought to the theoretical and technical aspects of the process [3]. Later, several works and books brought corrections and improvements and were more material oriented, with emphasis on the thin plasma polymer films [20, 25, 26]. However, the development of plasma diagnostics allowed in the 1990s and 2000s a better microscopic description of the process and significant advances [27, 28].

Today, the complex and interdisciplinary field of plasma polymerization roughly receives two main types of contributions. On one hand, the macroscopic approach tries to relate directly the film properties to the external plasma parameters, like power, flow, pressure [29], and is being said to be a "chemical point of view" [27, 30]. On the other hand, internal plasma diagnostics endeavor to correlate the film characteristics to the microscopic description of the plasma, like electron

density, ion and radical fluxes [31]. It is referrred as “physical point of view ”. Contradictions between the two points of view gave birth to a lively debate [9, 32–36], which resulted in a better permeation between them [27, 37], even if combined studies already existed [27, 35, 38]. In parallel, the increase in modeling capacities and in developing reaction rates database have astonishingly enhanced simulation of this complex process, mainly for small organic molecules like acetylene C_2H_2 [28, 39–41]. The plasma polymerization chemistry thus remains an prominent subject of investigation [2, 27] and needs to be fed with proper experimental studies [9, 27, 35].

Plasmas are complex mixtures of species, with many possible reaction processes. The conventional polymerization is the “monotonic” chemical assembling of many identical organic compounds to form long and regular molecular chains. The junction of these two fields is not straightforward and is actually rather a complete new kind of process, than a union of concepts. In the present chapter, the conventional polymerization will first be presented (Section 2.1). In a second step, it will help to understand the complete different mechanism which is plasma polymerization and the dominating model which emerges (Section 2.2 & 2.3). Then the parameters affecting the plasma polymerization will be presented (Section 2.4). Finally, the chapter will end with the classification both of plasma polymerization domains and of monomer groups (Section 2.5 & 2.6).

The present work is the first in the laboratory dedicated to the fundamental aspects of plasma polymerization. It seemed thus important to review significantly the basis of the process. All the elements presented here will therefore not be directly useful to interpret the obtained results. However they will be helpful for the overall comprehension of the process and to draw the work perspectives.

2.1 Conventional polymerization

Conventional polymerization is indispensable necessary introduction to plasma polymerization. The latter will effectively differ from many features presented in the present section.

2.1.1 Definitions

According to the International Union of Pure and Applied Chemistry (IUPAC), a polymer is a substance composed of “macromolecules” or “polymeric molecules”. They are defined as molecules of high molecular weight, formed by the large repetition of one or several molecule(s) of small molecular weight, called “monomers”. The definition applies to high repetition numbers,

generally above one hundred units. Below, from 2 to several tens of units, they are rather termed "oligomer molecules" and constitute in large amount the so called "oligomer" substance.

The repetitive structure of the macromolecule can be linear or form a tridimensional network. The constitutive unit, the monomer, is generally organic (containing carbon atoms) or more rarely inorganic. If all the monomers are identical, the substance is called "homopolymer", otherwise it is termed "copolymer".

Polymerization is the chemical process of formation of the macromolecule, starting from a large number of individual monomers. Modifying the original classification of Carothers of 1929, two main polymerization mechanisms were distinguished in 1953 by Flory: the "step" and the "chain" mechanisms.

2.1.2 Step-growth polymerization

The step polymerization can be considered to be a polymer formation mechanism without propagation of reactive sites. Each reaction occurs between two stable molecules: two monomers react to form a dimer, a monomer and a dimer form a trimer, a dimer and a trimer can produce a pentamer... All reactions are independent, without initiation or termination (see below), and are enabled by one or several chemical functionalitie(s) of the initial monomer:

$$M + M \rightarrow M_2 \quad (+H_2O) \tag{2.1}$$

$$M_2 + M \rightarrow M_3 \quad (+H_2O) \tag{2.2}$$

$$M_i + M_j \rightarrow M_{i+j} \ (+H_2O) \tag{2.3}$$

Where M stands for a monomer, M_2 a dimer, M_i and M_j for an oligomer/polymer molecules of order I and j, respectively. If every step reaction is accompanied by the release of small molecule like H_2O, the process is called "condensation" according to the Carothers classification (1929) [18]. On the contrary, without group loss, the reaction belongs to the so-called "additions". Most of step-growth polymerizations belong to the latter category. They generally occur through monomers containing a vinyl function (-CH=CH_2), like for styrene, or a double carbon bond, like for methyl methacrylate (MMA).

2.1.3 Chain-growth polymerization

The chain polymerization is a mechanism through which a functionality of the initial monomer react with a reactive site of the forming chain and for which the addition regenerates the reactive center. It is seen as a propagation of the reactive site through the successive addition of monomers. Indeed, a preliminary reaction is required to create the first reaction site: the so-called "initiation". On the other hand, the propagation reaction must be stopped by a "termination" reaction.

$$Initiation \quad M + h\nu \; or \; I \rightarrow \; M^* \tag{2.4}$$

$$Propagation: \quad M^* + M \rightarrow \; M_2^* \tag{2.5}$$

$$M_2^* + M \rightarrow \; M_3^* \tag{2.6}$$

$$M_i^* + M \rightarrow M_{i+1}^* \tag{2.7}$$

$$\ldots \tag{2.8}$$

$$Termination \quad M_n^* \rightarrow \; M_n \tag{2.9}$$

Where * stands for species bearing the reactive site, $h\nu$ represents a radiation and I an initiator. The reactive sites can be of three kinds:

(1) $M^{\bullet}$, a radical site leading to the so called "radical chain polymerization"

(2) M^{-}, an anionic site leading to the "anionic chain polymerization"

(3) M^{+}, a cationic site leading to the "cationic chain polymerization"

Olefin monomers (compound with at least one double carbon bond) especially tend to proceed through chain polymerization. The reactivity to one of the three chain mechanisms – radical, anionic or cationic – highly depends on the molecular structure and composition of the monomer. Therefore, a monomer will generally use a preferential path to polymerize and is seldom able to follow the three of them. Styrene is one of these exceptions [42].

The "living" polymerization is a chain-growth polymerization characterized by a lack of termination. The produced polymer thus still contains reactive sites, that's why they are qualified as "living". Initially discovered for anionic chain polymerization in 1956 by Szwarc [43], it was then observed for the cationic sites. The difficulty to obtain a stable radical explains the latest observation of the radical living polymerization, like the Atom-transfer radical-polymerization in 1995 [44].

2.1.4 Comparison

Step and chain polymerizations typically differ in their dynamic of polymer formation. With the reaction time, the percentage of monomer conversion increases. The chain polymerization will produce high-molecular-weight polymer molecules at all percentages of conversion. There are no intermediate-sized molecules in the reaction mixture, but only monomer, high-polymer and initiator species. On the other hand, the step polymerization produces high molecular-weight polymer only close to the end of the reaction, at very high monomer conversion (>98% conversion).

Three characteristics are stressed:

- The conventional polymerizations are generally carried out in liquid phase, the monomer being either pure or diluted in solutions.
- Both mechanisms require at least one chemically reactive functionality in the initial monomer.
- The conventional polymers are macromolecules, characterized by a high repetition of one or several identical unit(s).

2.1.5 Gas-phase polymerization

Gas phase polymerization (without plasma) generally requires high pressures. For the polymerization of ethylene, which is a gaseous monomer, pressures "down" to 20 atm need initiators or catalysts to operate the process [42, 45]. In that case, the mechanism is either via radical chain or coordination mechanisms [45]. To our knowledge and the one of Yasuda, no step growth polymerization has ever been reported for gas phase polymerization. According to Yasuda, the already low reaction kinetic of the step polymerization in solution hampers any occurrence of the process at the low concentrations of the gaseous phase [3].

One exception of polymerization, not only in gaseous state but in addition at low-pressure, is the "transport polymerization" [42]. Its mechanism requires no chemical initiation, proceeds through radical reactive sites and is out of known categories [42]. We will come back to its case later on.

2.2 Brief history of plasma polymerization models

Many attempts have been carried out to model plasma polymerization mechanisms. Bell, Biederman and Osada reviewed these attempts which we summarize in Table 2.1 [20, 24].

Among the reactor types (see third column "geo"), the capacitively-coupled plasmas (CCPs) dominate. An important fact is the usual investigation of alternative current (AC) discharges, as visible in the fourth column (frequency). It is explained for polymerizing plasma because of the covering of the electrodes by the dielectric plasma polymer films [5, 46]. These layers hamper the charge collection by the metallic electrodes and their removal by the power supply. Therefore, in direct current (DC) discharges or low frequency plasmas (<1 kHz), high potentials developed on the dielectric coating, attenuating the applied potentials and extinguishing the discharge. Otherwise, several parameters were varied as indicated in the fifth column of the table. Some are linked to the plasma itself, like the pressure, the power or the flow, and others to the substrate, via its temperature, position or the bias of the electrodes in the CCP case. In many studies, the proposed reaction rates were estimated by fitting the experimental results [46–51]. Incidentally, it is interesting to note that styrene was among the most investigated monomers [21, 47, 49, 50, 52, 53].

The last column of Table 2.1 summarizes the main features of the proposed models. When possible, the accent has been put on the following aspects:

- **Step growth or chain growth polymerization**? It is very interesting to note that no step mechanism was ever proposed. This is explained by Yasuda because of its already low kinetic of reaction in conventional liquid polymerization [3].
- **Surface reactions or plasma volume reactions**? The early models favor surface reactions on substrates or electrodes, by considering activation of adsorbed monomers by ionic or electronic bombardment. On the contrary, the second wave of models rather investigates where does the initiation occur, the propagation and the termination of the considered chain mechanism.
- **Ionic or radical chain growth**? Ionic mechanisms dominate the proposition up to 1974, then leading place to radical dominating processes. Strong evidences that radicals reactions are responsible for this evolution will be described later on.
- **Emergence of new concepts**: Reinitiation or reactivation by the Bell group, but already proposed by Yasuda and Lamaze in 1973 [63]. The competitive ablation and polymerization (CAP) mechanisms and the rapid step-growth polymerization (RSGP) of Yasuda.

As far as clues in favor for radicals are concerned, Bell interestingly summed up in its 1980 review [10] the studies carried out by its group: Kobayashi *et al.* [55, 56, 64], Morita *et al.* [65], Tibbitt *et al.* [51] and Brown *et al.* [66]. According to their works, radicals are the primary responsible for chain propagation and the ions must be set aside. The radicals would be produced either

Authors	Date	Geo	Freq.	Parameters varied	Main model characteristics
Williams & Hayes [21]	1966	CCP	10 k	Pressure - substrate T	Chain - Surface Ionic bombardment
Denaro [54]	1970	CCP	2 M	Time - power - pressure	Radical chain - Surface Electronic bombardment
Westwood [49]	1971	CCP	3 M	Substrate Bias	Chain - Surface Cationic bombardment / e^- bomb neglected
Yasuda & Lamaze [52]	1971	ICP	RF	Time - Noble gas - power - pressure	Chain - Volume initiation & propagation / Surface termination
Carchano [48]	1974	CCP	6-50 M	Freq. - pressure - substrate T	Chain - Surface Ionic and radical bombardment
Kobayashi & Bell [55–57]	1974	CCP	RF	Flow - pressure	Volume oligomerization Radical dominates - reactivation
Poll [46]	1976	CCP	unspec.	Flow	Surface - Volume at zero flow Adsorption - First layer bombardment
Lam [50]	1976	CCP	880 k	Pressure - time	Radical chain - 4 models whose best = Volume initiation / Surface propagation & termination
Tibbitt & Bell [51]	1977	CCP	RF	Flow - position	Radical chain - Surface and volume Reactivation/reinitiation
Yasuda & Hsu [3, 58]	1978 1985	ICP	RF	Flow - position	Poll model revised Competitive ablation/polymerization (CAP)
Bell [24]	1980	-	-	-	Review - favors radical chain - Surface & volume - reinitiation
Yasuda [3]	1985	-	-	-	Book - “Atomic Polymerization” “RSGP” mechanism (see next section)
Yasuda & Wang [53]	1985	CCP	10 k	Flow - power - substrate T	Stress distinction between plasma reaction and deposition step
Biederman & Osada [20]	1992	-	-	-	Book. Agreed RSGP but stress on the surface mechanisms with adsorb monomers
Friedrich *et al.* [30, 59, 60]	2000	CCP	RF	Power - DC	Very low W/F by pulsing, promotion radical grafting or chain propagation
Short *et al.* [27, 61, 62]	1990s	ICP	RF	W/F	Low W/F: ionic polymerization

Table 2.1: Summary of the main works proposing models or mechanisms for plasma polymerization.

in the gas phase by electron impact of the monomers or on surfaces by electronic and ionic bombardment. Their arguments are as follows.

- Free radical concentration is 3 to 5 orders of magnitude higher than the ionic ones in a non-thermal plasma at a pressure of 133 Pa. Consequently, taking into account the higher reaction cross sections of the ions, the rate of reaction of radical-stable neutral reactions are 10 to 100 higher than the ion-stable neutral reaction rates [66].

- The increase of the deposition rate has been correlated with the increase of radical concentration [56].
- High concentrations of radicals were observed in polymers exposed to plasmas. It favors the possibility of reaction of adsorbed monomers with these surface radicals [47].

Recently, Friedrich reviewed from the 1960s to 2010 the mechanisms of plasma polymerization [30], that could not be included in the present work. It is mainly based on the film characterization, referred as "chemical" point of view. The short complementary review of Whittle *et al.* (Short's group) provides more information on the microscopic characterization of the plasma by plasma diagnostic, whose point of view is rather said to be "physical"[27]. Both groups brought more insight in the plasma polymerization mechanisms with a specific focus on the regime of low W/F (define in Section 2.4.1), as indicated in the end of Table 2.1. This regime generally allows the highest retention of the monomer functionality and is thus of importance for functional coating. However, the plasma polymerization technique is thought to have shown its limitations concerning the monomer structure retention and other techniques are suggested to go beyond, like the initiated Plasma-Enhanced Chemical Vapor Deposition (iPECVD) or the Electro-spray deposition [30, 67].

2.3 Main model

2.3.1 Preliminaries

A major step forward has been made with Yasuda's statement that plasma polymerization is not a conventional polymerization process [3]. Three first considerations and observations support this assumption.

- A low pressure induces a reaction kinetics too low for a step growth mechanism (for which all models seemed to agree), but also for a chain growth mechanism. Thermodynamical limitations are proposed to strengthen this affirmation: the ceiling temperature above which any polymerization can occur decreases with pressure (see [68] on page 64).
- Monomers without chemically reactive functionality can be as well polymerized as the ones with functionality.
- Non-polymerizing gases like nitrogen can be copolymerized by plasma.

In addition, other observations must be taken into account.

- The role of the ionization is not essential for the plasma polymerization mechanism (but is for the plasma ignition indeed), as:

  - cations are highly reactive to impurities which are significantly present in plasmas;
  - cationic polymerization is only possible for a limited number of monomers.

- Radicals dominates in the plasma phase (as already advanced by Brown *et al.* [66]).
  - Bond energies in molecules (1-5 eV) are well below their ionization energies (10-20 eV).
  - The electron energy distribution function, considered to be maxwellian, provides only a small fraction of high energy electrons (>10 eV) and a large part of low energy electrons (<10 eV).
- The high concentrations of radicals observed in the plasma polymers [47] imply radical mechanisms without termination and where radicals dominate.
- The high crosslinking and the branching of polymers, observed via their insolubility, suggest complex mechanisms, with different steps.

2.3.2 Vacuum p-xylylene polymerization into parylene: biradical polymerization

Gas-phase polymerization at low-pressure or in "vacuum" is very rare. It occurs for very limited types of monomers, all bearing two unpaired electrons, which are [42]:

- carbenes, which are compounds where a carbon atom bears the two nonbonding electrons [69], like methylene H_2C:, ethenylidene $H_2C{=}C$:...;
- silylene and germylene, which are similar to carbenes but for which the diradical atom role is played by a silicon and germanium atom, respectively;
- p-xylylene derivatives for which, this time, the two unpaired electrons are in two different locations in the monomer.

The latter can be polymerized as follows, restricting to the simplest derivative: the unsubstituted one. The precursor is the [2,2]paracyclophane whose structure is shown on Figure 2.1 (A). Initially at solid state, it sublimes around 120-160°C in a vacuum chamber at pressures ranging between 10 to 100 Pa. The vapor is then cracked or pyrolyzed in a second chamber by heating at 600-680°C. The precursor then dissociates into two para-xylylenes radicals (structure B on Figure 3 - 1). The diradical nature has been established by Electron Spin Resonance and the cleavage of only one of the CH_2-CH_2 bonds has been ruled out [42]. The polymerization proceeds through the recombination of two p-xylylene radicals which form a diradical. The growth continues by the repeated addition of p-xylylene diradicals at both radical end sites.

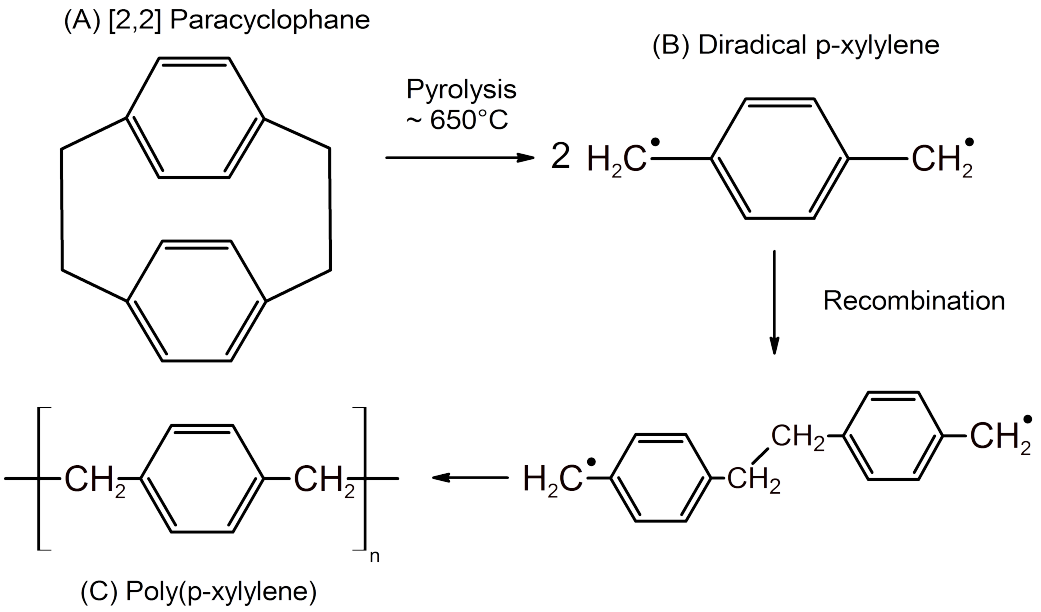

Figure 2.1: Different steps for the p-xylylene polymerization, forming parylene N or poly(p-xylylene).

According to reference [42], the polymerization occurs between the diradicals adsorbed on the reactor surface. For Yasuda, it is rather (unclearly) stated that "the polymer is deposited on surfaces", letting the possibility of gas-phase polymerization. Anyway, the reaction proceeds on sufficiently cold surfaces, not above 35°C.

The particularities of this polymerization are an extreme speed of reaction, within a fraction of a second and with an almost complete conversion of the initial monomer. In addition, the deposited polymer, namely parylene N, contains a high concentration of trapped radicals, as the process has no known termination. Finally the polymer film is highly insoluble.

It is interesting to note that the obtained parylene has advantages for material processing very similar to the one of plasma polymerization. Using no solvent nor catalyst, the polymerization is considered as a green polymer chemical process. Its high conformality (adapts to rough surfaces), high uniformity (pinhole free) and elevated chemical resistance make it very valuable as protective coating, encapsulating film, moisture and dielectric barriers. Its excellent mechanical and electrical insulating characteristics are of importance for the microelectronic industry. Other potential uses include coating of orthopedic parts (bone pins and joint prosthesis) to make them biocompatible but also conservation of archival and artifact objects.

The polymerization mechanism of p-xylylene is neither a step-growth (no reaction between stable molecules), nor a chain-growth (propagation by reaction of a stable monomer with an

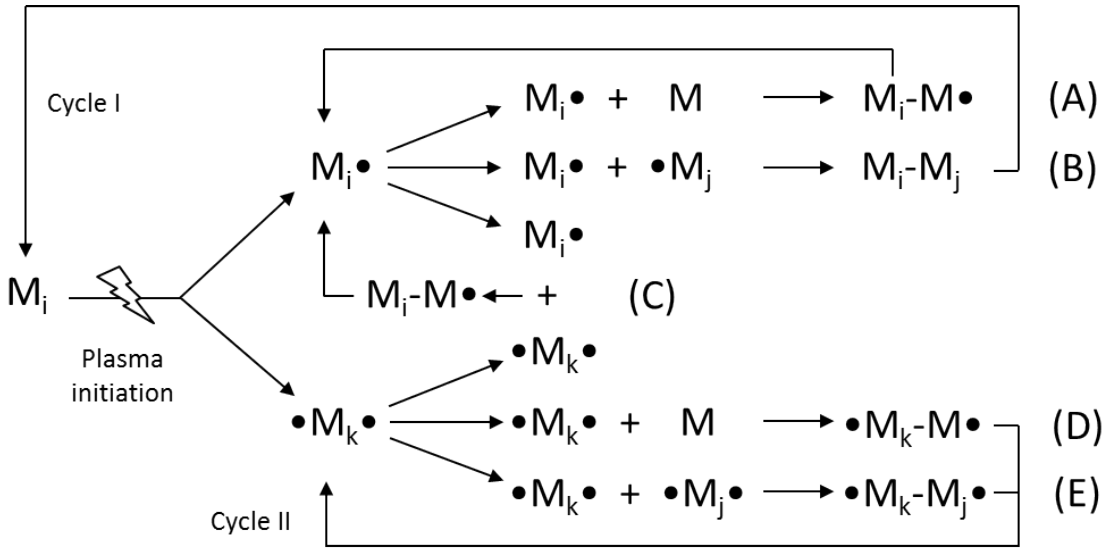

Figure 2.2: Schematic presentation of the RSGP mechanism, inspired from [70].

activated species). It is rather a repetition of fast step reactions between activated monomers, termed by Yasuda "rapid step-growth" mechanism. More recently, the mechanism was termed "transport polymerization" [42], suggesting the transport of the monomer from the gas-phase to the surface upon which it would polymerize.

2.3.3 RSGP mechanism

Considering the p-xylylene polymerization, Yasuda moved forward in 1985 a new mechanism to explain the observed features of the plasma polymerization. He called it the "Rapid Step-Growth Polymerization" (RSGP) [70], presented schematically on Figure 2.2. M stands for a monomer and M with subscript I, j and k indicate species of different sizes, which can be as small as an atom or as large as an oligomer. The symbol "•" stands for a reactive site, which can be, and this is important, a radical or an ionic site, or even can represent an electronic excitation of the considered species.

The preliminary step is an initiation of a species present in the plasma, M_i by plasma excitation. This species can be the monomer or already a stable product of the discharge. The initiation will mostly be an inelastic collision of the species with an electron, but it can also be an UV photon absorption or another inelastic collision with an activated species of the plasma, like ions or electronically excited molecules. This initiation step leads to the production of 2 kinds of species: mono-activated species $M_i^\bullet$ or species with a bi-functionality ${}^\bullet M_j{}^\bullet$. Then 5 different possible reactions are considered:

- Reaction (A) is a chain propagation, which regenerates the reactive site.
- Reaction (B) is termination-like but between two active species.
- Reaction (C) is a crossing reaction between mono- and bi-functional species, leading to the recombination and loss of two active sites. It is then similar to a partial chain termination.
- Reaction (D) is a chain propagation but with a bi-functional species which is new. The reacting site is regenerated.
- Reaction (E) is totally new and is inspired from the p-xylylene transport polymerization. It is termination-like but with conservation of the bi-functionality in the product.

Two main paths of the rapid step-growth are stressed. The first is the so-called "cycle II", which gathered reactions (D) and (E). Both preserve the bi-functionality in their respective products. They are expected to have very high rate coefficients to occur at the very low concentrations of low-pressure. In addition, cycle II has the advantage to explain the very high deposition rate during pulsed plasma [71]. Indeed, the termination-like reaction (E) preserves the reactivity in its product, unlike the termination reaction (B). The bi-functional sites of the species $^{\bullet}M_k^{\bullet}$ can virtually never disappear as long as they don't react with a mono-functional species via the cross reaction (C). It can then proceed ad lib in the plasma time off.

The second main path of rapid step-growth is called "cycle I". It is the reactivation of a stable plasma product and more generally the repeated activation of reaction products. The reaction (A), a conventional chain propagation, is stated to be present but of minor importance. It is supposed to have a slow reaction kinetic at low-pressure, except in particular conditions, like higher pressure and low substrate temperature (higher condensation on the substrate).

This latter remark shows that Yasuda considered this general scheme as well for gas-phase reactions as well as for surface reactions. Concerning the reactive sites, all kinds are taken into account but radical ones should dominate in general. Ionic sites could however be predominant in certain conditions, like on powered electrodes which undergo significant ion or electron bombardments.

2.4 Parameters of plasma polymerization

Studying plasma polymerization requires the variation of the external parameters of the process. Some of them are related to the power density or transmitted energy per molecule, like the pressure, the monomer flow, the power or the discharge pulsation. Other parameters are more related to the reactor design and geometry: power coupling, flow geometry or substrate position.

Finally, the substrate material, its temperature, bias and surface energy density have also showed great influence on the process. We will present here several parameters relevant for the present study or its perspective.

2.4.1 W/F and W/FM parameter

The W/F parameter is also termed "specific energy" and the W/FM parameter is often referred to as the "Yasuda parameter". Their different components are:

- W = wattage or power delivered by the power generator in [W]
  = applied power - reflected power (from the generator point of view)
  (the real power absorbed by the plasma is discussed in Section 2.4.2)
- F = the molar monomer flow rate in [mol/s]
- M = the molar mass of the monomer in [g/mol]

The **specific energy (W/F)** represents the mean amount of delivered energy per mole of monomer or per monomer. Thus, it is expressed in J/mol or eV/monomer, respectively, with the following equivalence: 10^{-3} J/mol = 1.036 ev/monomer or **1 W/sccm = 14.0 eV/monomer**. The **Yasuda parameter (W/FM)** is the mean delivered energy per unit of injected mass of monomer. Yasuda expressed it in [J/kg], but it can be expressed as well in more microscopic adapted units like eV/Da, with the equivalence: 10^8 J/kg = 1.036 eV/Da.

The interest of the specific energy (W/F) lies in its capture of the antinomic effect of the power and the flow on the mean energy available per monomer in a single parameter. Experimentally, it allows to determine transition in the deposition process: either the "critical energy" by monomer to reach full glow conditions (Section 2.5.1) or the "activation energy" required to activate the monomer and lead to its deposition (Section 2.5.2). It is largely used in the recent literature [31, 37, 38, 67, 72].

Interest of the W/FM parameter

To understand the Yasuda parameter (W/FM), let us consider the physical meaning of the same W/FM value on several monomers. In the third column of Table 2.2, a W/FM of 1 eV/Da is expressed in terms of specific energy (W/F). We calculated it for the five monomers we studied in the present work. The result is clear: a same W/FM means a higher delivered energy per monomer as the monomer mass increases.

Monomer	**Mass** (Da)	**W/FM** (eV/Da)	**W/F** (eV/monomer)	**Total BE** (eV/monomer)	**Ratio W/F over BE**
Acetylene	26	1	26	≈ 18	1.5
Ethylene	28	1	28	≈ 24	1.2
Benzene	78	1	78	≈ 56	1.5
MMA	100	1	100	≈ 59	1.7
Styrene	104	1	104	≈ 74	1.5

Table 2.2: Specific energy (W/F) evaluated for different monomer with the same W/FM parameter. Masses and total estimated bond energies of the same monomers. Ratio of the delivered energy to the total bond energy. (MMA = methyl methacrylate)

Bond	**Used bond energy** (eV)	**Bond**	**Used bond energy** (eV)
C-H	4.30	O-H	4.83
C-C	3.61	O-C	3.74
C=C (π)	2.74	O=C (π)	4.04

Table 2.3: Used values to estimate the total bond energy of monomers, taken from [3]

The bond energy of a molecule can be roughly estimated by summing the dissociation energy of all its bonds. The bond energies were taken from [3] and are summarized in Table 2.3. Back to Table 2.2, the fifth column shows that the total bond energy increases more or less with the mass of the monomer. We could have said that it increases with the number of atoms and so the number of bonds in the molecule. However, care must be taken, as this bond energy depends also on the kind of atoms and the kind of bonds of the monomer: benzene and MMA have almost the same bond energy but rather different masses. The last column of the table shows the ratio of the specific energy over the total bond energy per monomer. It is rather similar for the different monomers.

There are two interests in using the W/FM parameter. Firstly, it is more relevant to compare the mass deposition rate of different monomers under the same plasma conditions. Indeed, injecting the same number of acetylene molecules in the reactor will inject less mass than if the same number of styrene is introduced. This was observed by Yasuda as the **mass deposition rate is proportional to the molar mass** in the case of monomers of homologuous series (see [71] p170). Secondly, in the case of highly energetic deposition (high W/F), a styrene monomer can **"absorb" more energy by dissociation** than an acetylene molecule. This is embedded

in the ratio of the specific energy over the bond energy, which is similar for different monomers at the same W/FM. Thus, these two interest of W/FM allows to better compare the mass deposition rate of different (homologuous) monomers in the same plasma conditions (other than W and F) and the same reactor. It was thoroughly demonstrated experimentally by Yasuda [3, 73].

2.4.2 Reactor and flow geometry

The W/F and W/FM parameters are sometimes considered to allow comparison between reactors. However, the reactor design and geometry have a strong impact on the real values of the power and the flow participating to the polymerization process.

The **real power** participating in the process is delicate to define:

(1) Before reaching the plasma, a part of the power indicated on the power generator (or on the powermeter on the line between the generator and the source) is lost in the source and the matching system [9, 32]. The ratio of the power really emitted by the electrodes or the coil to the one send by the generator is termed the **coupling efficiency**. It varies with the reactor geometry but it can also change with the conditions, like power or pressure [74].

(2) A part of the power emitted by the electrodes and the coil is also lost in the reactor structure (walls). To account for these two effects, the power absorbed in the plasma can be directly measured by probes inside the plasma. However, care must be taken as different tools can report different values of absorbed power [35].

(3) According to Hegemann *et al.* [29, 75], only a region of the plasma volume (define as the interelectrode volume, for their CCP geometry) is really participating in the deposition process and is called the activation volume. The real power participating in the deposition process is then the power absorbed by the plasma, reduced by a geometrical correction factor equal to the activation volume over the plasma volume.

Regarding the **flow really entering the plasma region**, some flow designs effectively allow a large by-pass of the gas from the plasma region. The mean real energy locally absorbed in the plasma region per molecule is then much higher than W/F. This is especially true for the case of the bell-jar CCP. The ratio of the plasma volume to the reactor volume is often called to give a qualitative idea of the by-pass ratio [3, 72]. However, in our opinion, a ratio of surfaces is more correct, as flows are considered. It can be simply explained by considering a long tubular reactor with a coil or electrodes at one end, which create a small plasma region but across the

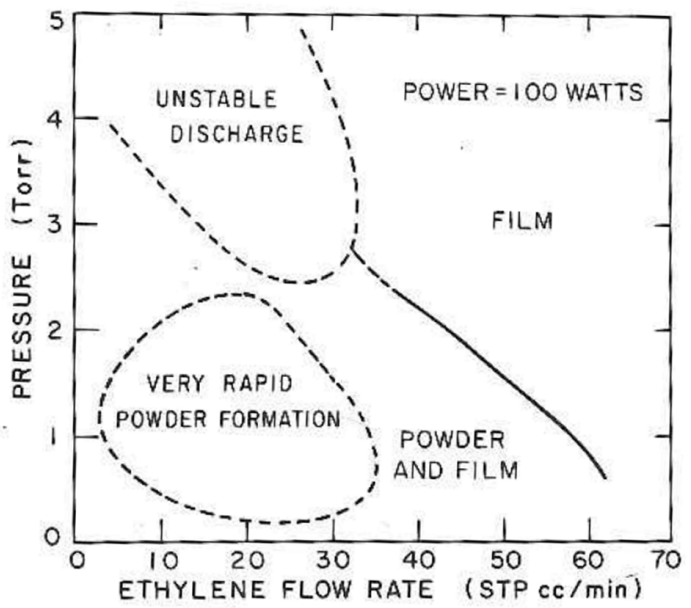

Figure 2.3: Domains of final product types obtained by plasma polymerization of ethylene depending on the pressure and the flow used and working at constant power (from [64]).

whole section of the tube. The plasma volume is small and the reactor volume is large, but no by-pass of the species is allowed.

2.4.3 Pressure

The specific energy or the Yasuda parameter are totally independent of the pressure. Experimentally, pressure shows a strong effect by changing the kinds of final products: soluble (oily) film, insoluble film or powder. This is best demonstrated by the results of Kobayashi *et al.* regarding the mapping of the final product type of Figure 2.3 [57, 64].

Microscopically, pressure strongly affects the **collision frequency** between the species and between the species and the reactor walls. Said in other words, it changes the reaction rate in the plasma bulk, as well as the transport of the activated species to the location of deposition. Another microscopic effect of pressure is the variation of the **rate constant of the three body recombination** (two-to-one association) [6, 28]. The recombination of two radicals for instance leads to an activated complex with high internal energy. A collision is required with a third body (wall or other species) to lose this excess energy and avoid the reverse reaction of decomposition.

A very strong effect when varying the pressure is the **change of the plasma volume**. As film-forming species can be lost or deactivated from their creation location to the deposition

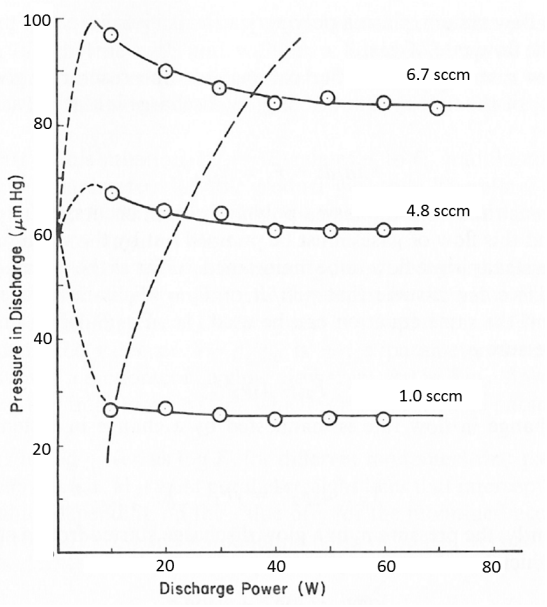

Figure 2.4: Values of the discharge pressure for different combinations of power and flow (taken from [5]).

location, this affect the **distribution of the mass deposited**. Accordingly, even if the total deposited has not changed, the variation of its distribution may affect locally the deposition rate. Therefore, not only the initial pressure before plasma ignition is important, but also the pressure during the discharge. The latter can vary markedly with the plasma conditions, as clearly shown on Figure 2.4: a power increase, for three sets of different flows.

2.4.4 Temperature and nature of the substrate

It is important to realize that the plasma volume reactions are one thing and the deposition step and the surface reactions are another. The substrate temperature effect shows it clearly: all other parameters kept constant, the deposition rate follows an exponential decrease with increasing substrate temperature [47, 53, 70, 76, 77]. In addition, it also changes the deposited film composition. Therefore the chemisorption of the polymerizing species from the plasma volume to the substrate surface is of uttermost importance.

These results reveal the interest of studying the sticking coefficient of the species onto the surface [38], but also the surface mobility of the physisorbed species. This mobility was shown to determine the access of the adsorbed species to the chemisorption sites and affect the roughness of the sample [38, 76].

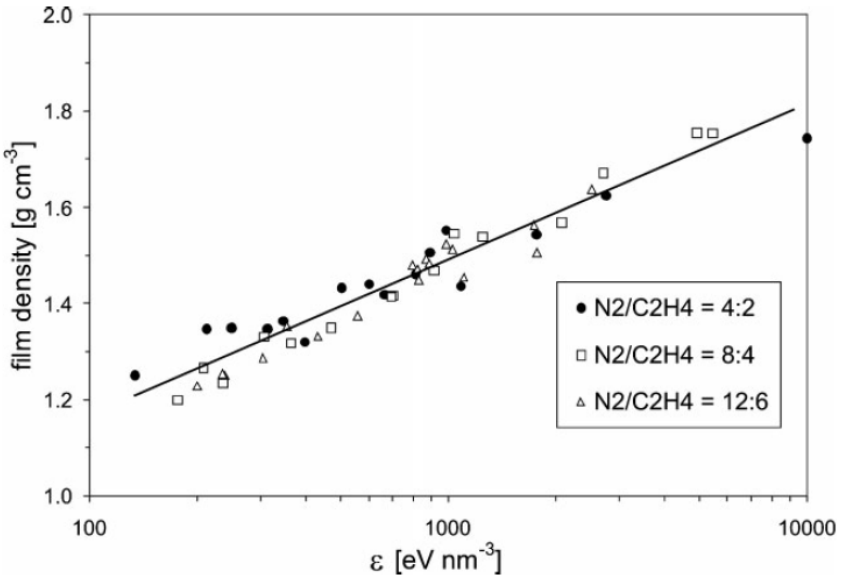

Figure 2.5: Film density of plasma polymer film deposited from a mixture of ethylene (C_2H_4) and nitrogen (N_2) depending on the surface energy density, ϵ_{surf} (from [78]).

2.4.5 Surface energy density

The bombardment of the growing film by ions has been proposed to be the cause of the growth in many studies. In early works (see Table 2.1), observations favor the polymerization initiation by impinging ions, especially for CCP geometries which can have large substrate electrodes bias. In the more recent works of Short *et al.* [27], the estimations in regime of low W/F input even shows that the whole mass can be transferred to the substrate by ion flux on the surface.

Moreover, the densification process of the depositing film revealed to depend on the mean energy dissipated by the bombarding ions per unit of volume of the growing film, ϵ_{surf} (in eV/nm^3). It is also called "surface energy density" and is given by:

$$\epsilon_{surf} = \frac{\Gamma_i E_i}{R} \tag{2.10}$$

where Γ_i is the ion flux at the substrate (ion/cm^2.s), E_i is the ion mean bombarding energy (eV) and R is the deposition rate (nm/s). The dependence of the film density on ϵ_{surf} is noticibly linear [37, 78], as shown on Figure 2.5.

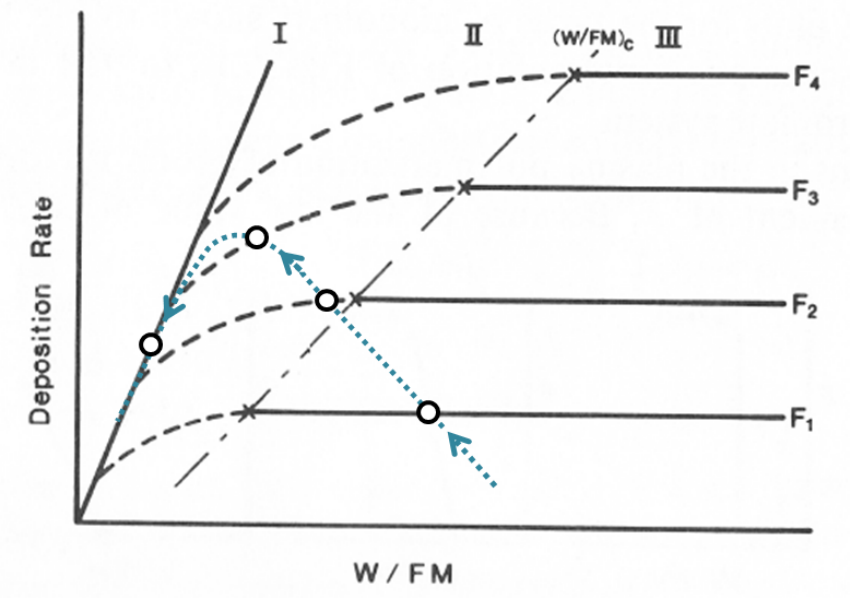

Figure 2.6: Description of the plasma polymerization domains through the general trends of deposition rate in function of the W/FM parameter (adapted from [5], p311).

2.5 Domains and trend of the DR in plasma polymerization

To investigate the parameters influencing plasma polymerization, many works adopted a macroscopic approach from the 1960s to recently. Hence, most results are related to the kind of produced material – powder, film or oil – and the evolution of the deposition rate (DR) in the case of the film. From these studies, the parameter giving the most distinctive and maybe intelligible variation of the DR are the W/F and W/FM parameters, i.e. the mean delivered energy per injected monomer or mass. We present here the domains defined by Yasuda on the DR trend (Section 2.5.1) and the approach of the macroscopic kinetics (Section 2.5.2).

2.5.1 Domains of Yasuda - critical W/FM - full glow

The study of the deposition rate (DR) while varying the discharge power and the monomer flow revealed three regimes of plasma polymerization [73, 79, 80]. It is best introduced by observing the general trend of the DR for increasing W/FM parameter, as shown on Figure 2.6. Each trend curve is actually obtained at a fixed flow while increasing the power. The four shown flows are by increasing order: $F_1 < F_2 < F_3 < F_4$. It is therefore important to have in mind the following aspect. Moving vertically (at constant W/FM) from one point of, let say, the F_1 curve to the F_2 curve is accompanied by an increase of the power.

The evolution of the F_3 curve starts with a linear dependence of the DR with increasing power or W/FM (region I). This regime is qualified as "**energy-deficient**", as this is the applied power which determines the DR. The F_3 curve ends by a region with no increase of the DR when increasing the power or W/FM (region III). In this domain, the only way to increase the DR is to increase the flow, e.g. up to F_3. Therefore the regime has been termed "**monomer-deficient**". Finally, between the two regimes (region II), the F_3 curve smoothly evolves with W/FM from linear dependence to saturation of the DR. The regime is called "transition".

Working at constant power but increasing flow leads to the dotted line we added on the initial figure. The arrows show that in this case the W/FM ratio decreases. The evolution of the DR then indicates an initial linear increase at low flow (and high W/FM), a bell shaped trend in the transition regime and ends with a linear decrease at the highest flow (above F_4).

For each curves on Figure 2.6, the "monomer-deficient" regime starts at different threshold value of W/FM. They are termed "**critical** W/FM" and are thus written with the subscript "c". For the present work, it is important to note that the $(W/FM)_C$ was also correlated to two other phenomena:

- the plasma has reached its maximal volume and is said to reach the regime of "**full glow**";
- the **discharge pressure becomes constant** for higher W/FM.

2.5.2 Macroscopic kinetics - Activation energy

The name "Macroscopic kinetics" in plasma polymerization refers to chemical kinetics applied to a macroscopic output of the polymerization: the deposition rate. We will see the different interpretation it gives from the above Yasuda's domains.

Chemical kinetics and Arrhenius plot

In chemistry, kinetics are the study of the reaction rates, R', which are the local numbers of reactions occurring per unit of time and volume ($m^{-3}s^{-1}$) between two reactants, A and B. Under the simplest conditions, this number is given by:

$$R' = k(T)\, n_A\, n_B \tag{2.11}$$

where $k(T)$ is the rate constant, and n_A and n_B are the number density of A and B, respectively. The number of reactions occurring within a volume (of gas or solution), V, is equal to R' $\cdot$ V.

Under conditions of thermal equilibrium, the rate constant, $k(T)$, follows an exponential increase with increasing temperature of the gas or the solution:

$$k(T) = A \cdot exp(-\frac{E_a}{k_b T}) \tag{2.12}$$

where A is the pre-exponential factor (m^3/s), E_a is the activation energy (eV), k_b is the boltzmann constant (eV/K) and T the temperature of the fluid (K). The activation energy is the energy needed for the reaction to occur. Equation 2.12 is called "**Arrhenius equation**".

The exponential term of Equation 2.12 may seem blunt but is actually justified microscopically. It is effectively equal to the proportion of microscopic collisions between the reactants, A and B, with (thermal) energy of collision above the activation energy, in the case of maxwellian distributions of speed (thermodynamic equilibrium). By comparing Equation 2.11 to Equation 1.8 (p17); it is found that the rate constant is given by:

$$k(T) = < \ \sigma v \ > \tag{2.13}$$

When taking the natural logarithm of equation 2.12, the equation becomes:

$$ln(k) = ln(A) - \frac{E_a}{k_b} \cdot (1/T) \tag{2.14}$$

which is the equation of a straight line, y = a + s · x, with a = ln(A), the negative slope s = -E_a/k_b and the variable x = 1/T. Hence, plotting k in function of 1/T on a semi-logarithmic scale provides a straight decreasing line as shown on Figure 2.7. This is the so-called "**Arrhenius plot**". The measure of the slope of experimental fits gives the very important parameter of the reaction, which is the activation energy, E_a.

Arrhenius-like dependence of DR in plasma polymerization

The central statement of macroscopic kinetics is the following. The general trend of the mass deposition rate (R) curve for increasing W/FM or W/F (like shown on Figure 2.6) was proposed to follow an exponential dependence like the Arrhenius equation [81–83]:

$$R/F = G \cdot exp(-\frac{E_a}{W/F}) \tag{2.15}$$

where G is the pre-exponential factor and E_a the activation energy of the monomer in the plasma.

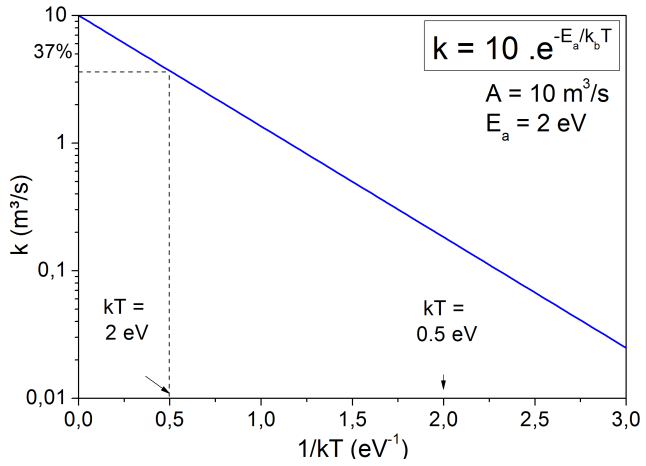

Figure 2.7: Arrhenius plot: ln(k) in function of $1/k_bT$ gives a straight line on a semilogarithmic scale.

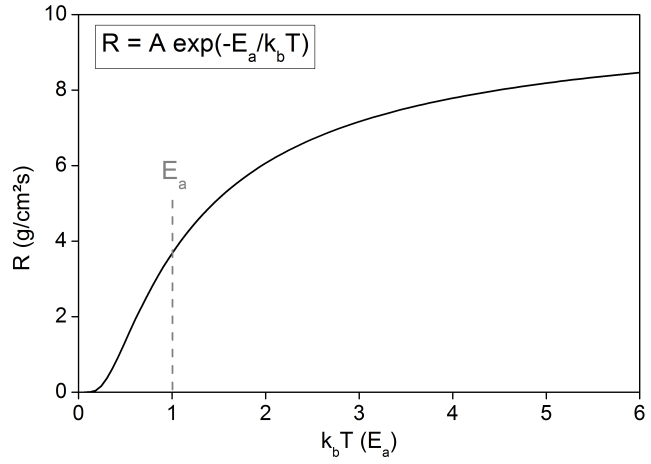

Figure 2.8: General trend of the exponential dependence of the deposition rate on the W/F parameter, assumed by macroscopic kinetics.

No convincing physical microscopic basis exists for this equation, whose widespread use by Hegemann *et al.* actually started the debate announced in the introduction of the present chapter. The general applicability of the equation to any reactor configuration seems rather negative [9, 32, 35], even integrating the corrections of the power and the flow really transferred to the active plasma zone (Section 2.4.2). The interest of Equation 2.15 may lie in its general shape in agreement with the general trend of the plasma polymerization deposition rate: initial threshold at low W/F and saturation at high W/F [9]. It captures with the single parameter E_a the whole DR relative dependence, as shown in Figure 2.8. The initial dependence at low W/F is closed to be linear, which is assumed by Yasuda (Section 2.5.1).

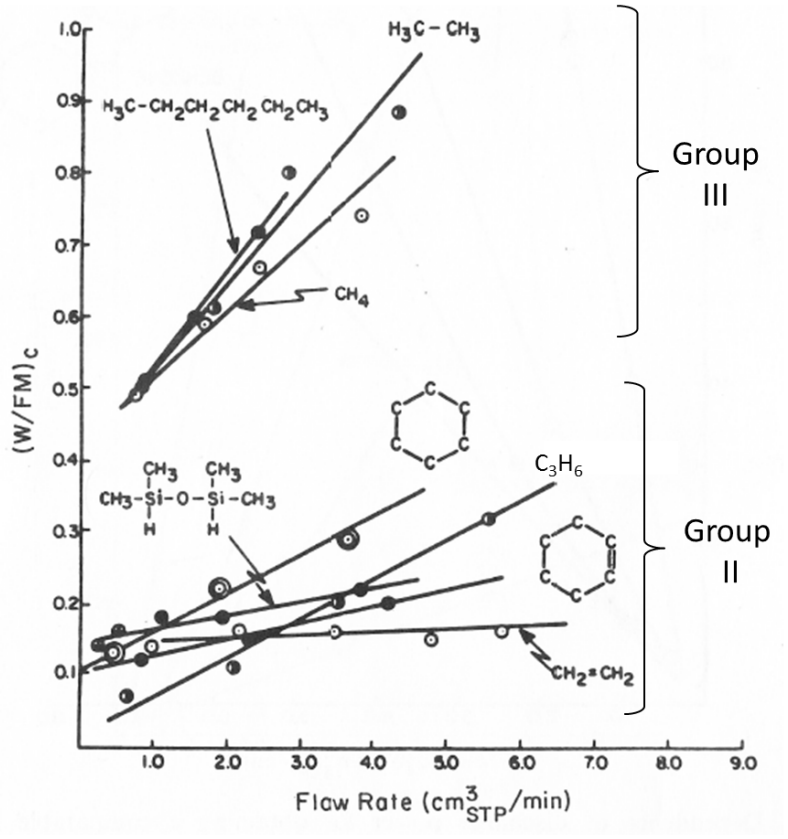

Figure 2.9: Evolution of W/FM$_C$ depending on the flow for: three saturated hydrocarbon monomers forming group III; four mono-unsaturated monomers and one silicon and oxygen containing monomers forming group II (taken from [3] p304).

2.6 Monomer classification

A considerable work has been carried out by Yasuda and Hirotsu to determine the critical W/FMs as a function of the flow for many monomers. The measurements are summarized in Figure 2.9 and Figure 2.10.

On Figure 2.9, three monomers show a strong dependence of W/FM_C with the flow. They are all saturated and were gathered in a group of monomers, termed "group III". The remaining monomers showed a moderate dependence of the critical parameter with the flow. They formed the "group II" of monomers, which are mono-unsaturated with a single double bond and/or a non-aromatic cyclic structure (or additionally containing atoms like Si or O). Finally, on Figure 2.10, no flow dependence is observed for the $(W/FM)_C$. The four monomers are highly unsaturated: containing aromatic cycle and/or triple bond.

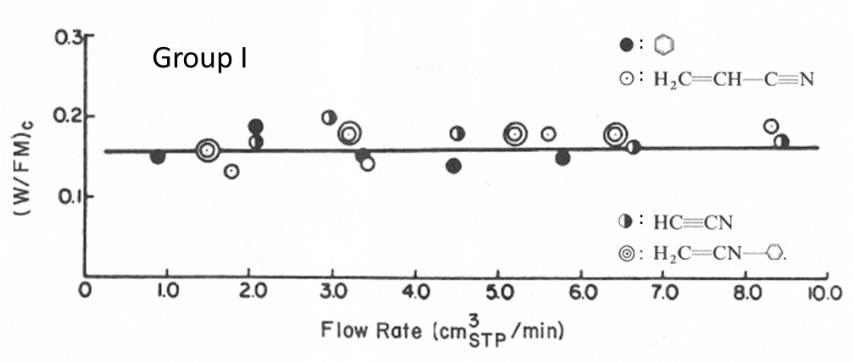

Figure 2.10: Evolution of W/FM_C depending on the flow for highly unsaturated monomers forming group I: benzene and three nitrogen containing unsaturated monomers (taken from [3], p305).

It is interesting to note that this monomer classification gave similar gathering for other aspects of plasma polymerization. For instance the formation of powder was observed with decreasing importance in the order: group I > group II > group III [84]. The hydrogen production in the discharge was observed with increasing importance to be: group I < group II < group III [85]. Moreover, monomers of group I tend to produce polymeric film with much higher concentration of trapped radicals than monomers from group III.

The **polymerizing behavior** led to a second proposed classification. Some monomers were observed to predominantly polymerize in plasma, while the others rather decompose [63, 86]. The first group, the "group A", corresponds to monomers which are aromatic, heteroaromatic, nitrogen-containing, Si-containing and olefinic. At the opposite, oxygen-containing, aliphatic hydrocarbon chains and cyclic hydrocarbon chains belongs to the second group of monomers, called "groug B".

Finally, a third classification distinguishes [79]:

- **chemically nonreactive gases**: mainly monoatomic inert gases, which are not consumed in chemical reactions. They can ionize other species or sputter surfaces.
- **reactive gases**: gases which do not form polymer when plasma is ignited in their pure vapors but can be incorporated into a film when mixed with a polymer-forming species or can chemically react with them during plasma. These are O_2, N_2, CF_4...
- **Polymer-forming gases**: the usual monomer of plasma polymerization.

Chapter 3

Electron ionization in Mass Spectrometry

Among ionization techniques for detection of gaseous molecules, Electron Ionization (EI) is widely used in organic Mass Spectrometry (MS). It is most often referred as Electron Impact, but this term does not render the quantum mechanical nature of this energy exchange reaction [87]. The ionization process has been extensively studied from atoms to molecules [88–90].

The aim of this chapter is to present the most relevant features for the ongoing study: the ionization cross section, the reaction time scale and a limited description of unimolecular ion decomposition. The chapter will then end by establishing a criterion to distinguish peaks in a mass spectrum and the interest of measuring the appearance energy in their case.

3.1 Ionization cross section and ion abundance

Electron ionization is the process during which a primary electron interacts with a target atom or molecule and induces the ejection of a secondary electron. The probability of this process depends on the primary electron energy. Indeed a minimum energy is required to release a bounded electron from an atom or a molecule. It is called the **ionization energy** (IE), often referred to as **ionization potential** (IP). Primary electrons with energies below this threshold cannot ionize the target. For primary electrons with energies far above the IE, the ionization is possible but very unlikely. In this case, the primary electron speed is so high that its interaction time is too short to transfer a part of its kinetic energy to the target. For energies in between, the ionization probability reveals a maximum.

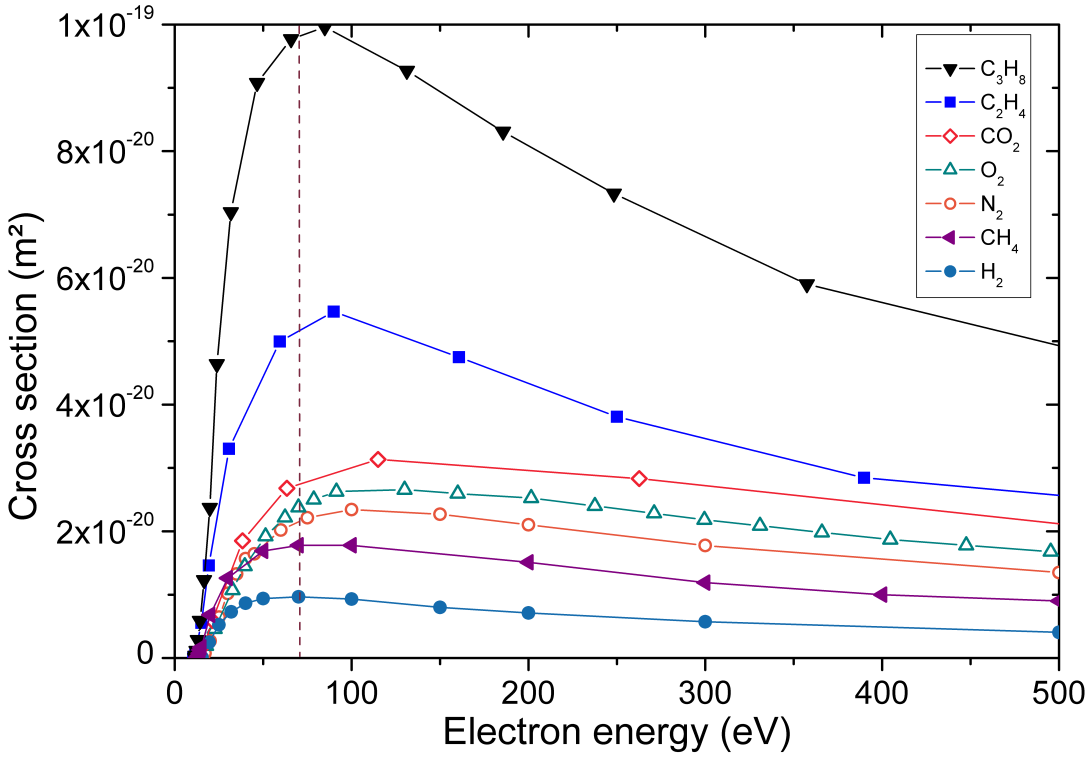

Figure 3.1: Ionization cross section of several molecules depending on the primary electron energy. Open symbols are for usual gases [15]. Filled symbols are for hydrogen and hydrocarbons. For the latters, the curve comparison shows that the cross section increases with the size of the molecule.

Figure 3.1 shows the electron energy dependence of the ionization cross section for several molecules. A maximum is observed for each curve, lying between 100 eV and 70 eV, marked by a vertical dashed line. The three gases marked with open symbols are very usual ones: oxygen O_2, nitrogen N_2 and carbon dioxide CO_2. The maximum of the cross section defines the typical order of magnitude for electron ionization cross section (3.10^{-20} m^2) which corresponds to a classical interaction radius of 1.0 Å. It is interesting to note that it is close but below the molecular diameter of nitrogen (3.1 Å) or oxygen (2.9 Å). The four remaining gases are marked with filled symbols. They include: hydrogen (H_2), methane (CH_4), ethylene (C_2H_4) and propane (C_3H_8). It is noticeable that the maximum of the cross section increases with the size of the molecule. This effect has been observed for primary electron energy ranging from 75 eV to 1.2 keV. It leads to the "**additivity rule**" for EI cross section [91, 92]: for the same electron energy, the cross section of a large molecule can be estimated by adding the known cross section of its different constituents.

The ion abundance A is defined by the number of ions produced per unit of time by the beam of the primary electrons. It depends on several factors. At constant electron energy and constant

temperature of the gas, the ion abundance induced by electron ionization is proportional to the gas pressure p [87] through the relation:

$$A = C\ p\ i\ V \tag{3.1}$$

where i is the electron current, V the volume within which the process occurs and C is a constant of proportionality which depends on the ionization cross section of the considered gas and on the gas temperature.

3.2 Timescale of fragment ions production

The electron ionization of a molecule is usually carried out at electron energies from 50 to 100 eV. It is an energy choice made for maximizing the ion abundances, as the cross sections are maximal in this range. During the EI process, approximately 10 to 20 eV of the primary electron energy is transmitted to the molecule [87]. The ionization energy of atoms and molecules generally lies in the range of 8 to 16 eV, with few exceptions like helium which requires 24.6 eV. As bonding energies between atoms in a molecule usually lay between 1 to 5 eV, the transmitted energy is largely sufficient to induce bond cleavage on the impacted molecule. However, it is important to underline that the formation of ions which are fragments of the initial molecule is a two-step process, described hereafter.

The electron impact firstly results in the ionization of the target molecule, before inducing any fragmentation. This is due to the much shorter time scale of electron motion in regard of the one of the atom cores. A primary electron of 70 eV has a classical speed of 5.10^6 m/s. Therefore it takes 0.2 fs to cross a region the size of 1 nm. The secondary electron emission is a process of the same timescale, below 1 fs [87]. This is supported by the possible ignition of hot plasma within 100 fs [93]. Secondly, the vibrational period of H_2 of 50 fs gives a lower time scale bound for motion of atom cores. For heavier atoms, it is generally considered to be on the order of 100 fs [94] and can be up to 1 ns for vibration of a large group of atoms [87]. Therefore, **ionization always takes place before dissociation**. Figure 3.2 depicts schematically the first step of ionization.

Once the ionization has occurred, the ionized molecule can carry internal energy in excess. The second step is then the possible decomposition of the produced parent ion, which depends on its internal excess energy.

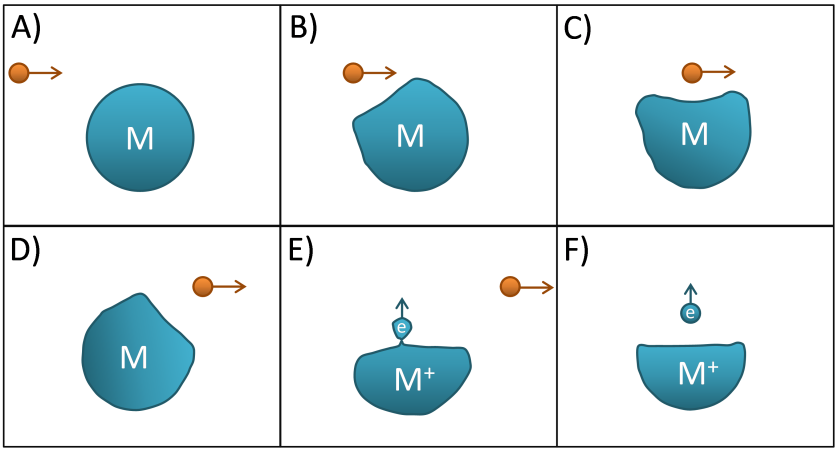

Figure 3.2: Illustration of the electron ionization in terms of electron cloud, according to Van Bramer [95]. The primary electron induces an electric field which modifies the atomic orbitals (step B, C and D). In the process, it transmitted a part of its kinetic energy by inelastic collision. Left behind, the excited atom releases a part of its exceeding internal energy by ejecting an electron (step E and F).

3.3 Conditions for unimolecular ion decomposition

In MS, the EI is carried out to ensure that the ion decomposition is unimolecular, which means that the decomposition occurs without any external influence. To this aim, two conditions are required.

Firstly, the pressure must be such that the parent ion does not collide with the remaining neutrals before reaching the detector. Typically, a pressure below 10^{-2} Pa (10^{-4} mbar) is considered sufficient [96]. Indeed, with a large ion-neutral collision cross section of 5.10^{-15} cm^2, this pressure would ensure an ion mean free path of 0.8 m. Practically, secondary electron multiplier (SEM) detector requires even lower pressure, below 5.10^{-4} Pa (5.10^{-6} mbar), so the pressure condition is plainly fulfilled.

Secondly, unimolecular decomposition requires the avoidance of multiple electron impacts. The electron currents are generally designed to provide an ionization degree of 10^{-3} of the entering neutrals at the maximal ionization cross section [87]. This is obtained under the condition of continuously injecting and pumping the neutrals in molecular flow conditions. A nitrogen molecule with a mass of 28 amu has a classical speed of about 10^3 m/s for an energy of 0.1 eV. It therefore takes 5 µs for it to cross a distance of 1 cm at constant speed, which is the size of the spectrometer ionization chamber. Concerning the ions produced in the ionization chamber, they are extracted by an attracting potential of around 10 V. It then takes around 5 ns to extract a nitrogen ion (N_2^+) from the same region. The conditions are then fulfilled as

the ions stay 1000 times less than the neutrals, for which only one is ionized per 1000 entering neutrals.

3.4 Theoretical elements of unimolecular decomposition

The process of unimolecular decomposition will now be described briefly. Two theories were independently proposed in 1952 to explain this reaction and the observed ion abundances. One is the quasi-equilibrium theory (QET) [97] and the other is the Rice-Rampsberger-Kassel-Marcus theory (RRKM) [98, 99]. Both theories are almost identical and are based on the same following assumptions and postulates.

A first assumption is that the rotational, vibrational, translational and electronic movements are independent. Concerning the independence of the electronic movement, this is justified by the shorter timescale of electronic transitions in molecules (10^{-18} s) or of their ionization ($<10^{-15}$ s). It is then a sort of Born-Oppenheimer approximation for calculation of energies and wave functions in atoms and molecules. The second assumption is that the nuclei movement can be described classically.

A first postulate is that all the microscopic states of the parent ion are equally probable. This means that the excess energy of the parent ion is equally distributed over all its degrees of freedom. This was experimentally observed in the so-called degree of freedom effect [100]. A second postulate is that the ion decomposition is irreversible or that recombination of products can be ignored. This is justified in the case of a sufficiently low pressure conditions.

3.4.1 Internal energy distribution - Decomposition rate - Appearance energy

The electronic excitation from the initial neutral state to the parent ion state occurs at constant interatomic distances, which is generally referred to as a "vertical transition". The electronic rovibrational states of the parent ion are then populated depending on their relative transition probabilities (Franck-Condon factors) and the energy distribution of the initial neutral. This gives a probability distribution function for the internal excess energy of the parent ion, namely $P(E)$. Two simple distributions are depicted on Figure 3.3a, but many complex shapes exists depending on the molecular ion structure and its distribution of states [101]. The impact of electrons with higher energy promotes the production of ions with higher internal energies. The $P(E)$ is then displaced towards higher energy, as illustrated by the dashed line distribution. In

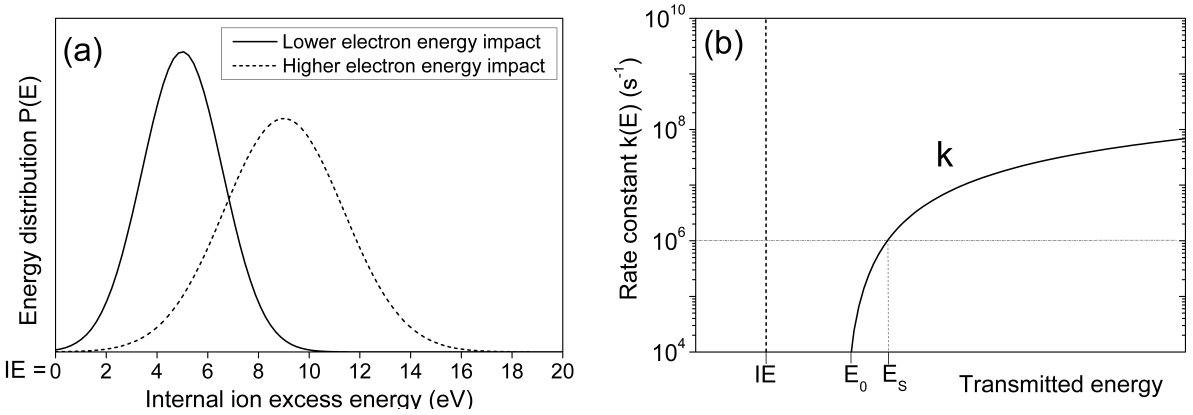

Figure 3.3: (a) Simple examples of two ion internal energy distributions P(E). (b) Example of rate constant evolution with threshold energies E_0. E_S is the minimum energy at which the fragment ions can be detected.

Figure 3.3a, the x axis is the internal ion energy in excess, that is to say the absorbed energy during the electron impact diminished of the IE.

The ion decomposition probability, which depends on its internal energy E, is expressed through the rate constant $k(E)$. Both theories lead to the same expression for it, taking into account all the degrees of freedom and the equal distribution of the internal energy. A simplified expression is often used:

$$k(E) = \nu \frac{E - E_0}{E^{n-1}} \tag{3.2}$$

where ν is the frequency factor, E is the internal parent ion energy, n is the number of vibrational degrees of freedom and E_0 is the threshold energy for the considered decomposition channel. The energy difference $E - E_0$ is the available energy for the dissociative translation. Structural changes of the initial neutral affect ν, n and E_0. The frequency factor is also directly proportional to $E - E_0$. An example of rate constant is shown on Figure 3.3b, which will be discussed further on. It is important to note that this approximate power dependence of $k(E)$ on $E - E_0$ is subject to important errors at low or high electron energies [13, 87]. However, it is still commonly used in quite recent works [90, 102, 103].

On Figure 3.3b, the $k(E)$ curve starts at the threshold energy E_0, which is the minimal internal energy for which the fragment ion can be produced. However, it is not the minimal energy at which the ion detection will occur in the spectrometer. This detection will actually be carried out at the minimal internal energy E_S, which will be called the "detection energy". It is defined as the internal ion energy corresponding to the minimal constant rate of detection of 10^6 s^{-1}, marked by a horizontal dashed line. To understand why the fragment ion is detected

at E_S, it is important to remember that the lifetime of the molecular ion is equal to the inverse of the rate constant. 10^6 s^{-1} then corresponds to a lifetime of 10^{-6} s of the parent ion, before it produces the fragment ion. This is the typical time needed for ions to leave the source and to enter the mass selector. For a lower rate constant, the lifetime of the molecular ion is higher and so it will reach the detector before decomposing. For rate constant above, it will decompose before leaving the ion source and the fragment ion will be detected.

The energy axis of Figure 3.3a and 3.3b are expressed with the origin taken at the IE of the molecular ion. The **appearance energy** (AE) of a fragment ion is then equal to the sum of the IE with the threshold energy E_0: $AE = IE + E_0$. It is also referred to as the **appearance potential** (AP). Concerning the energy difference between the detection energy and the threshold energy, $E_S - E_0$, it is called the "kinetic shift"İt is often below 0.01 eV, but can be as large as 2 eV [17]. Finally, for fragment ions other than the one of lowest AE, their detection occurred with a higher energy shift than the kinetic shift. As it is due to the competition of decomposition with fragments with lower AE, the energy delay $E_t - E_0'$ is termed "competitive shift".

3.4.2 Direct cleavage and cleavage with rearrangement

Two different typical channels exist for the decomposition of a molecular ion $ABCD^{+\bullet}$. They are shown on Figure 3.4 and explained hereafter.

- **Tight complex - cleavage with rearrangement**. For the top channel, the atom bonds can bend thanks to the ion internal energy and lead to a specific conformation of the parent ion, called "tight" activated complex. This conformation can promote the creation of a bond between the atom A and D, while the A-B and the C-D bonds are weakened. Valence electrons are redistributed and the decomposition ends with two products: the radical ion $AD^{+\bullet}$ and the closed-shell neutral B=C (with a double bond).
- **Loose complex - direct cleavage**. For the inferior channel of Figure 3.4, the ion internal energy leads to large vibrations of the B-C bond and the formation of a so-called "loose" activated complex. This conformation can lead to the direct cleavage of the B-C bond. The two dissociating products compete for the valence electron which is won here by CD, which forms a radical neutral ($CD^{\bullet}$). The remaining product then forms a closed shell ion AB^{+}.

To sum up, the tight decomposition only produces radical ion, like $AB^{+\bullet}$, while the loose fragmentation exclusively produces closed-shell ions, like AD^{+}.

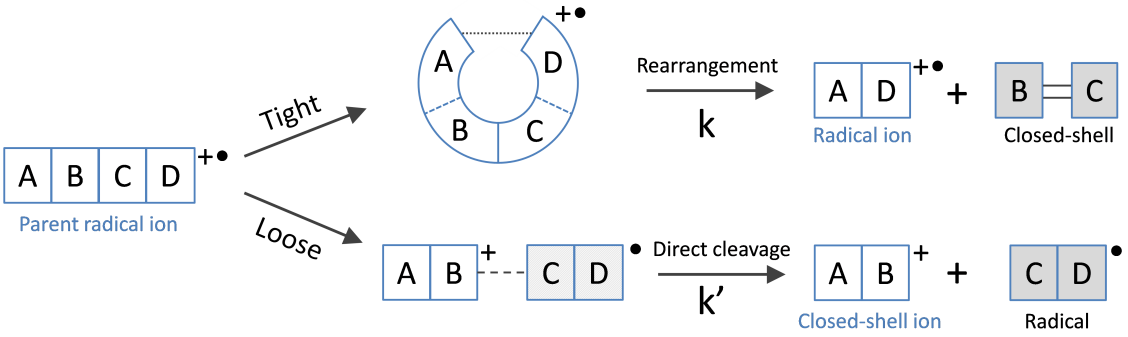

Figure 3.4: Schematic description of two decomposition channels of the $ABCD^{+\bullet}$ molecular ion, via its "loose" and "tight" complex conformations.

3.4.3 Prediction of the ion abundances

The ion decomposition probability of the "tight" and the "loose" channels are the rate constants k and k', respectively. Their precise dependence on the internal ion energy is now depicted at the bottom of Figure 3.5 and will serve to predict the relative abundances of the three ions: the molecular ion $M^{+\bullet}$, the fragment ion produced by rearrangement $AD^{+\bullet}$ and the fragment ion produced by direct cleavage AB^{+}.

On Figure 3.5, the threshold energies of k and k' are E_0 and E'_0 respectively and their detection energies are E_S and E'_S. The internal energy at which the rate constants cross each other is referred to as E_t. The upper part of Figure 3.5 is an ordinary distribution function for the molecular ion internal energy $P(E)$. The combined figure made of the rate constants and the ion energy distribution function is called a "Wahrhaftig diagram" [13]. It enables to determine the relative ion abundances of $ABCD^{+\bullet}$, $AD^{+\bullet}$ and AB^{+}, as follows.

- **Molecular ion intensity – $M^{+\bullet}$.** A part of the molecular ions will not decompose in the ionization source and will reach the detector as a whole. These are the ions with internal energies lower or equal to E_S. Indeed, their corresponding values of constant rate are small, which means a too long lifetime to decompose in the source. Their relative abundance is then determined by the relative surface area of the energy distribution below E_S.
- **Rearranged fragment ion intensity – $AD^{+\bullet}$.** The molecular ions which predominantly decompose in the ionization source via the tight complex are the ones with internal energies above E_S and below E_t. Above E_S, the value of the constant rate is high, which means that the decomposition lifetime of $M^{+\bullet}$ into $AD^{+\bullet}$ is sufficiently short to occur in the source. Concerning the upper energy bound, it is not E'_S, because a molecular ion with internal energy between E'_S and E_t will first decompose into $AD^{+\bullet}$ instead of AB^{+}. Indeed, in this

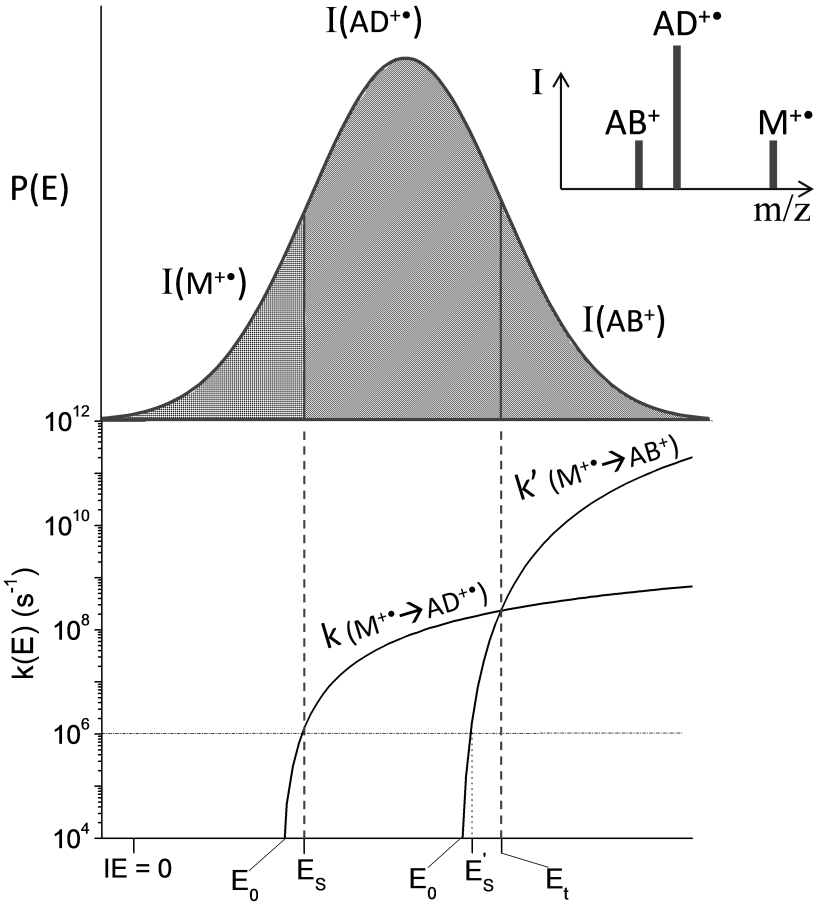

Figure 3.5: Wahrhaftig diagram: the combination of $P(E)$ and $k(E)$ determines the relative ion abundances of $M^{+\bullet}$, $AD^{+\bullet}$ and AB^{+}.

energy range, the $k > k'$ and then the lifetime before decomposition into $AD^{+\bullet}$ is shorter than the one into AB^{+}. All considered, the relative abundance of the rearranged $AD^{+\bullet}$ is determined by the surface area of the energy distribution between E_S and E_t.

- **Direct fragment ion intensity - AB^{+}.** Finally, above E_t, the life time of decomposition into AB^{+} is now shorter than the one into $AD^{+\bullet}$. The molecular ion with energy higher than E_t will then decompose into AB^{+}. Its relative abundance is given by the relative surface area of $P(E)$ above E_t.

As a conclusion, the relative surface areas below $P(E)$ give the three ions intensities observed in the mass spectrum, depicted on top right of Figure 3.5. It is now clear that a shift of the internal energy distribution $P(E)$ towards higher energies will change the relative surface area below $P(E)$, by decreasing the relative abundance of the molecular ion $M^{+\bullet}$ and increase the

one of AB^+ in the present example. Indeed this simplified description does not take into account metastable ions which decomposes "on flight" in the mass analyzer [13].

3.4.4 Typical relative features of loose and tight decomposition

The constant rate curves of Figure 3.5 illustrates typical relative features between the "loose" and the "tight" decomposition. A first feature is that the "tight" threshold energy E_0 can be lower than the "loose" one, E_0'. This can be explained via the net number of cleaved bonds. As seen on Figure 3.4, the tight decomposition proceeds through the cleavage of two bonds, A-B and C-D, but also leads to the formation of two bonds: A-D and the π-bond of B=C. The net number of cleaved bonds is then zero. On the contrary, the loose fragmentation requires the cleavage of one bond, B-C. Then the threshold energy is often lower for the tight channels than for the loose one. A second features is that the "loose" channel usually has a higher constant rate (above the E_t energy indeed). It is due to the fact that the formation of the A-D bond needs that A and D are within bond distance. It then requires very specific conformation of the $ABCD^{+\bullet}$ ion which are less probable at high internal energy. It is also said that the formation of $AD^{+\bullet}$ has the more favorable enthalpy and that the one of AB^+ has the more favorable entropy.

3.4.5 Factors affecting the constant rates and the ion abundances

The internal energy distribution $P(E)$ is needed to determine the ion abundances. This distribution can be estimated by dedicated experiments during which the energy lost by the primary electrons is measured. However, several empirical rules can help describe the observed abundances:

- **The stability of the produced ions** increases their abundances. Non-bonding electron sharing of heteroatoms like oxygen can increase the stability, as well as resonance stabilization of aromatic compound for instance.
- **The Stevenson's rule** is based on energy considerations [20]. During the decomposition of $AB^{+\bullet}$, two couples can be produced: either $A^+ + B^\bullet$ or $A^\bullet + B^+$. From the fragments A or B, the one with the lowest IE will be preferentially ionized. In other words, the radical fragment with the highest IE will retain the electron during the decomposition.
- **The loss of the largest alkyl** is an exception to the ion stability rule. For branched molecules, the abundance of fragment ions are favored if their counter products are large neutral alkyl radical. Thus the fragment ion produced by loss of an ethyl neutral radical $C_2H_5^\bullet$ is more abundant than the one produced by the loss of a methyl radical $CH_3^\bullet$.

- **The stability of the neutral counter product** of a fragment ion also enhances the ion abundance. If the neutral product is a radical, its stability is improved by electron delocalization, branching or electronegative heteroatoms. In the case of closed shell neutral product (tight decomposition), the small ones often have high stability like H_2, CH_4, H_2O, CO, CH_2CO...

3.5 Mass criterion for molecular ion peak

It is now clear that the electron ionization (EI) of a polyatomic molecule can produce a series of ions. The EI mass spectrum reflects the abundance of the molecular ion and the fragments ions. At fixed electron energy, the mass spectrum constitutes a fingerprint of the studied compound, called "Cracking Pattern" (CP). When two polyatomic molecules are mixed, the recorded mass spectrum will be a linear combination of their cracking pattern, with intensities proportional to their partial pressures [17].

In the post-discharge of hydrocarbon plasmas, the gas-phase is made of a mixture of potentially numerous stable compounds. The electron ionization mass spectrum is then a linear combination of many CPs, which makes the interpretation of such spectrum a complex task. The key point relies on the identification of the molecular ion peaks among the other peaks.

The so-called "**Nitrogen rule**" can help to discard peaks from being molecular ion peak:

"A neutral closed-shell species containing an even number of nitrogen atoms has an even mass number."

This rule is due to a fortunate correspondence between the mass of the most abundant isotope of an element and its valence: either the mass and the valence are even-numbered, or they are odd-numbered [17]. It stands for organic compounds with the most common elements. For instance, carbon's and oxygen's most abundant isotope, ^{12}C and ^{16}O, have even mass number and can form an even number of bonds, 4 and 2 respectively. On the contrary, hydrogen's most abundant isotope ^{1}H has an odd mass number and can only form one bond. Nitrogen is the only exception: ^{14}N can form 3 bonds. In the present study, all the organic compounds contain zero nitrogen atoms and thus all the neutrals have an even mass number. Therefore, as the molecular ion is produced by direct ionization, it has the same mass as its parent neutral and also has an even mass number. This will serve as a first criterion to discard a mass spectrum peak to be a molecular ion, that we called the "Mass criterion for molecular ion peak":

An odd mass ion is not a molecular ion / A molecular ion has an even mass

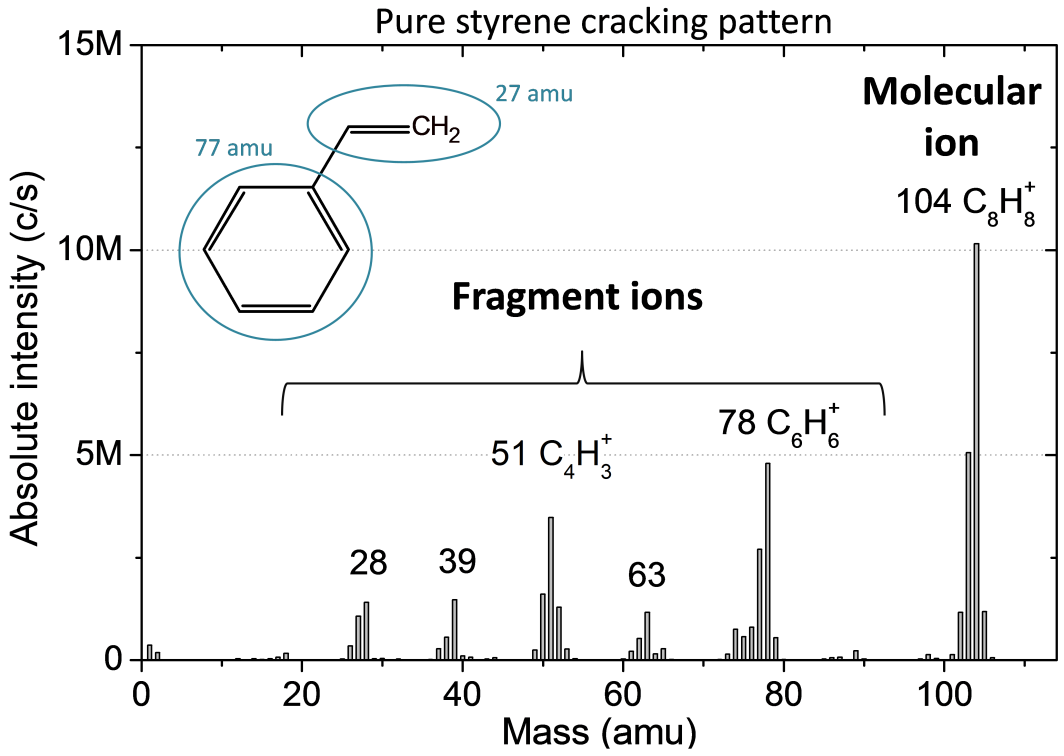

Figure 3.6: Cracking pattern and structure of styrene.

3.6 Cracking pattern of a single hydrocarbon: the styrene case

In order to apply some aspects of Electron Ionization MS, the styrene CP pattern will be discussed here. The styrene structure is shown on Figure 3.6. Its molecular formula is C_8H_8 with a molecular weight of 104. It is composed of phenyl functional group (C_6H_5- with 77 amu) and a vinyl functional group (C_2H_3- with 27 amu).

On the same figure, the styrene CP major peak (called "base peak") is at m/z = 104. It is thus the molecular ion peak. Among the main fragment ion peaks, we distinguish those having an even mass (m/z = 78 and 28) from those with odd mass number (m/z = 63, 51, 39).

3.6.1 Even mass fragment ions

In regard of the "reverse" nitrogen rule, for zero nitrogen containing compounds, the fragment ions with even mass are radical ions. Indeed, an even mass neutral has an even number of valence electrons. If ionized, it thus has an unpaired electron. Furthermore, as seen earlier (Section 3.4.2), radical ions are only produced through the "tight" decomposition channels.

For instance, the peak at m/z = 78 of the styrene CP is assigned to $C_6H_6^+$, which is most probably a benzene ion. A direct cleavage of the phenyl-vinyl bond of styrene (C_6H_5-C_2H_3) would give two fragments: C_6H_5 with a mass of 77 amu and C_2H_3 with a mass of 27 amu. Therefore the production of a fragment ion with m/z = 78 requires a hydrogen atom transfer from the vinyl fragment to the phenyl fragment. The C-H scission from the vinyl radical constitutes the second bond cleavage during the "tight" decomposition. The radical H atom recombines with the radical site of the phenyl group and thus it is the first bond formation of the tight process. The second bond formation is the triple bond creation in the vinyl fragment which has lost the H atom: the two radical sites recombine and the final product is acetylene HC≡CH. The net number of bond cleavage of the overall fragmentation is then zero.

The two rearranged fragment ions, $C_6H_6^+$ with m/z = 78 and $C_2H_2^+$ with m/z = 26, competes to keep the unpaired electron of the parent molecular ion of styrene. The IE of acetylene is 11.4 eV, well above the one of benzene with 9.2 eV. According to the Stevenson's rule, acetylene thus wins the electron and is produced as a closed-shell neutral. Benzene is preferentially ionized. Its ion abundance is effectively markedly higher at m/z = 78 than the one of acetylene at m/z = 26 on the styrene CP.

What is important to retain from all this is the fact that **even mass fragment ion are radical ions and are produced** by "tight" decomposition or said in other words **via rearrangement**. The consequence to interpret mass spectra of gas mixture is that they could be taken as molecular ions. Effectively, in an unknown mixture of hydrocarbon vapors, the $C_6H_6^+$ ion could originate either from the ionization of benzene or from a decomposition channel with rearrangement of styrene.

3.6.2 Odd mass fragment ions

Now let us consider the direct cleavage of the phenyl-vinyl bond. It produces two fragments via the "loose" activated complex (Section 3.4.2) with masses of 27 and 77 amu. Competing for the unpaired electron, the fragment with the higher IE ($C_2H_3^\bullet$ with 9.8 eV [13]) will keep the electron and become a radical neutral. The fragment with the lower IE ($C_6H_5^\bullet$ with 8.1 eV [13]) preferentially yields the electron and becomes a closed-shell ion: $C_6H_5^+$. Therefore the peak at m/z = 77 is more intense than the peak at m/z = 27 in the styrene CP.

3.6.3 Conclusion for mass parity of peaks

To sum up the situation, in the case of compounds containing zero (or even number of) nitrogen atom(s), the following statements, complementary to the mass criterion for molecular ion, can be made:

- An **odd-mass ion** is a closed-shell ion, which is:
  - not a molecular ion and
  - a **fragment ion produced by direct dissociation** of the parent excited molecular ion
- An **even-mass ion** is a radical ion and can be:
  - a **molecular ion** or
  - a **fragment ion** due to the decomposition **with rearrangement** of a heavier ion.

These statements will constitute the base of our methodology to deal with interpretation of mass spectra during hydrocarbon and oxygen containing monomer plasmas.

3.7 The electron energy spectrum

The last section of the present chapter introduces the electron energy spectrum (EES) of electron ionization. The EES is the record of the abundance of an ion while varying the primary electron energy. Several examples are visible on Figure 3.7. In solid symbols, the EES of the molecular ion of styrene, benzene and hydrogen are shown, with m/z = 104, 78 and 2 respectively. A simple measure of their IE is obtained at the crossing of their respective curves with the x axis at 40 c/s. It gives 8.8 eV for styrene (IE = 8.4 eV), 9.9 eV for benzene (IE = 9.2 eV) and 16.1 eV for hydrogen (IE = 15.4 eV). The shifts between these experimental values and the IE are not kinetic shifts (Section 3.4.1). Indeed the molecular ion requires no decomposition to be observed. Instead they are due to uncalibrated electron energy and to experimental errors, which will be established in Section 5.3.8.

In open symbol is the EES of the fragment ion at m/z = 78 of the styrene CP. This is the rearranged fragment ion discussed earlier (Section 3.6.1). The crossing of the curve with the x axis constitutes a simple measure of its appearance energy (AE) at around 11.4 eV. This time, being a fragment ion, a kinetic shift is present but cannot be evaluated. The uttermost interest of this measurement relies in the fact that the AE of this fragment ion of styrene (11.4 eV) appears 1.5 eV above the measured IE of benzene (9.9 eV).

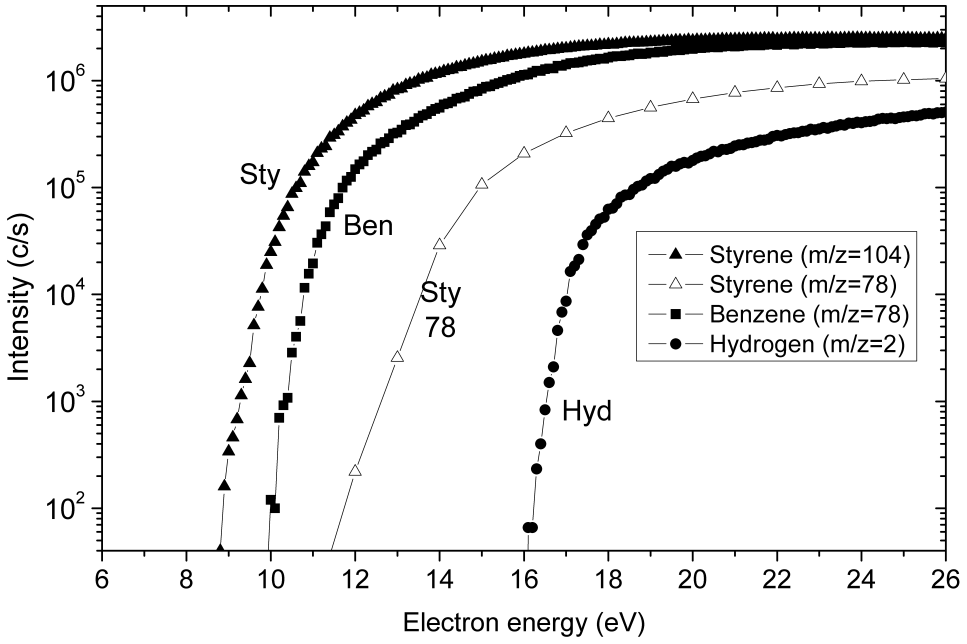

Figure 3.7: Electron energy spectra of m/z = 104 and 78 of a pure styrene vapor, of m/z = 78 of a pure benzene vapor and of m/z = 2 of pure hydrogen.

Said in other words, it is possible to **distinguish a molecular ion peak from a fragment ion peak** by measuring the appearance energy. This observation shows the interest of such measurement for an unknown mixture of hydrocarbons, like a hydrocarbon plasma. The detection of a peak at m/z = 78 in the mass spectrum of the mixture is not a guarantee of the presence of benzene, if peaks with higher masses are detected. Instead the measurement of a (calibrated) AE at m/z = 78 close to the IE of benzene constitutes a much stronger clue of benzene presence.

This approach is referred in the literature as Threshold Ionization Mass Spectrometry (TIMS). It will serve as a second criterion to confirm or rule out an even-mass peak as corresponding to a molecular ion in unsaturated hydrocarbon plasma (in Section 7.3.2).

Chapter 4

State of the art on styrene and MMA

4.1 Styrene plasma and plasma deposited styrene films

This section will start with a short bibliographic overview on the articles found on styrene plasma and/or on plasma deposited polystyrene (pPS) films (Section 4.1.1). Then the plasma-phase diagnostics of the styrene discharge will be screened first (Section 4.1.2), before reviewing the XPS characterization of the pPS films (Section 4.1.3). To finish, information brought by other characterization techniques on plasma polystyrene (pPS) will be summed up (Section 4.1.4), as well as the several mechanisms proposed for styrene polymerization (Section 4.1.5).

4.1.1 Bibliographic overview of styrene

Conventional PS has excellent properties of plasticity and of electric insulation. It is therefore used in preparation of various electronic devices and photo conductive thin films [104]. pPS films usually try to conserve these properties, while cross-linking and branching are looked at for higher resistance. Application as protective coating and corrosion resistance coating are reported [104–106], as well as resist for lithography [104], gate insulator [107, 108], ultrathin antireflective coatings [105], humidity sensor [109], optical biosensor [104] and increased biocompatibility surface [110].

In the literature, 45 peer-reviewed papers were found on the characterization of styrene plasma and/or on the surface analysis of pPS films. The first reports date back to 1966 and the last to 2014. The early papers are more oriented on the mechanisms of styrene plasma polymerization, which was actually one of the model system studied to understand plasma polymerization (Section 2.2), while applications dominate in the years 2000s.

From the characterization technique point of view, the following features are pointed out:

- Plasma diagnostics are seldom with only four Optical Emission Spectrometry (OES) and five Mass Spectrometry (MS) studies [62, 111–118].
- Chemical composition of the pPS film has extensively been studied as shows the 18 works using Infra-Red spectroscopy (IR) [21, 47, 59, 62, 104, 106, 112–115, 117, 119–125] and the 13 studies on X-ray Photoelectron Spectroscopy (XPS) [59, 62, 114, 117, 118, 121, 125–130].
- Five works reported on Secondary Ion Mass Spectrometry (SIMS) and Time-of-Flight SIMS [117, 118, 120, 127, 131].
- The Deposition Rate (DR) is often measured with 12 occurrences [47, 52, 53, 109, 115, 121, 123, 124, 129, 132–134].

Concerning power coupling, inductively coupled plasma (ICP) occupies less than a quarter of the studies, the remaining being capacitively coupled plasma (CCP). Our group is the only one to have reported on the styrene plasma polymerization in planar ICP [117, 118, 129, 130, 135].

Pulsation of styrene plasma is seldom investigated, with only 6 occurrences and not before 2001 [59, 117, 118, 128, 129, 131]. The group of Friedrich *et al.* showed the pulsation allowed to produce pPS films with composition and structure very close to conventional PS [59, 128, 131].

We concluded from this very short bibliographic overview that styrene plasma phase still needs further characterization, especially in a quantitative way. In contrast, XPS film characterizations are already well documented and have been helpful in the present work.

4.1.2 Diagnostics of styrene plasma

Table 4.1 summarized the styrene plasma diagnostics carried out by five groups. The column "comments" shows the coupling type (CCP/ICP) and if the system was with a continuous injection and pumping of styrene (flow) or with neither injection nor pumping (closed). In addition, the column exhibits the characterization method used: MS of neutral species and at which electron energy, MS of positive ion or OES.

Species in styrene plasma

The third column of Table 4.1 shows the neutral species detected. The excited species measured by OES are marked with a star "*", the radicals detected by MS with "•" and the stable closed-shell neutral with no sign. The species marked between brackets are not sufficiently

Authors	Comments	Neutral species	Indicators
Ferreiro *et al.* [111]	CCP – flow Neutral MS at 25 eV Positive MS	C_2H_2, C_2H_4, C_3H_4, C_6H_6, C_8H_6, C_8H_{10} and $C_{10}H_8$ ($C_7H_7^\bullet$)	
Ozden *et al.* [113]	CCP – closed Neutral MS at 70 eV	C_2H_4	
Chen *et al.* [114–116]	CCP – flow Neutral MS at 70 eV OES	C_2H_2, C_2H_4 (C_6H_6,$C_8H_7^\bullet$, $C_6H_5^\bullet$ and $C_4H_3^\bullet$) H*, H_2*, CH* by OES	From neutral MS: 78/104 = fragmentation
Beck *et al.* [62]	ICP – flow Neutral MS at 20 eV Positive MS	C_2H_2, C_2H_4, C_4H_2, $C_{10}H_8$ (C_6H_6)	From positive MS: $208^+/104^+$ = oligomerization $26^+/104^+$ = fragmentation
Li *et al.* [117, 118]	ICP – flow OES	H*, C*, CH*, C_2*, C_6H_6* by OES	

Table 4.1: Bibliographic summary for styrene plasma diagnostics.

proven in our opinion and experience of MS. For instance, the three radicals apparently detected by Chen *et al.* can most probably be due to the cracking patterns of heavier species.

The two neutral MS studies at 70 eV only revealed the stable closed shell species C_2H_4 for Ozden *et al.* and C_2H_2 and C_2H_4 for Chen *et al.* Lowering the electron energy at 25 an 20 eV revealed six additional neutral species: C_3H_4, C_4H_2, C_6H_6, C_8H_6, C_8*H_{10}* and $C_{10}H_8$. OES studies revealed six excited species: H*, C*, H_2*, CH*, C_2* and C_6H_6*. Concerning positive ions, many have been observed, with notably dimers for Beck and Ferreiro and trimers for Ferreiro only. No negative ions are reported.

Indicators for styrene plasma

The last column of Table 4.1 revealed indicators proposed to evaluate the state of the discharge:

- Chen *et al.* proposed the signal ratio of the peak at m/z = 78 to the one at 104 as an indicator of the monomer fragmentation. However, in our opinion, it is a delicate choice due to the large signal at m/z = 78 already present in the styrene cracking pattern.
- Beck *et al.* proposed two indicators from the positive ion mass spectrum: $208^+/104^+$ as oligomerization degree and $26^+/104^+$ as fragmentation degree. The first was observed to decrease with power and the second to increase with power.

Mechanisms in styrene plasma

In the styrene plasma of Beck *et al.* at low W/F, the two most intense ion signals are the one of the monomer with around 110 kc/s, followed by the one of the dimer with 40 kc/s. It was concluded they were the ions with the highest concentrations in the plasma. However no neutral dimer could be detected in the discharge. Therefore, the dimer ion was proposed to be produced by the recombination of a monomer ion with a neutral monomer. The ionization of a neutral dimer was logically excluded.

Additionally, due to the supposed high-concentration of monomer and dimer ions, Beck *et al.* proposed several schemes for their decomposition in the plasma, inspired by the theory of the unimolecular ion decomposition presented in Chapter 3. The proposed decompositions lead to the production of several of the observed neutral and ions. However, we must mention that the unimolecular decomposition theory applies at pressure below 10^{-2} Pa [87], well below the pressure of 1 Pa used in the work.

4.1.3 Surface characterization of pPS by XPS

We propose here to first describe the XPS spectrum of conventional PS and explain its features. Then we will resume the information extracted from the XPS spectrum of plasma deposited PS. The objective is to identify guides to decompose the pPS XPS spectra we acquired.

Conventional PS by XPS

The general photoelectron spectrum of conventional PS is shown on figure 4.1a. As a pure carbon and hydrogen containing polymer, PS only reveals one main peak at the carbon 1s binding energy (BE) around 285 eV. Figure 4.1b shows the same spectrum but at high resolution zoomed on the C1s peak. This so-called "C1s spectrum"is fitted with two components: an aliphatic component settled at 285.00 eV and an aromatic component with a chemical shift of -0.22 eV. This latter is justified by ab initio calculations which indicates a 0.2 eV shift [24]. It is also supported by the shift of 0.31 eV observed between gas phase C1s BE of benzene and methane [25]. Besides, an additional peak around 291 eV is observed. This peak toward higher BE comes from the energy loss of the photoelectron due to electronic excitation of unsaturated and/or aromatic Ï€ bond (valence electron). It occurs for electrons emitted from one of the 6 ring carbon atoms and to a lesser extent from the first neighbor carbon atom. The peak is commonly called "$\pi \rightarrow \pi^*$ shake-up"satellite peak. By comparison with gas phase C1s shake-up structure of benzene,

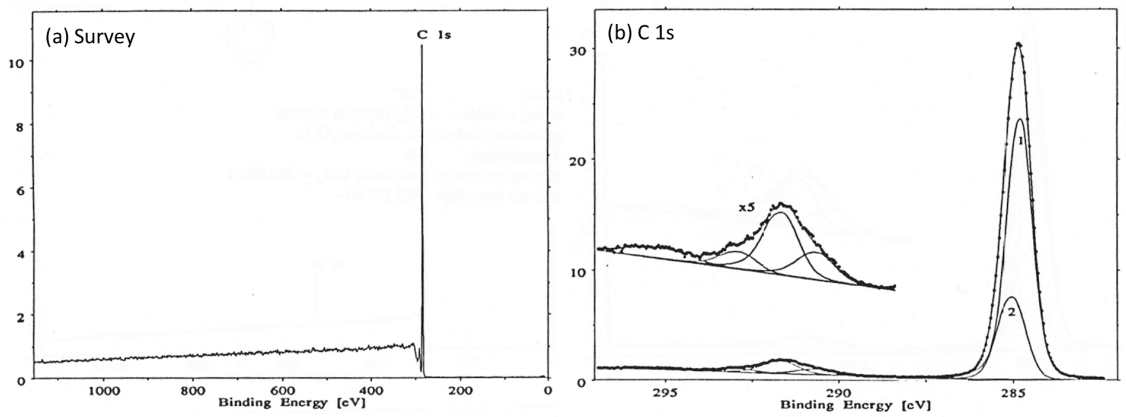

Figure 4.1: XPS spectra of conventional PS: (a) general survey and (b) high-resolution C1s region (from [136]).

	Beamson & Briggs [137]	Beamson [136]	Petrat [138]	Prohaska [121]	Haidopoulos [135]	Swaraj thesis [139]	Retzko [59]
Shake-up/C1s	10%	9%		7.9%			
Shake-up/total C1s	9%	8%	7.5%	7.3%	7.5%	7.1%	9.5%
Background	Linear	Seems linear	Shirley	-	Shirley	Seems Shirley	-

Table 4.2: Measured shake-up areas of conventional PS as measured by several workers, in addition with their choice of background, their method used to create the polymer thin film.

Beamson & Briggs fitted it with four components for PS. However they recommend in general the use of the minimum number of components required to obtain a reasonable fit, without necessarily physical meaning [25]. Their summed area of the shake-up components valued 10% of the main C1s core-line envelope.

Several workers measured the shake-up peak area and their results are shown in Table 4.2 [59, 121, 135–139]. Several points are outlined here.

- The relative shake-up area is either divided by the whole C1s surface area – including the shake-up itself – or just the C1s main peak area - excluding the shake-up. The first area will be referred here as "total C1s" and the second as "C1s". We chose the first one in the present work.
- Another observation is the measure of different values for the relative shake-up area. The two mainly used backgrounds as lower bound of the peak area may explain a large part of the difference. The used backgrounds were indicated in the fourth row of Table 4.2. Linear

Authors	Exposure time to air (ETA)	Oxygen uptake (at%)	Aromaticity retention
Prohaska *et al.*	Short ex-situ	<0.5%	42 – 72%
[121]	2 weeks	up to 10%	
Retzko *et al.*	In-situ or short ex-situ	<0.5%	75%
[59]	1 month	up to 4%	43%
Swaraj thesis	In-situ	≈ 1%	54 – 90%
[139]	3 months	3 – 16%	17 – 51%
Haidopoulos *et al.*	15 min	≤ 1%	≈ 88%
[135]	1 week	5 – 7%	≈ 62%

Table 4.3: Summary of results from XPS characterization of pPS. The aromaticity retention has been calculated from the specified shake-up relative area measured for conventional PS and pPS films.

background would lead to higher values of the relative shake-up area (8–9%), than for the Shirley one (7.1–7.5%).

- The relative shake-up area may serve as an aromaticity retention indicator because its signal was observed to be linearly decreasing with increasing alkane chain length in alkane-styrene copolymers [140].

Plasma PS by XPS

Among 13 works reporting on XPS characterization of pPS, four were selected and their results are summarized in Table 4.3. For each work, two rows are used as the film characterizations were done at two different exposure times to air (ETA) of the pPS samples (second column).

The second column of the table is the **exposure time to air** (ETA) of the pPS samples. It reveals a strong effect on the film composition. It can be seen from the third column, which is the range of **oxygen uptake** in the same pPS samples, in atomic percentage. It was measured via the oxygen 1s peak observed in the general photoelectron spectrum of the pPS. Clearly the oxygen content increases from less than 1% for in-situ measurement or short exposition to air, up to values ranging from 3 to 16% depending on the plasma conditions and on the ETA. Furthermore, the increase was generally observed to be fast in the first 24h and then progressively saturates.

The last column of Table 4.3 shows the **aromaticity retention** of the pPS. It was calculated from the reported values of the relative shake-up area divided by the same area but for conventional PS film deposited and characterized in each study. It seems the best method to compare the measured aromaticity, as each study has a different shake-up area for their conventional PS. Globally, the aromaticity retention can be as low as 17% and reaches values up to 90%. The exposure to air damages the aromaticity which is always observed to decrease with ETA. Aromaticity is then anti-correlated to the oxygen uptake.

The oxygen uptake and its increase with ETA is generally explained by the presence of a significant concentration of trapped radicals in plasma polymers [3]. For styrene, trapped radical has been measured by Electron Spin Resonance (ESR) and IR [113].

When measured, all the works observed that a hardening of the plasma conditions (higher power, lower flow) results in a larger oxygen uptake and a decrease of the aromaticity retention. It confirms their anti-correlation observed for increasing ETA.

The incorporation of oxygen in the pPS is also detectable via the appearance of new components in the C1s spectrum of the plasma polymers. A component is generally used at $\approx$ 286.5 eV of binding energy that is assigned to alcohol and/or ether groups (C-O). More rarely, for the highest oxygen uptake, a second component has been added at $\approx$ 287.6 eV, assignable to aldehyde/ketone groups (C=O). Concerning the main part of the C1s peak, a single component is generally used at $\approx$ 285.00 eV instead of the double component aliphatic/aromatic used by Beamson and Briggs. The double component seems delicate to carry out and is subject to large fitting errors [139]. This is mainly due to the fact that the components undergo significant peak broadening compared with conventional PS. The peak FWHMs of the pPS films generally ranges from 1.4 to 1.7 eV [130, 139], which is much larger than the 0.9 to 1.3 eV range of conventional PS.

Conclusions for XPS characterization

We draw here the main conclusions to guide our C1s fit. As our samples were generally exposed half a day before introduction to XPS spectrometer, we expect an oxygen uptake and a significant loss of aromaticity. We will use at least a C-O component as done by several workers and also a C=O component when necessary. Large FWHM are expected between 1.3-1.7 eV, generally attributed to a higher chemical environment diversity compared with conventional PS and then a larger range of possible chemical shift [141]. The imposition of aromatic and aliphatic

components won't be done as it is delicate and as the shake-up area is a sufficient aromaticity retention indicator.

4.1.4 Characterization of pPS by different techniques

Besides XPS characterization, we present briefly here other selected characterizations giving insight on the plasma deposited styrene films.

Crosslinking was stated by several workers because pPS were insoluble [47, 52, 113, 120]. In particular, Ozden *et al.* observed insolubility in more than 4 solvents: benzene, toluene, chloroform, CCl_4 [113]... Denaro measured a simultaneous oxygen uptake and a loss of solubility with aging [47]. The ToF-SIMS characterization of Oran *et al.* shows an increase of the branching and crosslinking with an increasing effective power [131, 142].

Methyl functions (CH_3) were detected by Infrared Spectroscopy (IR) in many studies [59, 119, 121, 122, 135]. The methyl substitution was less intense for pulsed plasma polymerized styrene films [59]. This methyl substitution was set aside by Legget by Secondary Ion Mass Spectrometry (SIMS) [127], but it could be due to the large difference of sampling depth between the two techniques: SIMS depth < 3 nm and IR is a bulk characterization [135].

Prohaska investigated the effect of the **substrate temperature** in 1984, varied from 20 to 180°C, around moderately hard conditions at $7.1 \cdot 10^7$ J/kg (77 eV/styrene) [121]. The deposition rate linearly diminishes with the temperature with two slopes. It is different from the observations of Yasuda & Wang in 1985 [53], who showed a decreasing exponential behavior from -60 to +75°C. Their measurements were done under very hard conditions at $17.6 \cdot 10^7$ J/kg (209 eV/styrene). However, the two reactor geometries are substantially different: ICP for Prohaska and CCP for Yasuda, which usually requires higher power to reach similar electron densities [53].

Prohaska is the only one to have significantly investigated the **styrene flow rate** effect [121]. Its observations are consistent with the general trends established by Yasuda & Hirotsu in 1978 for other monomers for increasing flow [73]: the **DR** shows an initial increase, then saturates and finally decreases at higher flows.

Aromaticity retention measured by XPS was correlated in some work by other characterization techniques. For instance, Retzko *et al.* measured a retention of 74% by XPS, confirmed by IR and NEXAFS with >75% retention [59]. Similarly, Prohaska *et al.* confirmed its XPS-measured aromaticity loss by IR [121]. Oran *et al.* observed an aromaticity decrease

with effective power by ToF-SIMS [131, 142], confirming the one measured by XPS in the same group by Swaraj *et al.* [128, 139].

Concerning the **oxygen uptake**, it was also confirmed by ToF-SIMS [131, 142] and by many IR studies.

4.1.5 Styrene polymerization mechanisms

Finally, the different proposed mechanisms of styrene plasma polymer production are reviewed in the present section.

Thompson investigated in 1972 the initial step of plasma polymerization with two original measurements [120]. Firstly, he added nitrogen dioxide in the styrene discharge to work as a radical scavenger. As it did not affect the polymerization rate, he excluded a radical initiation step. Secondly, the application of an additional DC potential to the plasma region hinted at a cationic initiation. However, Thompson's conditions were estimated extremely hard around $1 \cdot 10^9$ J/kg (around 1500 eV/styrene!) due to the very low stated flow: 0.061 g/h equivalent to 0.2 sccm.

Many workers favored **radical polymerization mechanisms** for styrene: Yasuda from 1971 [52] to 1985 [3], Prohaska in 1984 [121], Ozden in 1991 [113] and the Friedrich's group [59, 60, 128, 131]. For the latter group, they studied pulsed styrene plasma under very mild conditions: Retzko conditions were around $2 \cdot 10^6$ J/kg [59] and Friedrich conditions were around $0.2 \cdot 10^6$ J/kg (if the mentioned flow of 7 L/h is correct) [60]. They motivated a radical chain grafting polymerization mechanism by the observation of a very high polymerization rate during the plasma off time. Swaraj mentioned it applied to their mildest conditions, but not anymore at higher effective power [128].

Concerning the **location of the polymerization**, different conclusions were established for styrene. On one hand, the capacitive discharges with powered electrodes favored the observation of surface initiated mechanisms due to electron and ion bombardment [47, 132]. On the other hand, electrodeless and/or inductive plasma enhanced gas-phase polymerization mechanisms [52]. However, promotion of surface mechanisms or plasma-phase polymerization generally depends on the conditions. For instance, in our inductive system, Haidopoulos *et al.* deposited pPS on stainless steel substrates with a constant bias of +25 V DC [130]. The film morphology observed by SEM in that case showed that nucleation and growth started on the substrate defects, probably due to electron or negative ion bombardment.

4.2 MMA plasma and plasma deposited MMA films

Usually known as Plexiglass®, conventional poly(methyl methacrylate) or PMMA is appreciated for its optical clarity and UV resistance [117, 126]. However, in its unmodified form, this material is brittle. Therefore it often requires modification with comonomers or additives, for its numerous applications, as glass substitute for instance. As surface coating, PMMA has been used for intraocular lenses [143], biosensors [144], drug delivery systems [145], photosensitive and lithography material [146] or as gate dielectric for organic transistor [147].

The widespread use of conventional PMMA (cPMMA) may explain why plasma deposited PMMA (pPMMA) is among the first studied plasma polymers and why so many usages are reported. In photonics, pPMMA is applied as variable and graded refractive index [148], as waveguides [149], as wavelength transformer for solar cells or as gain medium for tunable solid-state dye lasers [150]. In photosensitive applications, lithography and thin films deposition, it has the advantages of PMMA, but with a higher purity and a better compatibility with other dry processing steps [146, 151]. In electronics, its higher dielectric constant than cPMMA made it useful as gate dielectric and its better linear response to humidity as humidity/moisture sensor [147, 152–154]. Finally, transparent protective coating for paints in automobile industry [155], enhanced bonding interface between nanoparticles and their matrix [156], membrane for gas separation and biomedical implants are also noted [157, 158].

4.2.1 Conventional PMMA and XPS characterization

The formation of cPMMA proceeds through the polymerization of its monomer, methyl methacrylate (MMA) [42]. From their structures on Figure 4.2, it can easily be seen that the polymerization can be carried out via the carbon double bond of the monomer, with a radical mechanism for instance. Pendant side groups from each side of the cPMMA backbone are the methyl function CH_3 (15 amu) and the methyl ester function $COOCH_3$ (59 amu).

The PMMA stoichiometry can be measured by XPS. Louette *et al.* reported 27.3 at% of oxygen, as compared to the theoretical 28.6 at% value [159]. The high resolution spectra of C1s is decomposed with four components due to the four carbon environments: C-C, β-shifted C-CO_2, C-O and O-C=O. Their respective measured positions and peak widths are shown in the four last columns of Table 4.4 [137, 159]. The systematic higher widths of Louette *et al.* are due to a lower energy resolution of the spectrometer. In both reference, the measured relative surface areas, using linear backgroung, show slight difference with the theoretical ones. The O1s

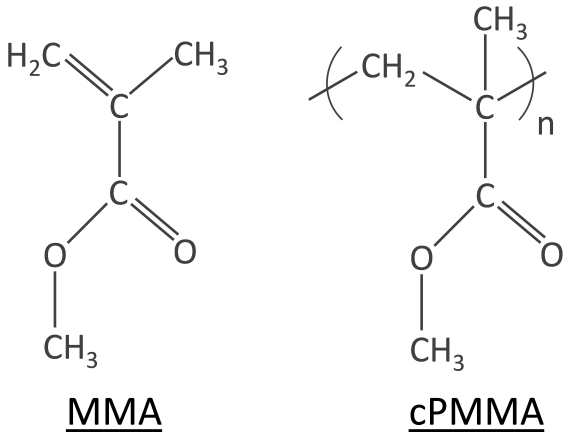

Figure 4.2: Chemical structure of the MMA monomer and the conventional PMMA polymer.

Components	Relative surface areas (%)			Position (eV)		Widths (eV)	
	Theory	Beamson	Louette	Beamson	Louette	Beamson	Louette
C-C	40	42	44	285.00	285.00	1.15	1.30
C-COO	20	21	20	+0.72	+0.84	1.06	1.30
C-O	20	21	18	+1.79	+1.81	1.28	1.30
O-C=O	20	17	18	+4.03	+4.00	0.99	1.21
O=C	50	51	49	532.21	532.28	1.27	1.40
C-O-C	50	49	51	+1.56	+1.51	1.39	1.57

Table 4.4: Relative surface areas, peaks positions and peak widths for the decomposition of the C1S and O1s high resolution spectra of conventional PMMA by XPS [137, 159].

high resolution spectra are decomposed with two components: O=C and C-O-C. The measured values of relative surface area, peak positions and peak widths are given in the two last rows of Table 4.4.

4.2.2 Surface characterization of pPMMA

Several characterizations of the pPMMA films are now described with the following order: deposition rate, chemical composition, structure and morphology.

Deposition rate of pPMMA

Usually, research groups measured either the deposition rate, DR (in nm/min), or the mass deposition rate, MDR (n g/cm^2.s). When measured as MDR (μg/cm^2.min), the DR was calculated from the usual glassy PMMA specific weight of 1.18 g/cm^3, when having no other indication.

The DR is generally rather low for plasma deposited MMA, between 1 and 20 nm/min [77, 146, 152, 153, 155, 160]. However two groups succeed to reach much higher values by increasing the initial pressure in their flow system [148, 151, 161, 162]. Fort the Short *et al.* group, 50 nm/min was reached on their grounded electrode and 200 nm/min on their powered electrode. For Morita *et al.*, 70 nm/min was reached on the supposed powered electrodes in RF field. 150 nm/min was achieved with the same system but at much lower applied field frequency, at which electron bombardment is enhanced.

Besides, the DR was generally observed to increase with W/F in MMA flow system [148, 160]. In closed system, higher power accelerates all reaction rates, resulting in an earlier appearance of the DR maximum with time and in higher maximal values [146].

Finally, the DR has been inversely correlated to plasma-phase dimerization, measured by MS as the dimer ion intensity over the monomer ion intensity ratio [160]. It was also simultaneously partially correlated with the MMA fragmentation, measured by MS as the ratio of the small ions intensity to the monomer ion intensity [160].

Chemical characterization of pPMMA

Qualitative retention of the initial monomer structure is a usual study in many works [77, 113, 117, 150, 152, 161, 163, 164]. Its evaluation is generally made by IR, XPS and SIMS (developed in the next section), while some works quantified more specifically the content of O and of the characteristic ester function (O-C=O) by XPS [150, 163, 164].

The theoretical value of **oxygen concentration** in cPMMA is 28.6 at%. Measured by XPS, pPMMA usually contains less oxygen, from 14 to 28 at% depending on the conditions and the reports [77, 150, 163, 164]. These values, when expressed as a percentage of the theoretical value of 28.6 at%, give an oxygen retention from 50% to 99%, as summed up in the second row of Table 8.1. The best retention value of 99% has been achieved at the very low W/F of 3 eV/MMA in a capacitive continuous-wave MMA plasma [77]. Other studies reported 80% of retention at 67 eV/MMA [163] and 79% at 42 eV/MMA [150].

Component	Theoretical cPMMA	pPMMA	Relative retention
Oxygen content	28.6 at%	14 – 28 at%	50 – 99%
Ester content (O-C=O)	20%	4 – 12%	20 – 60%
Ether/carbonyl content (C=O/O-C-O)	0%	4 – 7%	

Table 4.5: XPS measure of oxygen content, ester/carboxyl content and ether/carbonyl content in the pPMMA. Retention as compared to theoretical content in cPMMA, when relevant.

The C1s high resolution XPS spectra show the appearance of a C=O / O-C-O (carbonyl/ether) component that is not contained in cPMMA. Its relative surface contribution to the C1s peak can reach 7% [164]. Concerning the carboxyl/ester component O-C=O already present in the cPMMA, its theoretical contribution to the total C1s area of cPMMA is 20%. For the plasma polymer, the carboxyl/ester retention can be varied from 60% down to 20% as summarized in the third row of Table 8.1 [163, 164].

Unsaturation has been detected in several works. FTIR absorption lines assigned to C=C and C≡C were detected [151, 161, 164]. They are intense for the pPMMA collected on powered electrode and much lighter on the grounded electrode. pPMMA revealed photoluminescence properties, which are usually due to unsaturated bonds which can form conjugated-bond chromophores [150]. Raman Spectroscopy showed a R-C=C-R absorption line [77]. Finally ToF-SIMS positive spectrum revealed peaks characteristic of material containing aromaticity [164], but it will be discussed in more details below.

Diversity in chemical and structural environment was usually observed, as indicated by XPS, FTIR, NMR and photoluminescence, which all revealed peak broadening [117, 150, 157, 161, 163].

Structural characterization of pPMMA

As far as we know, only two works reported on the pPMMA characterization by Secondary Ion Mass Spectrometry (SIMS) [163, 164].

The research focused on secondary ion fragments assigned either to main polymer chain fragments (shortly “backbone fragments”) or to fragments originating from end group of the polymer chain or of pendant side chains (referred more shortly as “chain/side end groups”) [164].

When compared to cPMMA, pPMMA usually shows an increase of the main/side end group peaks and a decrease of the backbone fragments. This may indicate a higher concentration of end groups at the surface, showing a lower molecular weight (shorter chains) [145, 165, 166]. It could also indicate a higher degree of branching [164]. Both interpretations are supported by the oily appearance of the deposit, which indicates short chains and low crosslinking.

The increase of the W/F ratio from 14 to 210 eV/MMA revealed a decrease in the backbone fragments signals and an increase of the main/side end group intensities. It indicates an increase of the branching and/or that chains shorten.

From the positive spectra, several characteristic peaks of material containing aromaticity are detected [164]. However they also appear in unsaturated material or even in saturated material at high ion dose, which may be the case in the study (ion dose kept below 10^{13} ions/cm^2). When the W/F ratio is increased, the three peak intensities increase, indicating either an aromaticity increase or an unsaturation increase. Complementary IR measurements on the samples showed that aromaticity was below detection limit at low W/F and in small amount at high W/F [166]. Therefore the ion dose excess is finally considered as better explaining the presence of the three peaks.

Morphology of pPMMA

Deposited on Si substrate with roughness below 0.1 nm, pPMMA samples were studied by AFM [162]. Compared to the spin-coated PMMA roughness of 1.5 nm, pPMMA has a very small one, usually less than 0.5 nm. Moreover the pPMMA showed a better overall planarity at the tens of micron scale, with rare defects [162].

Proposed mechanisms for pPMMA formation

An original proposition arose from the work of Casserly *et al.* [77]. As simplification, the oxygen loss was considered to be carried out in two ways, assuming the same backbone structure of the pPMMA as the one of cPMMA. **Mechanism n°1** is the loss of the methoxy group by scission of the C-OCH_3 bond, like on Figure 4.3a. A loss of 10% of oxygen gives then a functional loss of 10%. **Mechanism n°2** is the loss of the complete methyl ester functionality by the cleavage of the C-$COOCH_3$ bond, as shown on Figure 4.3b. A loss of 10% of oxygen would then lead to a functionality loss of 5% as the function contains 2 oxygen atoms.

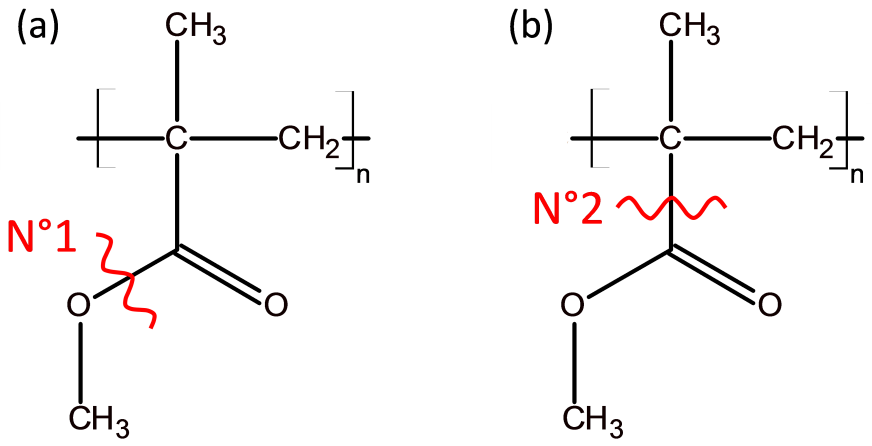

Figure 4.3: Functionality loss pathways for PMMA.

In this model, only the products of the MMA dissociation which contains the double carbon bond are assumed to participate to the polymerization process. These species are dimethylketene (DMK), allene (C_3H_4) and propene (C_3H_6), for instance, and will be discussed later on in Figure 4.4 and 4.5. However, it is well established that non polymerizing gases, like N_2 and more particularly CO, CO_2, can polymerize by plasma when injected with a polymer-forming gas, like a hydrocarbon monomer vapor [71] (see Section 6.5). Nevertheless their relative simplicity, the two mechanisms were worth mentioning.

4.2.3 Diagnostic of MMA plasma

Plasma diagnostic and detected species

Several works report on species identification in MMA plasma [113, 117, 146, 160, 161, 167–169]. The detection were carried out either ex-situ on product gases condensed on a nitrogen trap during the plasma [167, 168] or for the others directly in-situ. The used characterization techniques were different and complementary: Nuclear Magnetic Resonance (NMR) [167], Gas Chromatography coupled with Mass Spectrometry (GC/MS) [168], Fourier Transform Infrared Spectroscopy (FTIR) [161, 169], Optical Emission Spectroscopy (OES) [117] and Mass Spectrometry (MS) [113, 146, 160]. Interestingly, three studies focused on closed systems [113, 146, 169], the others being on conventional flow systems. The interest of closed systems is their known value of starting molecules, a conservation of mass in the reactor (nothing is pumped away) and an easier evaluation of the reaction rates when quantifying the product partial pressures [169]. It also allows one to determine the final stable products of reaction.

Species	Formula	Mass	Detection technique	Comment
Hydrogen	H_2	2	In situ MS [113, 146]	
Methane	CH_4	16	In situ FTIR [161] In situ MS [146]	
Water	H_2O	18	In situ OES [117]	Weak intensity
Acetylene	C_2H_2	26	In situ FTIR [161]	
Ethylene	C_2H_4	28	Ex situ NMR [167] In situ FTIR [113, 161] In situ MS [113]	
Carbon monoxide	CO	28	In situ FTIR [161] In situ MS [113] In situ OES [117]	
Ethane	C_2H_6	30	In situ MS [146]	Assignment?
Formaldehyde	CH_2O	30	In situ FTIR [161] Ex situ NMR [167]	
Oxygen	O_2	32	In situ OES [117]	Weak intensity
Methanol	CH_4O	32	In situ FTIR [161]	
Allene	C_3H_4	40	In situ FTIR [161]	Propadiene (not propyne)
Propene	C_3H_6	42	In situ FTIR [161]	
Propane	C_3H_8	44	In situ MS [146]	Assignment?
Carbon dioxide	CO_2	44	In situ FTIR [161] In situ MS [113] Ex situ NMR [167]	
Butene	C_4H_8	56	Ex situ GC/MS [168]	
Butane/isobutane(L)	C_4H_{10}	58	Ex situ GC/MS [168]	
DMK	C_4H_6O	70	In situ FTIR [161] Ex situ NMR [167] Ex situ GC/MS [168]	
Pentane/isopentane	C_5H_{12}	72	Ex situ GC/MS [168]	
Methyl Isobutyrate	$C_5H_{10}O_2$	102	Ex situ GC/MS [168]	CAS 547-63-7
Methyl Isopentanoate	$C_6H_{12}O_2$	116	Ex situ GC/MS [168]	CAS 556-24-1

Table 4.6: List of neutral closed shell species reported in MMA plasma. The comment "Weak intensity" indicates an OES detection with low signal. The comment "Assignment?" indicates a conflict with other possible assignments which was not considered in the reference.

Only reported in closed system, the total pressure in discharge was always observed to increase when specified [113, 146, 169]. It indicates a **significant production of**

non-depositing species in the MMA plasma phase. For Orhan *et al.* who observed no film deposition, this indicates that MMA belongs to the class B of monomers of Yasuda [63] (see Section 2.6), for which decomposition dominates [113]. In contrast, with the same closed system, styrene was observed to lead to large deposition and a total pressure drop. It belongs to class A monomers, known to lead to polymer formation.

Twenty neutral closed shell species were reported and are resumed in Table 4.6. Propane C_3H_8 (m/z = 44) and ethane C_2H_6 (m/z = 30) were suggested in one characterization by MS [146], without considering the possible production of CO_2 (m/z = 44) and formaldehyde CH_2O (m/z = 30), observed in several other studies. It explains the comment "Assignment?" in the table. It is worth mentioning that all MS studies were carried out at 70 or 80 eV. Among the neutral radicals, six were as well observed: $H^{\bullet}$*, $C^{\bullet}$*, $O^{\bullet}$*, $CH^{\bullet}$* by the unique OES study [117] and $[MMA+H]^{\bullet}$ and $[MMA+3H]^{\bullet}$ by MS [160]. Positive ions were also detected with a MS spectrometer directly in contact with the plasma [146, 160]. Small ions dominated, but high molecular weight ions were observed well above the MMA mass at low W/F. For one of the ion studies, the negative ions were mentioned to be under the detection limit, while they could be detected in the same system with a Freon discharge [160].

Mechanisms in MMA plasma

Reviewing the MMA plasma reactions, Pan *et al.* proposed two main dissociation pathways for MMA [169]. The first is the C-O bond cleavage with H rearrangement between the two dissociation products, as shown on Figure 4.4. It leads to formation of dimethylketene (DMK) with m/z = 70 and formaldehyde with m/z = 30.

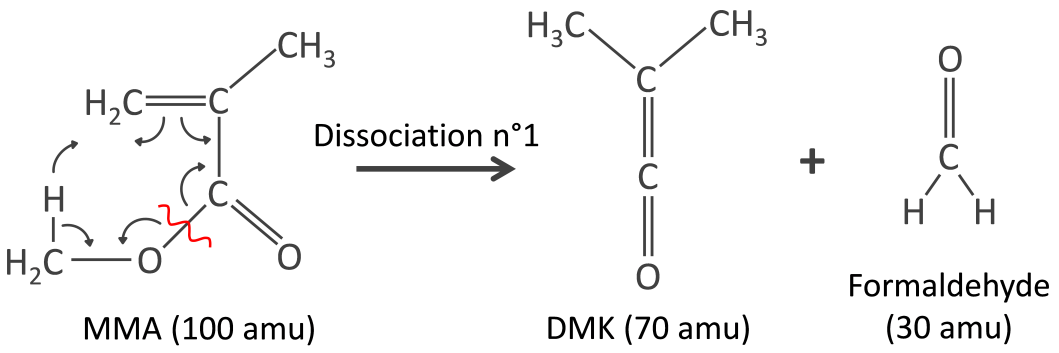

Figure 4.4: Dissociation pathway of MMA n°1, with atomic mass in amu indicated between bracket.

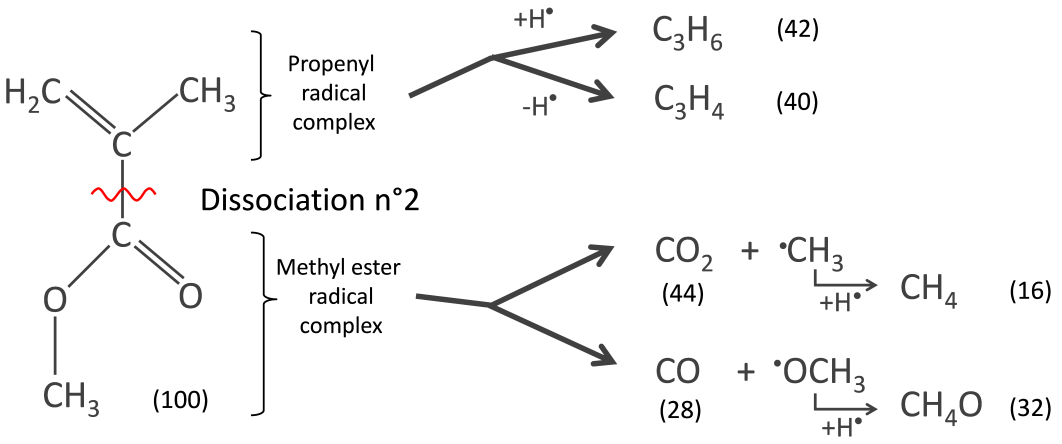

Figure 4.5: Dissociation pathway of MMA n°2, decarboxylation, with atomic mass in amu indicated between bracket.

The second main reaction is referred as decarboxylation [168]. It is the cleavage of the C-C bond between the methyl ester function $COOCH_3$ and the propenyl function C_3H_5, as shown on Figure 4.5. The propenyl radical can either gain or loss a H atom to the methyl ester function during the dissociation. It thus produces allene C_3H_4 or propene C_3H_6 (top two products on Figure 4.5). Concerning the methyl ester group, it is further dissociated to produce either a CO_2/CH_4 couple with H gain or a CO/CH_4O with H gain as well. The CO/CH_2O couple with H loss was not considered in the study [161]. Formaldehyde CH_2O was indeed not detected in plasma ignited in pure methanol CH_4O, while the methoxy radical $CH_3O^\bullet$ is likely produced in there [169].

The two pathways are interesting as they correspond to the previously mentioned functionality loss mechanisms of the pPMMA (see Figure 4.3). The MMA dissociation n°1 with production of DMK and formaldehyde corresponds to mechanism n°1 of methoxy group loss. The MMA dissociation n°2, which is the decarboxylation of MMA, with production of CO_2 and CO, is linked to the loss of the functional methyl ester group, or mechanism n°2.

A third mechanism in MMA plasma have been proposed by O'Toole *et al.* [160]. Indeed, monomeric and dimeric positive ions of MMA, $(M+H)^+$, $(M+3H)^+$, $(2M+H)^+$ and $(2M+3H)^+$, were detected in large amount in the MMA plasma at low W/F. For the same conditions, almost no neutral dimers were observed on the contrary of other monomers. It is concluded that dimerization is mainly conducted via monomer neutral – monomer ion collisions. This is one of the observation which leads the group of Short *et al.* to assume ion dominated polymerization mechanism at low W/F regime [27, 160] (Section XXX).

Quantification of MMA plasmas

Pan *et al.* determined the partial pressures of 8 neutral species in their closed system [169]. Considering the above mentioned dissociation pathways of MMA, n°1 and 2, they estimated their respective reaction rate. The C-O bond cleavage accounts between 41 and 54% of MMA dissociation, depending on conditions. On the other hand, under the same set of conditions, MMA yields 17-22% of propene and 7-8% of methanol, two decarboxylation products of MMA. The combined yield of propene and allene are expected to account to the total decarboxylation efficiency, but it could not be estimated for allene. The yield of CO and CO_2 were not used for it because they are decomposition products of other intermediates like DMK or formaldehyde. It was confirmed by their continuous increase with time during the discharge. This continuous increase was also observed in the two other studies with closed system (if mass 44 is assigned to CO_2 and mass 28 to CO in Zeuner *et al.* work) [113, 146]. It confirms they can be considered as final products of MMA discharge. On the contrary, partial pressures of all the other species showed a maximum value with time, indicating either further decomposition in plasma or deposition on the surrounding walls.

Chapter 5

Experimental setup and techniques

The present chapter will start with the description of the plasma reactor used to carry out the plasma polymerization process and the experimental method for measuring the flow of liquid precursor. Then the gas-phase mass spectrometer used to characterize plasma will be detailed. Finally, the surface characterization by X-Ray Photoelectron Spectroscopy (XPS) will be depicted, as well as the two spectrometers based on this technique used in the present study.

5.1 The plasma reactor

The plasma deposition system is composed of four major elements: the vacuum chamber (5.1.1), the injection system (Section 5.1.2), the plasma source (Section 5.1.3) and the substrate holder (Section 5.1.4).

5.1.1 The vacuum chamber

The vacuum chamber of the used reactor is a vertical cylinder made of stainless steel with 28 cm internal diameter (Figure 5.1 and Figure 5.2). The pumping is ensured by a primary pump via two collecting pipes symmetrically arranged at the cylinder bottom (see (1) on Figure 5.1). During deposition, a nitrogen cold trap precedes the pump and collects most of the monomer and condensable effluent gases of the process. This protects the oil pump from degrading from these exhaust molecules. The combined pumping reaches a vacuum pressure of 0.3 Pa. Beyond the deposition process, a turbo-molecular pump is used to lower the reactor pressure in order to limit the water and pump oil vapor contamination.

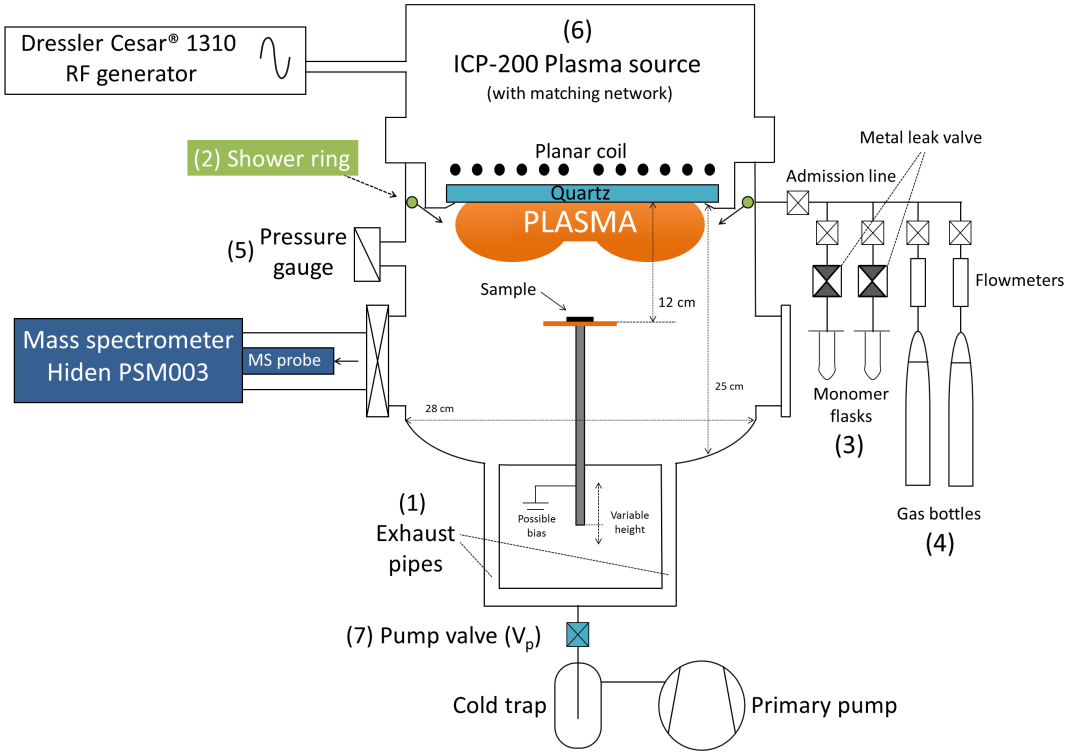

Figure 5.1: Schematic drawing of the plasma reactor.

5.1.2 The injection and pumping system

The gas injection system allows a symmetrical gas distribution via a "**shower ring**" (see (2) on Figure 5.1 and green part on Figure 5.2), which consists of a ring-shaped hollow pipe placed at the top of the chamber, just below the plasma source. Its 24 injection holes of 1 mm diameter are drilled on the pipe inside and are regularly spaced. Combined with the two pumping exists at the bottom of the reactor, this allows a symmetrical gas flow from the top to the bottom.

Upstream of the shower ring, two kinds of gases can be injected, either from a pressurized bottle or from an evaporated liquid precursor in a flask (see (3) and (4) on Figure 5.1).

- The flow of the **bottle gases** is settled via controlled flowmeters (MKS Multi Gas Controller 647c and MKS Mass-Flo®). Once the desired flow is established, the target pressure can be adjusted by adjusting a throttle valve, called "pump valve" (7), leading to the nitrogen cold trap.
- In contrast, the flow of **gases evaporated from a liquid precursor** is not automatically regulated. Indeed, the vapor diffuses towards the chamber thanks to the pressure difference through a mechanical leak valve (Varian® Leak Valve - Sapphire and copper gasket). As the evaporation process requires energy, the liquid cools down at its surface. The decrease

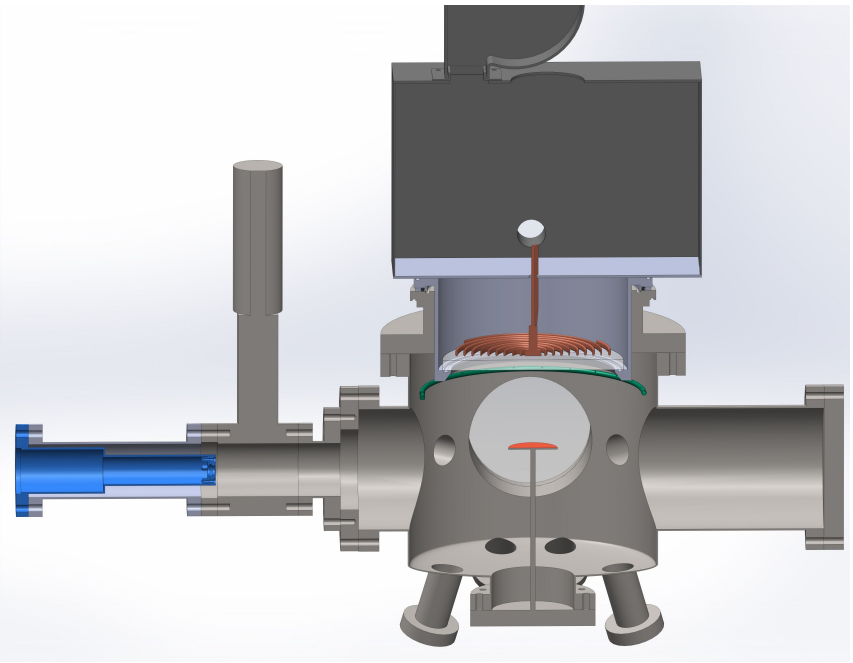

Figure 5.2: Reactor design drawn on Solidworks®. The blue part is the mass spectrometer described in section 5.3 used in the present study and protected by a valve. The collecting aperture of the spectrometer is located at 35 cm from the substrate holder.

in temperature slows down the evaporation rate and so the vapor pressure decreases in the flask. In turn, the injection is then lowered and requires an increase of the leak valve opening to keep the same flow and thus the same pressure in the reactor. The equilibrium often takes several minutes to be reached (further discussed in Section 8.2.2). Depending on the precursor, the temperature of the flask usually decreases of around 10°C for a flow of 28 sccm. To avoid any condensation of the evaporated liquid precursor along the admission line, the latter is heated at around 80°C, as well as the leak valve [148].

The **pumping system** is composed of a rotary vane pump (Pfeiffer® DUO 10MC, 10 m^3/h) protected upstream by a nitrogen cold trap. Despite this protection, the oil pump has to be regularly changed (every two weeks) during period of frequent plasmas with the monomers used in the present work. The tubing between the reactor and the trap is around 1 m long with flanges of CF 40 and about 40 cm long between the trap and the pump. The connecting flanges of the trap and the pump are DN 25 ISO-KF. The cold trap leads to strong differences in the pumping rate, according to the adsorption rate of the gas on cold surfaces. For instance, at a fixed pump valve opening, a pressure of 10 Pa could require a flow of 60 sccm of ethylene, but only 12 sccm of hydrogen.

The **pressure** in the reactor is measured with 1% accuracy by a Baratron® absolute capacitance gauge (see (5) on Figure 5.1). As its membrane can undergo deposition during the plasma, it is only briefly exposed to the discharge to measure the absolute reactor pressure during plasma. The continuous evolution of this latter during the discharge is instead monitored with a Convectorr® gauge. Its filament heated at around 250°C can effectively hamper the plasma polymer deposition on the filament, as its temperature is close or above the ceiling temperature of polymerization of the used precursors [68]. However, the measuring principle of this gauge has huge pressure errors which can reach up to 400%.

At the mainly used flow (F_s = 28 sccm=0.46 sccs) and pressure (p = 6.7 Pa), the vertical **mean drift speed** of the molecules in the reactor, v, values 11 cm/s. This speed can be established by dividing the real volume of gas (at the actual pressure p) injected per second by the section of the cylindrical reactor, A. The real volume, V, is connected to the standard volume, V_s, by $p \cdot V = p_s \cdot V_s$, with p_s the standard pressure. The following formula thus gives the mean drift speed, v, with F_s the standard flow [3] (p17):

$$v(cm/s) = \frac{F_s(sccs)}{A(cm)} \cdot \frac{p_0}{p} \tag{5.1}$$

5.1.3 The plasma source

The plasma source (ICP-P 200, JE PlasmaConsult GmbH, Germany) is placed on top of the vacuum chamber (see (6) on Figure 5.1). It consists in **planar spiral coil of 20 cm diameter**, separated from vacuum by a quartz window (Figure 5.3). The special four antennas and planar design enable a low inductance, scalable to industry size unlike the usual helical design [129]. The low inductance (0.54 μH) and the fact that the four coils are parallel allows the use of lower RF voltage [170], reducing the capacitive coupling (Section 1.2.3). Other characteristics of the source are the production of a high plasma density and the ability to homogeneously treat surfaces up to 10 cm diameter. Additionally, the coil housing integrates eddy current shielding, reducing the resistive losses [170].

The coil receives a radio-frequency signal (13.56 MHz) of variable power from a Dressler Cesar® 1310 **generator** (Advanced Energy, Germany). The coil heating is compensated by venting and by internal water cooling. To reach an optimal transmission of the power to the plasma, the impedance of the source-plasma couple must match the 50 Ω impedance of the generator. To this aim, the source integrates variable capacitances to compensate the plasma impedance which varies with plasma conditions and time. This matching unit can

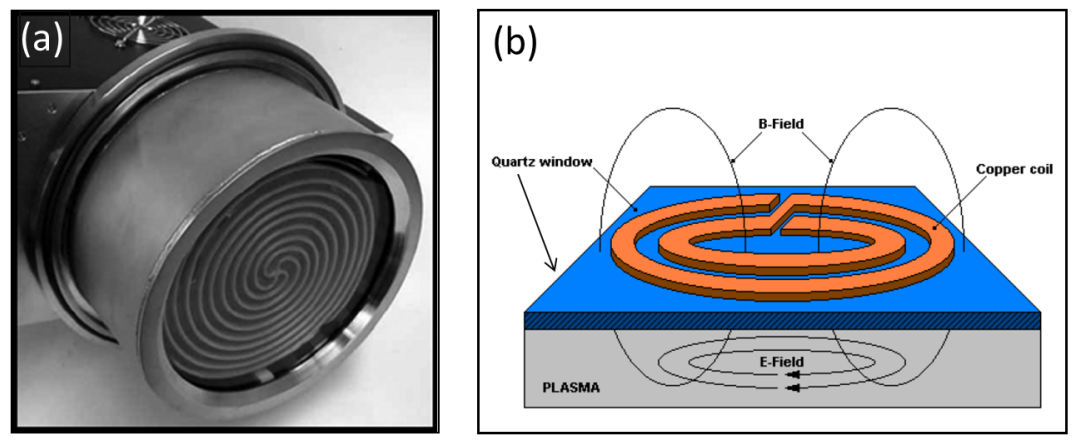

Figure 5.3: (a) Picture of the four antenna planar coil design of the plasma source, inserted in its stainless steel housing providing eddy current shielding (copyrights JE PlasmaConsult Gmbh) [129]. (b) Scheme of the magnetic and electric field produced by the source (from [170]).

be automatically driven by the generator unit, which measures the reflected power and tries to minimize it by adjusting the capacitances. Depending on conditions, manual or automatic compensation has been used in the present work and the reflected power was usually below 4 W for an applied power of 150 W.

The characterization of **electromagnetic fields distributions** for planar coil geometry [170, 171] shows that the electric field is parallel to the quartz window (see Figure 5.3b). Furthermore, as plasma is a conducting environment, the fields are absorbed by its free electron and ion currents. The field intensity is then exponentially decreasing with increasing distance from the quartz window. In other words, the field is evanescent. The skin depth is defined as the distance for which the electromagnetic field diminishes of a factor 1/e. A typical skin depth value is 2 cm for a plasma at 5 Pa and with a typical electron density of 10^{-11} cm^{-3} [170]. Therefore 63% of the electric power is absorbed in the volume between the quartz window and the skin depth. With a 20 cm diameter coil, it corresponds to a volume of 0.6 L. It is important to note that this absorption volume varies with conditions, from around 0.2 to 2 L.

5.1.4 Substrate holder

The substrate holder, which is electrically isolated from the reactor by ceramics, is placed horizontally on the rotary axis of the vacuum chamber (red on Figure 5.2). It consists in a stainless steel disc of 5 cm diameter on which the sample substrates can be fixed. Although it is possible to bias the sample holder, it was kept at **floating potential during the whole**

present work. Its vertical position can be varied but was kept unchanged at 12 cm from the quartz window all along this study. Due to this distance, the substrates are generally not in direct contact with the plasma volume. The gas flow path strikes the substrate holder perpendicularly.

5.2 Flow measurement

5.2.1 Standard volume flow

A standard volume is the volume that a gas would occupy in standard conditions of temperature T_S and pressure p_s. It is then equivalent to a precise number of molecules. Standard volumes injected in the reactor per unit of time are widely used in laboratories and industries to express the flow of a gas: sccm = standard square cube centimeters per minute, slm = standard liters per minute...

The Standard Temperature and Pressure (STP) conditions of the IUPAC (International Union of Pure and Applied Chemistry) are: $T_S = 273$ K and $p_S = 10^5$ Pa = 0.987 atm. In these conditions, 1 cm^3 STP of gas equals 44.6 μmol of the substance (in accordance with [80] p288). More importantly, the conversion factor between the standard volume flow and the molar flow is: **1 sccm = 0.743 μmol/s**.

The flow meters used in the lab express the flows in sccm and are used for pressurized bottle gases, like nitrogen, ethylene, acetylene... The standard conditions of the above mentioned MKS flow meters are 273 K and 1 atm = $1.01326 \cdot 10^5$ Pa [172]. Their standard volumes then contain 1.3% more mole of gas than the IUPAC standard volumes.

5.2.2 Measure of the flow rate of liquid monomer

The monomers in liquid precursor state, like styrene or benzene, are injected in the reactor with a mechanical dosing leak valve. A procedure to measure their flow is described by Yasuda ([80] p288). Once the vapor injection has stabilized, the procedure requires to suddenly stop the pumping (by closing the pump valve) and to measure the increase of pressure per unit of time $\Delta p/\Delta t$. The flow expressed in terms of standard volume of injected gas F_V can be calculated with the following equation:

$$F_V = \frac{\Delta p}{\Delta t} \frac{V_R}{p_s} \frac{T_s}{T} \tag{5.2}$$

where V_R is the reactor volume, T the temperature of the injected gas (in the reactor), and T_S and p_s the standard temperature and pressure (IUPAC convention). This equation differs

from ref [80] because we expressed it here with the (real and measureable) reactor volume V_R. Moreover we think an inversion of the ratio p_s/p_1 is needed in the Yasuda expression, according to the following ab initio development.

- The law of perfect gases stands: $pV = nRT$.
- The increased number of mole of a gas injected at constant temperature is: $dn = d(pV)/RT$.
- When injected in the constant available volume of the reactor V_R, it is the pressure that increases: $dn = V_R/RT \cdot dp$.
- Besides, this increased amount of mole can be expressed in terms of a standard volume increase dV_S, evaluated at the constant standard temperature T_S and pressure p_s: $\mathrm{dn} = \mathrm{p}_s/(\mathrm{RT}_S) \cdot \mathrm{dV}_s$.
- Equaling both expressions and isolating dV_S gives: $\mathrm{dV}_s = \mathrm{dp} \cdot \mathrm{V}_R/\mathrm{p}_s \cdot \mathrm{T}_S/\mathrm{T}$.

Clearly the standard pressure p_s stands at the denominator.

5.2.3 Pump valve opening

During the deposition process, the monomer vapor is continuously injected and pumped by the nitrogen trap and primary pump. Throttling the access to the pumping system, the pump valve can slow down the pumping rate. This valve was graduated with 16 intervals to reproduce its opening, noted V_P (for pump valve). For the same target pressure in the reactor, V_P has a great effect on the flow as can be seen of Figure 5.4a. A saturation of the flow can be observed at high opening of V_P.

When working at constant pump valve opening (usually fully open), a change of the reactor pressure requires a change in the flow. This is clearly shown on Figure 5.4b, where the different couples of flow/reactor pressure were measured for different valve opening. The present result is stressed as it is usual to see in the literature works investigating the pressure effect without even caring about the flow in the case of a liquid precursor. This greatly complicates the discussion of the results, as pressure and flow are two independent parameters of the plasma polymerization process [80].

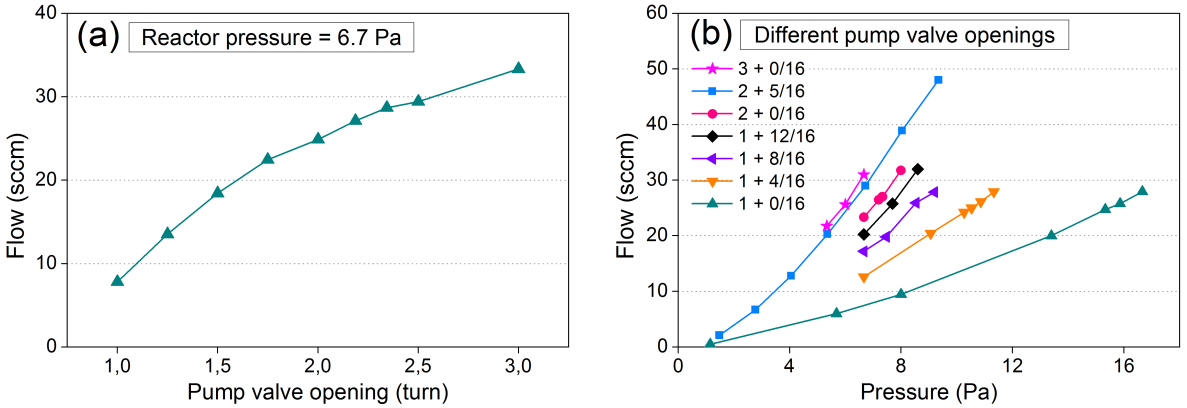

Figure 5.4: (a) Effect of the pump valve opening on the flow for the same equilibrium pressure of 6.7 Pa in the reactor. (b) Effect of the reactor pressure change on the flow, when working at constant pump valve opening.

5.3 Mass Spectrometry

Mass spectrometry (MS) is an analytical technique enabling to distinguish molecules originating from solid, liquid or gaseous samples. Celebrating its one hundredth birthday recently, the first MS instrument dates back to 1912 [87]. Today it is used in many fields like organic or inorganic chemistry, biology, atmosphere pollution, food control, forensic science, surface and material science, reaction kinetics,... [96]. Its widespread applications are due to several solid advantages: extreme sensitivity, high acquisition speed, delivery of structural and quantitative information.

Applied to plasma, MS provides essential data: detection of ions and their energy distribution function, identification of neutrals thanks to Threshold Ionization Mass Spectrometry (TIMS), relative or absolute species quantification and time evolution of species [96].

5.3.1 The mass spectrometer overview

The Hiden® PSM003 mass spectrometer is a compact instrument, build for versatile plasma analysis with moderate cost and intermediate performances. The spectrometer is equipped with a turbo-molecular pump reaching a typical pressure of 10^{-8} mbar (measured by a Penning gauge). This low pressure is ensured by an isolating cylindrical housing mounted on a flange as shown on Figure 5.5a. Its triple quadrupole design has a 1 to 510 Da mass range with a low mass resolution of 0.7 amu FWHM. The smallest of its three collecting apertures of 50, 100 and 300 μm diameters, enables to analyze plasma with pressure up to 0.5 mbar. Its energy filter

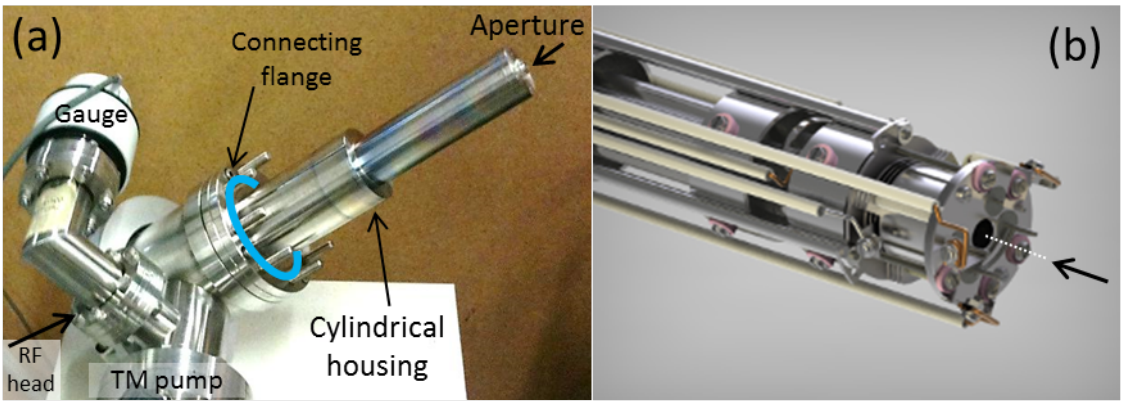

Figure 5.5: (a) Picture of the isolating cylinder housing mounted on a flange of the mass spectrometer. (b) Picture of the inside of the isolating cylinder: external view of the mechanical part of the probe (with the courtesy of Hiden®).

can measure entering kinetic energy of species up to 100 eV. The Secondary Electron Multiplier (SEM) detector has a large dynamic range of 7 decades.

The spectrometer probe shown on Figure 5.5a (mechanical part) is directly supplied by a RF power head (not shown on the picture). This latter is controlled by the electronic interface unit and sends to it the measured analogic signals. Communication with the computer is then ensured by a RS232 connection. Figure 5.5b shows a picture of the end of the probe when the cylindrical housing has been removed.

The instrument can operate in three different acquisition modes. Two acquisition modes are used for the detection of ions, either positive or negative. They were never used in the present work. The last acquisition mode, also called "Residual Gas Analysis"(RGA), is dedicated to the neutral detection. In their case, one usually considers that one ion is generated for 1000 sampled molecules ([87] p16), one of the generated ion over 100 reaches the detector ([13] p5).

Giving its name to the technique, the measurement of the mass of a species lies in its ionization and then its selection on the base of its mass-to-charge ratio (m/z). This operation requires five consecutive actions, linked to five consecutive parts composing the instrument. They are shown on the bottom of Figure 5.6 and are described hereafter: (1) the species collector (Section 5.3.2), (2) the ionization chamber (Section 5.3.3), (3) the energy selector (Section 5.3.4), (5) the mass selector (Section 5.3.5) and (5) the SEM detector (Section 5.3.6). Between each component, electrostatic lenses focused the ion beam. All numbers in the text of this section refer to the numbered parts of Figure 5.6.

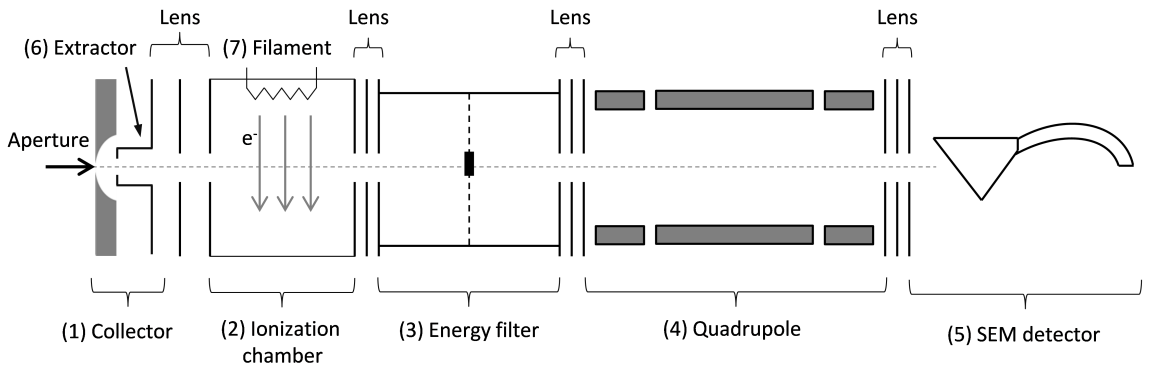

Figure 5.6: Schematic diagram of the Hiden® PSM003 mass spectrometer.

5.3.2 Species collector (1)

The species are introduced in the mass spectrometer through a collecting aperture of 50 μm diameter. In the case of ions, they are attracted thanks to the attracting potential of the extractor (6). In the case of neutrals, their diffusion is ensured thanks to a lower pressure in the spectrometer ($< 5.10^{-6}$ mbar in our case) compared to the reactor chamber (10^{-2} to 10^{-1} mbar). The design of the aperture is made to minimize interaction of the entering species with its surface, as visible from its flange section (1).

The plasma deposition process studied in the present work occurred everywhere in the chamber and thus also at the sample orifice. As a consequence, the flow of entering species in the spectrometer decreases with the reduction of the orifice and the measured intensities decrease as well. The reason for positioning the mass spectrometer 30 cm away from the discharge, as seen on Figure 5.2 (Page 75), was to limit this phenomenon. This distant position also allows using a closing valve to protect the spectrometer when venting the chamber to remove or set substrates. Despite all, plasma deposition occurred on the inside of the collecting aperture so that cleanings had to be done from time to time (around one a year). A signal increase of a factor of 5 to 10 was observed after the cleaning by keeping all other settings constant.

As ions and radicals species are not uniformly distributed in plasma, their collection is an important issue in the MS diagnostic of plasma. These species are effectively highly reactive and their mean free paths are short compared to the chamber size at the operating pressures of around 10^{-1} mbar. Therefore their detection necessitates locating the spectrometer in direct contact with the discharge, where they are produced. In contrast, neutral closed-shell species have uniform densities in the whole reactor volume, due to their stability and to diffusion [39]. In their case, the entrance slit of the mass spectrometer can be placed further away from the

plasma, which is the case here (see Figure 5.2). These species, actually considered as the effluents or by products of the process, can therefore be quantified during plasma by MS.

5.3.3 Ionization chamber (2)

After entering the mass spectrometer, species arrive in the ionization chamber (2). In the RGA mode, the neutrals undergo Electron Impact (EI) ionization, carried out with electrons emitted from a heated filament (7). The electron current is controlled and can be changed which has a direct influence on the ion signal intensity. The EI energy is generally set at 70 eV because many common compounds have their highest ionization cross section around that energy. However, it can also be varied from 5 to 100 eV so that ion decomposition of species like hydrocarbons or organic compounds can be studied too. The electron energy dispersion is generally considered to have an energy spread of 0.5 eV [96].

One considers that this system ionizes one species over 1000 ([87] p16). As the pressure is below 5.10^{-6} mbar because of the detector (see below), the ion mean free path is above 1 m. It definitely makes negligible any ion-molecule reaction in the ionization source and makes consistent the unimolecular ion decomposition hypothesis [13, 87], as seen in Chapter 3 on electron ionization (Section 3.3).

5.3.4 Energy selector (3) - Bessel box

A Bessel box is an energy filter (3) which has a cylindrical geometry as shown on Figure 5.7. The entrance and the output slits are both circular aperture in an electrode disk, which are at the same potential. The lateral horizontal cylinder is in electric contact with the central stop so that both are set at the same potential. The potential difference between the slits electrode and the central stop can be controlled. Only ions with specific energy (like ion A) can pass through this energy filter. Ions with higher kinetic energy (like ion B) would be stopped by the output electrode or by the central stop. Ions with too low energy (like ion C) would make a U-turn. So by tuning the potential difference one can measure the kinetic energy distribution of the collecting species/ions. The transmission of this energy selector is around 15%, much below a magnetic sector reaching 95%. However, it has the advantage to be very simple and has a very low cost.

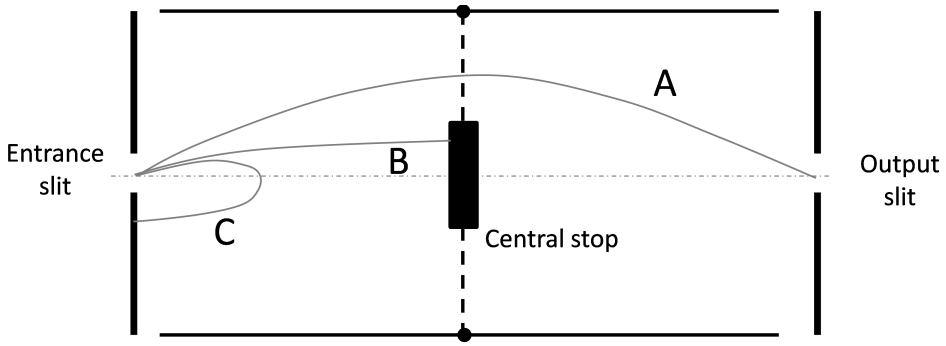

Figure 5.7: Section of the horizontal cylinder of the Bessel box energy selector. Among the three ion trajectories, only ion A with the right entering energy will pass through the box.

5.3.5 Mass selector (4) - Quadrupole

The mass analyzer is a triple quadrupole, made of 3 aligned quadrupoles with Molybdenum rods, used to increase the mass resolution. A quadrupole consists of four parallel rods, placed like shown on Figure 5.8. Applying specific RF potentials to them allows ions with an exclusive mass value to pass. Two opposite rods (like rods A and C) receive the same potential composed of a DC component U and a radio-frequency AC component with amplitude V. The two other rods (B and D) receive an opposite potential.

$$V_A(t) \;=\; V_C(t) \;=\; U + V.cos(\omega t) \tag{5.3}$$

$$V_B(t) \;=\; V_D(t) \;=\; -(U + V.cos(\omega t)) \tag{5.4}$$

A positive ion entering the field region parallel to the symmetry axis will be attracted towards the closest negative rod. However, the potential of this rod will change and draw him back toward the symmetry axis. The ion will exactly oscillate around the symmetry axis if it has the appropriate m/z ratio. Otherwise it will deviate from the central path so that it will strike the side walls of the quadrupole chamber. The complete equations of motion and calculation of the trajectories are available in many reference books [87] and will not be developed here. The important result is that a set of linearly dependent values of U and V enables to scan the m/z ratio which allows ions to go through the quadrupolar field area.

The widespread use of quadrupole is due to their main advantages: compactness, low cost, good transmission and fast response time. On the other hand they have the lowest mass range, a low mass resolution and mass dependent transmission [87, 96, 173].

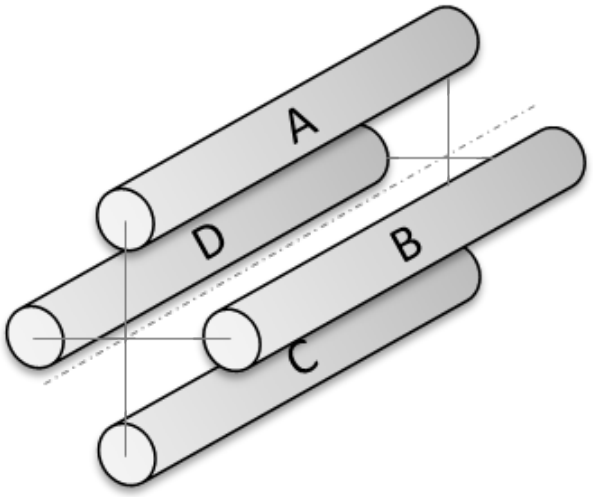

Figure 5.8: Quadrupole design.

5.3.6 SEM detector (5)

The role of the detector is to produce an electric current proportional to the abundance of the incoming ions. Among detectors, Secondary Electron Multiplier (SEM) detectors have good performances and are the most widely used. It uses the secondary electron emission occurring when an ion strikes a surface. The emitted electrons are then attracted toward another electrode surface with a higher positive potential and their collision on it emits additional electrons. The repetition of this process in cascade greatly amplifies the initial ion current and makes electron EM very sensitive. The design of the electrodes, called dynodes, can either be a succession of 10 discrete dynodes, each with its own potential, or continuous with a single and curved cone-shaped dynode. The latter sees its inner potential increased progressively all along the tube and is called a channeltron. The present spectrometer is equipped with this latter design.

To avoid arcs and damage, the SEM detector working pressure must be kept under $5 \cdot 10^{-6}$ mbar. Two important detector parameters must be tuned when acquiring a mass spectrum: the dwell time and the settle time. The settle time is the duration between the change of the instrument settings (e.g. change of U and V to select a new m/z ratio, change in electron emission current) and the beginning of the next acquisition step. Increasing this parameter will increase the stability of the changed instrument settings but also increase the measurement time. The dwell time is the time during which the ion signal is integrated. The longer it is, the lowest the noise signal is.

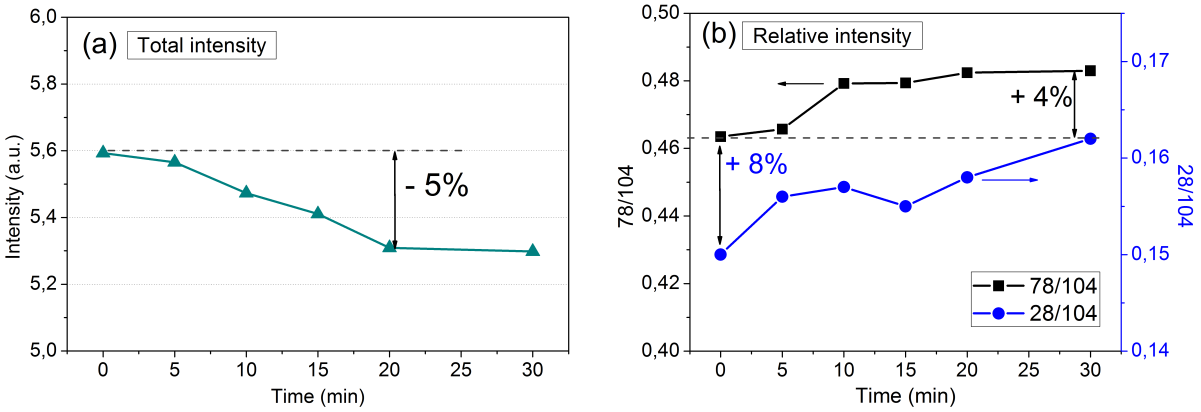

Figure 5.9: For styrene vapor at 7 Pa, evolution with time of: (a) the total mass spectrum intensity at 70 eV; (b) the ratio of the intensity at m/z = 26 and 78 to the one of the styrene molecular ion at m/z = 104.

5.3.7 Drift of the MS intensities

Even with all settings constant (including the species densities in the spectrometer), the absolute intensities of signal measured by MS are subject to change with time or "drift". This is generally attributed to drift of electrode voltages, which heat or can be contaminated by the sampled gases.

To quantify this intensity variation on a short timescale, we regularly acquired the mass spectrum of a styrene vapor at 7 Pa over a period of 30 minutes, at an electron energy of 70 eV and keeping all settings constant. The styrene vapor spectrum have been shown in Section 3.6. As absolute drift indicator, the total spectrum intensity is plotted in function of time of Figure 5.9a. Within 20 minutes, we observe a relative diminution of 5%. However, the intensity of individual peaks of the spectrum may also show relative change. As drift indicators of relative peak intensity, the two important signals (>10% of the base peak intensity, here at m/z = 104) at m/z = 26 and 78 were divided by the molecular ion intensity at m/z =104. Their evolutions with time are shown on Figure 5.9b. It reveals that the relative change of intensity of important signal can reach 8% over 30 minutes. In the case of small signal, it can reach 15%. We conclude to a **maximal drift of 5% over a period of 10 minutes**. These measurements brought us to shorten as much as possible the exposition of the mass spectrometer to vapor and plasma when absolute measurements are required. This will be further explained in Section 8.2.2.

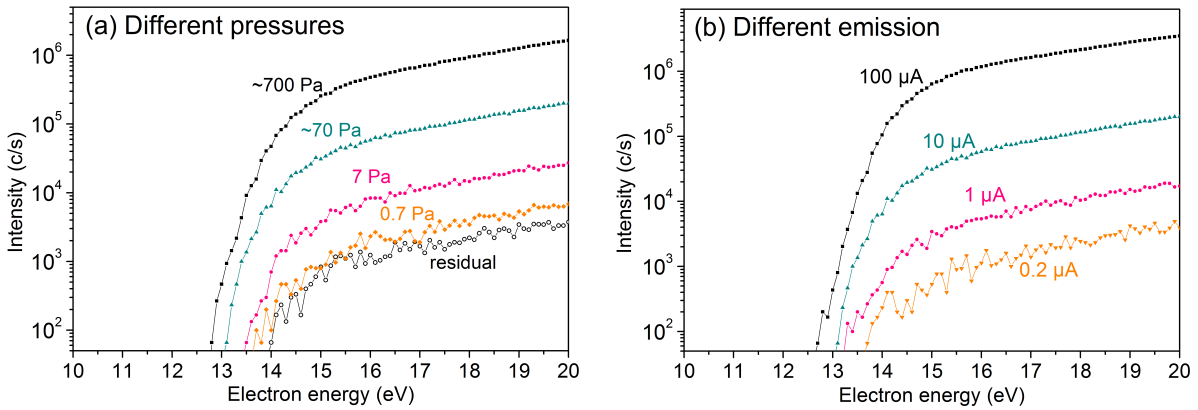

Figure 5.10: Electron energy spectra of the m/z = 32 signal of pure oxygen gas: (a) injected at different pressures, all other settings kept constant, (b) acquired at different emission currents, all other settings kept constant at a pressure of 7 Pa.

5.3.8 Error in appearance energy measurement

Another type of information brought by MS is the electron energy spectrum (EES) in the RGA mode (see Figure 5.10). The electron impact energy can be varied while acquiring the ion signal at a fixed m/z ratio. This allows the measurement of the Appearance Energy (AE) of a specific ion decomposition channel or the Ionization Energy (IE) for the molecular ion, as seen with more details in Chapter 3 (Section 3.7, Page 53).

In the present work, the AE is simply measured at the electron energy for which the acquired curve intersects the X axis, set just above the noise signal. On Figure 5.10, the Y axis was started at 50 c/s, because the noise was observed at 33 c/s.

To calibrate the electron beam energy, we measured the AE of several usual gases, injected pure at 6.7 Pa in the reactor. Those AEs were systematically higher of 0.6 eV ± 0.2 eV than the theoretical IEs. The shifts stayed similar over several months.

The EES at $m/z = 32$ were acquired when injecting pure oxygen in the reactor (see Figure 5.10a). This signal corresponds to the molecular ion of the oxygen molecule, O_2^+. We can see that the lower the pressure, the higher the measured AE, from 12.8 eV at 700 Pa to 13.9 eV at the residual gas pressure (<0.1 Pa). With regard to the theoretical IE of the O_2 molecule (12.1 eV), the measured shift increases from 0.7 to 1.8 eV when decreasing the pressure. On Figure 5.10b, the intensity of the same ion (32 amu) at a pressure of 6.7 Pa was plotted but for different electron emission currents. The energy shift increases from 0.6 eV at the highest current to 1.7 eV for the lowest one. From these two observations, we conclude that **the energy shift progressively decreases as the signal decreases**, whatever the origin of the intensity

reduction: pressure or emission current. This may contribute to explain the difference of shift observed in reference [173] from 0.8 eV to 2.3 eV.

As it is difficult to define a progressive shift correction to variable data, a unique diminution of 0.6 eV was applied to all the measured AEs, which we will call "corrected AEs" in this work. This correction stays stable over five months, and changes to another value when an optimization of the spectrometer was made. However, we will also keep in mind that an **additional decrease up to 1.0 eV is occurring for very weak signals**.

For the sake of precision, as the electron beam has an energy spread of 0.5 eV, the AE should be increased by about 0.5 eV [9]. However, the calibration shift would then increase by the same amount and the corrected AE would finally have the same value. It was therefore neglected for concision.

5.4 X-Ray Photoelectron Spectroscopy

Explained by Einstein in 1905, the photoelectric effect is one of the possible phenomena occurring when a photon meets an atom, with the Compton effect and, if the photon energy is higher than 1.022 MeV, the electron-positron pair production.

In the photoelectric effect, the photon is absorbed by an electron, which is then ejected from the atom. After the ionization, the photon has disappeared. The photoelectric effect explained by Einstein involved conduction electrons from metals: if the photon energy is higher than the work function of the metal, the photoelectron may be ejected. This corresponds to photons in the UV and part of the visible light.

This "first" photoelectric effect became a spectroscopy with the work of the Swedish physicist Kaï Siegbahn, in the beginning of the 1960s. Using X-Rays instead of UV or visible light, core levels electrons may be ejected. The principle of the X-Ray Photoelectron Spectroscopy (XPS) is very simple: a monochromatic X-Ray beam is used and an analyzer measures the speed of the photoelectrons. It is therefore possible to determine the energy of the core level from which the photoelectron has been ejected. Since the energy of the core levels is characteristic of each element, this is a tool to determine which elements are present on the sample. Indeed, the energy conservation states:

$$h\nu = BE + KE + \phi \tag{5.5}$$

where $h\nu$ is the photon energy, BE the binding energy of the electron to the atom, KE the kinetic energy of the photo-emitted electron and ϕ is the work function of the spectrometer

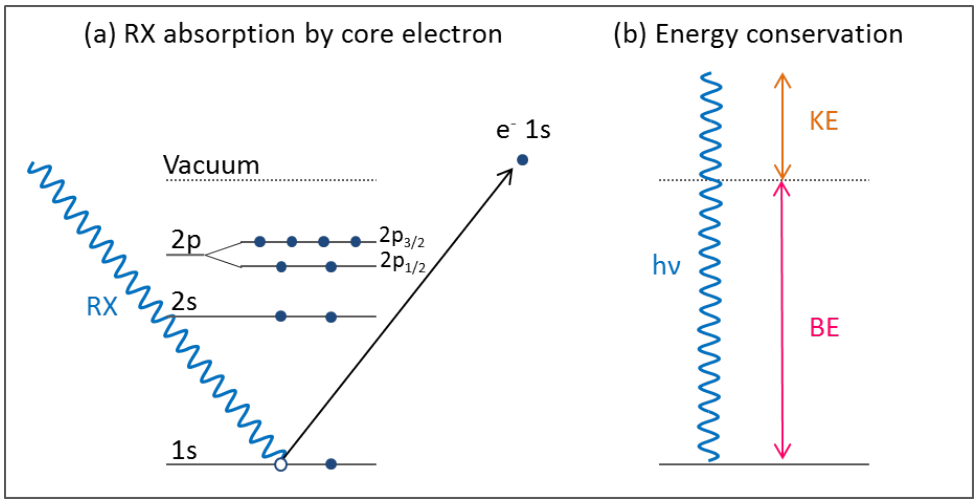

Figure 5.11: (a) A RX photon is absorbed by a core electron (1s) of one atom of the sample, leading to the electron ejection. (b) Schematic diagram depicting the energy conservation: the photon energy (hν) is distributed in BE and KE (the work function is neglected).

(and not the material). The work function is an adjustable instrumental correction factor. The phenomenon is schematically depicted on Figure 5.11.

XPS has two additional advantages that make it a very popular spectroscopy:

- This spectroscopy is semi-quantitative in that the intensity of the signal is proportional to the amount of the given element on the sample. As long as the sample is homogeneous, one can show that the relative amount of elements A and B is proportional to the relative measured intensities of the signals corresponding to these two elements, corrected by some factors such as the ionization probability (Scolfield factor), the inelastic mean free path and the transmission of the spectrometer. All these factors can be evaluated.
- By the measure of the chemical shift of a given binding energy, one can deduce the chemical environment of the atoms in the sample. XPS is then a chemical spectroscopy also known as Electron Spectroscopy for chemical analysis (ESCA).

The photoelectric effect is one of the major advances in modern physics: Einstein was awarded the Nobel Prize in 1921 for his explanation of the photoelectric effect and Siegbahn was awarded the Nobel Prize in 1981 for its use as a spectroscopy.

Three additional comments are important for our work:

- The depth analysis in XPS is generally evaluated to maximum 10 nm, but actually many parameters should be taken into account to give a more precise value.
- Insulating materials require charge compensation, because the emitted electrons leave a positive charge on the surface. item Hydrogen is not detected in XPS.

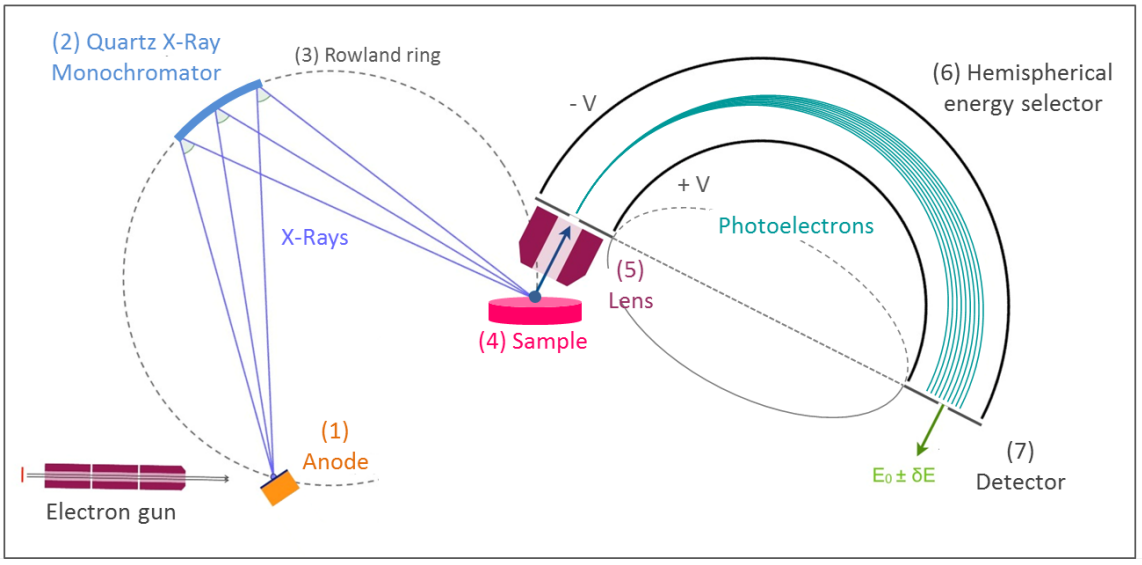

Figure 5.12: Schematic drawing of the XPS spectrometer.

Until 2013, the laboratory was equipped with three XPS instruments: SCIENTA, HP and SSX-100 spectrometers, the latter being the most used with moderate performances. At the start of 2013, they were replaced by two brand new and powerful instruments from Thermo Scientific®. The K-ALPHA for "routine"analysis with short acquisition times and the ESCALAB 250Xi built for research performance with high sensitivity, high energy and high imaging resolutions.

We describe here the two instruments used in the present study: the SSX-100 for the results from 2008 to 2012 and the ESCALAB for the latest results. Both were equipped with pumping systems reaching the 10-10 mbar range to allow high electron mean free path and to keep surfaces clean from contamination for several hours [174].

5.4.1 The former spectrometer - SSX-100

Figure 5.12 is a schematic diagram of the spectrometer and the numbers in the text below refer to it:

- The X-Ray production is usually carried out through bombardment of a metal anode with high energy electrons (10 keV) (1) generated in an electron gun. Aluminum or magnesium anodes are generally used because the energy width of their emitted X-Ray is small compared to other metals with heavier atomic nucleus. Our spectrometers use Al $K_{\alpha 1,2}$ emission line corresponding to photons of 1486.6 eV.

- To select this emission line, an X-Ray monochromator (2) is used, made of curved quartz crystals. Their crystalline planes serve as a Bragg network which reflects X-Ray of different energies with different angles. Picking the right angle allows one to select the desired X-ray energy. To improve the X-Ray beam intensity different quartz crystals are used.
- Since there are no lenses for X-Rays and because one needs to choose different sizes for X-Rays spot on the sample, a specific geometry is used: anode, cristals and sample are on a sphere called Rowland sphere or ring (3). In that configuration, the spot size on the sample has the same size than the spot on the anode. The electron gun has then a second role besides electron acceleration: it determines also the spot size on the sample.

The SSX X-Ray spot on the sample (4) can be varied, but the smallest spot size only reaches 300 µm diameter. The incidence angle of the X-Ray beam was 55° from the sample normal and the emitted photoelectrons were collected at 35° from it. The electron collection was ensured by an electrostatic lens (5) which focused the electron coming from a solid angle into the entrance slit of the analyzer.

Several geometries exist for energy selection but the SSX is equipped with the hemispheric one (6) which has the best performances. Two concentric hemispheric electrodes receive opposite potentials which produce a radial electric field. In this field, electrons are dispersed in energy: among all the entering electrons, only those with the right kinetic energy E_0 will be transmitted by the exit slit. The analyzer energy resolution ΔE (FWHM) is determined by the exit slit width ΔS, by the entrance beam angle α and the mean radius of the hemispheres R_0, according to the following equation [175]:

$$\frac{\Delta E}{E_0} = \frac{\alpha^2}{2} + \frac{\Delta S}{2R_0} \tag{5.6}$$

This equation shows that to acquire spectrum with constant energy resolution ΔE, the energy analyzer must be operated at constant pass energy E_0, by slowing down the electron before entering the selector. The decelerating ratio gives the energy position on the spectrum.

Finally, the photoelectrons are detected by a 2D multichannel plate (7). It operates as a 1D detector of 128 channels by integrating the signal on one direction. The width ΔS is then actually the width of one channel.

The best energy resolution achievable was 0.7 eV, due to the combined effect of the XR source width and the energy analyzer resolution [176].

Our plasma polymers required charge compensation as they were insulator. The SSX has a charge compensation system based on a low energy electron beam, but unfortunately the

system was inefficient and resulted in deformations of the peak shapes, leading in most cases to unworkable results for the chemical analysis.

5.4.2 The new spectrometer - ESCALAB

The new Thermo Scientific ESCALAB 250Xi spectrometer elevated analysis performances to a much higher level in the lab. This is due to optimized design at each steps of the process, from X-Ray production to electron collection, energy selection and electron detection.

The whole design follows the one of the SSX.

- The X-Rays are still produced by bombarding an aluminum anode with a finely focused electron beam. The Al Kα 1,2 emission line of 1486.6 eV energy is selected by two toroïdal quartz crystals placed on a 0.5 m Rowland circle.
- The sample receives the focused X-Ray beam with variable angle positions, thanks to the movable substrate-holder.
- The collection of the photoelectron is enhanced by a magnetic lens placed just above the sample. It has the advantage of ensuring a conservation of the electron kinetic energy and increase the current and then the sensitivity.
- The next lens system adapts the electron kinetic energy to a target value before entering the energy analyzer. As for the SSX, this is used to run the analyzer at constant passing energy and then with constant energy resolution.
- The photo-electron energy analyzer is a full 180° spherical sector analyzer.
- The detection system is made of two different detectors. The first consists in a 6 channel electron multiplier (EM), with large dynamic range. It is used for rapid acquisition of spectra. The second is two-dimension sensitive for image acquisition, made of two channel plate amplifiers. In addition, the spectrometer is equipped with state-of-the-art charge compensation. It combines low-energy electron sprayed from a flood gun with diffusion of Ar ions. It proved to work very well on the insulating plasma polymers studied in this work.

A very interesting feature of the new system is its unique argon sputtering gun: atomic ions of several keV are used for depth profiling of hard inorganic material, while large Ar cluster ions are used for sputtering of soft material. The latter proved to be very adapted for polymers, for which no degradation was detected while profiling.

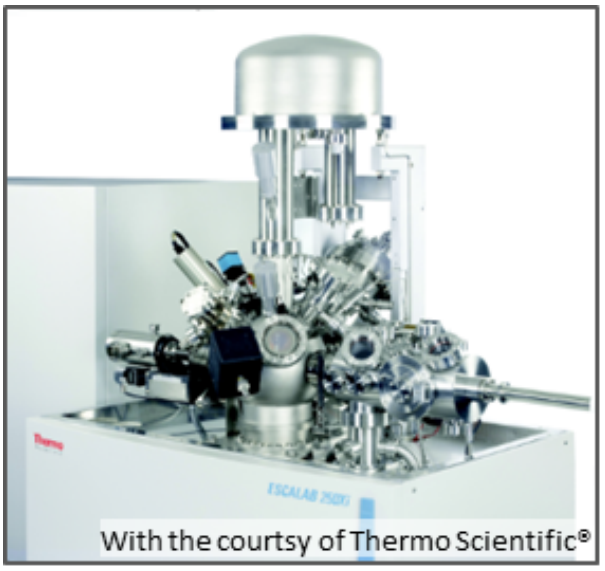

Figure 5.13: Picture of the ESCALAB spectrometer (with the courtesy of Thermo Scientific®).

The ESCALAB system is also equipped with a Reflection Electron Energy Loss Spectrometry (REELS), that can quantify H content on the topmost surface. This could especially be convenient for plasma-deposited polymers, for which H content can markedly vary.

The overall performances of the ESCALAB spectrometer are the following.

- The best energy resolution reaches 0.45 eV, defined as the measured FWHM of the Ag 3d5/2 photoelectron peaks.
- The best spatial resolution reaches 3 μm for chemical imaging. A set of slits enables one to collect photoelectrons coming from a smaller surface area than the XR spot size around 500 μm.
- Acquisition times are much shorter than before, enabling a survey and several high resolution regions in around 20 minutes.
- Prior to the introduction, a home-made system takes a picture of the substrate holder, that can be downloaded by the acquisition software. While the pumping is carried out, the user can already define on which part of the sample to acquire a spectrum, a line-scan or an image and with which settings.

Chapter 6

Surface characterization of plasma polystyrene films

The current chapter will present the characterization of plasma polystyrene (pPS) films by deposition rate (DR) and by X-Ray Photoelectron Spectroscopy (XPS), deposited at the substrate holder location (Section 6.2 & 6.3). The unusual results obtained led to investigate the light emitted by the plasma (Section 6.4), the discharge pressure and the monomer depletion (Section 6.5) and the distribution of the thickness and the mass deposited in the reactor (6.6). While discussing all these measurements, physical effects are proposed and bring a better comprehension of the specific reactor geometry (Section 6.7).

6.1 Plasma conditions

The results are presented for one series of pPS films, processed at varying power, from 90 to 240 W. All other parameters were kept constant: 3 min of deposition on silicon substrates, 6.7 Pa of pressure, 28 sccm of flow (21 μmol/s) and at continuous-wave (CW) conditions.

Initial pressure (Pa)	**Flow** (sccm)	**Applied power** (W)	**W/F** (eV/sty)	**W/FM** (eV/Da)	**W/FM** (10^8 J/kg)
6.7	28	90 – 240	45 – 119	0.43 – 1.15	0.42 –1.11

Table 6.1: Plasma conditions and ranges of W/F and W/FM, calculated here with the minimum and maximum applied power (1 W/sccm = 14.0 eV/monomer, as seen in Section 2.4.1).

The W/F ratio gives the mean energy delivered by the generator per injected monomer, in eV/monomer (see Section 2.4.1). It is indicated in Table 8.1 for the lowest and the highest power of the series. The W/FM ratio provides the mean energy delivered by the generator per mass of injected monomer in eV/Da (Section 2.4.1). The macroscopic units usually used by Yasuda are J/kg and are added in the last column to ease the comparison.

As no measurement of power coupling efficiency have been carried out, the power (or wattage, W) indicated on the graph of the present chapter will be the **delivered power**, which is the applied power subtracted by the reflected power, as measured by the RF generator. The reflected power was generally low, with values between 1 and 5 W.

6.2 Deposition rate at the substrate holder location

A Dektak profilometer was used to measure the thickness of the pPS films, deposited on silicon wafer at the substrate holder location. The "scoth tape" method was used to obtain a sharp step for the profilometer: a piece of scotch tape is stuck on the substrate before deposition (partly covering it) and is simply removed after the deposition.

On Figure 6.1, the DR progressively increases from 90 to 185 W, then abruptly rises to reach a plateau with a very high value of 650 nm/min. The first observation is that the DR qualitatively follows the general domains of plasma polymerization established by Yasuda [80], depicted in Section 2.5.1: a linear increase (region I, called energy-deficient region), finishing by a plateau (region III, called monomer-deficient region), with a transition region between them (region II). However, in our case, we detect an important difference. The transition to the plateau region is accompanied by a large increase of the DR, which is doubled.

The power at which the plateau region is reached is called the "**critical power**", written W_C (W for wattage). In our case, it occurs around 190 W and corresponds to a critical $(W/FM)_C$ of $8.8 \cdot 10^7$ J/kg or 95 eV/sty. It is delicate to compare this value for other geometries. Indeed, the coupling efficiency of planar ICP is known to be quite dependent on conditions, as discussed in Section 1.2.3 (and see reference [74]). Moreover, the flow by-pass, i.e. the possibility for the monomer to reach the pump without passing by the plasma region, is very specific in our case.

Applying macroscopic kinetics

Plotting the DR in a logarithmic scale against $(\mathrm{W/F})^{-1}$ gives the trend shown on Figure 6.2. Great care must be taken, as we measured the deposition rate (nm/min) and not the mass

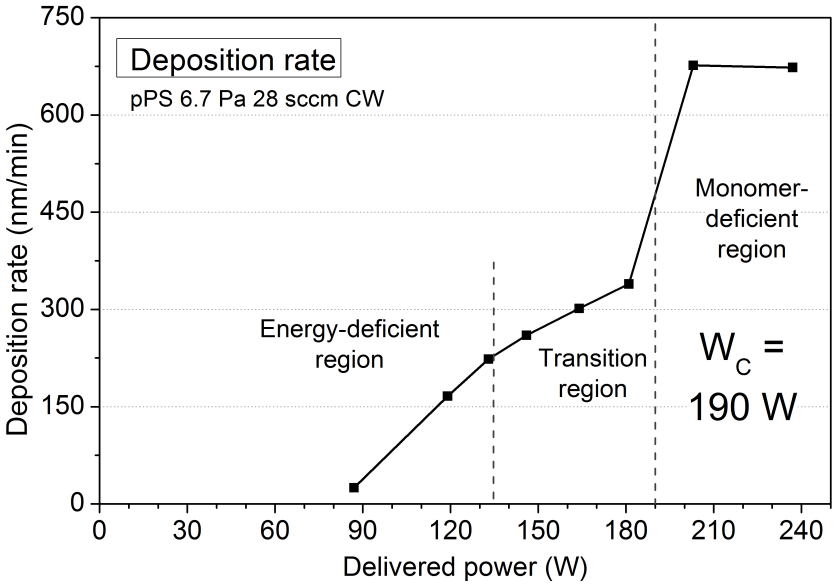

Figure 6.1: Deposition rate of pPS deposited at 6.7 Pa, 28 sccm and at continuous-wave.

deposition rate (g/cm^{2}s), which integrates the film density. Globally, no exponential dependence is observed by far, meaning there is no straight line similar to an Arrhenius plot (see Section 2.5.2).

The author would like here to shortly present a comment about the debate on the applicability of the macroscopic kinetics described in Section 2.5.2, on the base of the present data.

(1) A straight line may be observed from 0.010 to 0.017 (eV/monomer)$^{-1}$. Looking more accurately, a small bending of the data is occurring. The measure of the slope gives an activation energy of 176 eV/monomer.

(2) The point with the lowest DR at 90 W is clearly out from this straight line dependence.

(3) In addition, these data must be corrected by the film density, which has most probably a varying and increasing value with W/F. Therefore if we had any straight line initially, we should not anymore after the film density correction. However, the data could probably still be fitted by a straight line, for moderate correction, thanks to the visual effect of the data presented in "scatter" plot. It could also be argued that the slight bending mentioned in point (1) would then be corrected by the density correction.

In our opinion, this discussion shows for us the problem of the macroscopic kinetics: the general trend of the DR always allows more or less to fit a straight line among a part of the plotted data, as already mentioned [9]. Besides, many other corrections still has to be integrated of course, like the coupling efficiency, the "active plasma region" (smaller than the plasma volume, see [75]), the flow by-pass ratio and the remote location of the substrate from the plasma region.

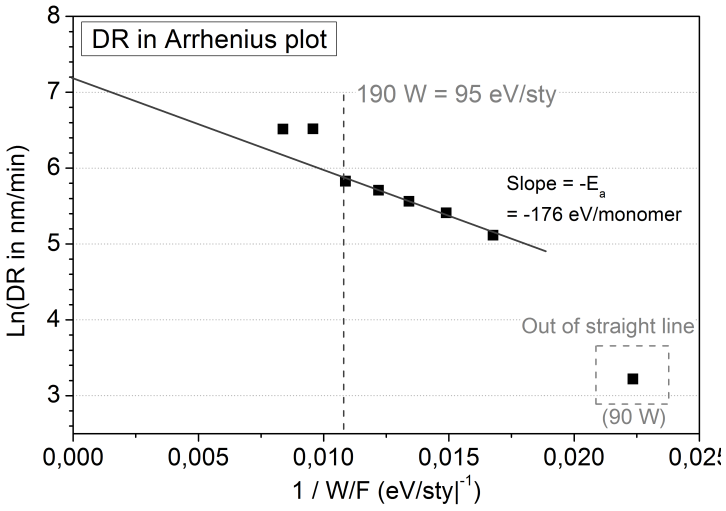

Figure 6.2: Arrhenius plot of the deposition rate (and not the mass deposition rate).

6.3 XPS characterization

In order to characterize the pPS films by XPS, their XPS spectra were compared to the spectra of a reference PS, spun coated on a Si substrate (0.5% styrene weight in toluene, 650 t/min for 18 s, 1 kt/min for 20 s, no annealing). From the general survey spectrum (not shown), pPS revealed oxygen incorporation. Figure 6.3 shows the XPS atomic concentration of oxygen of the same samples than for the previous DR measurement, after 6 days of exposure to air. The oxygen uptake reveals a steady value around 5% atomic concentration up to 165 W. Then a progressive increase up to 10% is measured from 165 to 210 W and above this value the increase slows down.

The oxygen incorporation trend does not follow the one established by Swaraj *et al.* [128], for which the increase of effective power leads to an increase of the oxygen uptake. This may be due to a difference in the geometry, which was a capacitively coupled reactor for Swaraj *et al.*, with the sample located between the electrodes. It can be also due to an unfortunate non-uniform light exposure of our different samples, which was not controlled. The trend does not also follow the sharp "discontinuity" of the DR around the critical wattage, but mostly evolved around it.

The C1s high resolution XPS spectra of conventional PS and pPS were also compared. In accordance with the literature (State of the art in Section 4.1.3), we used a smaller number of components in comparison to Beamson & Briggs [137]. A single component for the C1s main peak was used instead of the combination of an aromatic and an aliphatic one. For the shake-up satellite peak, the fit was done with a single component as well, instead of four different ones.

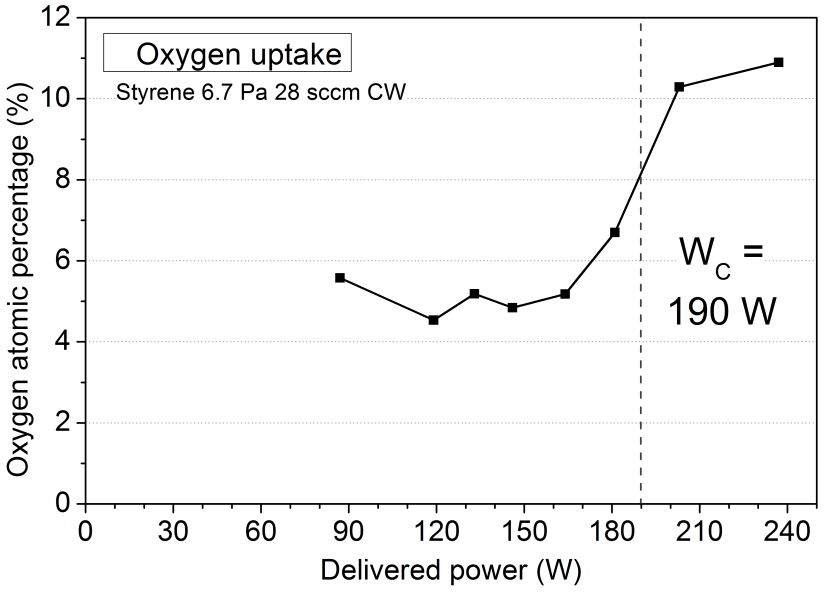

Figure 6.3: Atomic percentage of oxygen in the pPS films in function of power, as measured by XPS, with 6 days of exposure to air.

For the pPS, we added one oxygen containing component: the C-O (hydroxyl/ether), as done by many workers. This was not sufficient for the two highest powers, for which a C=O component (aldehyde/ketone) was needed. As the addition of a β-shifted component C-CO did not change significantly the results, we choose to not present it for simplicity. A "smart"background was used for the curve fitting.

The result of the decomposition of the C1s high resolution XPS spectrum acquired with the ESCALAB spectrometer can be seen on Figure 6.4a for the conventional PS and on Figure 6.4b for the pPS at 185 W (after 6 days of exposure to air). Comparatively to the spin coated PS, the pPS reveals: (i) a broader C-C component, (ii) the apparition of a C-O component and (iii) a diminution of the relative shake-up surface area.

(i) The FWHM of the conventional PS is 0.93 eV, while it lies between 1.18 and 1.33 eV for the present pPS (see Table 6.2). This is usually explained by an increase in the chemical environment diversity for the carbon atoms in the pPS [128, 130].

(ii) The C-O component systematically has a larger FWHM than the C-C one, as indicated in the same table. This is in agreement with the literature [128, 130].

(iii) Figure 6.5 shows the aromaticity retention, measured by dividing the relative shake-up area (to the total C1s area, including the shake-up) of the pPS samples by the same area but for the spin coated reference PS. From 90 to 150 W, a steady value around 63% is measured. Then a decrease is observed which slows down above 210 W. It confirms the

Component	**Measured FWHM (eV)**	
	Conventional PS	**Plasma PS**
C-C	0.93	1.18 – 1.33
C-O	-	1.35 – 1.70
Shake-up	2.10	2.10 – 2.40

Table 6.2: Measured FWHM of the different components used in the analysis of the C1s high resolution XPS spectrum.

anti-correlation of the aromaticity with the oxygen uptake already observed by other workers [128, 129, 177]. Besides, as for the oxygen uptake, the trend is not the same as the one observed by Swaraj *et al.* and does not follow the sharp variation of the DR around the critical wattage.

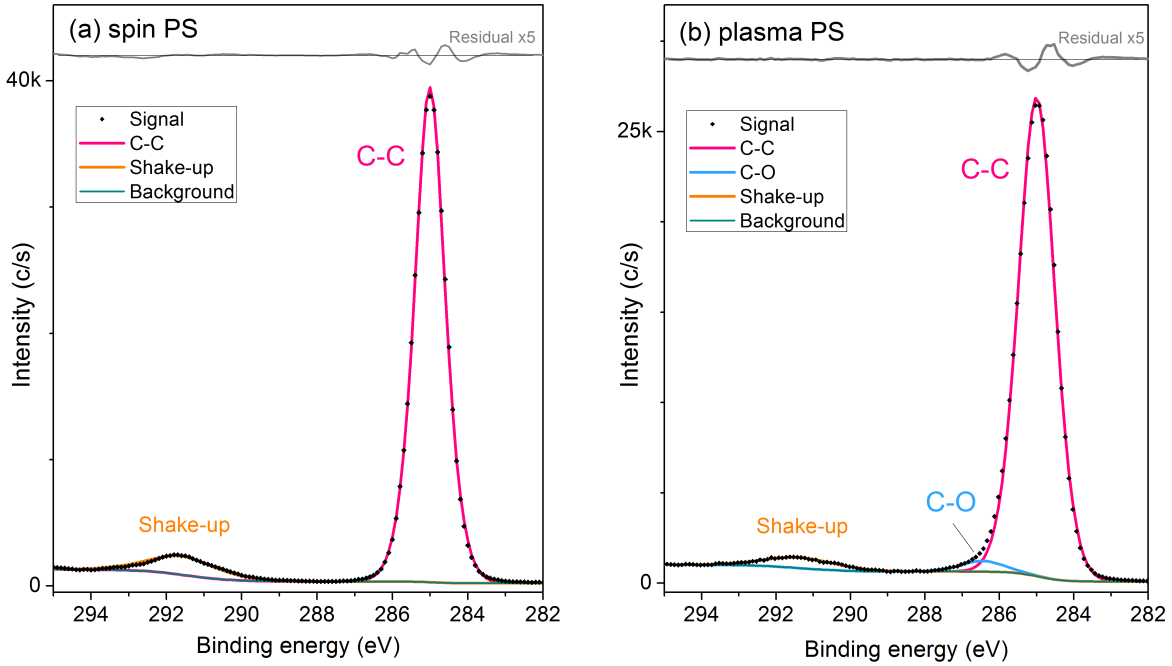

Figure 6.4: C1s high resolution XPS spectrum of: (a) spin coated PS and (b) plasma deposited PS at 6.7 Pa, 28 sccm and 185 W.

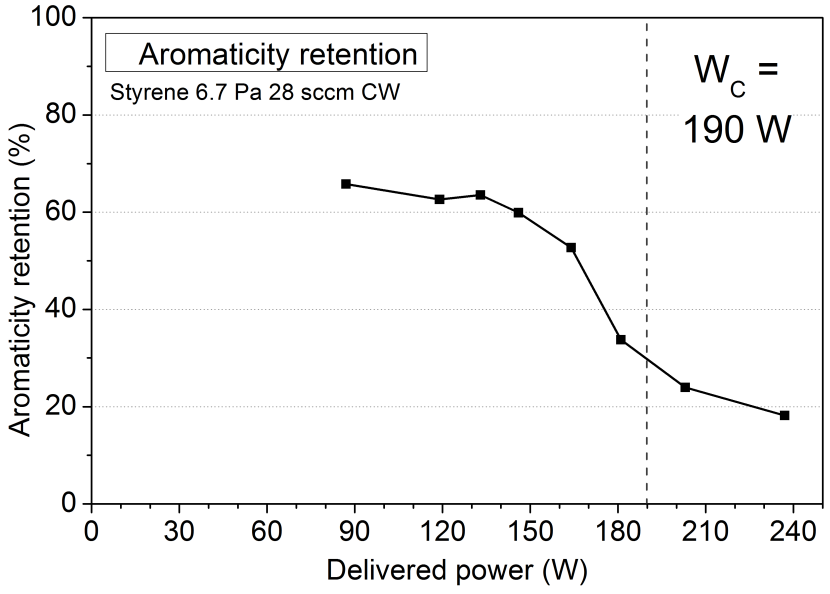

Figure 6.5: Aromaticity retention as measured by XPS: ratio of the shake-up area relatively to the total C1s area (including the shake-up) of the pPS to the one of the spin coated PS.

6.4 Light emission of the styrene plasma

To investigate the unusual discontinuity of the deposition rate at the critical power, the light emission was investigated. To this aim, an optical fiber collected the light generated by the styrene plasma through a reactor viewport, while all external light contamination was eliminated. The optical spectrometer was an Ocean Optics USB4000XR, with very low resolution but a large wavelength range, from 200 to 1000 nm. The plasma conditions were exactly the same as the ones of the plasma deposited coatings.

Figure 6.6 shows the evolution of the optical emission spectrum for the different powers, which are the applied ones (maximum reflected power is 4 W). Intensities are normalized to the exposition time which was of 30 s up to 195 W, and lowered to 10 s at 210 W. The spectrum at 195 W shows an unfortunate saturation. All spectra have spikes due to noise, which are not representative of any physical emission line. For each spectrum the background spectrum dependent on the exposition time have been subtracted.

The objective here is not to assign lines to excited species. The observed continua are shortly commented in Section 7.5.1. The aim was rather to integrate the intensity of each spectrum to measure their total intensity. This gives a relative value of the total emission, but which is flawed by the spectrometer transmission function (not corrected). The evolution of this indicator is plotted in function of the delivered power on Figure 6.7. The point at 192 W is underestimated due to the spectrum saturation (see Figure 6.6).

On Figure 6.7a, the linear scale clearly reveals an impressive increase of the emission around the critical power of the DR discontinuity. This kind of emission jump is characteristic in inductively coupled plasma reactor to a **transition from E-to-H** mode [8]. Without entering into the details described in Section 1.2.3, the E mode (for Electrical field) is a transmission of the source power to the plasma by capacitive coupling of the coil, which has a poor coupling efficiency. It is characterized by a low light emission correlated to a low electron density. In our data, it would correspond to the power range below 180 W. The sudden increase of emission around 190 W is due to a strong increase of the power coupling when passing to the H mode (for the H magnetic field). It is accompanied by a large increase of the electron density.

Figure 6.7b are the same data plotted in logarithmic scale. It shows that the light emission increase is exponential from 100 to 180 W (straight line) and that the increase is even stronger when reaching the critical power.

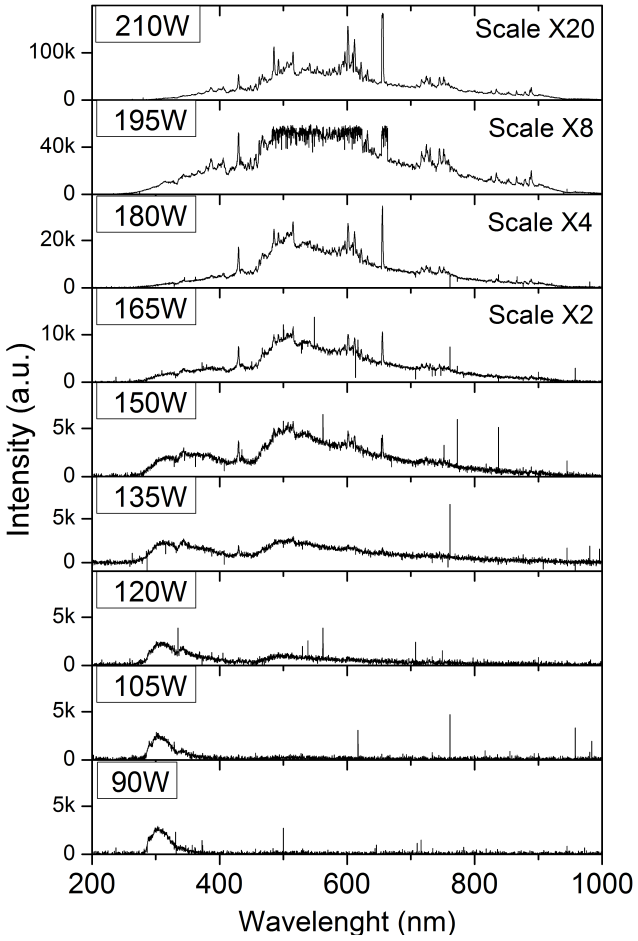

Figure 6.6: Optical emission spectra of styrene plasma at 6.7 Pa, 28 sccm and CW conditions, for different applied powers.

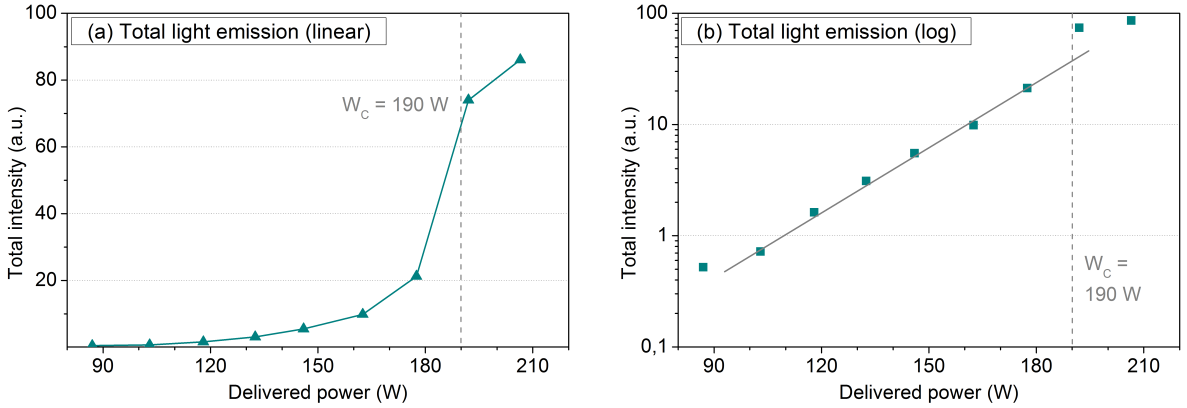

Figure 6.7: Total intensity of the emission spectra of Figure 6.6 in: (a) linear scale and (b) logarithmic scale.

6.5 Discharge pressure and monomer depletion

6.5.1 Discharge pressure

It is worth comparing the previous results to the discharge pressure, whose evolution is shown on Figure 6.8. It reveals a steady value at low powers, then a "bump" centered on 165 W and ends with a sharp drop of the pressure at 190 W.

Firstly, the value of the critical power based on the DR (see Figure 6.1) coincides well with the critical value based on the pressure stabilization criterion (Figure 6.8). Secondly, a possible explanation for the "discontinuity" in the DR evolution is the drop of pressure above the critical wattage. The mean free path of the species – electrons, ions, stable neutrals or radicals – is longer at lower pressure. Therefore, in that case, the **plasma volume is larger** and more reactive species could reach the substrate and deposit on it.

6.5.2 Pictures of the styrene plasma

In an attempt to visualize the plasma expansion with power, pictures of the plasma were taken at each power during the acquisition of the emission spectra of Section 6.4. A Pentax Kx camera (numeric reflex) was disposed at a viewport of the reactor chamber as shown on Figure 6.10. The angle of acquisition is in "low-angle shot", meaning from bottom to top. Thus the planar coil and the quartz window are at the center of the picture in the background. At the top of each picture, an irregular aluminum covered part of the wall is in the camera view angle (see Figure 6.9). This view angle is the best we could attain, considering the reactor geometry. The camera was settled in manual mode with manual focus. Thus all its settings were kept constant, except the exposure time which was ajusted when needed.

The pictures are shown on Figure 6.9. The intensity variation was so moderate from 90 to 180 W that the exposure time could be fixed at 200 ms (first top series of the figure). For higher power, the emission intensity changes so strongly that the exposure time had to be adjusted twice, as indicated.

Beside the intensity variation, the pictures reveal an **expansion of the plasma volume**:

(1) On the top series at 200 ms, the increase of power shows:
- a lateral expansion towards center, as the central darker zone is disappearing
- a lateral expansion towards side-walls can also be detected when comparing 135 W to 180 W, as the quartz window is not visible anymore

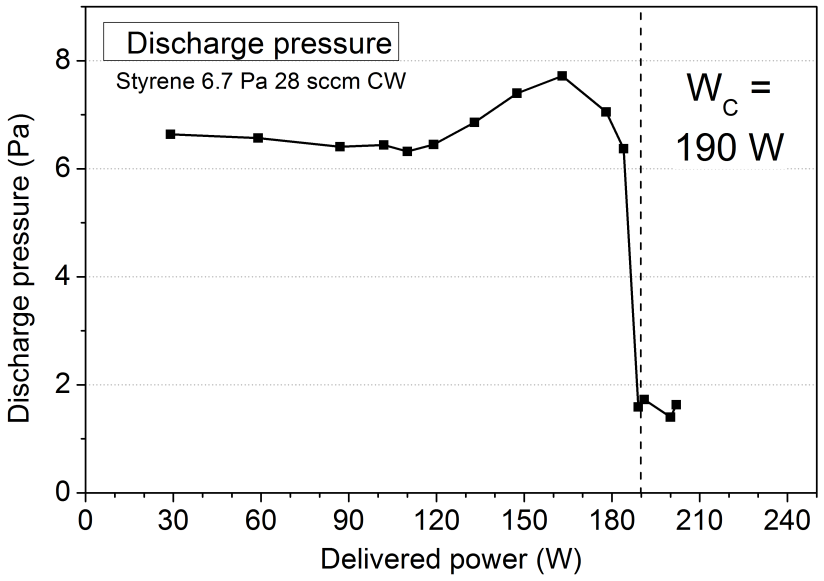

Figure 6.8: Discharge pressure during the plasma polymerization of the pPS samples.

(2) Comparing the power at 135 W to 240 W, an expansion of the plasma towards the substrate holder may be detected, but this is not very clear.

6.5.3 Monomer depletion

The evolution of the monomer depletion with power bring some answers about the pressure discontinuity of Section 6.5.1. The measure was made by mass spectrometry (MS), with a method fully described in Section 8.2. It consists in measuring the intensity of the molecular ion peak of styrene, once just before plasma and once after the discharge has stabilized, usually after 1 minute. The MS intensity is proportional to the partial pressures. Because the signal drift is very limited between the two measures which are very close in time, it allows to measure the partial pressure of styrene during the discharge with an error as low as 5% (see Section 5.3.7).

Instead of the styrene partial pressure, the monomer depletion (MD) is presented here and is defined as:

$$MD = \frac{p_{vap}^{sty} - p_{pla}^{sty}}{p_{vap}^{sty}} \tag{6.1}$$

where p_{vap}^{sty} is the pressure of the monomer before plasma (here a constant of 6.7 Pa) and p_{pla}^{sty} is the partial pressure of styrene during plasma.

The MD evolution depending on power is shown on Figure 6.11. It reveals a clear non linear increase with power and reaches a steady value of 99% when reaching the critical power of

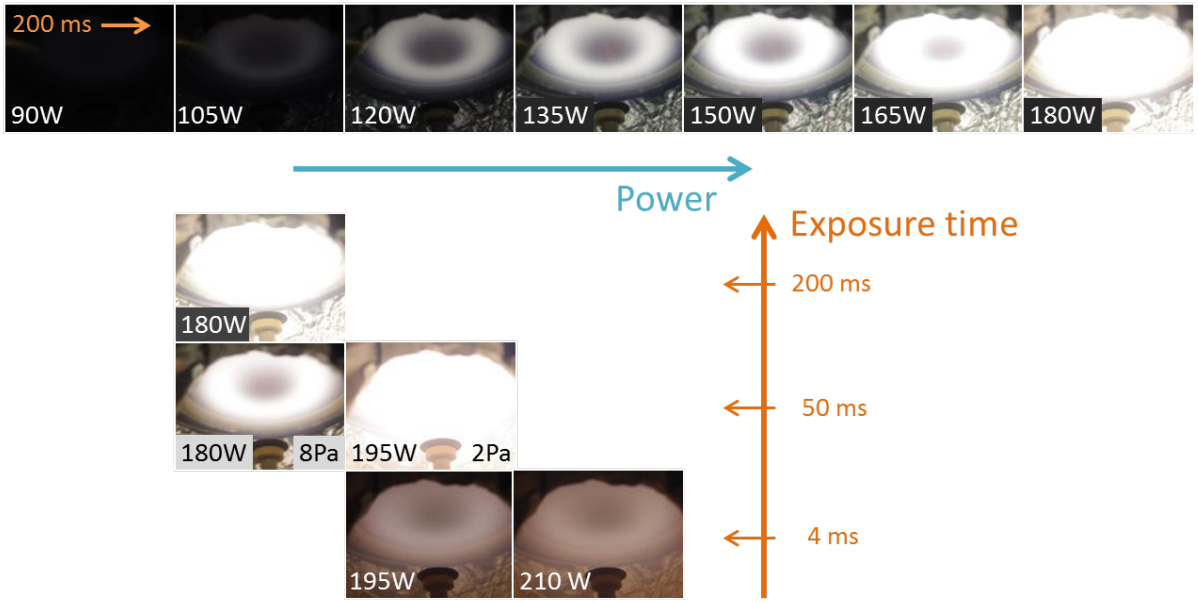

Figure 6.9: Pictures of the styrene plasma at 6.7 Pa, 28 sccm and CW conditions.

deposition rate and pressure at 190 W. What is important is the fact that the MD is already high at 180 W with a value of 95%. The E-to-H transition may be strong at 190 W but the **styrene was already almost completely depleted at powers just below the transition**. This will constitute another important piece for the discussion at the end of the chapter.

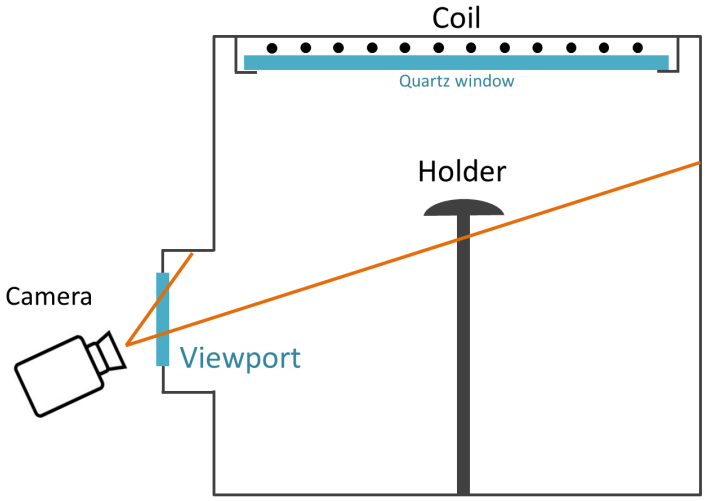

Figure 6.10: Scheme of the view angle of the camera.

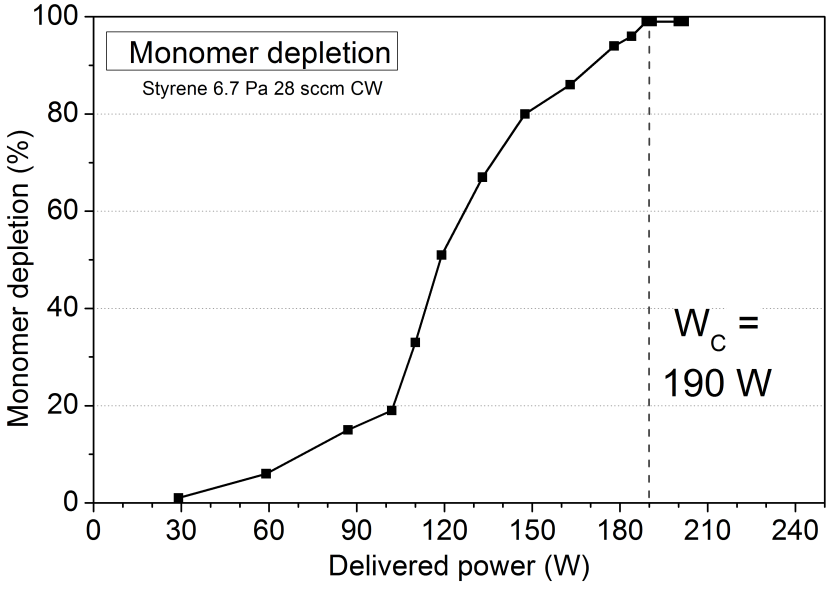

Figure 6.11: Monomer depletion of styrene during plasma at 6.7 Pa, 28 sccm and CW conditions

.

6.6 Thickness distribution and total mass deposited

6.6.1 Distribution of the film thickness

To further inspect the longer mean free path hypothesis above 190 W or the larger plasma volume, we studied the film thickness distribution in the reactor, deposited for 6 minutes at two different powers: at 120 W, below the critical wattage, and at 210 W, above it. The film was collected on long Si substrate of 10x1 cm^2, directly stuck on the quartz and the reactor wall. The thickness was measured by profilometry with the method of the "scotch tape" (Section 6.2). The results are shown on Figure 6.12.

On the quartz window (Figure 6.12a), at low power, the DR distribution exhibits strong variations. Two maxima of deposition are observed at 5 cm from the quartz center. The quartz stops at $r = 10$ cm and the slight increase above this value is due to the passage to the shielding metal maintaining the quartz. At higher power (and lower discharge pressure), the deposition is more uniform at the center, indicating either a higher plasma density at the center or that polymerizing species can diffuse on longer distance. Comparing both powers shows that the maxima are at the same position, but interestingly the highest thicknesses are the same. The amount of material deposited, slightly higher at high power, is then rather similar if densities are the same.

On the vertical wall (Figure 6.12b), thicknesses were measured only on the 9 first cm below the quartz window. The shapes are relatively analogous for both powers, but the thickness is markedly higher at 210 W, by a factor from 3 to 4. It is comparable with the same ratio of 4.1 at the substrate holder position, 12 cm below the quartz (see Figure 6.1). Again this increase of deposition can be explained either by a larger plasma volume and/or by a longer diffusion length of the polymerizing species. Assuming densities are close, a much higher amount of material is deposited at high power. Acting as a pump during the process, it could explain the considerable drop of pressure above the critical wattage.

Besides, it is interesting to compare these results to a simulation, carried out for the planar coil geometry of our reactor for another project. Carbon dioxide was studied with a continuous-wave power of 100 W and a pressure of 2.7 Pa. The result for the power dissipation density is shown on Figure 6.13. It reveals that this physical quantity is the highest close to the quartz window at around r = 6 to 7 cm. It coincides well with the positions of the maximum DR measured at 5 cm for styrene plasma deposition. The difference can indeed be due to the

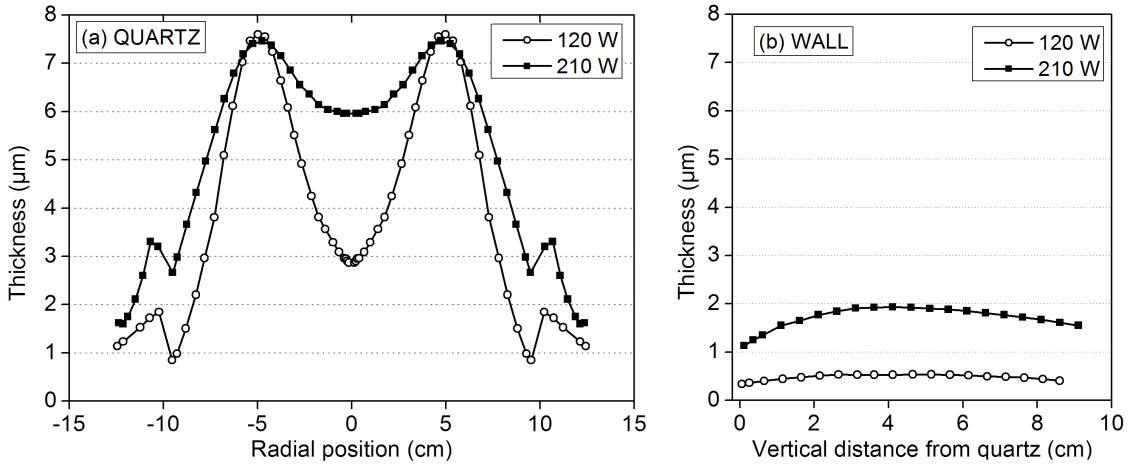

Figure 6.12: Distribution of the film thickness on: (a) the horizontal quartz window, (b) the vertical wall of the reactor.

gas and/or the pressure difference, but also to the flow path directed toward the center of the coil.

6.6.2 Total deposited mass

To further investigate the reason why the pressure drop above the critical power is so important, we wanted to have a better knowledge of the amount of material deposited. Therefore it is more accurate to evaluate the total mass deposited (g) than the deposition rate (nm/min). However it implies measuring the density of the deposited material, which was done at the sample holder position, 12 cm below the quartz. The conditions were kept identical with 6.7 Pa, 28 sccm and at continuous-wave regime for 6 minutes, with the two different powers at 120 W and 210 W. Large square Si substrates of 5x5 cm^2 were weighted before and after the deposition, with a balance precise to 0.01 mg. The weight was measured 15 minutes after deposition, so with low oxygen weight uptake due to the trapped radicals reaction with atmospheric oxygen. The thickness was measured all along the substrate diagonal every 5 mm, and the mean thickness was calculated from them (the thickness was highly homogeneous). The substrate surface areas were calculated by geometry. All these values, the DR, the density and the mass deposition rate calculated are summarized in Table 8.1.

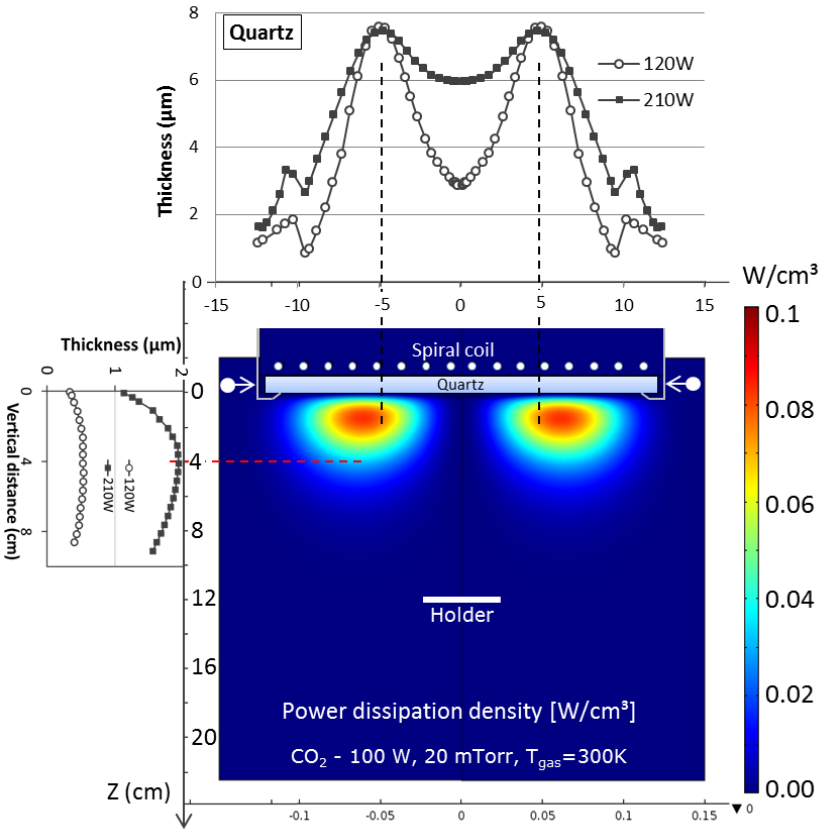

Figure 6.13: Comparison of the power dissipation density simulated in CO_2 plasma at 100 W and 2.7 Pa with the thickness distribution of plasma deposited styrene at 6.7 Pa and 120 W or 210 W. Kindly provided by Dr N. Baguer.

Power (W)	**Weight** (mg)	**Thickness** (μm)	**Area** (cm^2)	**DR** (nm/min)	**Density** (g/cm^3)	**Mass deposition rate** ($\mu g/cm^2.min$)
120	1.13	0.47	23.0	79	1.0	8.1
210	7.26	2.43	22.7	405	1.3	53

Table 6.3: Density and mass deposition rate of styrene at the substrate holder position (plasma duration = 6 min).

The first noticeable feature in Table 6.3 is the difference of DR with the values reported on Figure 6.1. Different plasma durations were used but Haidopoulos *et al.* showed deposition was linear with this parameter with our geometry [130]. So the DR should be the same. The discrepancy can rather be explained by the fact that the deposition was carried out on large Si substrates, completely covering the metallic substrate holder. Difference in the floating bias is therefore expected and then the results must be dealt with caution. The second feature from

Table 3 is the higher density of the coating at higher power. The ratio of weight is equal to 6.4, indicating that the amount of material deposited is higher than expected when we considered identical densities (factor of 4.1). A last feature is that the density of the pPS films is close to the glassy PS density at around 1 g/cm^3 and that the one at 210 W is higher than the one at 120 W.

To have a better understanding of the process above and below the critical wattage, we evaluated the mass balance, i.e. the mass injected during the deposition versus the mass deposited on all the surfaces of the reactor.

- The **injected mass** is the one of 28 sccm of styrene injected during 6 minutes. It corresponds to $6.95 \cdot 10^{-3}$ mol or 723 mg (using the correspondence of 1 sccm = 0.743 μmol/s).
- The mass deposited on the **samples** are 1.1 mg at 120 W and 7.3 mg at 210 W.
- The **reactor side wall** is a cylinder of 15 cm diameter and of 20 cm of height. As thickness, we used the mean value calculated for the 9 first "top" cm and the same thickness but divided by a factor two for the remaining 12 cm, to take into account that the DR should decrease in the lower part of the reactor. As density we used the one measured at the substrate holder, having no other indication. The deposited mass on the walls can then be estimated to 92 mg at 120 W and 437 mg at 210 W.
- On the quartz, we first calculated the volume deposited on individual flat ring for each radial position. The width of the flat ring was taken to be the difference between the radius of the selected radial position minus the one of the previous radial position. The area of each ring was then multiplied by the measured thickness for the corresponding radial position. The total deposited mass was then estimated by adding all the ring volumes and then multiplying it by the density measured at the substrate holder, having no other indication. However being directly exposed to the plasma, density is suspected to be higher on the quartz and therefore the deposited mass is under-estimated. The resulting mass is 150 mg at 120 W and 270 mg at 210 W.

All mass values are summed up in Table 6.4 in addition of the total mass deposited for both conditions. We see that around 33% of the injected mass is deposited at 120 W and almost 100% at 210 W. It can therefore explain why the pressure drops so much above the critical wattage.

Power (W)	Injected mass (g)	Mass on substrate (mg)	Mass on wall (mg)	Mass on quartz (mg)	Total mass (g)
120	0.72	1.1	92	150	≈ 0.24 (33%)
210	0.72	7.3	437	270	≈ 0.71 (98%)
	Increase factor:	6.6	4.7	1.8	3.0

Table 6.4: Estimated mass balance of the styrene deposition process.

6.7 Discussion

From the many measurements presented, it seems that two combined effects can contribute the DR "discontinuity" at the substrate holder location.

(1) **A discontinuity in the production rate of film-forming species**. The E-to-H transition observed at 190 W suddenly enhanced the coupling efficiency and the electron density which result in a sudden larger production of film-forming species and a sudden increase of the deposition rate [178].

(2) **A discontinuity in the transport of the film-forming species to the substrate**. The pressure drop occurring at 190 W has two effects. It increases the volume of creation of film-forming species (creation volume), because the mean free path of the electrons is longer (see [80] p286). It also increases the mean free path of the film-forming species which spread out further away from the "creation volume". It results in a sudden expansion of the "depositing volume", define as the creation volume improved by the spreading out distance of the film-forming species. Therefore the spacial distribution of the polymer deposition in the reactor may markedly evolve with the large pressure variation. Especially, the substrate holder enters suddenly deeper into the depositing volume and undergoes an abrupt increase of its deposition rate.

The following sub-sections will discuss these two effects with further details.

6.7.1 E-to-H transition versus pressure drop

The first effect due to the **E-to-H transition** has been recently reported for polymerizing plasma in the references [178, 179]. The DR shows an increase factor of 5 for the series at the initial pressure of 5 Pa, from just below to just above the transition power. Accordingly, the plasma polymer film composition changes drastically at the transition power. It can then explain our

significant change in the aromaticity retention and oxygen uptake, but which are smoother in comparison.

In opposition to the case of monoatomic or diatomic gases in closed conditions [180, 181], the increase of the initial pressure is observed to raise the threshold or transition power in flow polymerizing plasma [179]. In the latter work, the discharge pressure was maintained equal to the initial pressure by using a pressure-regulated throttling valve in front of a turbo-molecular pump [179, 182]. Thus the E/H transition may only be affected here by the plasma composition. The monomer studied is propanethiol, C_3H_8S, which has a high hydrogen content: large production of H_2 is thus likely, with a small collision cross section and an elevated ionization potential of 15.4 eV.

The E-to-H transition seems obviously sufficient to explain the DR discontinuity. However, in our view, the discharge pressure drop of the styrene discharge with a factor of 3.8 may also contribute and cannot be set aside considering the following points.

(a) The monomer depletion is close to 95% just before the E-to-H transition and reaches 99% at the transition. As styrene does not seem to produce stable effluents in large amount above the critical power, the pressure drop could maybe occur without the E-to-H transition and it may be a **coincidence** here. Considering the fact that a variation of pressure affect the value of the transition power, the pressure drop could also trigger the E-to-H transition. This must be temper in the present case, as the light emission started to increase already at 180 W.

(b) The above point may be supported by the fact that the study of the E-to-H transition has only started recently for flow polymerizing systems [178]. Significant differences can be expected from discharges of argon or nitrogen in closed system [181].

(c) At exactly the E-to-H transition power (190 W), the discharge pressure takes 3 minutes to stabilize. Just after plasma ignition, it actually starts to increase above the initial pressure of 6.7 Pa in the 10 first seconds and then slowly and regularly decreases to reach its final stable value of 1.7 Pa. For higher power, like 210 W, the pressure stabilizes at 1.7 Pa within the 30 first seconds. The study of the light emission with time should determine if the transition to the H mode is already present at the start of the discharge.

(d) Comparing the relative and the absolute increase of the deposited mass at different reactor location (Table 6.4) brings a further consideration. At the side-wall, the mass increase factor is of 4.7, against 6.6 at the substrate holder. Moreover, the side wall collect more than 60% of the total mass injected above the critical power. Thus, in our view, the **side-wall is the main cause for the pressure drop** (if no powder is produced, which

has to be verified) and the following reasoning may explain the higher mass increase factor at the substrate holder location. The side-wall has a very large surface and collects more and more mass as the power and the depositing volume increase. But being already almost in "full contact" with the depositing volume just below the critical power, its mass increase is lower than the one of the substrate holder when reaching the critical power. Indeed, if the substrate holder is further away from the depositing volume just before the critical power, the expansion of this volume with the pressure drop makes the substrate holder contact the depositing volume more abruptly than the side walls.

The three following sub-sections will discuss issues about the pressure with further details.

6.7.2 Full glow hypothesis

For CCP and helical ICP geometries, the critical power has been defined not only as a saturation of the DR and a pressure stabilization, but also as the achievement of the maximal plasma volume, referred as the achievement of "full glow" conditions [3]. To our knowledge, the present results could constitute the first report of a similar behavior for plasma polymerization in planar ICP, as well as the first application of the concept of full glow in such geometries for polymerizing plasma.

Yasuda and Morosoff studied the distribution of DR in helical ICP reactor at low and high W/FM [177]. For low W/FM, they observed much more localized DR distribution than at high W/FM, where deposition occurs more uniformly everywhere in the reactor. Concordantly, the DR was observed to be high at locations in the reactor corresponding to the "**glow region**" of the plasma (the plasma region emitting visible light). At low W/FM, the glow region was very located, while at high W/FM, it occupies the whole reactor.

For Yasuda, the plasma polymerization process occurs predominantly in the glow volume [80] (p292). Effectively, the glow region intuitively corresponds to the region where the inelastic collisions of the electrons leading to electronic excitation are the most abundant. The consecutive radiative deexcitations thus occur the most abundantly in the glow region, which is then the region with the highest light emission. As inelastic collisions of electron also lead to dissociation, the glow volume is as well the region of the largest radical production. At the base of the Rapid Step-Growth Polymerization (RSGP) mechanism (Section 2.3.3), these radicals must predominantly reach the surface to lead to large DR. Being highly reactive, the radicals should not propagate on distance much longer than their mean free path before reaching the surface and are therefore mainly localized in the glow region.

Applying these observations to our case is delicate, as the glow volume could not be visually well defined, especially at the highest powers (see Figure 6.9). However, it seems convincing to consider that, at low power, the glow volume is located close to the quartz window. The DR is therefore high on the window, as seen on Figure 6.12a at 120 W, and low or moderate everywhere else in the reactor. At higher power, the glow volume reaches the reactor walls and the substrate holder, which increases the DR at those places. In contrast, on the quartz window, the glow being already present at lower power, the DR does not increase anymore. The only change is a more uniform deposition along the quartz, as shown on Figure 6.12a at 210 W.

These reasoning must be tempered by the following consideration. The transition to the H mode is accompanied by a large increase of the electron density and therefore of the field screening: the skin depth diminishes [7]. This would accordingly tend to decrease the glow volume.

6.7.3 Pressure and mean free path

The estimation of the mean free path supports the fact that the deposition volume can be larger than the glow volume. To this aim, we will consider a radical the size of C_2H_2, like $C_2H^{\bullet}$. At low power (120 W), the dominating collision partner can reasonably be estimated to be the styrene monomer. The mean free path estimation is made as follows:

1) The elastic cross section of collision can be estimated by the geometric cross section (see Chapter 2, Section 4.3). The critical diameter of molecular sieve for benzene and toluene is 6.7 Å [183]. Slightly above, we will consider a molecular diameter of 7 Å for styrene. For acetylene, it is equal to 2.4 Å. The interaction radius d is the sum of the individual radii: $\mathrm{d} = \mathrm{r}_1 + \mathrm{r}_2 = 4.7$ Å. The geometrical cross section is then: $\sigma = \pi \mathrm{d}^2 \approx 7 \cdot 10^{-19}\ m^2$.
2) Considering a pressure of 6.7 Pa of styrene gives a density n of $1.6 \cdot 10^{21}\ \mathrm{m}^{-3}$
3) The mean free path is then: $\lambda = 1\ /\ \sigma \mathrm{n} = 0.9$ mm ≈ 1 mm.

At high power (210 W), the discharge pressure after a certain time is around 1.8 Pa and, as will be seen in a next chapter (Section 8.3.1), the main species present in the gas phase (and thus collision partner) is hydrogen.

1) The diameter of hydrogen is reasonably estimated to be 1.2 Å. The interaction radius is now: $\mathrm{d} = 2.4/2 + 1.2/2 = 1.8$ Å. The cross section is equal to: $\sigma = 1 \cdot 10^{-19}\ \mathrm{m}^2$.
2) A pressure of 1.8 Pa corresponds to a density of $4 \cdot 10^{20}\ \mathrm{m}^{-3}$.
3) The mean free path is equal to: $\lambda \approx 23$ mm.

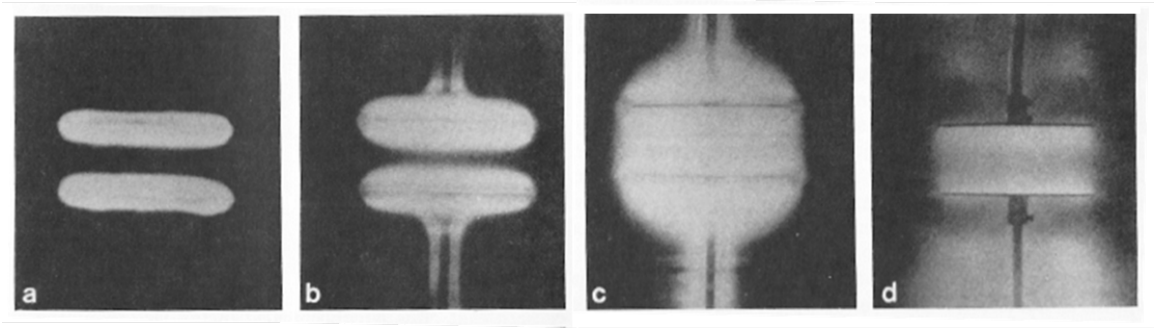

Figure 6.14: Pictures of the glow region in a CCP reactor with 4.5 cm of inter-electrode distance at different pressures: (a) 100 Pa, (b) 70 Pa, (c) 40 Pa and (d < 13 Pa (adapted from [2] p293).

So, below the critical power, $\lambda \approx 1$ mm and, above it, $\lambda \approx 23$ mm. Compared to our introduction of Section 6.7, the glow volume of Yasuda could correspond to our proposed creation volume, but the depositing volume could be markedly larger above the critical power, due to a mean free path of film-forming species of around 2 cm. Therefore, this must be considered when looking to the styrene plasma picture at the highest power on Figure 6.9. We could detect a slightly thicker plasma, so closer to the substrate holder, but the latter seems not immersed in the glow volume. However, the mean free path of 2 cm can significantly improve the deposition volume compared to the glow volume (or creation volume), as the distance quartz-holder is 12 cm.

Up to now, a typical radical mean free path was considered, to have an idea of the spreading of the radicals out from the glow region. In addition, a diminution of the pressure will also increase the mean free path of the electrons and therefore increase the glow volume itself. This latter effect of the pressure on the glow volume is best illustrated by pictures of the glow region for different pressures, visible on Figure 6.14, for a CCP reactor, at constant power. The discharge pressure diminishes from left to right. A clear increase of the glow volume is visible, which even spread out from the inter-electrode space at the lowest pressures.

As a test for our hypothesis of sudden immersion of the substrate holder into the depositing volume, we proposed to measure the evolution of the DR with time at the substrate holder location at exactly the critical power. The slow variation of the discharge pressure over 3 minutes should induce a DR increase with time, as the depositing volume expands.

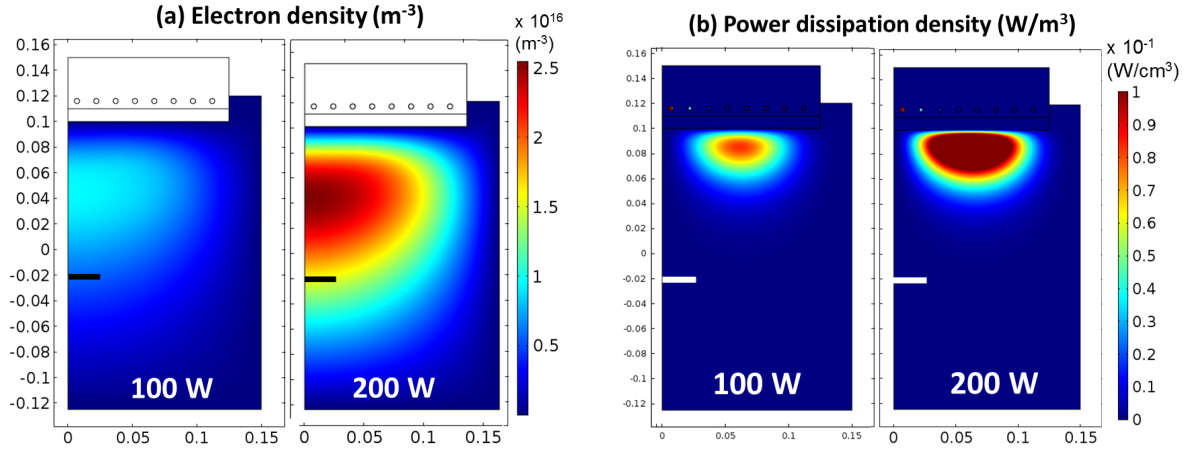

Figure 6.15: CO_2 plasma at zero flow and 2.7 Pa in our plasma reactor. (a) Electron density at 100 and 200 W. (b) Power dissipation density at 100 and 200 W. The substrate location is indicated by the black or white horizontal line.

6.7.4 Comparison with simulation of CO_2 plasma

The above mentioned simulations made on CO_2 plasma at 2.7 Pa can bring further understanding on the estimation of the glow volume which differs from the plasma volume, defined as the region of sufficiently high electron density.

On Figure 6.15a, the simulated electron density can be observed at 100 W and 200 W, with the same color scale. The position of the substrate holder at 12 cm from the quartz window is indicated by a black or a white horizontal line. At low power, it can be seen that the electron density does not overtake $1 \cdot 10^{16}$ m^{-3} or $1 \cdot 10^{10}$ cm^{-3}. At high power, it reaches $2.5 \cdot 10^{10}$ cm^{-3}. In both case, the density is located at the center of the reactor. However, at 200 W, a higher density is reached close to the wall. To our sense, the electron density indicates more or less the plasma volume.

On Figure 6.15b, the power dissipation density is plotted at the same two powers. It can be observed that at higher power, the region of high power dissipation is larger than at low power. The geometry of the region of high power dissipation is close to a toroid, or bluntly said, a doughnut. Comparing to the styrene plasma pictures on Figure 6.9, it is likely that region of high power dissipation corresponds to the glow region, and not to the region of higher electron density (to which corresponds the plasma volume). This is due to the fact that the electric field is the strongest close to the coil due to the skin depth, which elevates the electron temperature close to the quartz window (see Figure 6.16). Indeed, strong power dissipation requires at the same time a high electron density and a high electric field.

The simulation shows an increase of both the glow volume and the plasma volume. Now, it is hard to define a precise boundary from the simulation as in practice. However, the spread of the plasma volume towards the wall seems larger than the one of the glow volume.

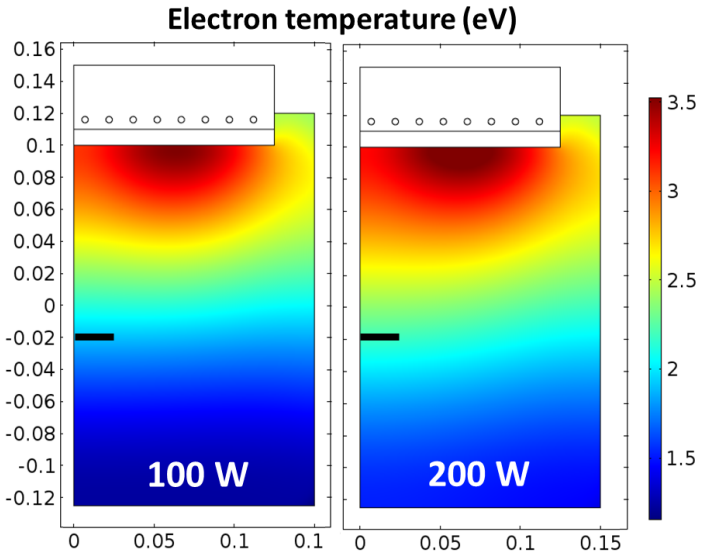

Figure 6.16: CO_2 plasma at zero flow and 2.7 Pa in our plasma reactor: Electron temperature at 100 and 200 W.

6.8 Conclusions

Plasma deposited polystyrene films at the substrate holder location have been characterized for different discharge powers. The deposition rate followed the general trends of the plasma polymerization domains, but revealed a sharp discontinuity at the critical power (Section 6.2). Surface characterization by XPS showed a significant but less sharp evolution of the oxygen uptake and the aromaticity retention at the same transition power (Section 6.3).

Two simultaneous phenomena occurred at the critical power: a transition towards an efficient power coupling (E-to-H transition), known to be accompanied by a large electron density increase (Section 6.4); and a sharp drop of the discharge pressure with an almost complete depletion of the monomer (Section 6.5).

While the effect of the E-to-H could explain the DR discontinuity, the pressure drop also retains our attention (Section 6.7.1). To have such a disappearance of the mass from the gas-phase, a surface is needed close to the location of creation of film-forming species. The investigation of the distribution of mass deposited in the reactor showed that the side-walls

collected the majority of the mass above the critical power (Section 6.6). Therefore, an expansion of the depositing volume up to contact the side walls is proposed. This is consistent with the achievement of full glow conditions: at a critical power, the DR and the pressure stabilizes and the plasma reaches its maximal volume (Section 6.7.2).

Attempt to estimate the depositing volume is qualitatively made by pictures of the styrene discharge (Section 6.5.2) and by estimating the mean free path (Section 6.7.3). Comparison with simulation made in our geometry, but for CO_2 plasma, helped to further discuss the volume expansion and distinguish the plasma volume from the glow/creation volume (Section 6.7.4). The depositing volume has also been proposed to be the glow volume increased by the mean free path of the radicals, spreading out from the glow/creation region (introduction of Section 6.7). This would be needed to explain the DR discontinuity by pressure drop.

To test to which extent the pressure drop affect the DR discontinuity, compared to the E/H transition, we propose:

- to find conditions for which the E/H transition is not simultaneous with a pressure drop, if it is possible;
- to measure an evolution of the DR with time at the critical power at substrate location (Section 6.7.3): the regular decrease of the discharge pressure over 3 minutes should affect the depositing volume expansion;
- to measure deposition distribution in the whole reactor at the same flow but with a lower initial pressure: the objectif would be to detect a different “deposition” volume;
- to simply reduce the distance between the substrate holder and the coil, in an attempt to detect a transition in the DR and accordingly detect a “boundary” of the depositing volume.

Original results could come out from these investigations, by contributing to the advances on the E/H transition in flow polymerizing system and by applying for the first time the full glow hypothesis to polymerizing plasma with planar ICP geometry.

Chapter 7

Identification of neutral stable species in unsaturated hydrocarbon plasmas

The present chapter deals with the identification of species in the plasma of unsaturated hydrocarbons. Due to the mass spectrometer location outside the plasma zone, the detectable species are restrained to neutral closed-shell molecules. As it will be seen, the detection of as many stable neutrals as possible can reveal intermediates of reaction. This is the main objective of the chapter, and will be reached by the advantages of Mass spectrometry (MS): high sensitivity, detection of all species regardless of their electronic excitation and species identification by Threshold Ionization Mass Spectrometry (TIMS).

The main difficulty in determining neutral species by MS lies in their indirect measurement by ionization. Indeed the electron impact on the incoming neutral, often carried out at the standard electron energy of 70 eV, produces an ion with high internal energy. If the initial neutral is not an atom but a polyatomic molecule like a hydrocarbon, the excited ion can dissociate and produce a series of smaller ions. The measured mass spectrum then forms what is called the "**cracking pattern**" (CP), or a set of several peaks, all with m/z ratio below the initial ion's one. In hydrocarbon plasma, several neutral species are produced and all of them have their own CP, which superimpose when acquiring the mass spectrum. To deal with this "peak forest", the great difficulty of the experimentalist resides in the proper interpretation of each observed peak: is it due to a real species existing in the discharge or to the CP of a heavier species? To answer this question, a systematic 2-step approach was followed, inspired by the literature [62, 111, 184, 185].

(i) A set of MS peaks that could indicate species produced in the discharge was established by use of different low ionisation electron energies. (ii) The measurement of the appearance energy (AE) of all the candidate peaks allowed to definitely confirm them or not as neutral species produced in the plasma. The AE is the threshold electron energy at which an ion signal is detected.

After briefly presenting the selected monomers and the plasma conditions, we will demonstrate the interest of performing MS at low electron impact energy. Then we will focus on the measure of the AE of molecules, as well as the AE of the fragment ions dominating the CP of a molecule. The species identification methodology will then be applied to the four monomers. The chapter will end with the comparison of the species detected in the four plasmas and its implication in term of plasma chemistry.

7.1 Selected monomers and plasma conditions

Four different hydrocarbons are studied: styrene, benzene, ethylene and acetylene. Their structures and raw formulae are shown on Figure 7.1. They are all unsaturated hydrocarbons, with an H/C ratio of 2.0 for ethylene and of 1.0 for the three others. Styrene was the primary investigated monomer and is the only one for which the polymerized films have been characterized. The three others were chosen because they can be easily produced from styrene. Indeed the C-C bond between its phenyl group (C_6H_5-) and its vinyl group (CH_2=CH-) is the weakest one. During dissociation, hydrogen atom rearrangement is a common process. The phenyl radical $C_6H_5^\bullet$ can gain H atom to produce benzene. The vinyl radical $C_2H_3^\bullet$ can either gain or loose H atom to produce ethylene or acetylene, respectively.

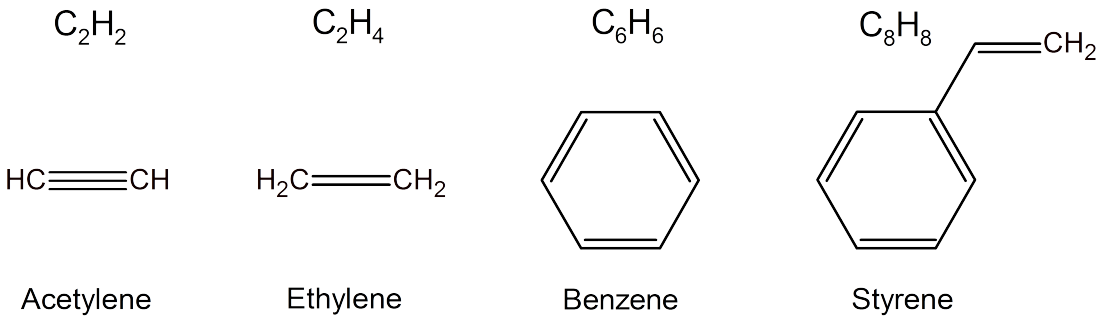

Figure 7.1: Structure and raw formula of acetylene, ethylene, benzene and styrene.

Monomer	**W/F** (eV/monomer)	**Bond energy** (eV/monomer)	**W/FM** (eV/Da)	**W/FM** (10^8 J/kg)
Styrene	80	74	0.77	0.75
Benzene	80	56	1.0	1.0
Ethylene	80	24	2.9	2.8
Acetylene	64	18	2.5	2.4

Table 7.1: Calculation of discharge characteristic ratios based on wattage W (in J/s), molar flow F (in mol/s) and molar mass M (in kg/mol). 28 sccm corresponds to $20.8 \cdot 10^{-6}$ mol/s.

Before plasma ignition, the injection conditions are the same for the four monomers with a pressure of 6.7 Pa and a flow of 28 sccm. Their discharges were carried out at a continuous-wave applied power of 150 W, except for acetylene which required softer conditions at 120 W. The automatic impedance matching system allowed a reflected power of maximum 4 W.

The rough estimation of the internal bond energy per monomer is reminded in Table 7.1 (Section 2.4.1). It can be compared to the mean delivered energy per monomer (W/F) for the four monomers in our conditions (Section 2.4.1). The conditions were chosen to give mass spectra with the most intense signals of the process effluents (see Section 8.3). They may seem quite energetic, but regarding styrene it is below the E/H transition and thus in capacitive coupling which has a moderate coupling efficiency (Section 1.2.3). To ease comparison with data from the literature, the mean delivered energy per mass of injected monomer (W/FM) has been also added in the table.

Each reactor having its own coupling efficiency and its own flow by-passing ratio, it is not straightforward to compare W/FM values between different reactors. However, just to give an indication, for the helical ICP system with no by-pass investigated by Yasuda and Hirotsu [73], W/FM above $2 \cdot 10^8$ J/kg were considered to correspond to quite hard conditions or high "plasma intensity" [80] (p307). In our case and assuming similar coupling efficiency and by-pass ratio (which is not the case, our by-pass can be large), it would indicate that styrene and benzene plasma are carried out with moderate plasma intensity, while ethylene and acetylene with high plasma intensity.

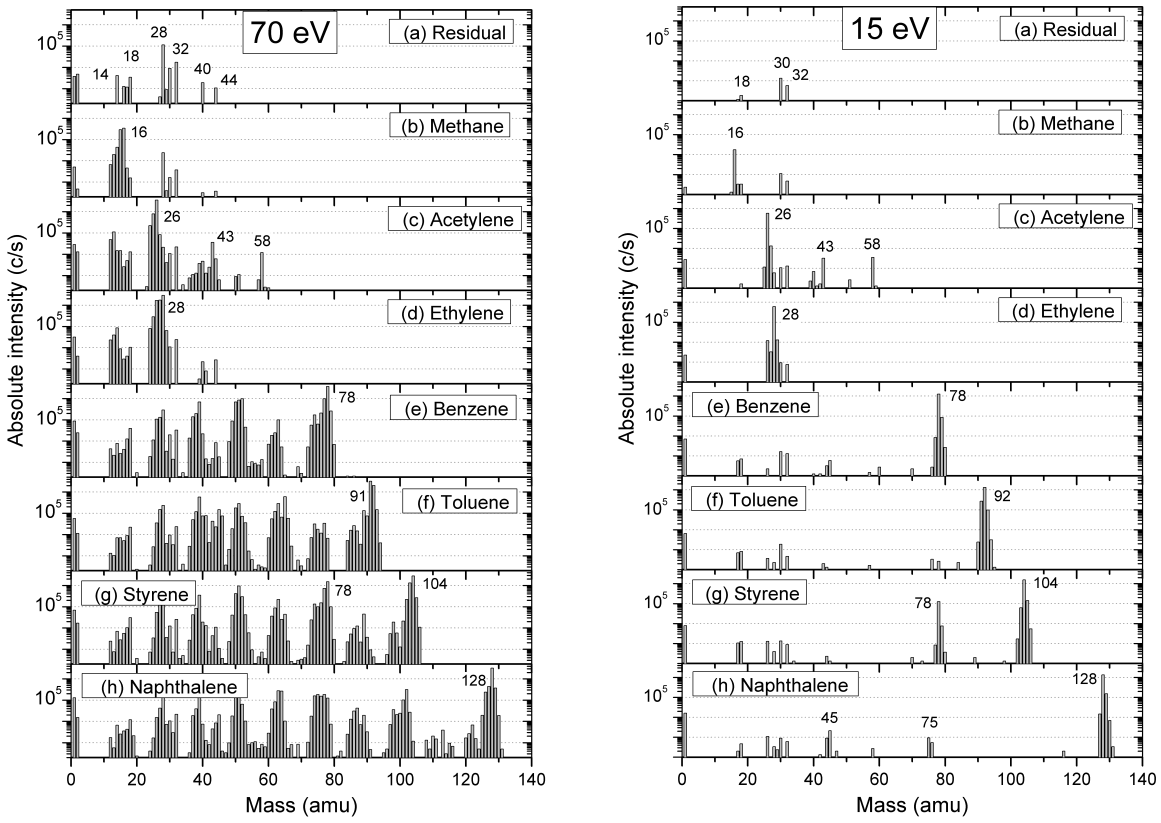

Figure 7.2: Cracking patterns of residual gas and seven pure gases/vapors injected at 6.7 Pa in the reactor: (left) at standard 70 eV electron energy, (right) at 15 eV electron energy.

7.2 Cracking patterns at low electron energy

To demonstrate the interest of working at low electron impact energy, seven gases/vapors were injected pure in the chamber at 6.7 Pa: naphthalene, styrene, toluene, benzene, ethylene, acetylene and methane. Their cracking patterns recorded at the standard ionization electron energy of 70 eV are shown on Figure 7.2-left. Keeping all the other settings constant, their CP were acquired a second time at 15 eV and are shown on the right of the same figure. The comparison of the 70 eV CPs to the ones at 15 eV clearly shows that the fragmentation is drastically reduced at low electron energy. This is partly due to the fact that they are all unsaturated or aromatic compounds, exhibiting high stability in their ionized state [186]. As will be seen, the mass spectra interpretation of hydrocarbon plasma, which are mixtures of gases, will be greatly simplified.

The drawback of working at such low electron energy is that some species yield very weak signals like methane or are plainly invisible like hydrogen, thanks to their respective ionization energies (IEs) of 12.5 eV and 15.4 eV. But this approach becomes interesting to minimize residual gases signals like the one from water H_2O (IE of 12.6 eV) or oxygen O_2 (12.1 eV), or simply to remove any interference from them like for nitrogen N2 (15.6 eV) and Ar (15.8 eV). This can be seen by comparing the mass spectrum of the residual gas at 70 eV and at 15 eV, on Figure 7.2a-left and -right respectively. By the way, at 15 eV, the residual gas peaks are: m/z = 18 assigned to H_2O+ and 32 to O_2^+. The unusual m/z = 30 peak is assigned to COH_2^+, that may come from residual acetone or formaldehyde. They can be seen in almost all the MS of the seven gases/vapors at 15 eV.

The last interesting feature lies in the intensities of the molecular ions. With our settings and at the same pressure in the reactor, they are very similar: just above 6 Mc/s for the four heaviest and just below 6 Mc/s for ethylene and acetylene. The only exceptions are methane with 20 kc/s and hydrogen which produces no signal. As other hydrocarbons like 1-propynyl-benzene (m/z = 130), the 1-butynyl-benzene (m/z = 116) or phenyl hexane (m/z = 162) gave also intensities close to 6 Mc/s in our system (not shown here), it is expected that other hydrocarbons yield similar intensities. This fortunate "**almost constant intensity" of the molecular ion peaks at 15 eV** can be explained by three considerations.

- Firstly, the transmission of quadrupole decreases with the mass of the ions [91, 187].
- Secondly the total ionization cross section is known to follow an "additivity rule": at the same electron energy, the cross section of a large compound can be estimated by adding the known cross sections of its different smaller parts (as seen in Section 3.1) [91, 92]. Established for electron energies ranging from 1.2 keV to 75 eV, an extension towards smaller energies seems probable.
- Thirdly, as the fragmentation is very low for highly unsaturated hydrocarbon at 15 eV, almost all the total ion intensity is concentrated in the molecular ion peak: indeed the "additivity rule" is established for the total ionization cross section and not for a single ion decomposition channel.

As a conclusion, for increasing mass, the decrease of quadrupole transmission seems compensated by an increase of the ionization cross section, mainly concentrated in the molecular ion production cross section. Hence, when discussing the mass spectra during plasmas, **high intensities will roughly indicate high partial pressures**. The individual intensity of one gas in a gas mixture is indeed generally considered proportional to its partial pressure [13].

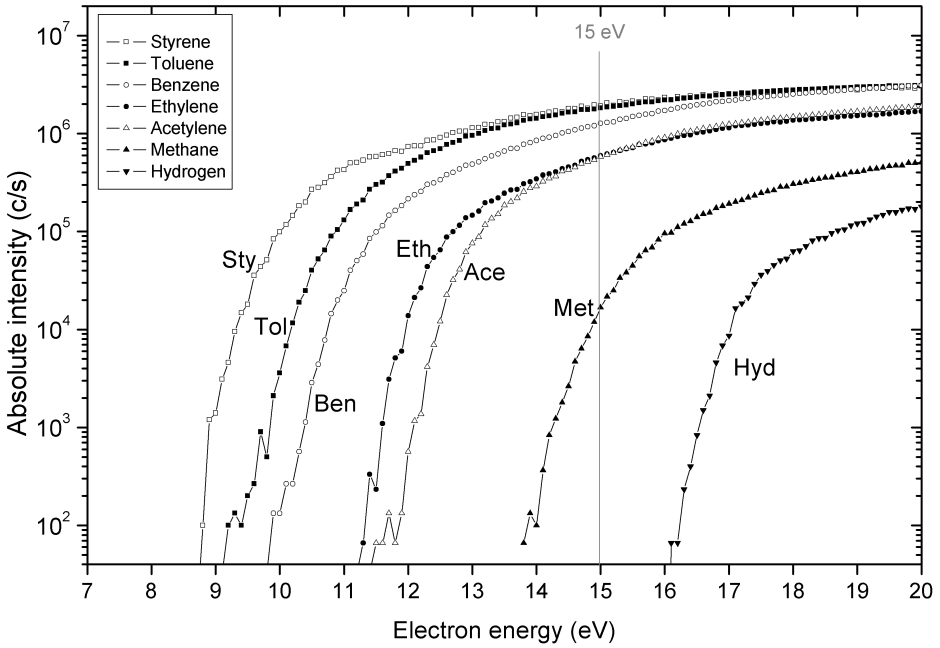

Figure 7.3: Non-corrected measured electron energy spectra at 10 μA of hydrogen (m/z = 2) and six hydrocarbons: styrene (m/z = 104), toluene (m/z = 92), benzene (78), ethylene (28), acetylene (26) and methane (16).

7.3 Appearance energy

7.3.1 Ionization energy of hydrocarbons

In the case of the molecular ion, the appearance energy (AE) is a measure of the ionization energy (IE) of the parent neutral. For hydrocarbons, the IE usually tends to decrease with an increasing number of carbon atoms in the molecules [13]. Figure 7.3 illustrates this aspect with the measured electron energy spectra (EES) of hydrogen and the above mentioned hydrocarbon gases/vapors, except naphthalene. The spectra are shown just above the noise signal at around 40 c/s. The IEs are simply measured at the electron energies for which the curves intersect the X axis (40 c/s). On the figure, the IEs clearly decrease with the mass of the gas. It is also interesting to note that the slopes at 15 eV are relatively low for hydrocarbons with masses higher than 26 amu. This means that small variations in the electron beam energy will have only a moderate effect on their observed intensity.

Reminding Section 5.3.8, the measured IEs are systematically shifted of 0.6 ± 0.2 eV towards higher energy compared to the theoretical IE, at the time of the currently presented results. All

the measured IEs/AEs are reduced by 0.6 eV in the present chapter, but an overestimation of the IE/AE up to 1.0 eV is likely to occur for small signals.

7.3.2 Criterion for detection of molecular ion in unsaturated hydrocarbon plasma

The aim of the rest of the present section is now to establish an important criterion for our overall objective: distinguish a molecular ion peak from a fragment ion peak in the mass spectrum of an unknown gas mixture, like a hydrocarbon plasma. To this goal, we must remind two features from the Chapter 3 on Electron Ionization. All the sections mentioned below referred to that chapter.

- In the CP of a single compound, we have seen two kinds of fragment ions in the case of zero nitrogen containing species (see nitrogen rule, Section 3.5): either odd mass fragment ions which are obtained by direct cleavage of bonds, via the "loose" complex; or even mass fragment ions which are obtained by decomposition with rearrangement, via the "tight" complex (Section 3.4.2).
- A typical feature of the even mass fragment ions (tight decomposition) is a possible low AE, thanks to a net number of cleaved bonds which is equal to zero (Section 3.4.4).

However, this second feature is not observed for highly unsaturated hydrocarbons, as we show it now. Figure 7.4 exhibits the non-corrected electron energy spectra of different peaks from the cracking pattern (CP) of pure styrene vapor. Several observations can be made:

- The odd mass fragment ions at m/z = 1 and m/z = 103 have low AE, very close to the IE of styrene (within 1 eV of energy difference). This may be surprising as the energy required to break a bond is around 3 to 4 eV. However electronic structure reorganization in the dissociation products may provide this energy [13]. Furthermore less energy is generally needed to ionize a radical and then produce a closed-shell ion (see table A.3 in ref [13], p278).
- The even mass fragment ions at m/z = 26, 78 and 102 have AE at least 2 eV above the AE of the styrene ion. This is rather surprising because the C-C bond between the vinyl and the phenyl groups (C_2H_3-C_6H_5) is the weakest and because H rearrangement are usually easily occurring. Apparently, the rearrangement decomposition channel requires a significant amount energy to occur.

What is important is that the same minimal energy shift for the AE of even mass ions was observed for other highly unsaturated hydrocarbons, like benzene, acetylene and toluene, and

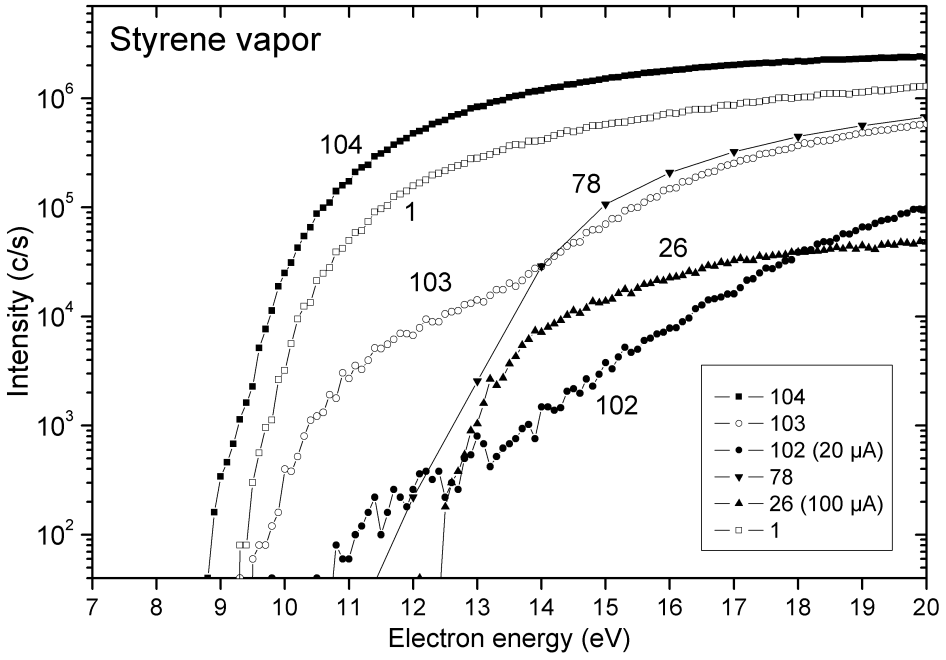

Figure 7.4: Non-corrected measured electron energy spectra of peaks of the styrene cracking pattern, acquired at 10 µA, excepted for m/z = 102 at 20 µA and m/z = 26 at 100 µA.

even for ethylene which is less unsaturated. This important observation will be used to discuss the even mass peaks measured during hydrocarbon plasmas. Thereby, an "AE criterion for molecular ion" is stated as follows:

An even mass peak with sufficiently low AE corresponds to a molecular ion in the case of highly unsaturated hydrocarbons

7.4 Species identification

In this section, we will systematically compare the mass spectra with no discharge at several low electron energies to the mass spectra under plasma conditions. The aim is to identify as many neutral closed-shell species as possible, by detecting in the spectra a maximum of molecular ion peaks, which have even m/z ratios. As already said, the radicals are not considered because of the distant location of the spectrometer from the plasma and hence the odd m/z peaks are neglected. The first plasma investigated, the one of styrene, will serve to establish the methodology in details. The three next plasmas – benzene, acetylene and ethylene – will be presented more briefly.

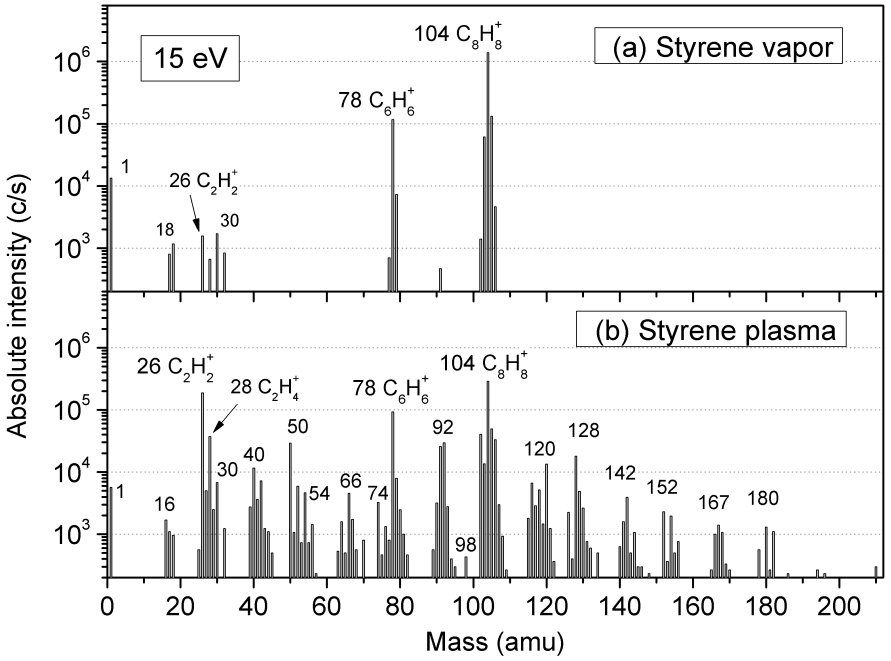

Figure 7.5: Mass spectra at 15 eV and 10 μA of styrene: (a) vapor at 6.7 Pa, (b) plasma at 6.7 Pa, 28 sccm, 150 W.

7.4.1 Styrene plasma

Figure 7.5a shows the vapor mass spectrum (VMS) by electron impact at 15 eV of styrene at 6.7 Pa. The molecular ion peak is observed at m/z = 104 amu. Even at such a low electron energy, fragmentation inside the mass spectrometer still occurs as the peak at m/z = 78 amu appears, assigned to the ion $C_6H_6^+$. Peak at m/z = 1 amu is attributed to ion H^+ and at m/z = 26 to $C_2H_2^+$. On either side of the m/z = 104, often referred as the M peak, we observed that M± 2 peaks (m/z = 106 and 102) are 2 orders of magnitude lower than the M peak. M±1 peaks have odd m/z ratio and are not discussed. The other last peaks at m/z = 18, 28, 30 and 32 are observed at 15 eV in the residual gas mass spectrum on Figure 7.2 a-right.

When switching the plasma on, at 150 W at continuous-wave (CW), the styrene plasma mass spectrum (PMS) at 15 eV is shown on Figure 7.5b. It reveals three main features compared to Figure 7.5a: (i) a strong decrease of the molecular ion signal at m/z = 104, (ii) a very weak decrease of the peak at m/z = 78 and (iii) the appearance of a series of new peaks.

To quantify the diminution of the molecular ion peak, we defined the "**monomer depletion**" (MD) as:

$$MD = \frac{I_{104}^{off} - I_{104}^{on}}{I_{104}^{off}}.100\% \tag{7.1}$$

where I_{104}^{off} is the intensity of the molecular ion without plasma and I_{104}^{on}n is the same intensity when the plasma is on. The MD depends on the experimental conditions and usually increases with power and reaches 79% in the present conditions. In the literature, a similar indicator has been found and is referred as "depletion" [188], "decomposition fraction" [189] or "fragmentation degree" [190]. The two latter names seem inappropriate in our setup because the monomer decrease can be due as well to fragmentation than to deposition without fragmentation on the surrounding surfaces. The signal at m/z = 78 is barely not decreasing. The signal ratio of 78/104 increases from 8% without plasma to 32% with plasma. This clearly indicates that benzene is produced in the discharge.

The number of new peaks with even m/z number that appeared in the styrene PMS is important. From the styrene VMS at 15 eV, we conclude that M±2 signals that diminishes less than 2 orders of magnitude below the M signal must be taken into account. This enables to count 44 new peaks with even m/z, ignoring signals below 300 c/s. We saw in section 7.2 that fragmentation is low at 15 eV. Those 44 peaks then seriously indicate the presence of neutral species produced in the plasma, which undergo direct ionization in the ionization chamber. To make it clear, the main part of the $C_2H_2^+$ ion signal measured at m/z = 26 for instance should come from neutral C_2H_2 existing in the plasma. Only a minor part of it may come from the fragmentation of a heavier species inside the mass spectrometer.

Styrene plasma mass spectrum at 12 eV

Hydrocarbons with four C atoms and more usually have IE below 10 eV [13]. Hence, to go further, we acquired the mass spectra at 12 eV, shown on Figure 7.6a. The styrene VMS shows almost a single peak, at the exception of the M+1 peak due to the well-known molecules containing one ^{13}C isotope [13]. Compared to the 15 eV, the PMS at 12 eV Figure 7.6b shows with no surprise peaks that disappear or drastically diminish below m/z = 50 due to the higher IE of light species [13]. Above this m/z ratio, we observe **five features**:

(i) confirmation of the prevalence of the even m/z peaks, like the series at m/z = 50, 52, 54 and 56 for instance;

(ii) confirmation for different peaks which were ambiguous at 15 eV as peak due to neutral species in the plasma at m/z = 82, 90, 94, 106, 130 and 132;

(iii) the neat decrease of the m/z = 167 peak shows that peak with m/z = 166 and 168 are serious candidate for neutral species;

(iv) decrease below 200 c/s (but no complete disappearance) for m/z = 98 and 178;

(v) enhancement of the peaks at m/z = 110, 134, 192, 194, 208, 210.

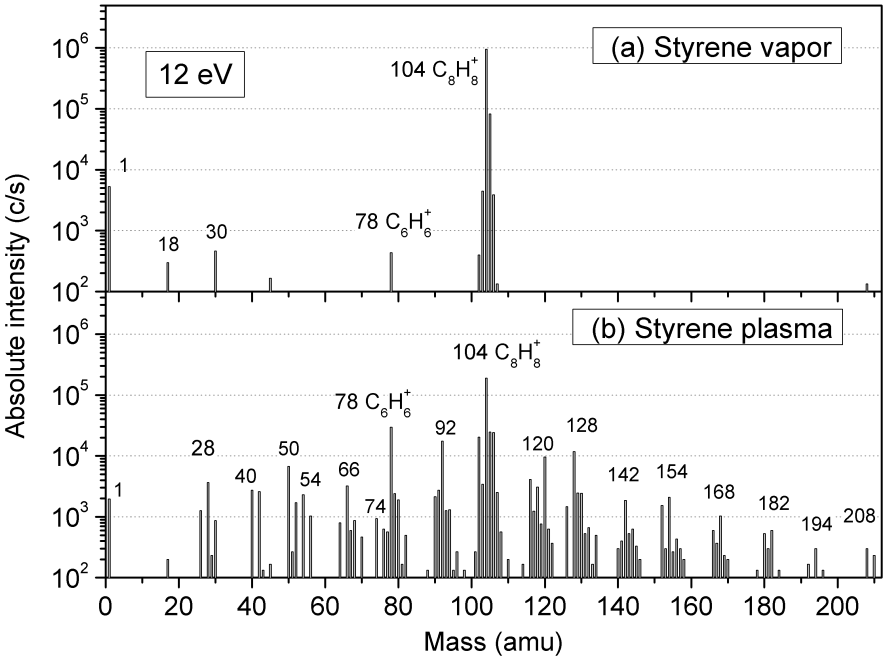

Figure 7.6: Mass spectra at 12 eV and 50 μA of styrene: (a) vapor at 6.7 Pa, (b) plasma at 6.7 Pa, 26 sccm and 150 W.

In addition to 12 eV measurement, we also recorded the styrene PMS at 20 eV (not shown here), which shows a strong peak at m/z = 2. This indicates a significant production of neutral H_2, for which the ionization potential is 15.4 eV. Including m/z = 104, 78, 166, 168 and 2, we therefore have a list of 55 peaks that seriously indicate the presence of numerous neutral species in the styrene plasma.

Appearance energies in styrene plasma

To evaluate if the 55 peaks are definitely due to neutral species, we measured their AEs while the plasma was turned on. The signal below 10^5 c/s in the 15 eV PMS, were taken with emission current of 100 μA to enhance their EES intensity and to minimize the AE over-estimation of weak signals (Section 5.3.8). The intense peaks with signals above 10^5 c/s were recorded at 20 or 10 μA chosen in order to prevent the SEM detector saturation. The corrected values of all their AEs are summarized in the fourth column of Table 7.2 for the styrene plasma. No indicated AE means that no signal was measured. For comparison, we added in the last column ionization energies of one or several isomers for the corresponding chemical formula. Above m/z = 50, all the corrected AE values are below 10.0 eV. In our sense, this is sufficiently low to fulfil the "AE

criterion for molecular ion" (Section 7.3.2). Hence this comforts us in the fact that the 55 peaks are actually due to the direct ionization of neutral species produced in the plasma.

The species detected are all **unsaturated hydrocarbons**. The determination of the **isomer** forms for each raw chemical formula is out of the scope of the present study. The number of isomers increases considerably with mass, which complicates any attempt of isomer identification from simple chemical considerations. Moreover, a priori deduction of isomer may lead to wrong conclusion, as highlighted by Güthe *et al.* [191]. Their work allows to exclude naphthalene isomer for the m/z = 128 species in a benzene discharge, for which it would have been highly expected. Furthermore, several isomers can coexist in the plasma for a given mass. Therefore, starting from here, we will indicate each of the identified peaks by its assigned chemical formula followed by its m/z value between brackets, but for convenience we will refer to it as a single species in the text.

In the literature, identification of species in styrene plasma was mainly carried out by Optical Emission Spectroscopy (OES) and MS [62, 111, 113, 116, 117]. OES revealed H, H_2, CH, C_2, N_2, $C_4H_2^+$ and C_6H_6 [116–118], from which only H_2 (2) and C_6H_6 (78) are neutral closed-shell species. Working at 25 eV of electron energy, Ferreiro *et al.* stated seven neutral closed-shell species by MS: C_2H_2 (26), C_2H_4 (28), C_3H_4 (40), C_6H_6 (78), C_8H_6 (102), C_8H_{10} (106) and $C_{10}H_8$ (128) [111]. Decreasing electron energy down to 20 eV, Beck *et al.* detected four neutral species, but only one is new: C_4H_2 (50) [62]. The remaining works carried out at 70 eV did not detect any other species [113, 116]. To summarize, 10 closed-shell species were already observed, including styrene. Comparatively, the present work confirmed these 10 species, and with stronger evidence. In addition, **45 never reported species are identified**. The observation of new species can either be due to the difference of geometry (planar ICP in our case), and/or to the position of the mass spectrometer in post-discharge in our case, and/or to deeper analysis.

N°	m/z	Assigned chemical formula	Corrected Appearance Energy in plasma (eV)				Ionization Energy (eV) [13, 192]
			Styrene	Benzene	Ethylene	Acetylene	
1	2	H_2	15.1	15.1	15.1	15.2	15.4
2	16	CH_4	13.0	13.1	13.1	13.6	12.5
3	26	C_2H_2	11.0	11.2	11.2	11.1	11.4
4	28	C_2H_4	10.4	10.5	10.5	11.2	10.5
5	30	C_2H_6	11.8	12.5	12.2	12.3	11.5
6	40	C_3H_4	10.1	10.0	10.1	10.5	9.7 / 10.4
7	42	C_3H_6	9.7	10.1	10.1	10.4	9.7
8	44	C_3H_8	11.6	-	11.4	-	11.0
9	50	C_4H_2	9.9	10.2	10.3	10.0	10.2 (diacetylene)
10	52	C_4H_4	9.6	10.0	9.7	10.1	
11	54	C_4H_6	9.3	9.8	9.6	10.2	9.6 / 9.1
12	56	C_4H_8	9.5	9.9	9.7	-	9.6 / 9.2 / 9.1
13	64	C_5H_4	9.7	9.9	10.0	10.2	
14	66	C_5H_6	8.9	9.1	9.1	9.3	
15	68	C_5H_8	9.4	9.3	9.5	-	
16	70	C_5H_{10}	9.8	9.7	9.6	-	
17	74	C_6H_2	9.7	9.9	10.2	9.7	9.6
18	76	C_6H_4	9.4	9.8	9.7	9.8	
19	78	C_6H_6	9.2	8.7	9.5	9.8	9.2 (benzene)
20	80	C_6H_8	8.9	8.9	9.1	-	
21	82	C_6H_{10}	9.2	9.2	9.4	-	
22	90	C_7H_6	8.8	-	9.9	9.9	
23	92	C_7H_8	8.5	8.8	9.2	10.1	8.8 (toluene)
24	94	C_7H_{10}	8.6	8.9	9.1	-	
25	96	C_7H_{12}	9.3	9.3	-	-	
26	98	C_8H_2	9.6	-	-	9.6	
27	100	C_8H_4	-	-	-	9.8	
28	102	C_8H_6	8.8	9.4	9.8	9.7	8.8 (phenylacetylene)
29	104	C_8H_8	8.2	8.8	9.5	9.6	8.4 (styrene)
30	106	C_8H_{10}	8.3	9.1	9.3	-	
31	108	C_8H_{12}	8.6	-	9.3*	-	
32	110	C_8H_{14}	9.1	-	-	-	
33	116	C_9H_8	8.5	9.2	9.2	10.2*	
34	118	C_9H_{10}	8.3	9.7	9.4	-	
35	120	C_9H_{12}	8.3	10.4*	9.2	-	
36	126	$C_{10}H_6$	9.2	10.3*	-	9.9*	
37	128	$C_{10}H_8$	8.3	8.8	9.1	9.5*	8.1 (naphthalene)
38	130	$C_{10}H_{10}$	8.5	9.1	9.0	-	
39	132	$C_{10}H_{12}$	8.8	9.3	9.4*	-	
40	134	$C_{10}H_{14}$	8.9	9.5*	-	-	
41	140	$C_{11}H_8$	8.9	-	-	-	
42	142	$C_{11}H_{10}$	8.4	8.9	9.4*	-	
43	144	$C_{11}H_{12}$	8.5	9.2	9.5*	-	
44	146	$C_{11}H_{14}$	9.0	9.5	-	-	
45	152	$C_{12}H_8$	8.3	8.6	-	-	
46	154	$C_{12}H_{10}$	8.4	8.5	-	-	
47	156	$C_{12}H_{12}$	8.5	8.6	9.9*	-	7.5 (anthracene)
48	166	$C_{13}H_{10}$	8.4	8.8	-	-	
49	168	$C_{13}H_{12}$	8.5	8.8	-	-	
50	178	$C_{14}H_{10}$	8.7	10.2*	-	-	
51	180	$C_{14}H_{12}$	8.4	8.9	-	-	
52	182	$C_{14}H_{16}$	8.5	9.0	-	-	
53	192	$C_{15}H_{14}$	9.0	-	-	-	
54	194	$C_{15}H_{16}$	8.7	-	-	-	
55	208	$C_{16}H_{18}$	8.5	-	-	-	
56	210	$C_{16}H_{20}$	8.7	-	-	-	

Table 7.2: List of the investigated neutral species in the styrene, benzene, ethylene and acetylene plasmas based on MS at 12, 15 and 20 eV. Corrected measured appearance energies (cell with hyphen means no signal was measured). The * denotes very weak signal probably having AE overestimation risk close to 1.0 eV, as seen in Section 5.3.8.

From all the identified neutral by-products in the styrene plasma, several features can be highlighted.

- From the 15 eV PMS, 10 species dominate the spectrum and should have the highest partial pressures: C_2H_2 (26), C_2H_4 (28), C_4H_2 (50), C_6H_6 (78), C_7H_8 (92), C_8H_6 (102), C_8H_{10} (106), C_9H_{12} (120), $C_{10}H_8$ (128) and of course C_8H_8 (104).
- Both fragmentation and plasma state polymerization of styrene occur in the gas phase.
- Species with every numbers of carbon atoms are present: C_1, C_2, C_3,..., up to C_{14}. In each mass sub-region, the dominant species is highly unsaturated: C_2H_2 (26), C_3H_4 (40), C_4H_2 (50), ..., up to $C_{14}H_{12}$ (180). These two observations suggest that radicals with one carbon atom and low H content are likely to participate to species production, like methylene radical CH_2, the $CH^\bullet$ and/or the $C^\bullet$ radicals. The two latter were observed in our experiment by OES [118].
- In the high mass region, above m/z = 104, the decreasing intensities with increasing number of carbon atom indicate that their partial pressures diminish with size. This strongly suggests that they are successively produced by the repeated addition of a one carbon atom radical. On the contrary, association of two activated styrene monomers is not likely to occur, as can be seen from the very low intensity of peaks with 16 carbon atoms around m/z = 208.
- In the low mass region, below m/z = 104, species with even C atom number dominates slightly. This may be explained simply for C_2H_2 (26), C_2H_4 (28) and C_6H_6 (78) by similarity with the unimolecular ion decomposition: a cleavage of the weakest C-C bond in the styrene monomer under electron impact of a few eV, accompanied by H rearrangement during the dissociation. For diacetylene C_4H_2 (50), a reaction between C_2H_2 and an ethynyl radical $C_2H^\bullet$ is the most likely mechanism to explain its significant production (as will be discussed in the acetylene plasma section below). But the C_2 radical should be considered as it has been observed in our plasma by OES [118]. The fully saturated methane CH_4 (16) produced in the discharge can be explained by the significant presence of H_2 (2) seen in the 20 eV PMS.

7.4.2 Benzene plasma

Without plasma, the benzene VMS in Figure 7.7a shows peaks at m/z = 78 and 1, assigned respectively to $C_6H_6^+$ and H^+. Peaks at m/z = 18, 30 and 32 are due to residual gases. When plasma is ignited (Figure 7.7b), the reduction of the molecular ion peak of benzene allows one to

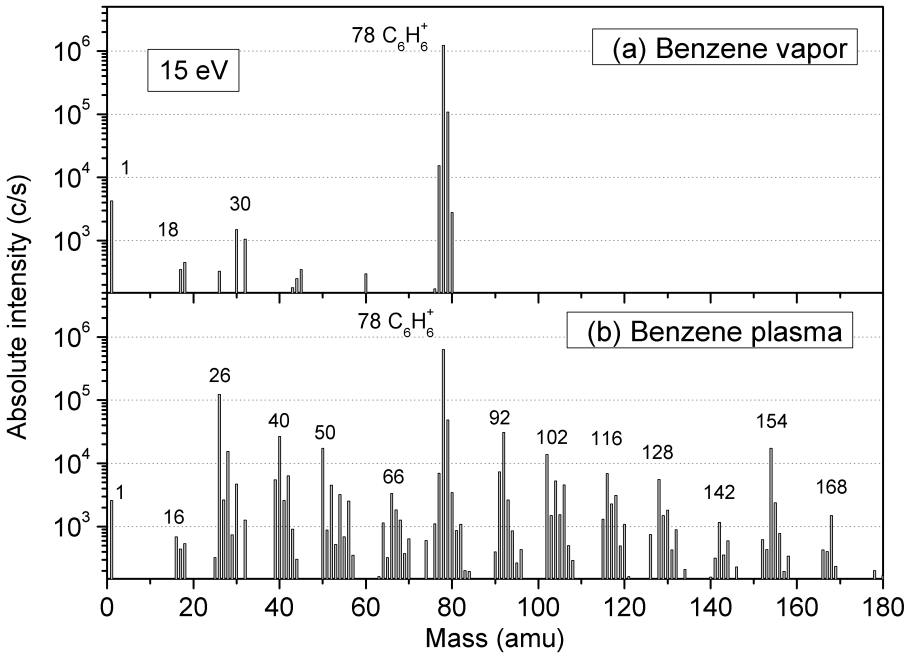

Figure 7.7: Mass spectra at 15 eV of benzene: (a) vapor at 6.7 Pa, (b) plasma at 6.7 Pa, 28 sccm and 150 W.

measure a benzene depletion of 58%. It shows a better stability than styrene which reaches 79% depletion in the same conditions. Moreover numerous new even m/z peaks appeared. The six most intense peaks are at m/z = 26 assigned to $C_2H_2^+$, 28 to $C_2H_4^+$, 40 to $C_3H_4^+$, 50 to $C_4H_2^+$, 92 to $C_7H_8^+$ and 154 to $C_{12}H_{10}^+$.

As for styrene, we acquired the benzene PMS at 12 eV (not shown here). Combined with the 15 eV PMS, it allowed to identify 44 even m/z peaks indicating a likely production of neutral species in the plasma. All their measured and corrected AEs are listed in the fifth column of table of Figure 7.2. As can be seen, their corrected AEs are almost all below 10.0 eV starting from m/z = 54. This confirmed them to originate from direct ionization in the ionization chamber of stable closed-shell species coming from the benzene plasma. However the AE of signals above m/z = 100 show a systematic increase comparatively to styrene plasma, especially at m/z = 120 and 126 peaks with a corrected AE above 10.0 eV. A close look to the benzene PMS at 15 eV shows that many of those signals are one order of magnitude below the same m/z signal during the styrene plasma. The overestimation risk of the AE we highlighted for weak signals in Section 5.3.8 may then explain an increase up to 1.0 eV. Moreover different isomers can exhibit differences in their IE up to 0.7 eV (see ionization energy of C_3H_4). With this in mind, the only signal we excluded from being due to neutral species in the plasma is at m/z = 120, because of its

increase of 2.1 eV with respect to styrene plasma. Finally, the PMS at 20 eV showed an intense peak at m/z = 2 indicating strong hydrogen production. To conclude for benzene, 44 peaks indicate production of 44 stable closed-shell species in the benzene plasma, including hydrogen and benzene and excluding the m/z = 120 peak.

Discussion of benzene plasma species

Three works report on species identification in pure benzene discharge [193–195]. Biphenyl (m/z = 154) reported by Weisbeck can likely correspond to our species $C_{12}H_{10}$ (154), by far the dominant species in its mass region [193]. Duval determined several optical lines and bands due to 6 radicals – H, CH, C_2, C_2H, C_7H_7 and C_6H_4 – and excited benzene [194]. Smolinsky and Vasile also studied benzene discharge by MS, at 20 eV electron energy for the neutral but reported none of them [195]. Other studies were carried out with benzene diluted in noble gases. In the case of argon discharge with around 1% or 10% of benzene, Shih identified acetylene and a list of 21 polycyclic aromatic hydrocarbons (PAHs) [189, 196], starting from the 2-ring naphthalene (128) to a 7-ring coronene ($C_{24}H_{12}$ - 300). The five species we could have in common are then acetylene (26), naphthalene (128), acenaphthylene (C_12H_8 - 152), acenaphthene ($C_{12}H_{10}$ - 154), phenanthrene ($C_{14}H_{10}$ - 178) and anthracene ($C_{14}H_{10}$ - 178). They deduced from their observation that the formation of PAHs proceeds mainly by the hydrogen abstraction and the HACA mechanism, as, unlike us, they did not seem to observe other species than acetylene, benzene and the PAHs. HACA or "hydrogen abstraction and C_2H_2-addition" is a mechanism, established in hydrocarbon flames, which explains the growth of particle in the flame-phase via the following two-step reaction [197]:

1) a hydrocarbon reacts with a $H^\bullet$ radical and yields one of its H atom to form H_2 and a hydrocarbon radical: M-H + $H^\bullet$ → $M^\bullet$ + H_2
2) the hydrocarbon radical reacts with an acetylene molecule and forms products, which can be a $H^\bullet$ radical and its closed-shell counterpart: $M^\bullet$ + C_2H_2 → M-C_2H + $H^\bullet$.

For benzene also diluted in argon, the MS of neutral species of Niinomi [198], most probably recorded at 70 eV, showed intense peaks at the even m/z = 26, 78, 102 and 154, that could correspond to our observed species. Finally, Güthe observed so many species by resonant two photon ionization spectroscopy, that comparison is difficult [191]. However their special reactor design probably allows inaccessible processes for usual low-pressure discharges, thanks to the gas expansion from a several bar chamber. Neglecting this last report, 7 species of the present study are in common with the already reported neutrals: C_2H_2 (26), C_6H_6 (78), C_8H_6 (102),

$C_{10}H_8$ (128), $C_{12}H_8$ (152), $C_{12}H_{10}$ (154) and two isomer forms of $C_{14}H_{10}$ (178). Therefore **37 new closed-shell neutral species are detected**.

In our case, the set of the observed species requires other mechanisms in addition to the HACA mechanism. As for styrene, the observation of unsaturated species containing all number of carbon atoms, from C_1 to C_{10}, very likely indicates radical intermediates containing one carbon atom and low H content, like methylene CH_2, CH or C. This is supported by the radicals observed by Duval [194]. Furthermore the high intensity of $C_{12}H_{10}$ (154), also observed by Weisbeck, Shih and Niinomi, indicates a likely reaction between 2 one-ring species, possibly benzene itself or the phenyl radical $C_6H_5^{\bullet}$.

7.4.3 Acetylene plasma

The 15 eV VMS of acetylene shows several peaks due to acetone, which are at m/z = 40, 43, 51 and 58 (Figure 7.8a). Indeed, as acetylene is unstable at high pressure in gas bottle, acetone is used as a stabilizer [199]. Acetone is well detected despite its concentration below 0.5% because its IE (9.7 eV) is 1.7 eV lower than acetylene IE (11.4 eV). Otherwise the CP of acetylene is very simple with its molecular ion peak at m/z = 26 and secondary peak at m/z = 1 due to H^+ production in the ionization chamber. Peaks at m/z = 18, 30 and 32 are due to the usual residual gas peaks.

Concerning the acetylene discharge, the monomer depletion and the pressure drop were so important at 150 W that we present here results at 120 W. When the discharge is switched on, the 15 eV acetylene PMS on Figure 7.8b revealed a MD of 59% for acetylene and a decrease of 70% for acetone. The PMS is very simple in contrast with styrene and benzene plasmas. 13 new peaks appeared and the signals at m/z = 28, 40, 42 and 45 increases slightly. At 20 eV, a moderate peak at m/z = 2 appeared as well. At 12 eV, 6 new peaks were highlighted at m/z = 54, 90, 92, 104, 116 and 126. Therefore the EES of 23 selected peaks was acquired, including m/z = 26 but excluding m/z = 45 which is an odd m/z peak. Their corrected measured AEs are shown in the 7th column of table of Figure 7.2.

For several peaks, it is not straightforward to conclude for production of neutral species in the plasma. For m/z = 40, the measured AE is equal to the AE due to acetone. However the neat increase of its signal from 1600 c/s to 8200 c/s and the decrease of acetone bring us to consider the production of C_3H_4 in the plasma. For the slightly increasing peak at m/ = 28, its AE is 0.8 eV higher than the one of ethylene. However the acetylene contribution to this peak is definitely not responsible of all the intensity, as it should be reduced comparatively to the

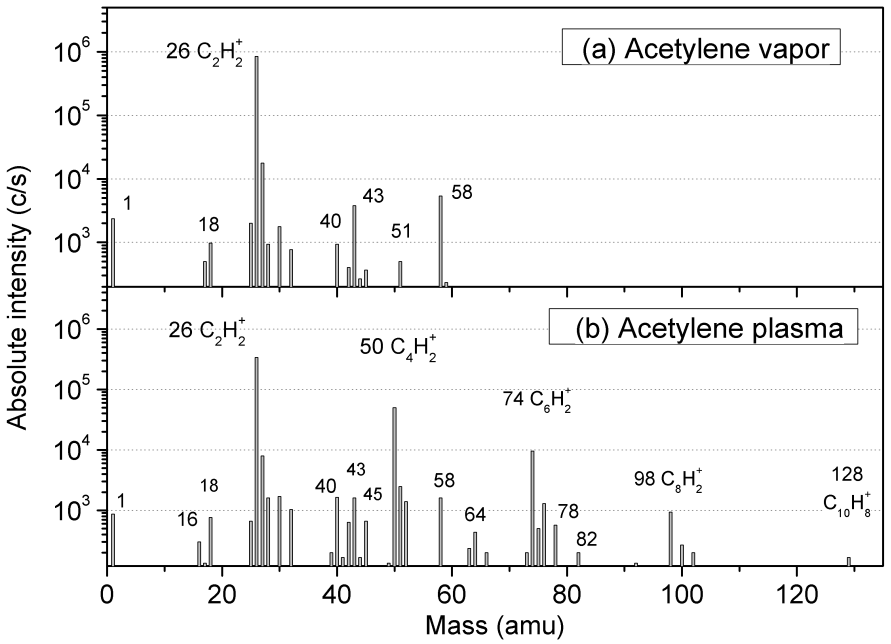

Figure 7.8: Mass spectra at 15 eV of acetylene: (a) vapor at 6.7 Pa, (b) plasma at 6.7 Pa, 28 sccm but only 120 W.

vapor case. Furthermore the signal is weak and can then suffer the overestimation risk of the AE observed in Section 5.3.8. We therefore estimate that a small production of C_2H_4 is likely in the discharge, especially as a moderate H_2 production has been confirmed. The m/z = 42 AE confirmed as well a small C_3H_6 production. Hence 23 closed-shell species are stated for the acetylene plasma, including acetylene itself.

Discussion of acetylene plasma species

Either in pure acetylene vapor or with acetylene mixed with noble gases, numerous works report neutral closed-shell species by MS [55, 185, 188, 199–203]. H_2 was identified in four of them [188, 200, 204, 205]. Polyyne species $C_{2n}H_2$ (wrongly called polyacetylene in many papers) were almost always reported, only with n = 1 and 2 for some works, up to n = 5 for Platzner *et al.* [201]. Otherwise, to our knowledge, only three groups observed other species. In addition to 13 neutral radicals including carbenes, Benedikt *et al.* confirmed by Threshold Ionization Mass Spectrometry (TIMS) 5 species in expanding thermal plasma of acetylene with Argon: methane (16), C_3H_4 (40), C_5H_4 (64), C_5H_6 (66) and C_6H_6 (78) [185]. In another work, they also reported 6 extra species by MS at 70 eV, but with no mention of TIMS measurement, in a combined capacitive and inductive reactor: C_4H_4 (52), C_6H_4 (76), C_8H_6 (102), $C_{10}H_6$ (126),

$C_{10}H_8$ (128) and $C_{12}H_{10}$ (152) [199]. In the same group, Consoli *et al.* observed C_2H_4 (28) and C_3H_6 (42) [202]. In the continuous-wave mode of a pure acetylene magnetron discharge, De Vriendt *et al.* observed no new species below 100 amu [205]. However, when the plasma is pulsed, heavier hydrocarbons are observed and particularly an important series of PAHs between 350 and 460 amu is revealed. To sum up, 17 of the 23 neutral closed-shell species we observed were already reported in the literature. We therefore **measured 6 new species**, but did not observe $C_{10}H_2$ (122), $C_{12}H_8$ (152) nor PAHs above 160 amu.

What strikes the most with acetylene PMS is the lack or very low intensity of species with an odd number of C atoms. This strongly indicates that one carbon atom radicals are not likely to be produced and to work as intermediate polymerizing species. The three polymerization products observed at m/z = 50, 74 and 98 are assigned to polyyne species $C_{2n}H_2$. They are consistent with those observed in the literature [188, 199, 201, 202, 204–207]. To account for their production in the gas phase, the simplest radical is the ethynyl radical $C_2H^\bullet$ [199]. The production of diacetylene C_4H_2 (m/z = 50) can hence be explained via the following reaction: $C_2H_2 + C_2H^\bullet \rightarrow C_4H_2 + H^\bullet$. At first proposed for combustion of acetylene [208–210], the reaction constant of this mechanism was used for modeling low-pressure pure acetylene plasma [39]. It is also intensively studied for comprehension of outer planet atmospheres [211]. The repeated addition of the ethynyl radical can in turn explain production of C_6H_2 (m/z = 74) and C_8H_2 (m/z = 8) via: $C_4H_2 + C_2H^\bullet \rightarrow C_6H_2 + H^\bullet$; $C_6H_2 + C_2H^\bullet \rightarrow C_8H_2 + H^\bullet$. A second production mechanism was proposed via a neutralization between ions [199], but will not be discussed here. Formation of the first ring C_6H_6 (m/z = 78) occurs through several proposed mechanisms [208], but higher ring species like naphthalene $C_{10}H_8$ (m/z = 128) is mainly proposed through the H-abstraction and C_2H_2-addition or HACA mechanism [197, 208, 212]. Concerning the moderate hydrogen production in the discharge, it may explain the measured small production of methane and ethylene in our acetylene plasma, which were not especially expected.

7.4.4 Ethylene plasma

The 15 eV ethylene VMS on Figure 7.9a shows the molecular ion peak at m/z = 28, but also a major peak at m/z = 26 assigned to C_2H_2+. The corrected measured AE of this peak is 13.1 eV in pure ethylene, well above the ionization potential of acetylene (11.4 eV). Hence the two pathways for the $C2H_2^+$ ion production should be well distinguished by measuring the AE during the plasma.

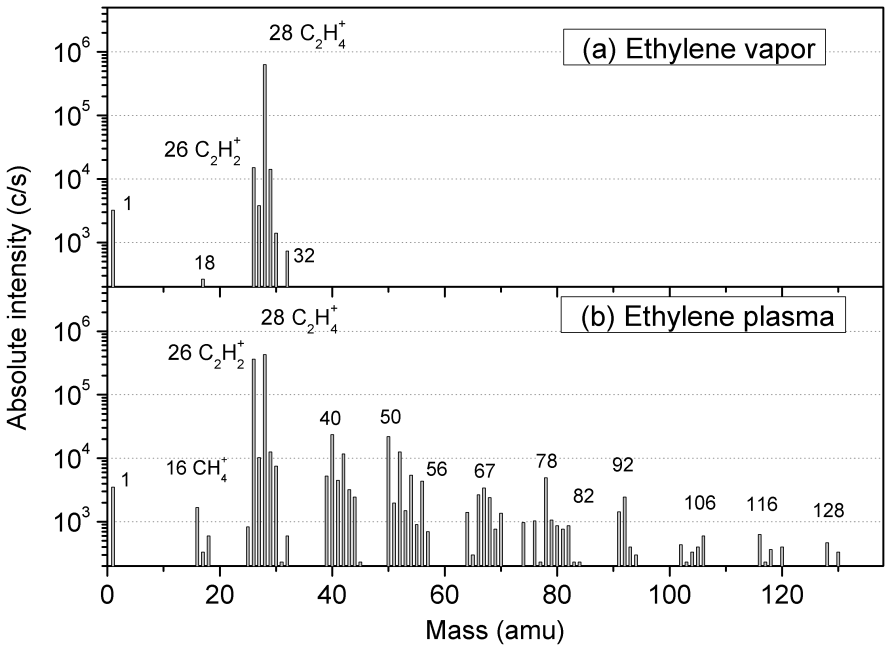

Figure 7.9: Mass spectra at 15 eV of ethylene: (a) vapor at 6.7 Pa, (b) plasma at 6.7 Pa, 28 sccm and 150 W.

When the plasma is switched on at 150 W, the PMS at 15 eV in Figure 7.9b indicates a consumption of only 35% of the ethylene monomer. It is hence by far the least consumed of the four studied monomers of the present work. The important increase of peaks at m/z = 26 and 30 shows with no doubt a significant production of neutral C_2H_2 and C_2H_6. In addition, we also counted 24 new peaks with even m/z. The PMS at 12 eV was needed to decrease the signal at m/z = 67 and revealed two additional peaks at m/z = 66 and 68. The same 12 eV spectrum also revealed 7 new peaks at m/z = 90, 96, 108, 132, 142, 144 and 156. The PMS at 20 eV showed an intense H_2 peak at m/z = 2. Hence we measured the AE of 37 peaks, including m/z = 28. The low value of their corrected AEs in the 6th column of table of Figure 7.2 indicates that they are very likely due to neutral species produced in the plasma. Especially for the m/z = 26 peak, its corrected AE during plasma is 11.1 eV, effectively below the AE at the same peak due to ethylene. We conclude hence to the production in the ethylene plasma of the 37 closed-shell species listed in table of Figure 7.2 (↪ *Page 128*), including ethylene itself.

Discussion of ethylene plasma species

Several neutral species identification are reported on low-pressure pure ethylene discharges by MS [55, 57, 184, 204, 213]. Supposedly working at 70 eV, Kobayashi observed C_2H_2 (26) and

heavier hydrocarbons, but without identifying the last [55, 57]. Smolinsky & Vasile identified five light neutrals by using 20 eV electron energy: H_2, CH_4, C_2H_2, C_2H_4 and C_2H_6. Working as low as at 15 eV, Dilks reported 8 species [184], but 7 others can be inferred from the shown PMS, with only 2 in common with Smolinsky & Vasile. The 13 new peaks are: C_3H_4 (40), C_3H_6 (42), C_4H_2 (50*), C_4H_4 (52), C_4H_6 (54*), C_4H_8 (56), C_5H_6 (66*), C_6H_8 (68*), C_6H_{10} (70), C_6H_6 (78), C_7H_8 (92), C_8H_8 (104*) and C_8H_{10} (106). The species marked by a star * are the one we added by observing the published PMS. As a conclusion, 18 of the 37 species we observed were already reported and the **19 remaining closed-shell species are then new**.

Not surprisingly, when comparing to acetylene plasma, many peaks in ethylene discharge that appears or has higher intensities correspond to species with much higher hydrogen content. Indeed the CH_4 (16) signal is higher, C_6H_6 (78) dominates instead of C_6H_2 (74), or C_8H_{10} (106) dominates instead of C_8H_2 (98). This is consistent with the higher H content of ethylene and the important H_2 production inferred from the intense peak at $m/z = 2$ observed at 20 eV. Moreover signals of species with an odd number of carbon atoms appear or are more intense than in the case of acetylene: C_3 around $m/z = 40$, C_5 around 66, C_7 around 92 and C_9 around 118. As proposed in the literature by Dilks *et al.* [184], ethylene is then likely to produce methylene as probable radical to explain its plasma polymerization features, on the contrary of acetylene. However this radical alone cannot explain the intense production of diacetylene (50), which indicates a direct production. The significant production of acetylene (26) and its suggested ethynyl intermediates $C_2H^\bullet$ in the previous section would rather be responsible for it, which also agrees with the conclusion of Dilks *et al.*

7.5 Comparison between the four plasmas

Among 55 neutral species, styrene plasma notably produces significant amount of benzene, ethylene and acetylene. In turn, discharge ignited in a pure vapor of those three species revealed numerous species. In this last section, we will compare the sets of observed species in the four plasmas to discuss common features and differences. To ease the comparison, the four PMS at 15 eV are reminded on Figure 7.10.

(1) All monomers polymerize in the gas phase and produce species with higher mass than the monomer.

(2) The four PMS were stopped at the highest detectable species. Therefore it can be seen that species containing more than 8 carbon atoms than the monomer have densities too

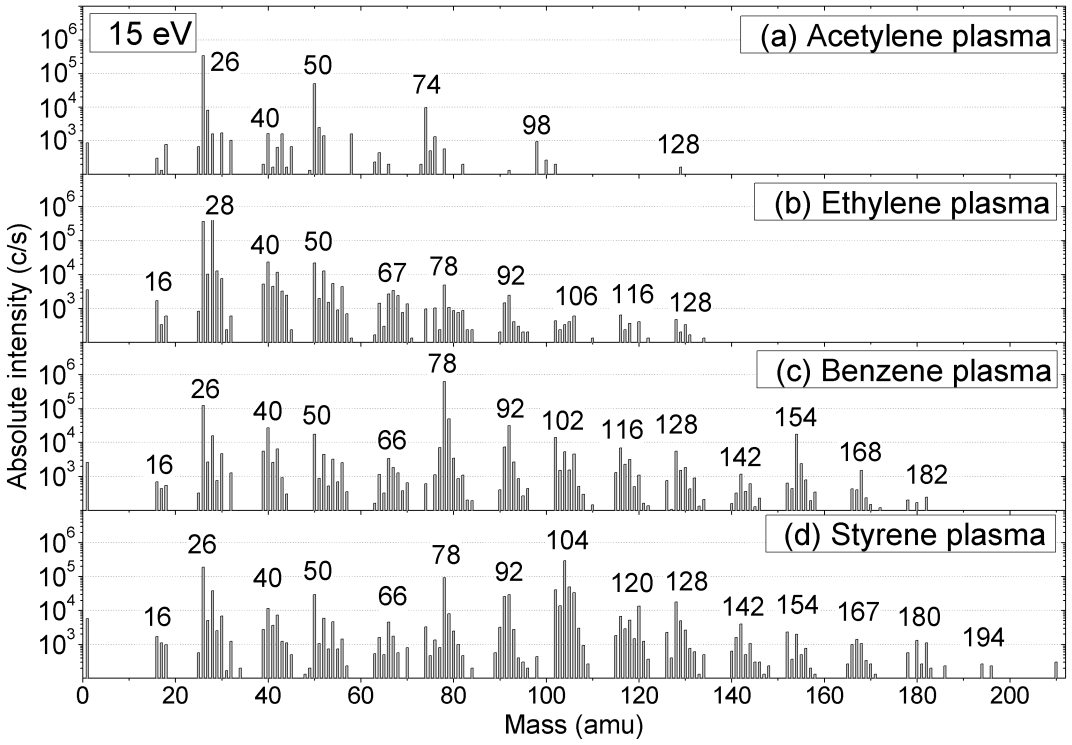

Figure 7.10: Reminder of the PMS at 15 eV of: (a) acetylene, (b) ethylene, (c) benzene and (d) styrene.

low to be detected. Furthermore intensities usually decrease with increasing number of carbon atoms, above the monomer mass. This strongly suggests a production of heavier species by the repeated addition of intermediate containing one or two carbon atom(s).

(3) Ethylene, benzene and styrene have species with every number of carbon atoms, unlike acetylene. This suggests that radicals with one carbon atom play an important role in their plasma chemistry. Having intense emission lines, C and CH were observed by OES in our system for styrene plasma [117, 118]. On the contrary, no emission line could be found for the biradical methylene $^{\bullet}CH_2^{\bullet}$, which is expected to play a significant role in some studies [184]. The presence of one carbon atom radicals also shows that double bond or aromatic bond does not hamper a hard fragmentation in styrene, benzene and ethylene plasma. The acetylene case suggests that a triple bond is needed for that.

(4) Unlike the three others, acetylene drastically favours even number of carbon atom species in its discharge. Its preferred products are the highly unsaturated diacetylene (50) and C_6H_2 (74). Their production are proposed via reaction of acetylene with the ethynyl radical $C_2H^{\bullet}$ or via HACA mechanism in the literature. For both of them, the intermediate contains 2 carbon atoms with low H content. Furthermore, we proposed C_2 as a third

likely intermediate containing 2 carbon atoms. Indeed, two small C_2 emission lines were possibly observed in acetylene plasma [214], and three other lines were detected in styrene plasma in our reactor and conditions [117].

(5) Acetylene is the product with the highest intensity in the other three discharges, above 105 c/s for each of them. It could therefore explain the quite intense peak at m/z = 50 for each plasmas and the series of peak at m/z = 50, 74 and 98 of the styrene discharge. It could also contribute to the species production via two carbon atoms intermediate in each discharge.

(6) In benzene plasma, intensity decreases for species increasing from 2 to 5 carbon atoms. This indicates that a direct fragmentation to C_2H_2 followed by an addition of one or two carbon atom species is favoured. An analogue reasoning can be followed for styrene. Its 2 most intense products of fragmentation are C_2H_2 and C_6H_6, from which the other species are produced. This could explain the low intensities of C_5H_6 (66) and C_7H_8 (92) for styrene plasma.

(7) The polymerization in the plasma phase via intermediates containing more than 2 carbon atoms does not seem likely to occur. Indeed in styrene discharge, peaks are very weak around 208 amu, 2 times the mass of the monomer. An exception to this observation is the rather intense species measured at m/z = 154 in benzene discharge. A reaction of benzene with a phenyl radical $C_6H_5^{\bullet}$ followed by H abstraction seems therefore likely to occur. The relatively high intensity around 180 amu in styrene discharge and the significant drop above it could also be explained by the addition of a 6 ring carbon atoms to styrene.

(8) The four discharges produce hydrogen, despite the high unsaturation of styrene, benzene and acetylene. This could contribute to the presence of methane in each of them. In addition, except for acetylene with the least hydrogen production, the three other PMS revealed series of species which increase by 2 amu. The most striking is the C_4H_2 (50), C_4H_4 (52), C_4H_6 (54) and C_4H_8 (56) series. Addition of H_2 could explain the systematic decrease of their intensities with increasing hydrogen content. However the limited amount of H in the initial monomer combined with the H_2 production in the plasmas could explain it as well. The first explanation is favoured by ethylene. Indeed, despite its higher H content, the same decreasing intensities are observed.

Finally, we will end this section by briefly comparing the AEs measured at the same m/z ratio between each discharge from table of Figure 7.2 (Page 128). The overestimation of the measured AE for weak signals can be clearly seen from e.g. the m/z = 128 line. The measured

AE increases from styrene to acetylene. Observing the four PMS at 15 eV, it can be seen that the signal of the m/z = 128 peak decreases from styrene to benzene, to ethylene and finally to acetylene. Experimental errors or different isomer forms can also contribute to the discrepancies. Nevertheless we think that some of our measured AEs could be used to approximate unknown IEs of several highly unsaturated species.

7.5.1 Perspectives on light emission of the four hydrocarbon plasmas

For the record, the optical emission spectra from discharge of styrene, benzene, ethylene and acetylene, will be very shortly commented. They were acquired in 2009 in collaboration with Dr Li. The conditions differ from the ones of the present chapter and are: 150 W of applied power, pulsed with a frequence of 10 Hz and a duty cycle of 50%. The pressure and flow conditions are not exactly known as the Convectorr gauge was used at that time but the expected values are indicated in the caption of Figure 7.11. The acquisition was made with an ACTON SP2756i spectrometer (Princetown Instruments), detailed in reference [118]. The spectra are shown on Figure 7.11.

While the conditions are not similar, there are stricking differences in the continuum part of the spectra, on which we will restrain our comment. As schematically depicted on the figure, four continuum contributions (A, B, C and D) may seem to appear from the acetylene to styrene spectra. We will try to connect them to the conclusions regarding the effluent detection of MS. Doing so, we will have in mind that a continuous emission spectrum is characteristic of a non-resonant recombination or association between two products of reaction: for instance, electron-ion or neutral-neutral recombinations. The relative energy of collision follows a distribution due to the speed distribution of the reactants. Therefore the complex formed by the recombination has an internal distribution of excess energy. It results in a distribution of energy of the photons emitted during the deexcitation of the complex and thus a continuous spectrum of light emission.

- The continuum A is the only present in the optical spectrum of acetylene plasma. The latter is characterized by a low amount of hydrogen produced (Section on pressure quantification 8.3.3) and is dominated by C_2 stable species and radicals. It suggests that recombination reactions with C_2 ions or C_2 radicals are causing this continuum.
- Compared to acetylene, the continuum B is appearing in ethylene plasma. This discharge is characterized by the production of a very large amount of hydrogen and a moderate amount of methane (Section 8.3.4). It suggests that recombination reactions with ions or radicals of H_2 or CH_4 are causing this continuum.

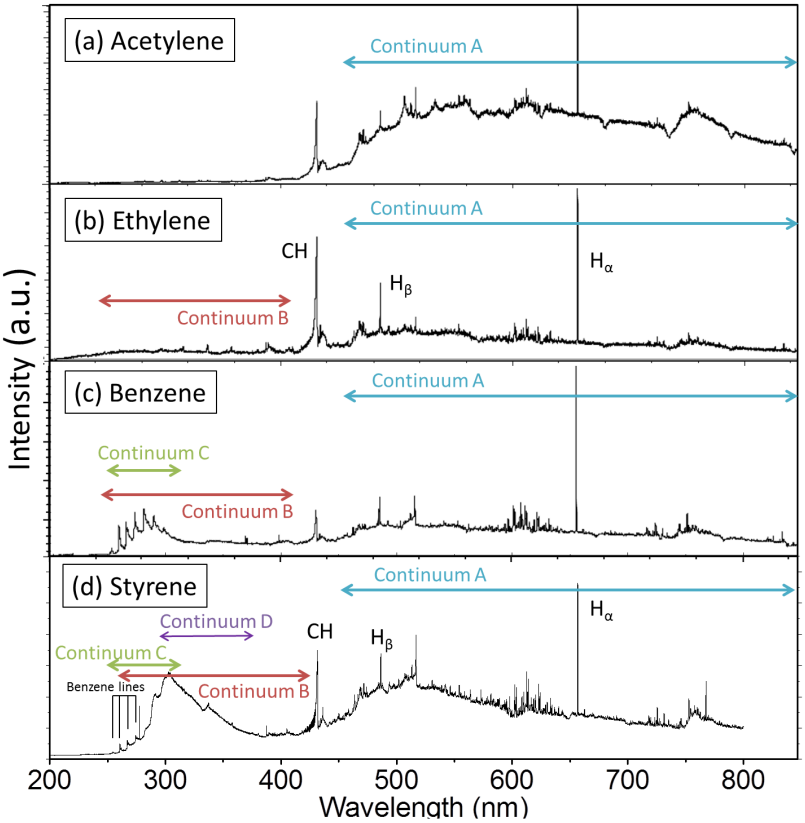

Figure 7.11: Optical emission spectrum at 150 W and a pulsation of 10 Hz and 50% of: (a) acetylene plasma at around 14 Pa and 18 sccm, (b) ethylene plasma at around 14 Pa and 18 sccm, (c) benzene plasma at around 9 Pa and 22 sccm, (d) styrene plasma at around 7 Pa and 28 sccm. The approximated values are due to the use of the Convectorr gauge, whose pressures had to be corrected (see Section 5.1.2). Line assignment of styrene plasma are made on the base of reference [117].

- Benzene and styrene potentially shows two other continua, C an D. We propose to link them with recombination reactions of heavy hydrocarbon ions or radicals.

A much more detailed and much deeper work is needed to analyze those data, which may provide original contributions. However, this first observation will serve for further discussions.

7.6 Conclusion

In the low pressure RF plasma of four hydrocarbons, identification of numerous neutral closed-shell by-products was performed by Mass Spectrometry, following a successful two-step approach. Firstly we determined all the MS peaks suspected to be directly due to neutral species present in the hydrocarbon plasma. This was reached by lowering the electron impact energy to avoid analysis fragmentation which greatly simplifies the cracking patterns (Section 7.2).

Secondly, we confirmed or excluded the suspected peaks with the "Appearance Energy criterion for molecular ion", by measuring their AEs (Section 7.3.2). This criterion that we established applies for highly unsaturated hydrocarbon and states that: "An even mass peak with sufficiently low AE corresponds to a molecular ion in the case of highly unsaturated hydrocarbons". For styrene, 45 never discussed closed-shell species were highlighted, in addition of the 10 already identified in the literature. Benzene, ethylene and acetylene plasma revealed 44, 37 and 23 neutral species respectively. Comparison to literature showed that respectively 37, 18 and 6 species had never been reported in pure or diluted hydrocarbon discharges. No isomer determination could be performed due to experimental errors in the AE determination.

Each discharge was discussed by thoroughly analyzing the different observed species. The highest intensities in each PMS allowed us to identify the species with the highest concentration in the discharges. Intermediates and mechanisms were briefly suggested. As acetylene, ethylene and benzene are substantially created in the styrene discharge, comparison of the species produced in their four respective plasmas revealed interesting features. The main conclusion is that the repeated action of intermediates containing one or two carbon atom(s) with low H content dominates the production of the species. Very unsaturated radicals like C and C_2 are proposed to be considered among intermediates as they were observed by OES in our system [117, 118]. The presence of the small intermediate compounds in ethylene, benzene and styrene shows that double bond and aromatic bond are not sufficiently strong to prevent their dissociation, on the contrary of triple bond in the case of acetylene. The production and the repeated action of the small intermediates support the "atomic polymerization" concept and the Rapid Step Growth Polymerization mechanism proposed by Yasuda [3]. This makes sense as the discharge intensities employed in the present work are intermediate to high, as seen in Section 7.1.

It must be noted that the discussion of the present chapter was restrained to plasma-phase processes. Surface processes should also be considered, especially when considering the specific design of the source: the plasma intensity is high at the quartz window and etching or release of species formed on the surface may affect the measured composition of the plasma.

Now that MS allowed us to identify the maximum of neutral products in the hydrocarbon discharge, it is time to take advantage of another of its features: the partial pressure quantification, which is the subject of the following chapter.

Chapter 8

Pressure quantification in unsaturated hydrocarbon plasma

The ignition of plasma in a monomer vapor leads to its transformation towards a large variety of different species: stable neutrals, radicals, electrons and ions. Downstream of the discharge, only the stable closed shell molecules remain from this complex mixture, and usually they are in their ground electronic state. Mass Spectrometry (MS) has proven to be an efficient technique to investigate stable gas blend. Especially, when recorded under the same conditions, the mass spectrum of such mixture is a linear superposition of the compound mass spectra, in proportionality with the partial pressures [13].

The present chapter takes the advantage of this property by attempting partial pressure quantification within the discharge of four unsaturated hydrocarbons, which are: styrene, benzene, ethylene and acetylene. The chapter will start with experimental considerations and the description of the quantification procedure (Section 8.1 and 8.2). Then the partial pressure results will be shown when varying the discharge power for each individual hydrocarbon (Section 8.3).

The measured partial pressure will then be compared between the four hydrocarbon discharges (Section 8.4). Discussing the results will lead to propose possible effects due to hydrogen production (Section 8.4.4) and regarding the specificity of the reactor geometry 8.6. The results will also be compared to the monomer classification established by Yasuda (Section 8.4.5). In addition, estimations will be made for the number of effluent released by consumed styrene (Section 8.5.1) and about the mass content of the plasma-phase (Section 8.5.2). Finally,

the interplay between the E/H transition and the discharge pressure will be discussed (Section 8.6).

8.1 Experimental verification in flow conditions

The measurement of absolute partial pressures is a common task in MS. For spectrometer with a single differentially pumped stage like ours and in the studied pressure range, the gas densities in the ionization chamber are effectively linearly proportional to the absolute partial pressures in the reactor [96]. However this proportionality was verified in the case of our flow system, which means that the process is carried out with a continuous injection and pumping of the gases. As these verifications brought very fruitful information, they were worth mentioning in a fully dedicated section. The presented results include the case of a single gas and then the case of two gas mixture. All the measurements have been done with a primary pump, without nitrogen trap. The effect of the nitrogen trap will be discussed in a next chapter (Section 10.4.6).

8.1.1 Injection of single gas

Two interesting preliminary information were observed through the single gas injection. Firstly, the injection of a gas in our reactor generally takes two minutes before reaching pressure stabilization. However, after 80 seconds, the pressure has already reached 96% of the asymptotic pressure. This is important as all the pressure measurements during the plasma studies were done after 80 seconds. Secondly, when injecting the same amount of flow of two different gases, like Argon and nitrogen, systematic pressure differences were observed. Argon pressure was up to 10% higher than the nitrogen one. The Baratron® pressure gauge was set aside as a cause, being a manometer capacitance gauge. To verify if this was due to differences in the pumping rate depending on the gas nature, the flow was measured using the Yasuda method, presented in the experimental chapter (Section 5.2). This measurement method is based on the pressure increase in the reactor, when the pumping is suddenly switched off. The argon flow revealed to be 4% higher than indicated, at every investigated flow. Inverting the two used flowmeters gave exactly the same results. This showed that the flowmeters were not accurate and this was taken into account in all the presented measurements.

Figure 8.1a shows the reactor equilibrium pressure when pure nitrogen is injected at different flows. The base pressure was high with 1.0 Pa, due to the leak rate of the used flowmeter. The shown measured pressures were diminished by this value for correction. A dashed line is added on

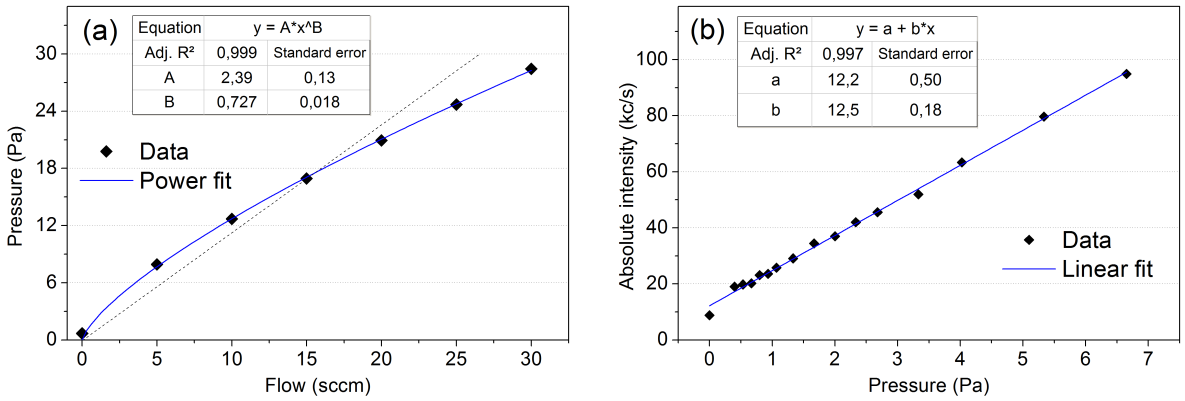

Figure 8.1: (a) Corrected reactor pressure for different nitrogen flow. (b) Absolute intensity measured at m/z = 28 and 20 eV as a function of the nitrogen pressure in the reactor.

the figure to show that the increase of pressure is not linear with the flow and shows saturation. This is due to the **increase of the pumping rate** of the primary pump at higher pressure. Yasuda and Hirotsu showed that the pressure p is empirically related to the flow F via a power dependence: $p = a F^b$ [215]. According to them, the value of the exponent generally lies between 0.5 and 1, but is more often close to 0.5. The same relation was observed when using nitrogen trap for condensable gases. In our case, this empirical relation gave by far the best fit, shown on Figure 8.1a. The exponent coefficient b is equal to 0.74.

Pure nitrogen was injected at different pressures in the reactor. The very low pressures were obtained by pumping with a throttled turbo-molecular pump. After two minutes, the mass spectrum was acquired for each of them. Figure 8.1b shows the intensity of the molecular ion peak of nitrogen at m/z = 28 as a function of the nitrogen pressure in the reactor. The experimental points are best fitted with a linear function with an offset at a null pressure of nitrogen. This offset is due to residual nitrogen in the ionization chamber of the mass spectrometer. The relative standard error on the slope is equal to 1%. We conclude from this result that the nitrogen density in the ionization chamber is effectively linearly proportional to the nitrogen pressure in the reactor in the range of pressure from 1 to 10 Pa.

8.1.2 Injection of two gases

Before any quantification, a very important aspect must be understood when injecting two gases sequentially. This is illustrated with an injection of argon at 20 sccm, followed by an injection of methane at 60 sccm. Figure 8.2 shows the time evolution of molecular ion signals of argon

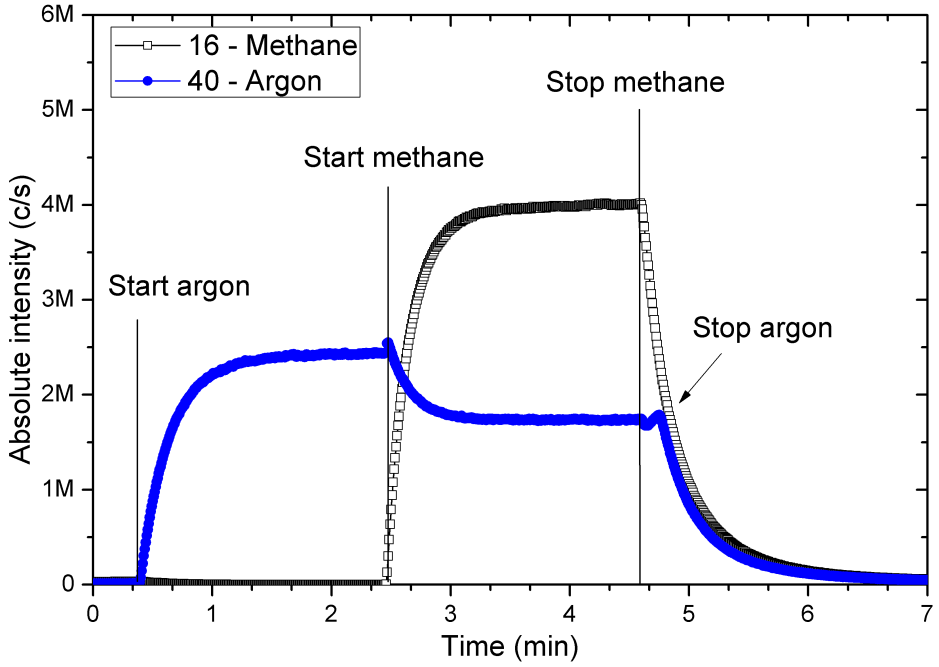

Figure 8.2: Time evolution of the molecular ion intensity of argon at m/z = 40 and of methane at m/z = 16, when those gases are injected consequentially (argon 20 sccm, methane 60 sccm).

(m/z = 40) and of the methane (m/z = 16). At 20 s, the argon injection starts and its related intensity increases. After 2 minutes, its signal stabilizes, as does the measured pressure of the reactor at 23.3 Pa, indicating the injection equilibrium is reached. At around 2'30, the methane injection starts. Its related intensity increases and takes 2 minutes to stabilize, like the reactor pressure at 68.0 Pa. It is striking to see that the argon signal markedly decreases as soon as the methane injection starts, with a stabilization following the one of the methane signal. Its relative signal decrease is equal to 29%.

On the basis that gas mixture can be quantified by MS, this is interpreted as the partial pressure of argon diminishes of 29%. Its partial pressure goes from 23.3 Pa when it was injected alone, down to 16.6 Pa when methane is injected. This is explained by the fact that the pumping rate is significantly higher at the total pressure of 68.0 Pa, than at 23.3 Pa. Therefore the same amount of sccm of argon gives a lower argon pressure in the reactor when the second gas is injected.

If methane is injected with the same flow as argon, i.e. 20 sccm instead of 60 sccm, the argon partial pressure decrease is lower with only 12% reduction. Said in other words, the partial pressure reduction decreases from 29% to 12% if the ratio of the second gas flow to the first gas flow (named "flow ratio") goes from 3 to 1.

	Total pressure (Pa)	**Argon pressure** (Pa)	**Relative difference**
Argon 20 sccm	23.3	23.3	
Argon + methane 20 sccm + 60 sccm	68.0	16.6	- 29%

Table 8.1: Effect of the injection of a second gas (methane) on the partial pressure of the first gas (argon).

Total pressure = 68.0 Pa	**Proportional to flow** (theoretical)	**Measured by MS** (experimental)	**Relative difference**
Argon pressure (Pa)	17.0	16.6	2%
Methane pressure (Pa)	51.0	51.4	0.8%

Table 8.2: Comparison for gas mixture of argon and methane of the theoretical partial pressures (based on the flow proportion to total flow) with the measured partial pressure by MS.

This effect has an important fortunate consequence for so many experiments on the partial pressure of residual gases in vacuum chambers. In our case, the reactor leak rate is quite high with 0.2 sccm. The injection of 20 sccm of argon (a flow ratio of 100) is expected to decrease much more than 29% the residual gas pressure. This was observed on the methane signal at the beginning of Figure 8.2 (too small to be seen). The methane flowmeter has a small leak rate around 0.1 sccm. The injection of 20 sccm of argon decreases the methane intensity from 33 kc/s down to 1 kc/s. This is a relative decrease of 97%!

This strong effect on the gas mixture has been taken into account for quantification of partial pressures of methane and argon mixture. As the two gases have the **same pumping rate curves**, their partial pressures are the mirror of their partial flows. To be clear, with 20 sccm of argon and 60 sccm of methane, the partial pressures are 25% and 75% of the total pressure of 68.0 Pa. This means a pressure of 17.0 Pa for argon and of 51.0 Pa for methane. The agreement is good between this argon pressure proportional to the flow with the one deduced by MS: 16.6 Pa. The relative difference is only 2%. The complete results are not shown here, but the agreement was usually within 2.5% and degrades to 5% for small pressures and MS signals.

8.2 Quantification procedure

8.2.1 Principle

Eight gases were chosen based on their high MS intensity in the plasma mass spectrum (PMS) of styrene at 20 eV. With their chemical formula and their atomic masses in amu between brackets, they are: hydrogen (H_2 - 2), methane (CH_4 - 16), acetylene (C_2H_2 - 26), ethylene (C_2H_4 - 28), benzene (C_6H_6 - 78), toluene (C_7H_8 - 92), of course styrene (C_8H_8 - 104) and naphthalene ($C_{10}H_8$ - 128). Implicitly, isomer choices are then made here which were not made for rigor in the previous chapter (Section 7.4.1). However, the isomers selected here seem the most likely. The aim was to quantify their partial pressures in the plasmas of styrene, benzene, ethylene and acetylene. The quantification procedure is explained hereafter.

One after the other, the eight gases were injected pure in the reactor at 6.7 Pa. Their mass spectra were recorded at 20 and 15 eV each time, with all other settings kept constant. For each spectrum, the molecular ion intensity was divided by the reactor pressure to give a value that is called hereafter "**conversion factor**". This factor gives the absolute intensity of the gas molecular ion per unit of reactor pressure. After this gas calibration step, the plasma was ignited in the reactor to record its PMS. Then, the absolute intensities of the peaks at the eight m/z of interest were divided by their corresponding conversion factor, to provide partial pressures.

The cracking patterns (CPs) of the eight chosen molecules are shown on Figure 8.3 at 20 eV and 15 eV. They were all recorded with the same settings and with the same pressure of 6.7 Pa. The 20 eV electron energy was chosen to quantify partial pressure of hydrogen and methane. Indeed, at 15 eV, hydrogen gives no signal and methane a very small one, while their signal is sufficient at 20 eV. Besides, it can be seen on Figure 8.3-left, that the seven molecules other than hydrogen give very small contribution to the peak at $m/z = 2$, with maximum 2 kc/s. Compared to the 300 kc/s of hydrogen, it means contribution smaller than 1% for the same pressure of 6.7 Pa. The same observation can be done for the peak at $m/z = 16$ of all the gases except methane.

The 15 eV electron energy was chosen to quantify the partial pressure of the six remaining vapors. This energy effectively reduces the overlapping of their CP. At 20 eV, ethylene has a strong peak at $m/z = 26$, whose intensity values 14% of the intensity of the same peak for acetylene at the same pressure. At 15 eV, this contribution goes down to 2%. The same reasoning can apply for the styrene contribution to the peak at $m/z = 78$, which corresponds to the molecular ion peak of benzene. This contribution goes from 25% at 20 eV down to 10% at

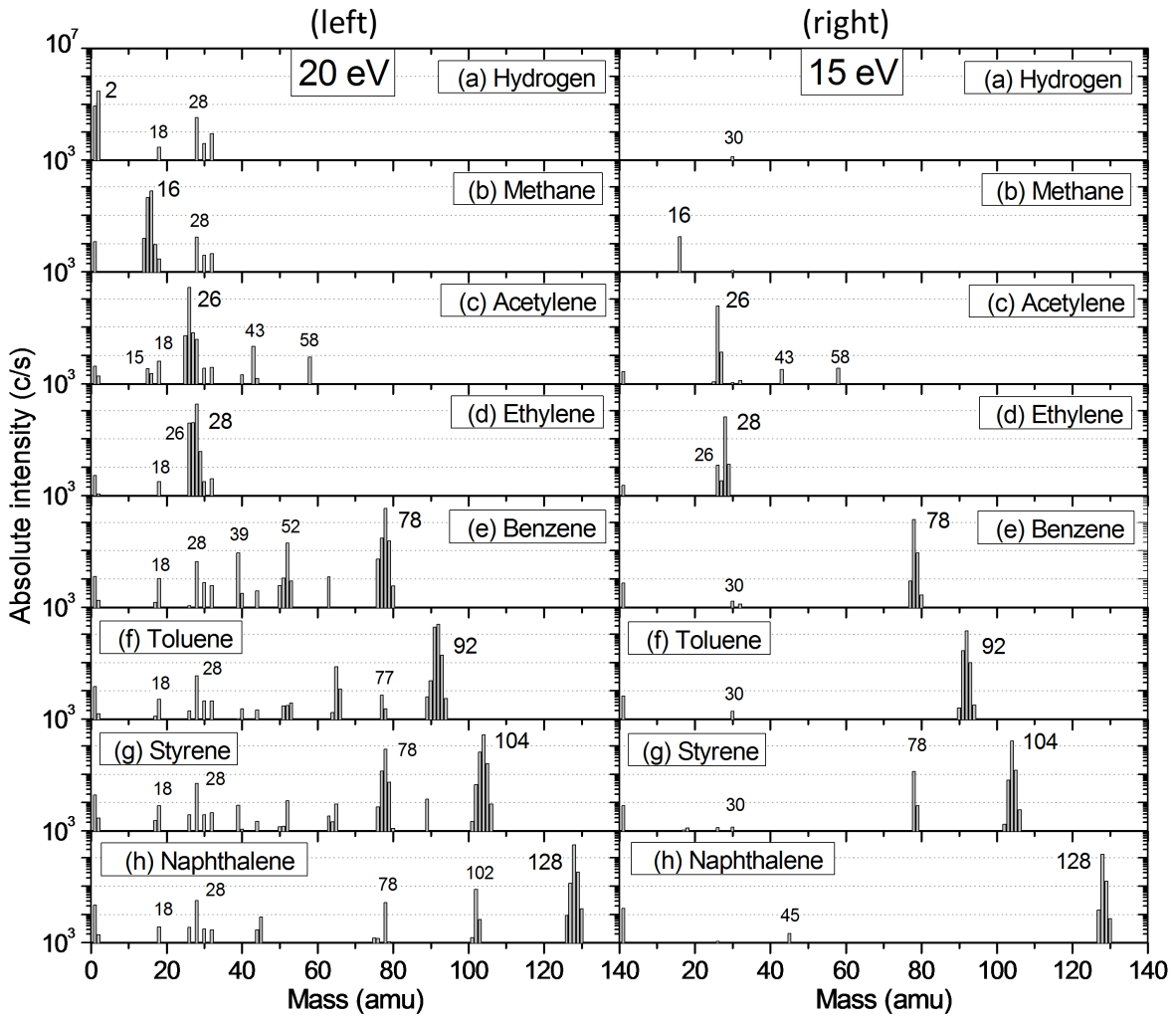

Figure 8.3: Cracking patterns at 20 eV (left) and 15 eV (right) of: (a) hydrogen, (b) methane, (c) acetylene, (d) ethylene, (e) benzene, (f) toluene, (g) styrene and (h) naphthalene. All recorded at 10 μA, 6.7 Pa and within the same two hours.

15 eV. Of course, these two still significant overlappings were taken into account when calculating the partial pressures of acetylene and benzene.

It is now clear that the quantification of partial pressures during plasma relies on MS absolute intensities. Depending on the undertaken measurements, these intensities should keep the same values during minutes or even days. The method to deal with these two timescales is considered in the next section.

8.2.2 Drift of absolute intensities over time

Absolute MS intensities are subject to drift with exposure of the spectrometer to vapors and plasmas. We showed in Section 5.3.7 that the maximal variation of the relative intensities is 5% over a period of 10 minutes. Considering these results, it was decided to limit as much as possible the spectrometer exposure to vapors and plasmas. However, this was complicated by the liquid monomer precursors, like benzene or styrene. They effectively require an injection equilibrium before igniting the plasma, as explained below.

The evaporation of a liquid induces its cooling. In turn, the temperature decrease of the liquid reduces its vapor pressure, its rate of evaporation and then its injection. The latter reaches equilibrium when the temperature of the monomer is stabilized, usually 10 minutes after starting the injection. Temperature regulation was not very helpful to achieve a quicker steady state of injection. The best strategy found is to heat the monomer or to increase its heating when the injection is started. This enabled to achieve equilibrium within 3 minutes.

With the same objective of reducing exposure time, the mass spectra were acquired with an increasing mass step of 1 amu to reduce the number of steps. Because several measurement were done on plasma pulsing at 10 Hz and with 50% duty cycle, the detector acquisition time (dwell time) was settled to 100 ms to integrate a complete pulsation period. A settle time of 50 ms was chosen to adjust the potentials of the spectrometer at each step. Therefore a complete mass spectrum from 1 to 150 amu was recorded within 20 s.

Typically, all the measurement presented here were carried out as follows: wait 3 minutes to established a steady monomer pressure, take 1 minute to acquire mass spectrum at 20 and 15 eV, start the discharge ignition, wait 1 minute before the pressure and the reflected power stabilize and finally take 1 minute to acquire the mass spectra during plasma at 20 and 15 eV. Between each of these runs, the reactor was pumped with a turbo-molecular pump down $1 \cdot 10^{-3}$ Pa during 10 minutes. The objective of this latter step was to partly degas the remaining volatile species on the reactor walls, but also to clean the mass spectrometer, whose electron emission current was kept high. Then the pumping of the nitrogen trap combined with the primary pump was settled back and the turbo molecular pump switched off, before starting the next run.

Generally a series of around ten runs (powers) were done for each monomer plasma before totally cleaning the reactor and proceed to the next monomer. As the reactor cleaning and pumping takes time, all the measurements were done over three days. The strategy to deal with the intensity drift over this much longer timescale is described hereafter.

	Monomer	**Other gases**	**Hydrogen**
Relative error	5%	20%	30%

Table 8.3: Relative errors on partial pressures, taken to be the maximal difference of measured conversion factors from the mean conversion factor.

All the conversion factors were measured before and after the four plasmas series (styrene, benzene, ethylene and acetylene plasmas). In addition, several conversion factors were also measured between each plasmas series. All the partial pressures were calculated by using the **mean conversion factor** from the several measured ones. Expressed in percentage of the mean conversion factors, the maximal deviations of the conversion factors were all between 10 and 20%. We then decided to consider a rounded up deviation of 20% for all of them. However, there were two exceptions. Firstly, the maximal deviation of hydrogen conversion factor reaches 30%. Secondly, for the monomer in whose vapor the plasma is ignited, the conversion factor was measured each time before the plasma. Its maximal deviation can then reasonably be estimated to reach only 5%. Considering all this, the errors on the calculated partial pressures were evaluated to be of 20% for all the gases, except for hydrogen and the monomer, for which 30% and 5% were used respectively, as resumed in Table 8.3.

8.3 Variation of power

The quantification procedure will now be applied to the discharges of styrene, benzene, acetylene and ethylene. Different powers were used, but all the other conditions were kept constant and are indicated in Table 8.4, except the pumping valve opening which has to be adjusted to reach the targeted pressure.

Monomer	Flow (sccm)	Initial pressure (Pa)	Pumping valve opening (turn)
Styrene	28	6.7	2 + 0/16
Benzene	28	6.7	2 + 2/16
Acetylene	28	6.7	1 + 15/16
Ethylene	28	6.7	1 + 15/16

Table 8.4: Plasma conditions used for the present chapter.

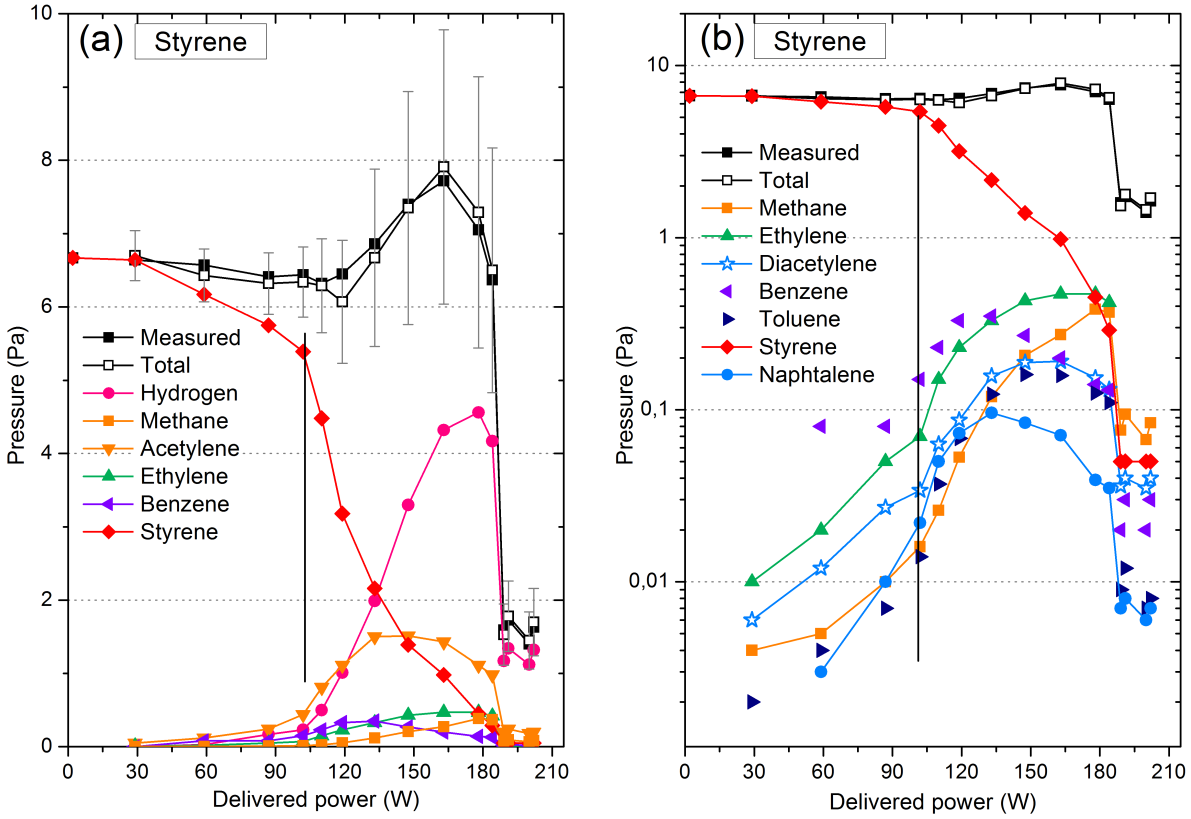

Figure 8.4: Calculated partial pressures, total pressure and measured pressure of styrene plasma at 6.7 Pa, 28 sccm and CW, with: (a) a linear scale and (b) a logarithmic scale.

8.3.1 Styrene plasma

The partial pressures were calculated in a series of styrene discharges while varying the plasma power. They are shown on Figure 8.4a with a linear scale for the vapors whose partial pressures reach at least 0.2 Pa. This was not the case for toluene and naphthalene. Therefore only the partial pressures of styrene, hydrogen, methane, acetylene, ethylene and benzene are shown. On Figure 8.4b, the same results are presented but with a logarithmic scale to show the trends of the smallest pressures, including toluene and naphthalene this time. On both figures, the measured discharge pressure is indicated, along with the total calculated pressure obtained by adding the eight estimated partial pressures. To lighten the graph, the error on the calculated partial pressures is only indicated for the total calculated pressure. Its error bars were simply obtained by adding the errors of every individual partial pressure. It is worth mentioning that the power values of the X axis were the transmitted power to the discharge and not the applied power.

Styrene plasma effluent	H_2	C_2H_2	C_2H_4	CH_4	C_6H_6	C_7H_8	$C_{10}H_8$
Maximal partial pressure (Pa)	4.7	1.5	0.5	0.4	0.4	0.17	0.10
Applied power for maximal pressure (W)	180	150	165	180	135	150	135

Table 8.5: Maximal partial pressures by decreasing order and the applied powers at which they are attained for the seven quantified effluents in the styrene discharge.

The first and most striking result is the excellent agreement between the measured pressure and the total calculated one. This confirms the quantitativeness of the procedure, even for a gas as delicate to quantify as hydrogen (due to its light mass, it is very sensitive to potentials drift in mass spectrometer and is generally subject to larger errors).

Several simple observations can be made from the graph. The partial pressure of the styrene monomer monotonically decreases. From 30 to 120 W, despite an apparent rather constant measured pressure, the styrene pressure is reduced by a factor of two. At the highest power, the depletion of the monomer reaches 99%. The dominating discharge products are indicated by decreasing maximal partial pressure in Table 8.5, with in addition the power at which it occurs. Hydrogen and acetylene are the two main effluents.

Going further, several more detailed observations can be revealed. Firstly, a distinct change of slope in the styrene pressure curve is observed around 100 W, marked by a vertical line on both figures. It also corresponds to the start of a regime of larger production of all the species. Secondly, a sharp drop of the total pressure occurs around 185 W. All the individual pressures are markedly reduced. The remaining product above this power is hydrogen, explaining 80 to 90% of the measured pressure. Therefore, almost no carbon atoms (integrated in hydrocarbon molecules) are remaining in the gas-phase and should have been deposited on the reactor walls.

Between the two transition powers, the individual pressures other than styrene all reach a maximal value, but this occurs at different powers. A first group of products has maximum pressures appearing early, like benzene around 120 W, naphthalene around 135 W and acetylene and toluene around 150 W. A second group of products have their maximum pressure around 175 W, which is the case of hydrogen, ethylene and methane. This second group corresponds to much more saturated species.

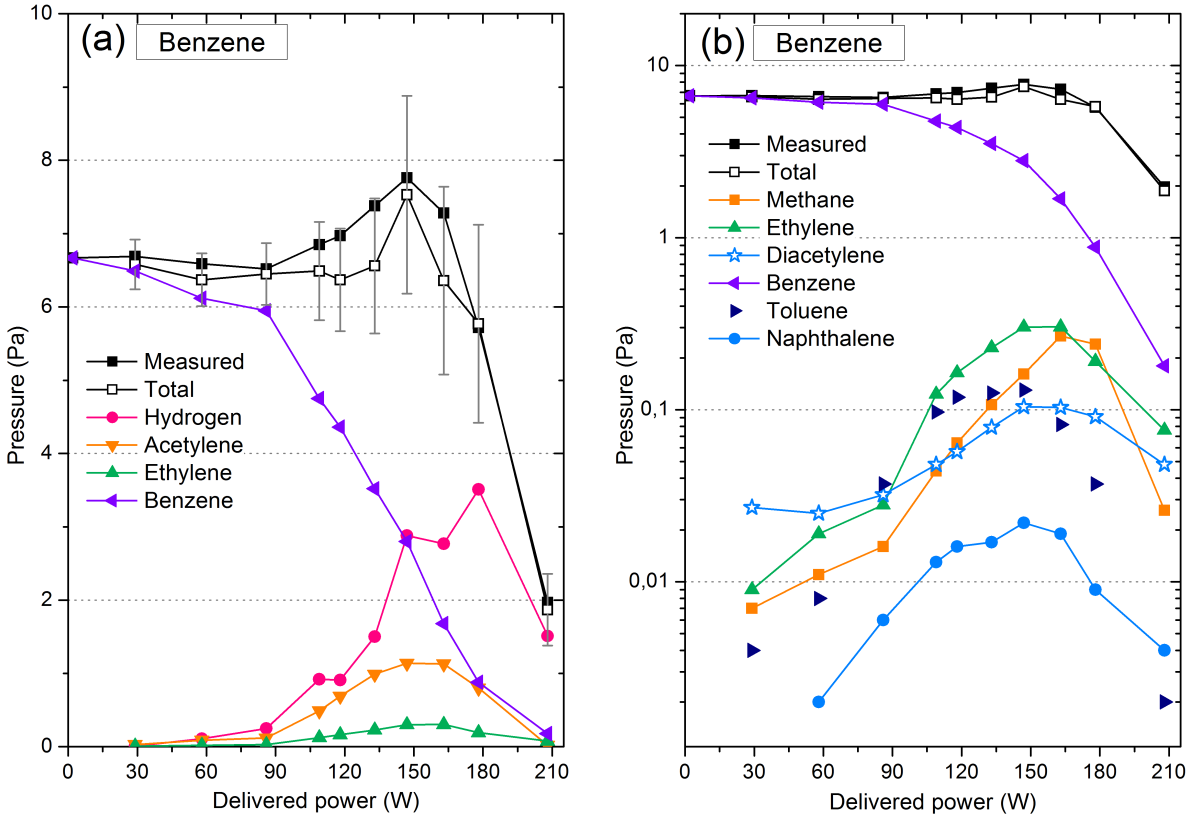

Figure 8.5: Calculated partial pressures, total pressure and measured pressure of benzene plasma at 6.7 Pa, 28 sccm and CW, with: (a) a linear scale and (b) a logarithmic scale.

8.3.2 Benzene plasma

Similar pressure graphs are shown on Figure 8.5 for the benzene discharge. The same scales of transmitted power and pressure are used. The total calculated pressure still agrees remarkably well with the measured pressure, within the error bars at three powers (120, 135 and 165 W). However, hydrogen pressure values may seem under-estimated at these powers on Figure 8.5a, which cause a slight under estimation of the total pressure. The 10 discharge conditions were done during the same series, but randomly, with no monotonic increase of the power. However the 120 W discharge condition was subject to a small pressure instability. The 135 and 165 W conditions were done at the end of the series and of the night, which may have induced a less careful respect of the procedure.

The benzene pressure shows the same monotonically decreasing trend with power than styrene. The dominating discharge products are once again indicated by decreasing maximal partial pressure in Table 8.6. The two main products are hydrogen and acetylene, as for styrene.

Benzene plasma effluent	H_2	C_2H_2	C_2H_4	CH_4	C_7H_8	$C_{10}H_8$
Maximal partial pressure (Pa)	3.9	1.1	0.3	0.3	0.1	0.03
Applied power for maximal pressure (W)	180	150	165	165	150	150

Table 8.6: Maximal partial pressures by decreasing order and the applied powers at which they are attained for the quantified effluents in the benzene discharge.

As seen from the benzen PMS in the previous chapter (Figure 7.7 on page 130), several peaks have absolute intensities close to the one of toluene, at m/z = 40, 50, 102 and 154 at 150 W. Hypothesizing conversion factors for those species similar to the one of toluene, their contribution should be limited to 0.2 Pa at the most.

Table 8.6 also shows for each effluent the power at which the corresponding pressure is observed to be maximal. As for styrene, the more hydrogenated is the species (hydrogen, methane and ethylene), the higher the power is needed. This could suggest that ethylene and methane require high hydrogen concentration to be produced.

The decreasing curve of the benzene partial pressure in Figure 8.5a shows a sudden change of slope at 90 W. At the same power, a clear increase of all the effluents pressure can be simultaneously observed. A similar behavior was also detected for styrene.

8.3.3 Acetylene plasma

Pressure graphs for acetylene can be seen on Figure 8.6, still with the same scales of power and pressure. In the previous chapter, polyyne species ($C_{2n}H_2$) were the dominating species in the acetylene plasma chemistry. Therefore, the partial pressures of diacetylene C_4H_2 (50 amu), C_6H_2 (74 amu) and C_8H_2 (98 amu) were estimated. The mean value of the factors of acetylene and benzene was chosen as reasonable conversion factor. To mark the lesser confidence in their estimated partial pressure, they are shown on the figures with open symbol. By the way, the shown diacetylene pressures in the styrene and benzene figures were estimated with the same conversion factor.

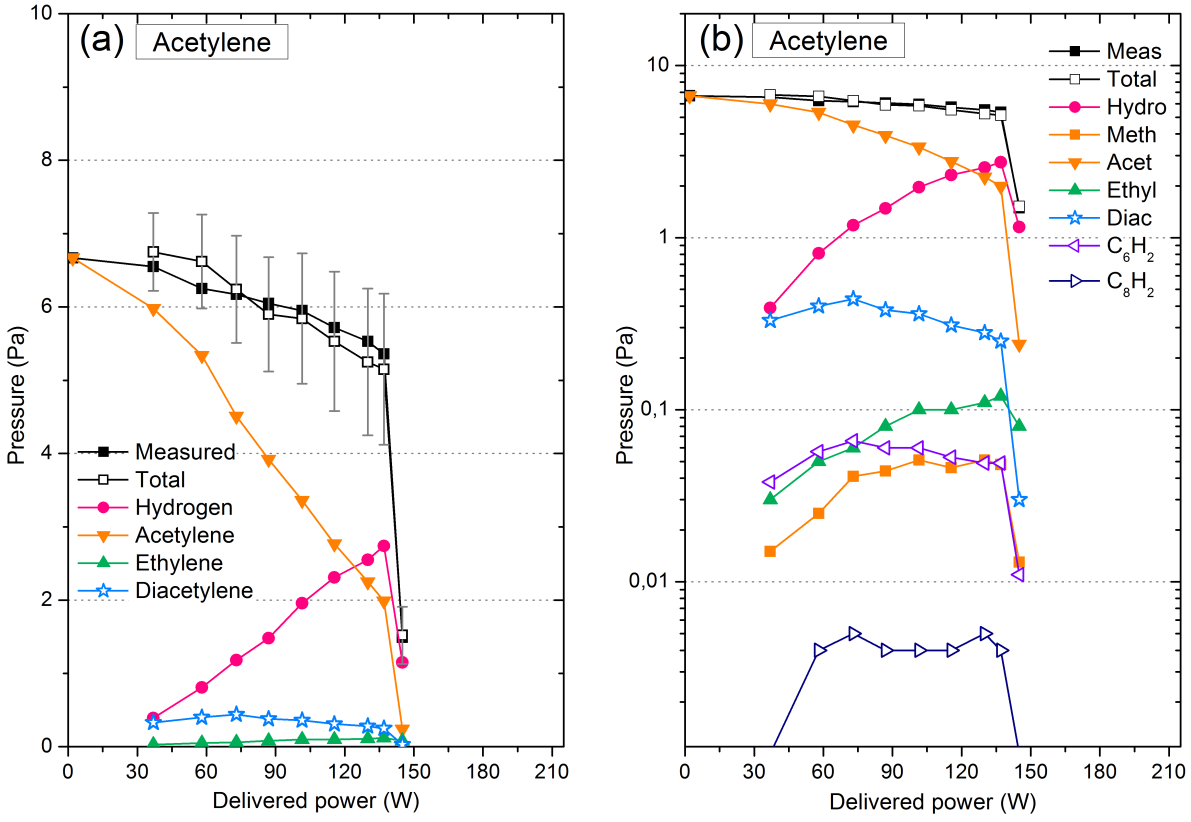

Figure 8.6: Calculated partial pressures, total pressure and measured pressure of acetylene plasma at 6.7 Pa, 28 sccm and CW, with: (a) a linear scale and (b) a logarithmic scale.

Acetylene pressure does not follow the same trend as the styrene and benzene ones in their respective plasma. Its decrease is linear with the power and with no change of slope. The main product of the discharge is hydrogen. Its pressure trend also differs from the one during benzene and styrene plasma: it increases linearly to reach the maximal value of 2.7 Pa. The same linear increase is observed for C_2H_4 and CH_4 but reaching the much lower maximal pressures, as reported in Table 8.7. The second product by pressure importance of acetylene discharge is diacetylene with a maximal pressure of 0.4 Pa. The pressure increases up to 75 W and then decreases at higher power. The three polyyne species have similar trends and their pressures are separated by an order of magnitude, as visible on Figure 8.6b and observable from Table 8.7. This almost constant ratio between their pressure values at each power will be called a "**pressure structuration in stages**". A similar "pressure structuration" is observed for the highly hydrogenated species: H_2 pressure is always around 20 times higher than the one of C_2H_4 and 40 times higher than the one of CH_4.

Acetylene plasma effluent	H_2	C_2H_4	CH_4	C_4H_2	C_6H_2	C_8H_2
Maximal partial pressure (Pa)	2.7	0.12	0.05	0.4*	0.05*	0.005*
Applied power for maximal pressure (W)	142	142	135	75	75	75

Table 8.7: Maximal partial pressures by decreasing order and the applied powers at which they are attained for the quantified effluents in the acetylene discharge. The pressures marked by a star (*) have been calculated with an estimated conversion factor.

Acetylene discussion

More visible on Figure 8.6a at a power of 40 W, it is interesting to note that the acetylene pressure decreases by 0.7 Pa and that the hydrogen and the diacetylene pressure are equal to around 0.35 Pa. This strongly suggests that the depletion of acetylene is not due to deposition at that power. Rather, the following balance of molecules is very likely to occur: 2 $C_2H_2 \rightarrow C_4H_2 + H_2$. To account for the production of diacetylene, a two stages reaction mechanism via the ethynyl radical ($C_2H^\bullet$) has been proposed [39, 199]:

(1) $C_2H_2 + e^- \rightarrow C_2H^\bullet + H^\bullet + e^-$

(2) $C_2H^\bullet + C_2H_2 \rightarrow C_4H_2 + H^\bullet$

(3) $H^\bullet + H^\bullet \rightarrow H_2{}^* \rightarrow H_2 + h\nu$

As a first step, the acetylene undergoes a hydrogen loss under electron impact at low electron energy (1). The second step is an acetylene addition on the produced ethynyl radical (2). Along the two steps, two $H^\bullet$ are produced which can recombine to form H_2 (3).

The "pressure structuration in stage" (constant pressure ratio between the species) of the polyyne species supports the repeated addition mechanism of $C_2H^\bullet$ to explain their formation, via reaction (4) and (5) [96]:

(4) $C_4H_2 + C_2H^\bullet \rightarrow C_6H_2 + H^\bullet$

(5) $C_{2p}H_2 + C_2H^\bullet \rightarrow C_{2p+2}H_2 + H^\bullet$

The simplest vinylidene radical, $H_2C{=}C{:}$, is a biradical. A triplet state has an activation energy of isomerization of only 2.1 eV ± 0.1 eV from acetylene HC≡CH [216, 217]. Its lifetime of 0.4 μs, before isomerization back to acetylene, is long enough to significantly react, as the mean free period of acetylene at 6.7 Pa is around 1 μs (300K, acetylene diameter 2.4 Å). Therefore, two other reactions could be:

(6) $C_2H_2 + H_2C{=}C{:} \rightarrow C_4H_2 + H_2$

(7) $C_4H_2 + H_2C{=}C{:} \rightarrow C_6H_2 + H_2$

In the previous chapter, we also proposed the biradical $^{\bullet}C_2{}^{\bullet}$ as additional intermediate because it was observed in our system by OES. This would give the two following reactions:

(8) $C_2H_2 + {}^{\bullet}C_2{}^{\bullet} \rightarrow C_4H_2{}^*$

(9) $C_4H_2 + {}^{\bullet}C_2{}^{\bullet} \rightarrow C_6H_2{}^*$

Several considerations must be enumerated for the $^{\bullet}C_2{}^{\bullet}$ biradicals:

- The complexes formed by the association reactions (8) and (9) generally carry important internal energy due to loss of initial kinetic energy and to formation of bonds. Mostly, their stabilization requires a collision with a so-called "third-body" within a sufficiently short time. At low pressure (<100 Pa), this type of process is not likely, due to very low rate constant [96, 199, 218].
- The production of $^{\bullet}C_2{}^{\bullet}$ is not favorable, as it requires a significant amount of energy.
- While being not expert in the field, the possibility of radiative deexcitations should be also considered for the stabilization of the excited complexes. Indeed, association reactions allow production of continuous optical spectrum. This would be consistent with the emission continuum observed in acetylene plasma, which were proposed in Section 7.5.1 to be due to association of C_2 ions or radicals.
- The $^{\bullet}C_2{}^{\bullet}$ biradical has been included, in addition of $C_2H^{\bullet}$, in a model accounting for the plasma polymerization of acetylene [219]. The highest calculated densities were of $6 \cdot 10^{11}$ cm^{-3} for $^{\bullet}C_2{}^{\bullet}$ and of $6 \cdot 10^{12}$ cm^{-3} for $C_2H^{\bullet}$.

The two biradicals, $H_2C{=}C{:}$ and $^{\bullet}C_2{}^{\bullet}$, proposed here are attempts to take into account their importance in the Rapid Step-Growth Polymerization (RSGP) mechanism proposed by Yasuda: the fast polymerization at low pressure is best explained by the high reactivity of biradicals (as seen in Section 2.3.3). The repeated addition of $C_2H^{\bullet}$, $^{\bullet}C_2{}^{\bullet}$ or $H_2C{=}C{:}$ may constitute pathways for acetylene depletion in the discharge. However, the rather constant pressures of

the polyyne species while the power increases do not explain the increasing acetylene depletion. Deposition on the wall would rather account for it. Moreover, it must be also acknowledged, that so far, we proposed mechanisms in the framework of plasma-phase reactions. Thereby, **surface processes** have shown to significantly influence the composition of the plasma [96]. This has to be investigated deeper.

The addition of the three proposed intermediates all results in molecular hydrogen (H_2) production at some stages, by direct production or by recombination of radical hydrogen atoms ($H^\bullet$). Concerning **ethylene** (C_2H_4) production, it can be explain by associative recombination of $H^\bullet$ with acetylene to produce $C_2H_3^\bullet$ [199]. This radical may in turn recombine with hydrogen atom to form C_2H_4. However, these are association reactions, whose products require stabilization, and in addition the decomposition reaction of $C_2H_4^* \rightarrow C_2H_2 + H_2$ have been considered by Kobayashi *et al.* [55]. In both case, the ethylene production is correlated to the amount of produced hydrogen, as suggested by their partial pressure positive correlation of Figure 8.6b. This would explain why the ethylene pressure is always one order of magnitude below the one of hydrogen.

Concerning **methane**, its production would be best explained via ethylene. As seen in the previous chapter (Section 7.4.4), the triple carbon bond seems robust enough to resist to fragmentation in the plasma. This was not observed for double and aromatic bonds which more easily fragment. Therefore, the fragmentation of the produced ethylene may seem a more probable path to explain the amount of methane observed in the present acetylene plasma. The fact that the methane pressure is half the one of ethylene may support this assumption.

Other reactions have been proposed in the literature for other detected stable species or radical intermediates, like C_4H_4 [96, 199].

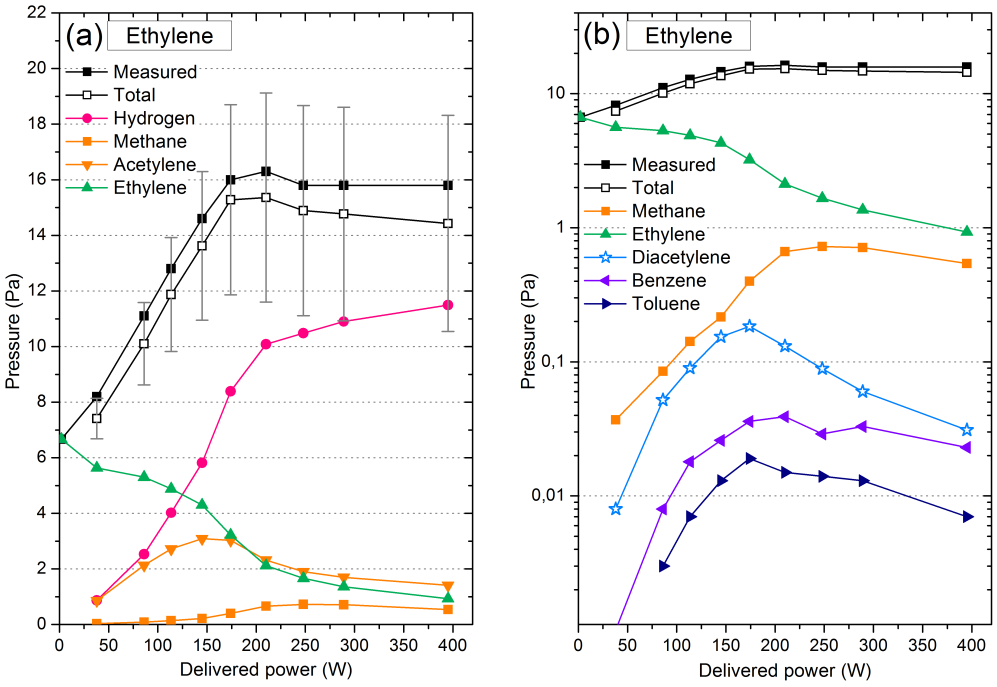

Figure 8.7: Calculated partial pressures, total pressure and measured pressure of ethylene plasma at 6.7 Pa, 28 sccm and CW, with: (a) a linear scale and (b) a logarithmic scale.

8.3.4 Ethylene plasma

Pressure graphs for ethylene are shown on Figure 8.7. For the power, as the ethylene depletion was still low at 200 W, higher powers were investigated up to 400 W. The measured pressure contrasts than for the three previous monomers with an increase up to 16 Pa.

Starting with Figure 8.7a, the measured discharge pressure linearly increases up to 175 W, above which it stabilizes. When compared to the total calculated pressure, once again the agreement is good. The main product of ethylene plasma is hydrogen, which increases monotonically to reach 11.7 Pa at the highest power. Acetylene is the second one with a maximal value of 3.1 Pa. The other effluents are reported in Table 8.8.

On Figure 8.7a, at the lowest power, it is also interesting to note the equal production of hydrogen and acetylene. It suggests a simple dehydrogenation reaction of ethylene under electron impact at a few eV in the plasma: $C_2H_4 + e^- \rightarrow C_2H_2 + H_2 + e^-$ [55]. When the power increases, hydrogen and acetylene pressures diverge. This is best explained by the ignition of the acetylene plasma chemistry, as supports the increase of diacetylene pressure on Figure 8.7b. The production of benzene is small but significantly higher than in the acetylene plasma.

Ethylene plasma effluent	H_2	C_2H_2	CH_4	C_4H_2	C_6H_6	C_7H_8	$C_{10}H_8$
Maximal partial pressure (Pa)	11.7	3.1	0.7	0.2	0.04	0.02	-
Applied power for maximal pressure (W)	400	150	250	180	210	180	-

Table 8.8: Maximal partial pressures by decreasing order and the applied powers at which they are attained for the quantified effluents in the ethylene discharge.

This means that a more hydrogenated plasma environment is required for its production. It must be reminded that other important products of ethylene plasma have not been quantified and should play significant roles. C_3H_4 (40 amu), C_3H_6 (42), C_4H_4 (52) and C_4H_6 (54) have effectively MS intensities higher than the one of benzene.

A change of slope can be observed on the hydrogen pressure curve of the ethylene plasma around 200 W. Reaching this power enabled to produce 10.0 Pa of hydrogen. Doubling the power brings only 1.7 Pa of additional hydrogen. This suggests several possibilities. Firstly, most of the hydrogen that can be easily extracted from ethylene has been produced at 200 W. We saw that at low power the dissociation of ethylene into acetylene and hydrogen is very effective. However ethylene still remains in the discharge at 200 W with 2.1 Pa. This could be due to recombination between hydrogen and acetylene, as already mentioned in acetylene discussion [55]. So hydrogen production has saturated because its high concentration induces an increase of the reverse reaction. Secondly, the hydrogen is consumed to form other species, like methane. However, the pressure of this latter has a change of slope at the same power and does not increase anymore. This maximal production suggests that its production (in smaller amount than hydrogen) either depends on the hydrogen concentration, or saturates due to the same reason of hydrogen production saturation. A third possibility is that a regime of full glow is reached at 200 W. The plasma occupies its largest volume, up to the reactor side-walls. The following picture can be depicted and will be further discussed in other sections:

- Below the critical power of 200 W, increasing the power expands the plasma volume and decreases the by-pass. This would result in an increase of the quantity of ethylene undergoing the plasma activation and the production of hydrogen.
- Above the critical power, increasing the power only allows more hydrogen production by intensifying the fragmentation within the existing plasma volume at lower power and not anymore by its expansion.

8.4 Comparison and discussion between plasmas at varying power

The quantification procedure of the partial pressures applied to the four hydrocarbon plasmas is convincing. The slight but still acceptable pressure differences observed for the benzene plasma show the importance of a careful application of this procedure.

The present section will compare the partial pressures between the four hydrocarbon discharges. To ease the discussion, styrene, benzene and acetylene will be referred as the three "highly unsaturated monomers" or as the "$C_{2n}H_{2n}$" monomers. Four features of the plasmas will now be compared in detail: the total pressure, the monomer pressure, the hydrogen pressure and the acetylene pressure.

8.4.1 Overview of the pressure differences between the four hydrocarbons

The discharge pressures of the four hydrocarbons are compared on Figure 8.8a. Ethylene is the only monomer to show an important increase of its discharge pressure and this constitutes an important feature which will be discussed. In contrast, the three $C_{2n}H_{2n}$ monomers revealed a very distinct pressure drop. Acetylene shows no pressure increase, unlike styrene and benzene. Furthermore, its pressure drop occurs at a distinctly lower power than the one of styrene and benzene.

Several competitive processes determine the discharge pressure in plasma. The fragmentation of a monomer into two (or more) stable products increases the pressure. On the contrary, the reaction between two molecules leading to their attachment without secondary product decreases the pressure and is termed "recombination" or "association". Regarding the boundary surfaces of the plasma, the physisorption or the chemisorption of a species on it decreases the pressure. They both will be referred as "deposition". Finally, the etching of molecules from the surface increases the pressure.

As already said (Section 8.3.3), associative recombinations are not likely in our pressure range [96, 218]. It indeed requires a third body stabilization, except in the case of a radiative deexcitation of the excited complex.

The dominating species identified in the four plasmas are always the monomer, hydrogen and acetylene. Their partial pressures are shown on Figure 8.8b, 8.9a and 8.9b, respectively. As those species generally constitute 90% of the pressure discharge, the addition of their three pressures accounts rather well for the total discharge pressure.

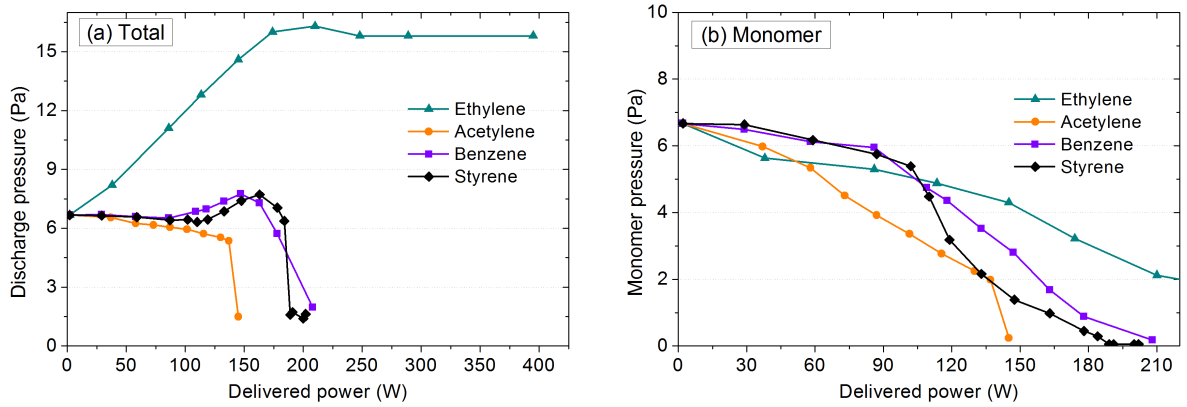

Figure 8.8: Comparison of: (a) the four measured discharge pressures and (b) the four monomer partial pressures.

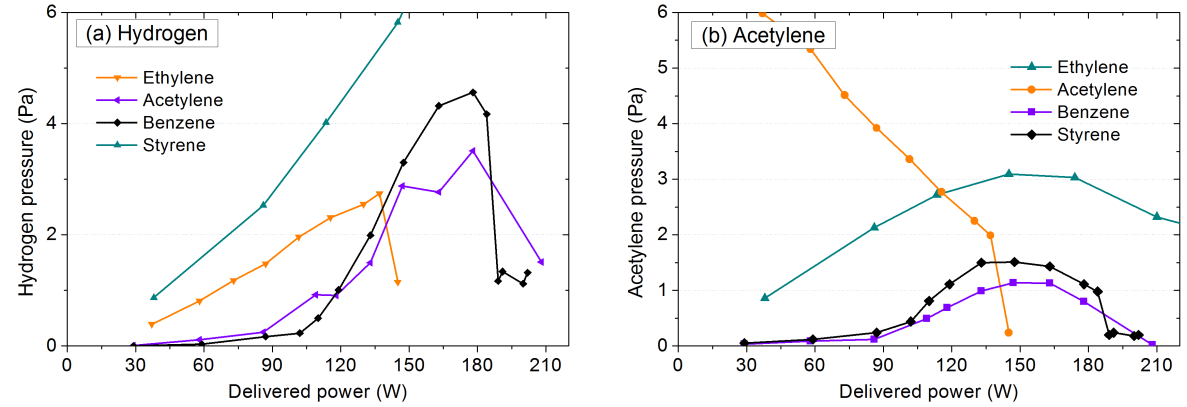

Figure 8.9: Comparison of: (a) the hydrogen production in the four discharges and (b) their acetylene content.

A quick comparison shows that the **discharge pressure of ethylene is explained by its large hydrogen production**, accounting for 74% of the pressure at the highest power. Fragmentation is then the dominating mechanism regarding ethylene, which should lead to a limited deposition in the reactor. In contrast, the deposition is of uttermost importance to explain the discharge pressure trends of the three $C_{2n}H_{2n}$ monomers. Indeed, species containing carbon atoms almost disappear at high power from the gas phase. Only a small amount of hydrogen remains, suggesting that **small dehydrogenation is needed to carry out the large deposition**.

The pressure drop (and the supposed deposition rise) occurs at the lowest threshold power for acetylene. This could suggest that acetylene plasma chemistry induces a faster deposition, by producing very easily a fast polymerizing intermediate. It could be supported by styrene

and benzene plasmas for which the discharge pressures start to decrease when the maximum of acetylene is produced. The need to be firstly decomposed into acetylene may explain their pressure drop towards higher power. This is consistent with the statement in the literature that acetylene is the main **precursor** of plasma polymer deposition for saturated and unsaturated monomers [55]. However, we are convinced that this hypothesis is not correct.

The measure in high concentration of a product in a plasma does not generally mean it is a precursor for deposition [38]. It rather indicates the combination of a significant production and a good ability to survive in the plasma when produced. This has been already discussed by Yasuda (in [71] p132-138) regarding the proposition of acetylene as deposition precursor in hydrocarbons plasmas [55]. Three such cases of precursor elucidation in silane, methane and C_xF_y plasmas have also been recently resumed by Von Keudell [9]. In the present case, it is well comprehensible for hydrogen, which does not polymerize, but less for acetylene whose discharge is one of the most polymerizing.

This is best illustrated in the present case by the ethylene discharge: it produces the largest amount of acetylene but shows no pressure drop and thus supposedly no deposition enhancement. In addition, hydrogen is detected in significant amount at power just below the pressure drop in the styrene, benzene and acetylene discharges. It does not certainly make hydrogen the polymerization precursor responsible for their pressure drop.

8.4.2 Focus on monomer pressure evolution

For the ease of the lecture, the monomer pressure evolutions are reminded on Figure 8.10. In the acetylene plasma, the acetylene partial pressure decreases linearly, while the hydrogen one increases linearly. Moreover, we have seen in the previous chapter that acetylene plasma chemistry virtually indicates no fragmentation of the triple carbon bond. These observations could indicate that dehydrogenation occur as soon as a small power is applied and linearly increases with the mean energy transmitted per monomer to the plasma. However, this seems unlikely as the C-H bond has much higher bond energy in acetylene (5.7 eV) than in ethylene (4.8 eV) or in methane (4.5 eV) [14]. Therefore, an effect related to an increase of the **plasma volume** seems more likely. At low power, the plasma volume is small, the energy density is already quite high in that small volume and dehydrogenation can already easily occur. With increasing power, the plasma volume increases, the energy density increases only slightly and the depletion increase could be mainly explained by the smaller by-pass of acetylene.

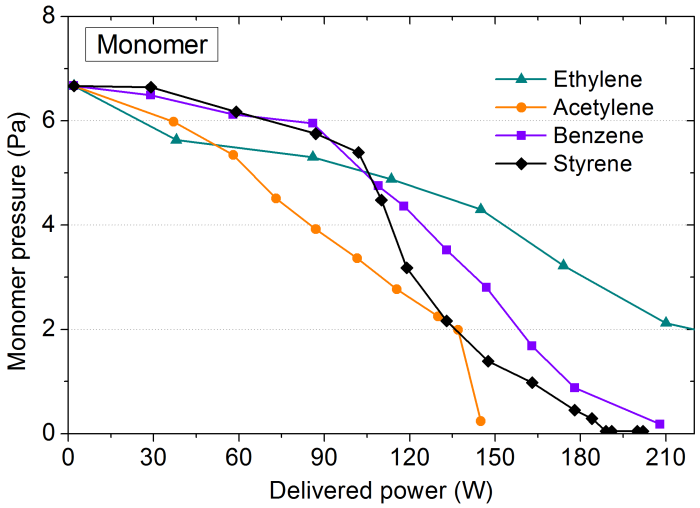

Figure 8.10: Reminder of the monomer pressure evolution as a function of pressure.

Ethylene is the most depleted at low power (Figure 8.10) and with the largest hydrogen and acetylene production (Figure 8.9). However, these two high productions may be induced by another path of production than single dehydrogenation. Instead of a single radical H atom loss, dissociation with rearrangement could occur: $C_2H_4 + e^- \rightarrow C_2H_2 + H_2 + e^-$. This has been suggested for electron impact on the basis of photolysis of ethylene [55].

Monomer pressure trends are different in the plasmas of styrene and benzene. At powers below 90 W, they are much less depleted than acetylene and ethylene and produce much smaller amount of hydrogen. Where goes the power delivered by the generator? Their larger size relatively to acetylene and ethylene induces a larger geometrical cross sections for collisions with the electrons. Their rate constant and reaction rate being larger, it could affect the electron temperature and density and thus the coupling efficiency. Moreover, their larger size also offers much higher ability to absorb energy by vibrational excitation, but also by fragmentation, than in the case of acetylene and ethylene.

Above 90 W, the monomer pressure trends of benzene and styrene both show a change of slopes but the values of these slopes are different: styrene is depleted faster than benzene and produces more acetylene (Figure 8.9b). This suggests the following hypothesizes. Firstly, the change of their monomer slopes could indicate the start of their decomposition. Most likely it would occur through dissociation of both carbon bonds and C-H bonds, as the hydrogen and acetylene production starts to increase for both of them (Figure 8.9). Secondly, the higher styrene depletion may occur via the easier cleavage of its phenyl-vinyl bond. This is also suggested by the slightly higher acetylene production of the styrene discharge.

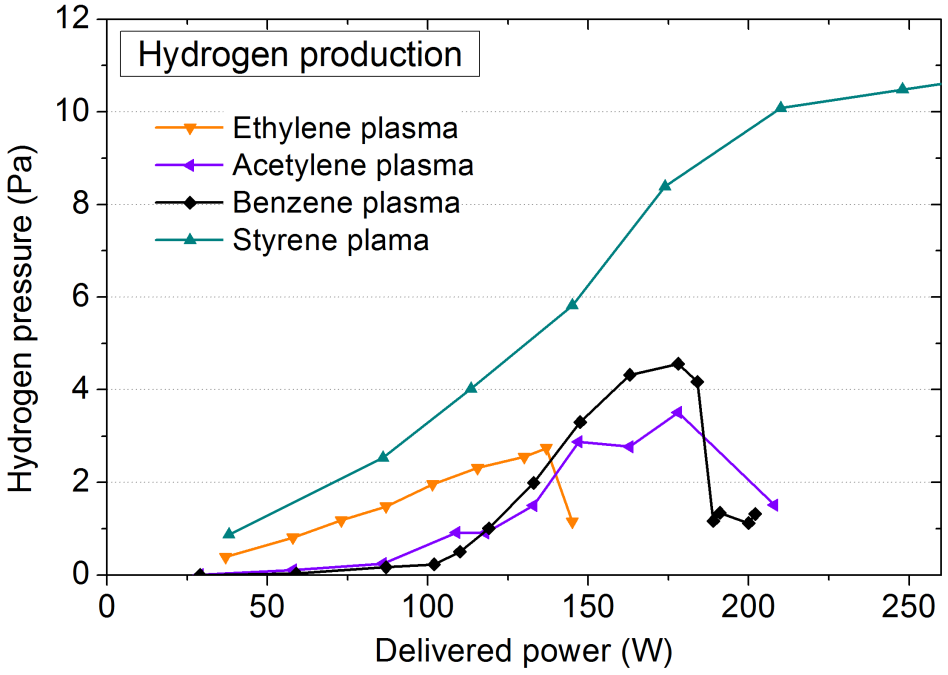

Figure 8.11: Reminder of the hydrogen production in the discharge of the four monomers.

8.4.3 Hydrogen production in more details

The presence of molecular hydrogen in hydrocarbon discharge has been proposed as responsible for reducing deposition rate [55]. The main reason for that is its potential ability to scavenge acetylene and convert it into ethylene, which much less polymerizes under plasma conditions. As we disagree with this hypothesis, we wanted to discuss the hydrogen production in more details. For the ease of the lecture, the hydrogen pressure evolutions are reminded on Figure 8.11.

The main common feature of the four studied discharges is their large production of hydrogen. It is always the dominant product, except for styrene at low power. Ethylene produces hydrogen with a maximal observed pressure of 11.5 Pa, which is much more than the ones of styrene (4.6 Pa), benzene (3.5 Pa) and acetylene (2.7 Pa), as summarized in Table 8.9. This may be explained by the very low enthalpy of reaction for hydrogen production from ethylene: $C_2H_4 + e^- \rightarrow C_2H_2 + H_2 + e^-$ (1.8 eV) [56]. In addition, the relative hydrogen content and the relative injection rate of hydrogen atoms may also give qualitative answers and are explained hereafter.

The relative hydrogen content of the monomer or more briefly the "H content" is defined as its H/C ratio. The H content of ethylene (C_2H_4) is equal to 2, which is twice higher than the H/C ratios of the three $C_{2n}H_{2n}$ monomers, as summarized in Table 8.9. However, it is different in terms of the relative injection rate of hydrogen atoms (stated as "H rate" for concision). Indeed,

Monomer	**Relative H content**	**Relative H rate**	**Maximal H_2 production** (Pa)
C_2H_4	2	2	11.5
C_2H_2	1	1	2.7
C_6H_6	1	3	3.5
C_8H_8	1	4	4.7

Table 8.9: Relative H content and relative H rate of the four monomers.

being injected at the same flow, styrene (C_8H_8) introduces twice more H atoms in the reactor per second than ethylene. Setting the H rate of acetylene (C_2H_2) to 1, the relative H rates are equal to: 2 for ethylene (C_2H_4), 3 for benzene (C_6H_6) and 4 for styrene (C_8H_8) (see Table 8.9).

The doubled H content of ethylene is definitely the dominant factor to explain its much higher hydrogen production in discharge. However, for the three $C_{2n}H_{2n}$ monomers which have the same H/C ratio, the H rate is qualitatively correlated with the higher maximal hydrogen pressure as visible in Table 8.9.

In addition, it is expected that styrene and benzene produces more hydrogenated species and more hydrogenated films on the reactor walls than acetylene, because they produce only slightly more H_2 than acetylene but have a much higher H content and H rate. Concerning the higher production of hydrogenated species in styrene and benzene discharges, it has been shown in the previous chapter when comparing their plasma mass spectra. It is confirmed here when comparing the production of methane and ethylene in the logarithmic pressure figures of the three $C_{2n}H_{2n}$ monomers (Figure 8.4, 8.5 and 8.6).

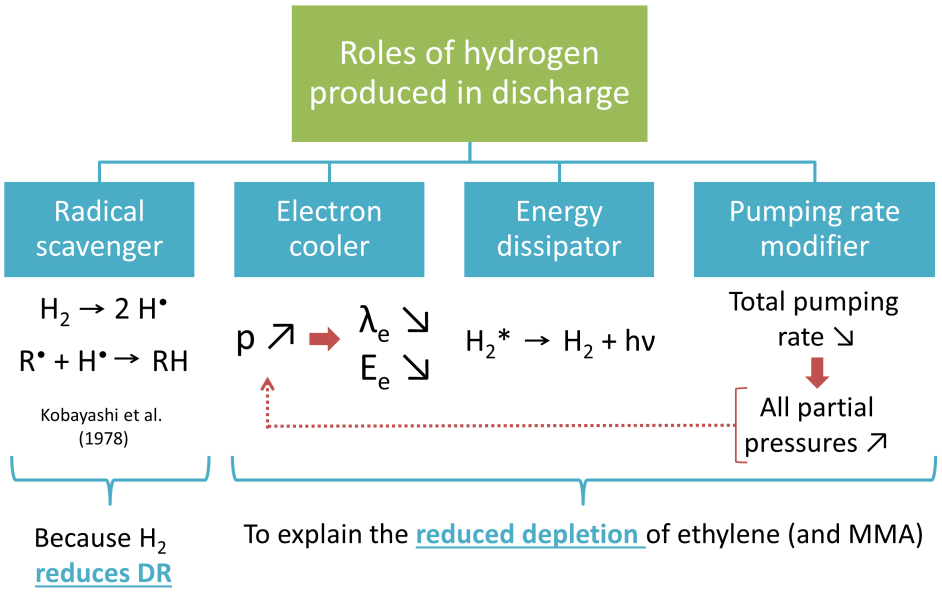

Figure 8.12: Scheme of the different effect proposed for hydrogen produced in hydrocarbon discharges.

8.4.4 The roles of hydrogen

In addition to the above mentioned "scavenging effect" of hydrogen on acetylene, we are convinced that presence of hydrogen plays other roles, summarized on Figure 8.12.

A first hydrogen role is the "**electron cooler**": the reduction of the electron temperature and the mean energy absorbed by species in the plasma. Here is our reasoning. The large amount of produced hydrogen in the ethylene plasma increases the pressure. This reduces the mean free path of electron and then shifts their energy distribution function towards lower energy. With lower energy on the average, electrons are less able to carry out fragmentation and radical formation. They are also less able to ionize species which reduces the electron density. This latter effect also reduces the fragmentation. This first hypothesis of the role of hydrogen may explain the highly reduced monomer depletion of ethylene, compared to the three $C_{2n}H_{2n}$ monomers. However, the effect of the partial pressure increase of H_2 may be more complex than depicted [180]. Direct measurement of electron density and temperature are required to test this assumption.

A second hydrogen role is the "**power dissipator**". Electronic excitation is indeed an energy consuming mechanisms, contributing to deplete the high energy part of the electron energy distribution function (Section 1.4.2). The consecutive radiative deexcitation produces UV photons of significant energy which can be reabsorbed by another species or can be absorbed

by the walls. In the latter case, the energy is lost by the plasma. This is supported by the large H_2 continuum observed in the optical emission spectrum of styrene in our conditions, visible on Figure 6.6 (page 101) and discussed in Section 7.5.1 (Page 137). It can also be seen, but in other conditions, in the work of Li *et al.* [117].

Finally, a last role of hydrogen is the "**pumping rate modifier**". Indeed, on one hand, by increasing the total pressure, the presence of hydrogen increases the overall pumping rate of the primary pump, as we saw in Section 8.1.2. On the other hand, hydrogen does not condense on the nitrogen trap, which reduces the overall pumping rate as we will see in detail (Section 10.4.6). The latter effect is actually must stronger than the first and therefore, as indicated by the dashed arrow on Figure 8.12, the partial pressures of all the other species increases.

Those three hydrogen roles can have an important effect on the deposition process. The first one as "electron cooler" would lead to less deposition, due to its lowering of the fragmentation and the activation of species. The second role as "power dissipator" also favors less deposition. For the third role, an decrease of the pumping rate would increase the residence time of ethylene and thus increase the chances of its fragmentation. However, the overall effect of the pressure increase is expected to soften plasma conditions by softening the plasma intensity in our conditions (decrease the electron temperature). This will be supported by the low MMA depletion at the very high power of 500 W (Section 10.4.1).

At this stage, it is not possible to judge if those roles are more important than the presumed "scavenging effect". However, now that it has been discussed, it could help to explain the evolution of the deposition rate (DR) observed in chapter 6 on styrene plasma deposition (see Figure 6.1, page 95). Indeed, the DR of styrene at the substrate holder location had been observed to decrease with a decreasing slope from 120 to 185 W. Figure 8.11 shows that this power increase corresponds to a burst in the hydrogen production: its pressure increases from 1 to more than 4 Pa. On Figure 8.10, we can also observe a decrease of the styrene depletion on the same power range: the negative slope is slightly reduced. This indicates a potential strong effect of hydrogen on the plasma chemistry and at the same time on the deposition process. But through which of the above mentioned roles? This is an opened issue.

8.4.5 Monomer classification and critical power

The monomer classification and the concept of critical power proposed by Yasuda can apply to discuss some observations (Section 2.5.1).

As explained in section 2.6, hydrocarbon monomers can be classified into three groups. To belong to group I, the monomers must contain triple bonds or aromatic cycle accompanied or not by a double bond. This is the case of styrene, benzene and acetylene. Moderately unsaturated, group II monomers contain a single double bond and/or a non-aromatic cycle. Ethylene therefore belongs to group II. The last group, the group III, corresponds to the fully saturated monomers.

The critical power (or wattage) W_C is empirically defined to be the input power above which several simultaneous phenomena are observed in a plasma polymerization process. It is the power above which the deposition rate (DR) becomes constant, at which the discharge pressure stabilizes and for which the plasma volume reaches its maximal value [3]. Above this power, it is then considered that the plasma is in "full glow" conditions

The critical power value for group II monomers (ethylene) has been observed to be generally much higher than for group I (styrene, benzene, acetylene). It explained why, in the same conditions of flow and power, group II shows less deposition than group I. In our case we did not study deposition characteristic of the four monomers, but their depletion in the discharge. However it seems reasonable to consider that higher deposition requires higher monomer depletion. As ethylene belongs to the less depositing group II, this could explain why ethylene is less consumed than styrene, benzene and acetylene in the same conditions. Going even further, this could actually be **the cause of the Yasuda classification,** as many of his works are dealing with cold trap as pumping system. The high release of hydrogen increases the total pressure which softens in turn the plasma conditions. Indeed, the Yasuda classification was also correlated with the hydrogen release [71] (p84).

According to the definition of critical power (pressure stabilization), the one of ethylene should be around 200 W. It is interesting to note that the plasma composition continues to evolve above this critical power. For styrene, the critical power would be at 185 W, if a pressure drop can be taken as such. We saw in the corresponding chapter that the aromatic content of the styrene plasma deposited film continues to vary above 185 W (Section 6.3). These two observations indicate that above the critical power investigation of the plasma and the deposition process are still useful.

Finally, it is worth mentioning that the critical power has been established for capacitively coupled (CC) and inductively coupled (IC) reactors. For the IC geometries, only the helical coil has been studied. Thus it has never been evaluated for our kind of planar IC geometry. Therefore, the observation of a pressure stabilization for ethylene could constitute a first observation of critical power in planar ICP. Moreover, the reaching of a full glow conditions for ethylene at 200 W suggests that a full glow condition has reasonably occurred for styrene at 185 W. This supports the assumption we made about the achievement of styrene full glow at 185 W. This was stated on the basis of the DR discontinuity in the chapter on styrene plasma deposited films.

8.4.6 Conclusions of the four discharges comparison

Several relevant conclusions can be drawn on the comparison of the partial pressures between the four hydrocarbon plasmas.

(1) The highest depletion of ethylene at low power and its highest hydrogen production indicates an easy fragmentation pathway, with a low activation energy, such as : $C_2H_4 + e^- \rightarrow C_2H_2 + H_2 + e^-$.

(2) The lowest depletion of ethylene at high power and the absence of pressure drop of the ethylene discharge support the following assumption. The increase of the discharge pressure due to hydrogen softens the plasma conditions. This could be highly important if it was actually the original cause of the monomer classification of Yasuda.

(3) The pressure drop of acetylene at the lowest threshold: acetylene produces no other product than H_2 and thus its total pressure can not increase. The lower pressure may initiate a E/H transition at a lower threshold power, suspected because of the jump of monomer depletion from 70% to 100% at the threshold, in contrast with styrene and benzene.

(4) The very low hydrogen production above the power threshold of acetylene, benzene and styrene means that very large deposition can occur without deposition. This may be explained by our particular reactor geometry. When the plasma expands laterally to the side-walls, there is no flow by-pass anymore which enhanced the monomer depletion. The softer plasma conditions at the side wall and just at the entrance location of the monomers (shower ring) may allow a very soft activation and deposition of the monomer, before reaching the hard plasma volume in front of the source.

(5) The very low depletion of styrene and benzene below a threshold around 100 W is raising questions.

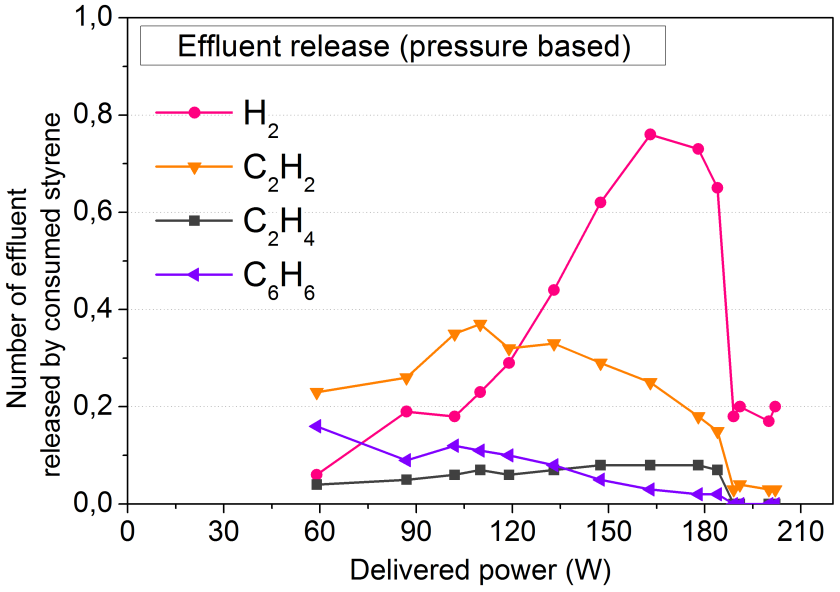

Figure 8.13: Number of effluent molecules released by consumed styrene monomer.

8.5 Taking advantage of absolute pressures

The objective of the present section is to extract the type of information available from absolute partial pressures: the number of effluent produced by consumed monomer (Section 8.5.1) or the amount of mass contained in the plasma-phase (Section 8.5.2).

8.5.1 Number of effluent released by consumed styrene and survival rate

The interest of quantifying the partial pressure is the possibility to answer to the following type of question: how many acetylene molecules are produced and survive by consumed styrene in the discharge? It allows to evaluate if the amount of acetylene detected is really important. This can be roughly estimated on the basis of the measured partial pressures and is presented here in the case of styrene. However, all the results presented here will have to be corrected by the overall pumping rate change demonstrated in Section 10.4.6.

Considering a complete decomposition of styrene exclusively into acetylene and that no deposition occurs in the reactor, each styrene monomer (C_8H_8) would produce at the most four acetylene (C_2H_2). This gives the maximal theoretical release of styrene for acetylene. A first estimation of the experimental number of acetylene produced by styrene molecule can be made by dividing the pressure of acetylene by the pressure of consumed styrene. The latter is simply obtained by subtracting the remaining styrene pressure in the discharge from the initial

Number released by consumed styrene	$\mathbf{H_2}$	$\mathbf{C_2H_2}$	$\mathbf{C_2H_4}$	$\mathbf{C_6H_6}$
Theoretical maximum	4	4	2	1.33
Experimental maximum	0.76	0.37	0.08	0.12
Applied power (W) at experimental maximum	165	115	165	115

Table 8.10: Theoretical and experimental number of effluents released by consumed styrene monomer.

pressure of 6.7 Pa. However, care must be taken as this implies the incorrect assumption that the pumping rate is constant (see future Section 10.4.6). Nevertheless, it is worth at this stage and the results will revealed to be an upper bound for the species production. The production estimation has been made for every power of the series investigated, as well as for other molecules than acetylene: hydrogen, ethylene and benzene. The result is on Figure 8.13.

The results at 30 and 60 W are neglected as the styrene depleted pressure is small and may induce large errors when dividing the effluent partial pressures. For hydrogen, the maximal release by styrene molecule reaches 0.76 at the most productive power of 165 W, as summed up in Table 8.10. Knowing that the maximal theoretical release is four, this is limited. For acetylene, it is maximum 0.37. The ethylene and benzene release is below 0.12 and toluene and naphthalene are both below 0.03 (not shown). Based on the produced pressures, which over estimate the results (see Section 10.4.6), we observe that the release of effluents from decomposition of styrene is moderate to small.

The initial question can be answered. The partial pressures of hydrogen and acetylene may seems important, but in terms of release by consumed styrene, it is moderate. This simply shows that the deposition process is efficient.

Benzene and acetylene are worth to be compared, as they can be produced in equal amount from the dissociation of the weakest bond in styrene, between the phenyl and the vinyl groups. More acetylene is released by consumed styrene than benzene. This can be explained by the possible decomposition of the produced benzene into acetylene in the plasma. It is quite clear from the acetylene production in the benzene plasma. However, a main difference between benzene and acetylene is their mass and the fact that, at room temperature, benzene, which is a liquid precursor, must condense much more easily on the surrounding surfaces or less escape from them than acetylene which is a gaseous precursor. Said in other words, light species should have a better **survival rate** at the exit of the plasma than the heavy ones, if they would interact

with a surface on the way. Surface processes have been effectively shown to influence greatly the plasma compositions [220] and diffusion of species could be estimated [221]. This aspect have been very few considered in the present work and should be worth to be considered in future works in the laboratory.

8.5.2 Tracking the mass in styrene plasma

In addition to the analysis of the effluents released by consumed monomer, we can go further by correlating the partial pressures to the total deposited mass estimated at two powers in Section 6.6.2 (120 and 210 W). The objective is to think now in terms of **mass conservation**: how much has been consumed and where does it go, into the pump or onto the wall? Regarding the gas-phase, it will be done on the basis of the partial pressures, which once again is not correct but constitute an upper bound to estimate the mass contained in the gas-phase, as we will demonstrate later.

At 120 W, the total deposited mass was estimated to be 33% of the total injected mass of styrene (see Table 6.4 on page 109). This calculation was made on the basis of the film density at the substrate holder. As we expect a higher film density, for instance, on the quartz window, this is a lower bound for mass deposited on the walls.

At 120 W, the (pressure based) monomer depletion is of 52.3%, which means a depletion of 3.5 Pa of styrene. Instead of calculating exactly the mass, we propose to invent the following (pressure or density based) mass indicator. By multiplying the lost pressure of styrene (3.5 Pa) by the mass in Da of the styrene molecule (104), we obtain a value proportional to the mass of consumed styrene, expressed in "Dalton Pascal" units, which will be written "DaPa": 3.5 Pa x 104 = 364 DaPa.

Beside, the discharge produces several effluents whose partial pressures have been measured and are indicated in Table 8.11. The third line of the same table reveals the number "DaPa" for each effluent, obtained by multiplying their mass by their partial pressure. The fourth line of the same table is the percentage of these latter values relatively to the DaPa of the consumed styrene (364 DaPa). They are the values which interest us: the percentage of the consumed mass of styrene took away by each effluent. The last column of Table 8.11 is the sum of each line.

We can conclude to the following picture at 120 W. From the total styrene injected and in term of mass:

- 52% has been consumed as measured by MS.

Depleted styrene = 364 DaPa	H_2	CH_4	C_2H_2	C_2H_4	C_6H_6	C_7H_8	$C_{10}H_8$	Total
Partial pressure (Pa)	0.23	0.05	1.11	0.23	0.33	0.07	0.07	1.87
Mass x pressure (DaPa)	0.5	0.8	29.0	6.3	26.0	6.2	9.4	77.7
Relative mass	0.1%	0.2%	8.0%	1.7%	7.1%	1.7%	2.6%	21.3%

Table 8.11: Relative distribution of the consumed styrene mass into the effluents.

Depleted styrene = 691 DaPa	H_2	CH_4	C_2H_2	C_2H_4	C_6H_6	C_7H_8	$C_{10}H_8$	Total
Partial pressure (Pa)	1,32	0,08	0,20	0,00	0,03	0,01	0,01	0,33
Mass x pressure (DaPa)	2,64	1,35	5,27	0,09	2,24	0,69	0,91	10,55
Relative mass	0,4%	0,2%	0,8%	0,0%	0,3%	0,1%	0,1%	1,5%

Table 8.12: Relative distribution of the total mass contained in the gas phase.

- 33% has been deposited (lower bound, due to film density under-estimation)
- 21% has been transformed into effluents (upper bound, due to pressure over-estimation)
- Total: **52% consumed ≈ 54% deposited and transformed** !

For the pleasure, we do it again for the power of 210 W, above the critical/transition power, with a monomer depletion of 99.2%. The values are indicated in Table 8.12 and the result is:

- 99.2% has been consumed as measured by MS.
- 98% has been deposited (lower bound, due to film density under-estimation)
- 1.5% has been transformed into effluents (upper bound, due to pressure over-estimation)
- Total: **99.2% consumed ≈ 99.5% deposited and transformed** !

As a conclusion, the estimation of the mass in the gas phase is in agreement with the difference between the mass injected and the mass deposited. This may be a fortunate compensation between the mass deposited, which is certainly under-estimated (based on the film density at the substrate holder, where it should be lower than at the quartz window) and the partial pressures, which over-estimate the real amount of effluents produced (to be demonstrated in Section 10.4.6). However, the calculation was interesting by showing that:

- acetylene and benzene take away the major part of the mass in the gas-phase at 120 W;
- hydrogen is negligible in term of mass, even if it has the highest partial pressure;
- it is possible to do such estimations.

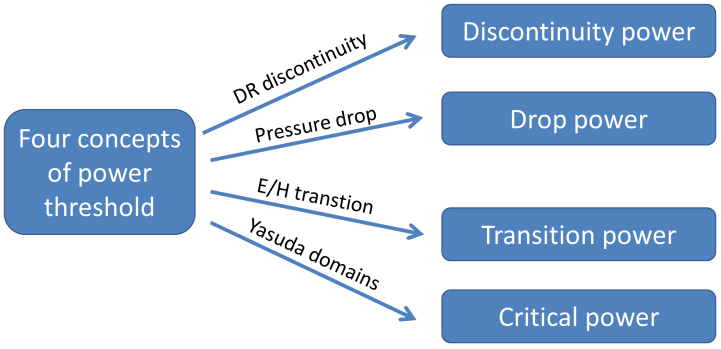

Figure 8.14: Summary of the four concepts of power threshold, defined on several observations: DR discontinuity, discharge pressure, E/H transition and domains of plasma polymerisation.

8.6 Pressure drop and simultaneous threshold powers

The objective of the present section is further discussing the questions left unanswered in the chapter on styrene plasma deposition about the simultaneous occurrences at the same threshold power of: the deposition rate (DR) discontinuity, the pressure drop and the E/H transition. Moreover, it had been detected that the monomer depletion was already very high just below the transition/drop/discontinuity power observed for styrene (Section 6.5.3).

The simultaneity of the three above mentioned phenomena may be fortuitous. Therefore, it seems important to give to each of them a different name for their threshold, as summarized in Figure 8.14.

At the present stage of our reflexion, our comprehension is not clear but we present on Figure 8.15 a scheme which could help visualizing the interconnections. As was summarized in Section 6.7, the starting point is that the **DR discontinuity** can be both explained by a discontinuity in the **production of film-forming species** and a discontinuity in their **transport to the substrate holder**, which is only one local point of the reactor. The whole following discussion will then be about detecting the potential causes of the observed DR discontinuity.

In our opinion, the production rate of the film-forming species is largely determined by the electron density and the electron temperature . Here lies the direct connection of the E/H transition, with its sudden increase of the coupling efficiency, due to the **positive feedback "A"** (on the scheme of Figure 8.15) between the electron density and the power absorbed, described in Section 1.2.3). It results in an abrupt increase of the electron density and thus a burst in the production rate of film-forming species.

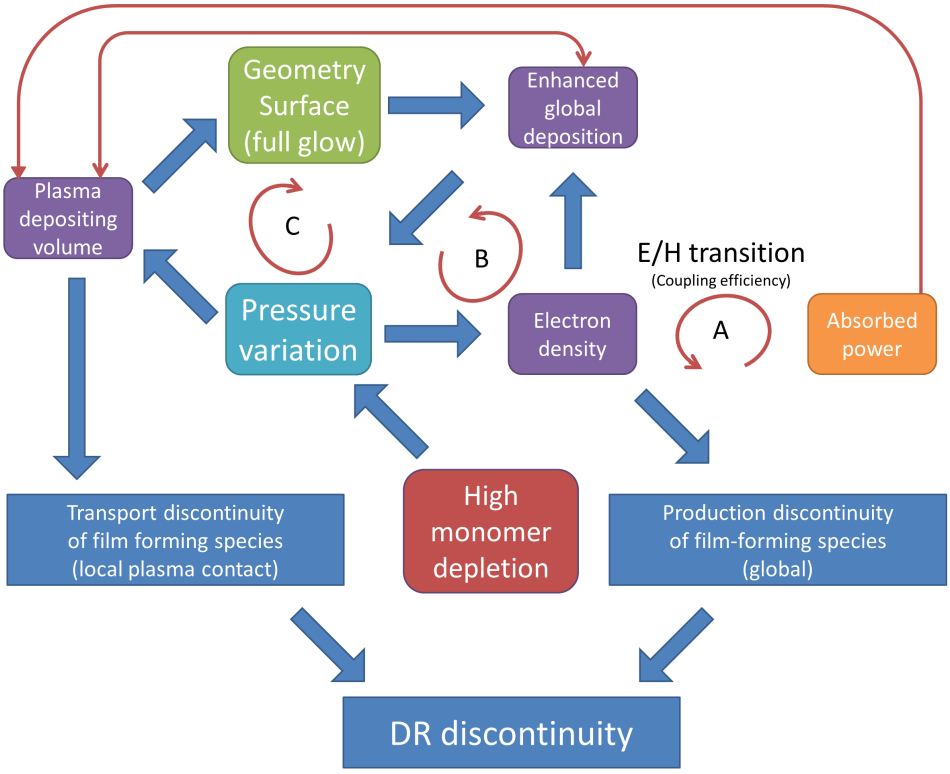

Figure 8.15: Scheme summarizing the interconnections regarding the discussion of the critical/transition/drop powers and the three positive feedbacks which could allow to explain the DR rate discontinuity of Section 6.2.

However, at the same time, this film-forming increase induces a global enhancement of the deposition, which can result in our flow system to a change of the total pressure, which is well-known to affect in turn the electron density. It shows another potential feedback process (the B circle arrow on the scheme) which may provide an abrupt variation of pressure. If strong, the pressure change affect the plasma volume and and thus directly the local deposition at the substrate holder. But, on the other hand, the change of the plasma volume may enhanced the global deposition depending on the surfaces geometry: for a moderate lateral increase of the plasma volume in our system, the plasma may suddenly contact the side-walls and increase the global deposition. In turn, this will decrease the pressure and starts a third positive feedback (C on the scheme). This shows a potentially high dependence on geometry to explain a pressure drop: the availability of surfaces which allows pumping of the activated species, which can otherwise deactivate. We could also remind that the E/H transition is also dependent on the pressure, as shown for closed systems with simple gases [180].

Clearly, the situation is highly complex and finding a solution with our very limited observations is impossible. The measure of the electron density, electron temperature, coupling

efficiency, plasma volume and also radicals fluxes would be necessary. The local measure of the deposition rate at the substrate holder location is depending on a large number of local and global quantities and their related phenomena. Moreover the occurrence of a E/H transition is even not known in acetylene and benzene plasma at their respective pressure drop power (the E/H transition has been observed for acetylene and is shown in Appendix A). Nevertheless, several observations made on our measured partial pressures may contribute to answer.

A first observation is: acetylene has a pressure drop well before reaching full monomer depletion. Indeed, on Figure 8.8b, the acetylene partial pressure is of 2 Pa at a power just below the drop power at 140 W (MD = 70%). Thus, we conclude from this observation that a pressure drop is not necessarily occurring with a progressive reach of 100% of monomer depletion, like it was suggested for styrene. Thus the arrow between "high monomer depletion" and the "pressure variation" may be weakened if not completely removed on the scheme of Figure 8.15.

A second observation is: ethylene has no pressure drop. Thus monomer producing large amount of non-polymerizing gases are less subject to abrupt transition. It would be very interesting to measure if a E/H transition is occurring in ethylene plasma on the investigated power range. It could reveal to which extend the total pressure of discharge affect the possibility of a E/H transition. (This has been done and is shown in Appendix A).

A third observation favors the "geometry effect" of the Figure 8.15 and thus the full glow hypothesis made in Section 6.7.2.

- The total mass deposition in the case of styrene plasma is enhanced on the reactor side walls above the critical power, as seen previously (Section 6.6.2).
- The small production of hydrogen (H_2) above the critical power means that the hydrogen atoms stay in their parent monomer and are incorporated into the polymer films. Moreover, quantitatively, acetylene, benzene and styrene discharges produce more or less the same amount of hydrogen above the critical power (1.0 to 1.5 Pa). This indicates that very soft dehydrogenation is sufficient for high deposition.
- Anticipating results from Section 10.4.6, a rapid estimation of the real number of hydrogen molecules released by consumed styrene can be made. Above the critical power, on Figure 8.13, the number of H_2 released by consumed styrene is 0.2. In these conditions, as the gas-phase is mainly composed of hydrogen, the pumping rate is much lower and the measured partial pressures over-estimate with a factor of 3 the number of molecules produced (Section 10.4.6). Therefore the real number of H_2 released by consumed styrene is divided by 3. It means that in these very energetic conditions, only **1 styrene molecule over 15 is releasing a hydrogen molecule**.

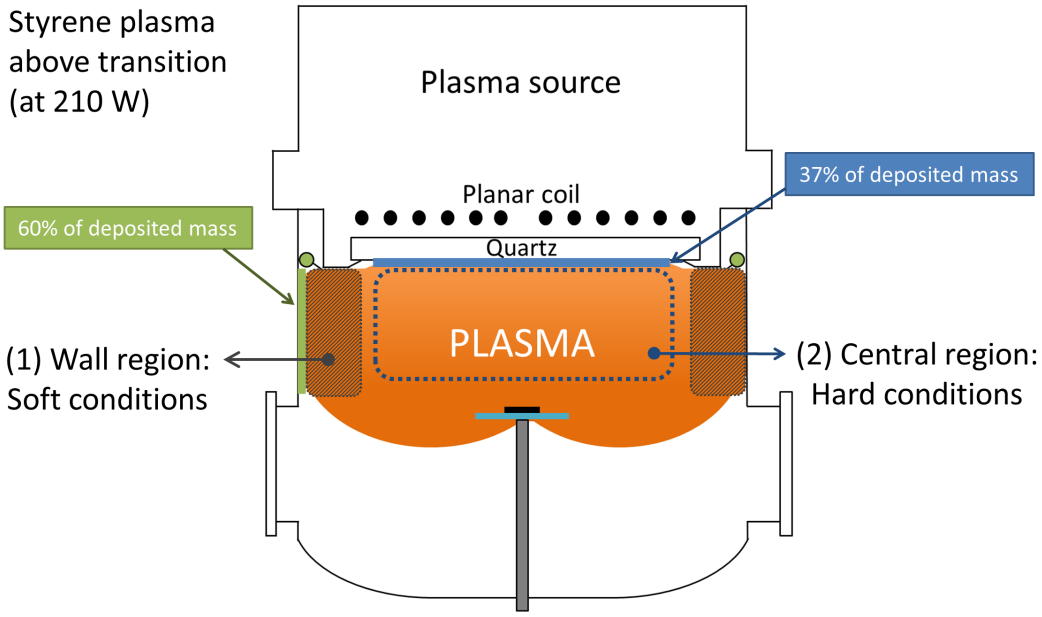

Figure 8.16: Scheme of plasma volume to explain the lower hydrogen production above the E/H transition through differences in the local plasma intensity.

- We develop hereafter a reasoning already reported in Section 6.7.1 allowing us to explain this very low number of released hydrogen. Our reasoning is based on the geometry of the reactor and especially the plasma volume, depicted on Figure 8.16. The best explanation in our opinion is that the plasma has expanded close to the reactor walls and almost up to the shower ring. However, the plasma is much weaker there (Region (1) on the figure) than just in front of the quartz window (Region (2)). Thus, a soft activation of the styrene monomer occurs and with no possibility to by-pass anymore the plasma region. Moreover the very large surface of the side walls available for deposition allows a very large deposition and the consequent pressure drop. In contrast, the plasma conditions are much harder in the central region (2). However, as much fewer styrene access this region, a much lower fragmentation and thus dehydrogenation occur.

As a test for this latter scenario, we propose to compare the film aromaticity at the substrate holder location to the one at the side wall. A higher aromaticity retention should then be expected at the side wall.

Now, this scenario does not exclude the E/H transition, as it could initiate the required lateral expansion of the plasma volume. But the reverse is possible, the change in the pressure could initiate the E/H transition. The ethylene case, with its very large pressure increase, could serve as a test by observing if any E/H transition occurs within the power range investigated.

8.7 Conclusion

The present chapter was dedicated to the partial pressure quantification in unsaturated hydrocarbon plasma. The agreement was excellent between the total pressure measured by absolute pressure gauge and the total pressure estimated by Mass Spectrometry.

The discussion of the partial pressure trends for acetylene allows one to discuss mechanisms proposed in the literature to account for the observed species. The author also proposed two biradicals as intermediates of reaction, in better agreement with the "Rapid Step-Growth Polymerization" mechanism proposed by Yasuda to explain the very fast polymerization under low pressure conditions (Section 8.3.3). However, this has to be better compared to the existing literature on acetylene [96].

A sharp pressure drop at a threshold power was observed for the three $C_{2n}H_{2n}$ monomers (acetylene, benzene and styrene) but not for ethylene. Measuring the light emission to evaluate the occurrence of a E/H transition has been suggested, and especially for ethylene. It should bring interesting data to disuss this transition and its relation with the occurrence of pressure drops or not.

The careful analysis and discussion of the hydrogen production in each discharge lead to propose three roles for hydrogen in addition of the "radical scavenging" role: the "electron cooler" role, the "energy dissipator" role and the "pumping rate modifier" role. The two firsts are in agreement with the observed effect of reduction of the deposition rate of hydrogen [55], as long as it is related to the monomer depletion. The third effect increases the overall pressure of the discharge which is thought to soften the plasma conditions, while the W/F is kept constant. This is supported by available but unshown measurements in styrene discharge: the monomer depletion decreases when the pressure is increased while keeping constant both power and flow.

The absolute partial pressures allowed the interesting estimation of the number of effluents released by consumed monomer, but also to quantify the mass contained in the gas phase, in total and for each effluent.

Finally, the complex interconnections were depicted between the physical quantities in the plasma and the transition phenomena occurring in our discharges. The discussion is not at its end, but several observations allow to progress. Notably, the very low amount of hydrogen produced at the highest power indicates a very low fragmentation for these conditions with the largest deposition for styrene. As this fragmentation is lower than at lower power, it supports an expansion of the plasma up to the reactor wall or said in other words a regime of full glow.

At the side-wall location, the plasma should be softer than at the center of the reactor and could explained a very soft deposition process, with very limited fragmentation. The question to known if the cause of the plasma expansion is in first place the E/H transition or the pressure diminution is opened and requires further measurements.

Chapter 9

MMA plasma: species identification by mass spectrometry

The present chapter will deal with the identification of the effluents from the methyl methacrylate (MMA) plasma by mass spectrometry (MS). The results are interesting as they are significantly different from the ones of unsaturated hydrocarbons. Indeed, the presence of two oxygen atoms in the MMA molecule revealed a new challenge for species identification by MS: peaks in the mass spectrum during plasma have multiple assignments. Manage this difficulty required both the use of low electron energy and Threshold Ionization Mass Spectrometry (TIMS), but also a heavy consultation of the NIST database. In addition, the comparison of plasma mass spectrum between MMA and the previously studied hydrocarbons allowed an important assumption. The method developed in the present chapter is also presented to serve more generally as reference for species identification in oxygen-containing monomers, like acid acrylic or methyl acrylate.

The vapor mass spectrum (VMS) of MMA will be presented first (Section 9.2). It will be followed by the plasma mass spectrum (PMS) of MMA (Section 9.3), for which the focus will be set on the identification of the high-mass region. Finally, the appearance energies (AEs) of the all the peaks observed in the PMS will be presented in Section 9.4. Their extensive discussion for the low-mass region of MMA PMS required the concept of the "hidden secondary AE"(Section 9.4.3) to establish the species assignments (Section 9.4.4).

Pressure (Pa)	**Flow** (sccm)	**Power** (W)	**BE** (eV)	**W/F** (eV/MMA)	**W/FM** (10^8 J/kg)
6.7	28	50 – 500	≈ 59	26 – 262	0.25 – 2.5

Table 9.1: Conditions used for the plasma polymerization of MMA. "BE " stands for the bond energy of MMA, roughly estimated in Section 2.4.1

9.1 Plasma conditions

The conditions used are summed up in Table 9.1. They were chosen similar to the ones of the styrene plasma polymerization for better comparison. The pump valve opening to achieve a flow of 28 sccm is 2.31 turns (2+5/16), compared to 2.00 turns for styrene (2+0/16).

9.2 Mass spectrum of MMA vapor

The CP of MMA at the conventional 70 eV electron energy can be seen on Figure 9.1 It reveals a very high fragmentation of MMA: the three fragment peaks at m/z = 69, 41 and 39, have higher intensity than the molecular ion at m/z = 100. As for styrene and highly unsaturated hydrocarbons in the previous chapters, we recorded the CP of MMA at several low electron energy: at 16 eV, 12 eV and 10.5 eV on the Figure 9.1b, c and d respectively. Obviously the MMA fragmentation decreases with lower electron energy. However, the main important difference, when compared to the unsaturated hydrocarbons, is the still significant fragmentation, even at 12 eV. This is mainly due to the higher degree of saturation of MMA and its aliphatic structure [186]. At the lowest energy of 10.5 eV, MMA mass spectrum still shows two significant even mass-peaks at m/z = 68 and 70. Their appearance energies (AEs) are below the ionization energy (IE) of MMA. This tends to support the presence of impurities, due either to the decomposition of MMA or to the stabilizer of MMA. The stabilizer used in MMA is the mono methyl ether hydroquinone (MEHQ) of chemical formula $C_7H_8O_2$ (124 amu) with IE at 7.5 eV, well below the one of MMA (9.7 eV) [192]. The possibility that these peaks are due to fragment ions of MMA is not likely, as no mention of fragment ion appearing at lower electron energy than the IE could be found in the literature, to our knowledge, and considering the inherent timescale.

The assignments of the main characteristic peaks of MMA at 70 eV are shown on Table 9.2. They can be explained by the simple bond cleavages shown in Figure 9.2. The C-O and C-C bonds are the weakest bonds in the monomer with very similar energy at around 3.6 - 3.7 eV. The "A cleavage" is the C-O bond scission between the DMK-H (dimethylketone) functional

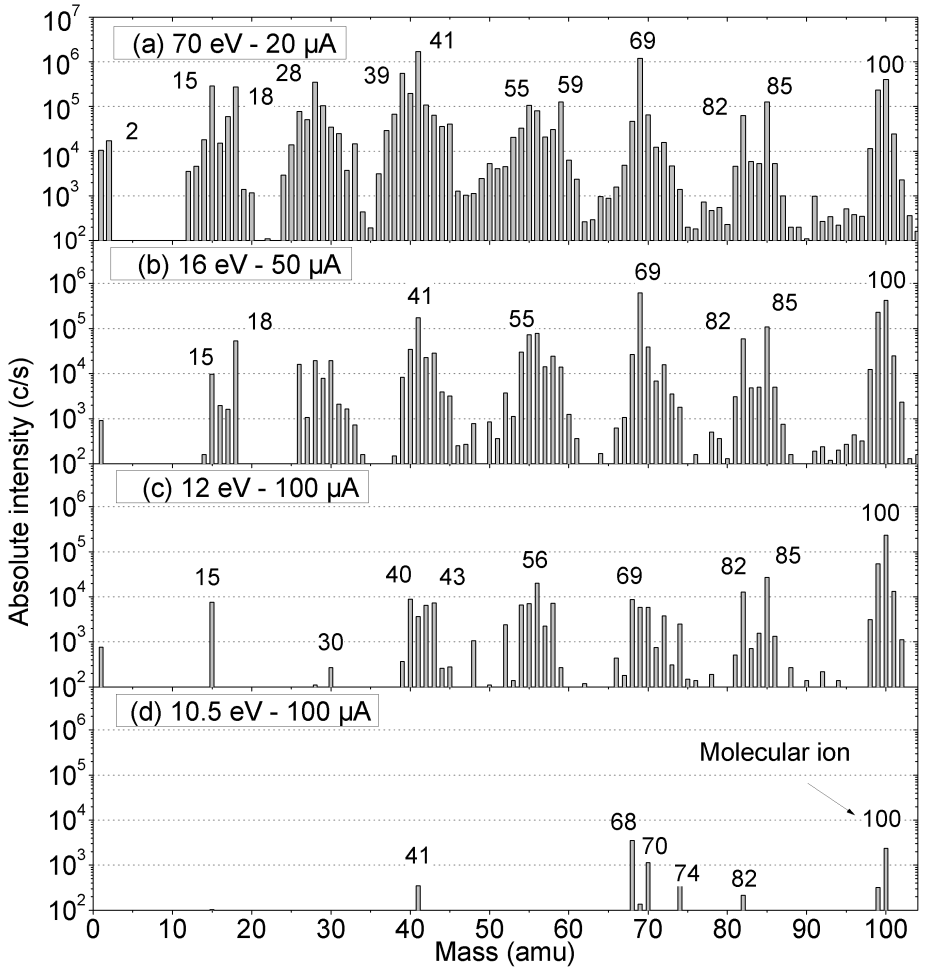

Figure 9.1: Cracking patterns of MMA with decreasing electron energy of: (a) 70 eV, (b) 16 eV, (c) 12 eV and (d) 10.5 eV.

group and the methoxy OCH_3 group. It leads to large production of 69^+ ions but almost no 31^+ ions. It is due to the high IE of the methoxy radical $OCH_3^\bullet$ (9.8 eV), which disfavors this fragment ion (Stevenson's Rule in Section 3.4.5) [13]. The "B cleavage" is the scission of the C-O bond between the methyl ester function and the propenyl group. It produces large amount of ions at m/z = 41 and 59. Other easy cleavages are the ones of the two methyl C-C bonds, referred as C and C' cleavages. Formation of ions of m/z = 15 and 85 are their consequences. The peak at m/z = 82 is characteristic of a neutral H_2O loss, which is familiar for the molecular ions of ketones and ethers [13]. As even-mass peak, it is not explained by a direct cleavage but it is produced by a "tight decomposition" (see unimolecular ion decomposition in Section 3.4.2) or a rearrangement during the dissociation [13]. It is thus marked by the symbol "(R)" in Table 9.2.

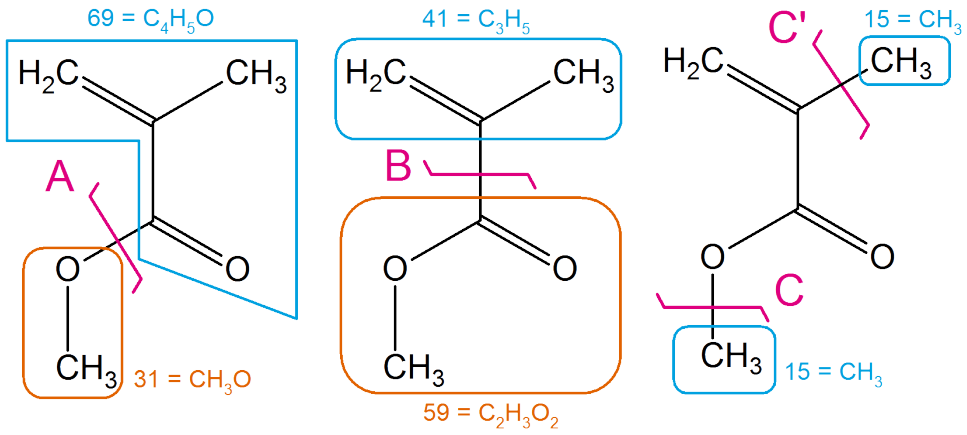

Figure 9.2: Four dominant cleavages of MMA.

Ion	Assignment	Origin/cleavage
15^+	CH_3^+	C or C'
28^+	CO^+	A and B
41^+	$C_3H_5^+$	B
55^+	$C_3H_3O^+$	A and C
59^+	$C_2H_3O_2^+$	B
69^+	$C_4H_5O^+$	A
82^+	$C_5H_6O^+$	H_2O loss (R)
89^+	$C_4H_5O_2^+$	C or C'
100^+	$C_5H_8O_2^+$	Monomer

Table 9.2: Peak assignments of the MMA cracking pattern and their most probable cleavage origin.

9.3 Mass spectrum of MMA plasma

From the shown vapor mass spectra (VMS) of MMA, significant overlapping of cracking patterns can be expected in the plasma mass spectra (PMS) of MMA. However, even if the lowering of the electron energy does not produce a single peak CP, it can be useful. Indeed at 70 eV, the peaks at m/z = 15, 28, 39, 41 and 69 are more intense than the molecular ion peak. At 12 eV, this latter is almost one order of magnitude higher than the second more intense peak at m/z = 85. Moreover, the AE can help to identify species. All the methodologies developed for styrene will be used here, but with more difficulties due to the higher fragmentation.

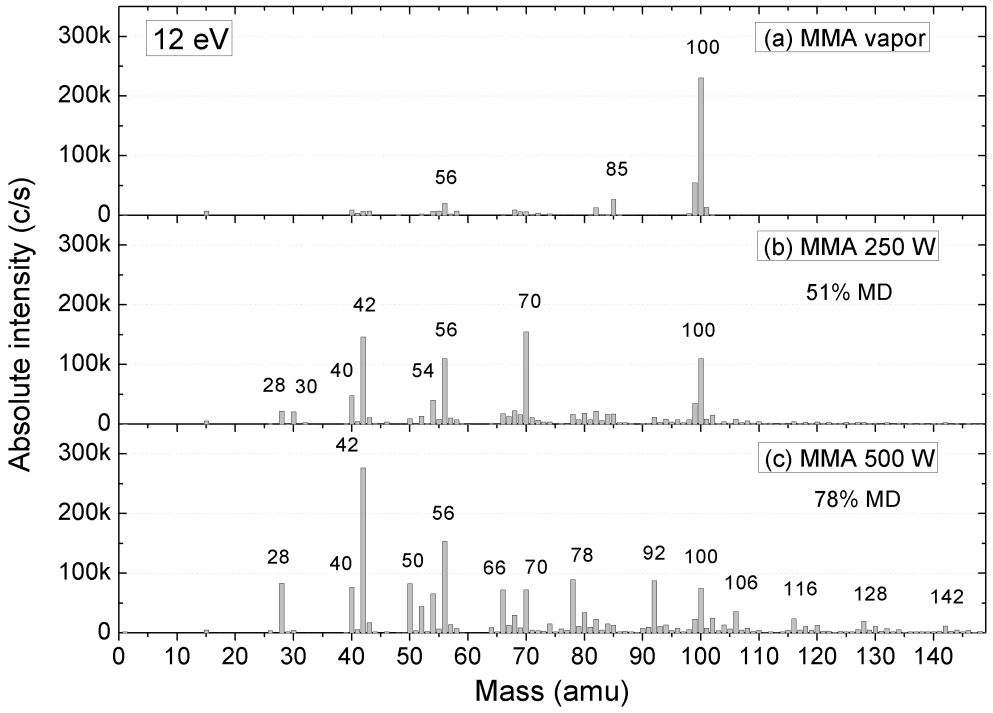

Figure 9.3: Mass spectrum at 12 eV in linear scale of: (a) MMA vapor at 6.7 Pa, (b) MMA plasma at 6.7 Pa, 28 sccm, 250 W and CW conditions and (c) MMA plasma at 6.7 Pa, 28 sccm, 500 W and CW conditions.

9.3.1 Mass spectrum with linear scale

As a first step, the MMA VMS at 12 eV of Figure 9.3a is compared to the PMS at 250 W and at 500 W on Figure 9.3b and c, respectively. The electron energy is kept the same, as well as the plasma conditions: 6.7 Pa of initial pressure, 28 sccm and continuous-wave conditions. It is presented with a linear scale for the intensity to clearly show the most significant peaks.

At 250 W, below 100 amu, seven peaks increase or appear: at m/z = 70, 56, 54, 42, 40, 30 and 28. They indicate the possible production of the following neutral species: dimethyl ketone (DMK, 70 amu), butene C_4H_8 or acrolein, which is the most probable isomers of C_3H_4O (56 amu), isomers of C_4H_6 (54 amu), propene C_3H_6 (42 amu), allene C_3H_4 (40 amu) and formaldehyde CH_2O or ethane C_2H_6 (30 amu). The last peak at m/z = 28 is assigned to ethylene C_2H_4 as its ionization potential of 10.5 eV is below 12 eV, on the contrary of CO whose IE is 14.0 eV.

At 500 W of applied power, some of the previously mentioned peaks becomes more intense, like at m/z = 56, 54, 42, 40 and 28. The 70 amu peak diminishes and the 30 amu peak almost disappears. A series of new peaks arises at m/z = 92, 80, 78, 68, 66, 52 and 50 below 100 amu. Above this mass, we mainly observed signals at m/z = 102, 106, 116, 128 and 142.

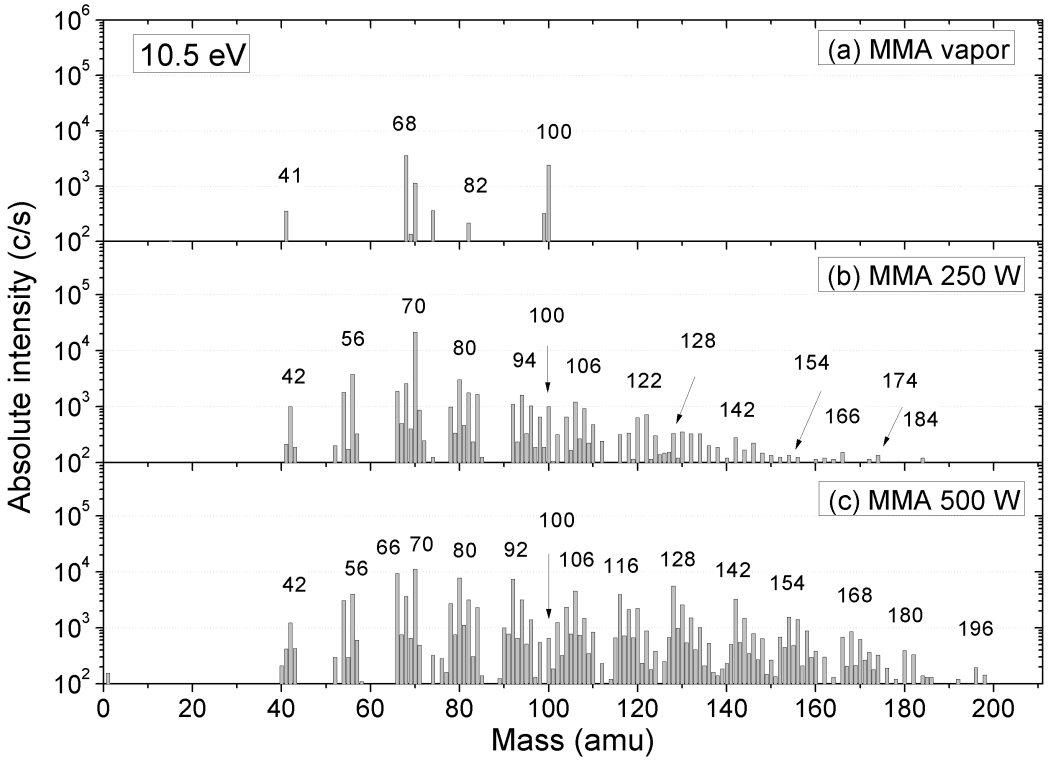

Figure 9.4: Mass spectrum at 10.5 eV in logarithmic scale of: (a) MMA vapor at 6.7 Pa, (b) MMA plasma at 6.7 Pa, 28 sccm, 250 W and CW conditions and (c) MMA plasma at 6.7 Pa, 28 sccm, 500 W and CW conditions.

9.3.2 Mass spectra with logarithmic scale

As a second step for species identification, the MMA VMS at 10.5 eV is compared to the PMS with the same electron energy at 250 W and at 500 W, all being on Figure 9.4. A logarithmic scale is used this time, to reveal as many peaks as possible. As already said, for the MMA VMS, the mass peaks at m/z = 68 and 70 are suspected to originate from degradation of the MMA or from its stabilizer. For the 250 W plasma, we can see that additional peaks are highlighted when comparing to the linear scale: at m/z = 92, 94, 96 and 98 for instance. At 500 W, peaks with masses above the MMA mass have large intensities, with usually one order of magnitude higher than at 250 W. Plasma polymerization in the gas-phase is then significant.

The assignment of all these peaks is much more difficult than for hydrocarbons. Indeed, many masses can correspond to species with zero, one, two, three or even four oxygen atoms. For the sake of clarity, high mass peaks above 90 amu will only be considered in the following section, leaving peaks with masses below 90 amu for the appearance potential section.

	Hydrocarbons	1 oxygen atom	2 oxygen atoms	3 oxygen atoms	4 oxygen atoms
92	C_7H_8	C_6H_4O	-	$C_3H_8O_3$	-
106	C_8H_{10}	C_7H_6O	-	$C_4H_{10}O_3$	-
116	C_9H_8	-	$C_6H_{12}O_2$	$C_5H_8O_3$	$C_4H_4O_4$
128	$C_{10}H_8$	-	$C_7H_{12}O_2$	$C_6H_8O_3$	-
142	$C_{11}H_{10}$	-	$C_8H_{14}O_2$	$C_7H_{10}O_3$	$C_6H_6O_4$
154	$C_{12}H_{10}$	- $C_{11}H_6O$	$C_9H_{14}O_2$ -	$C_8H_{10}O_3$ -	$C_7H_6O_4$ -
168	$C_{13}H_{12}$	- $C_{12}H_8O$	$C_{10}H_{16}O_2$ -	$C_9H_{12}O_3$ -	$C_8H_8O_4$ -
180	$C_{14}H_{12}$	- $C_{13}H_8O$	$C_{11}H_{16}O_2$ -	$C_{10}H_{12}O_3$ -	$C_9H_8O_4$ -
182	$C_{14}H_{14}$	- $C_{13}H_{10}O$	$C_{11}H_{18}O_2$ $C_{12}H_6O_2$	$C_{10}H_{14}O_3$ -	$C_9H_{10}O_4$ -
196	$C_{15}H_{16}$	- $C_{14}H_{12}O$	$C_{12}H_{20}O_2$ $C_{13}H_8O_2$	$C_{11}H_{16}O_3$ -	$C_{10}H_{12}O_4$ -

Table 9.3: Possible assignment of the high-mass dominant peaks according to the NIST Chemistry ebbook [9]. Hyphen "-" means that no assignment was found in the database.

9.3.3 High-mass region of MMA PMS

For the high mass region, the existence of the possible assignments was evaluated as follows. On the NIST Chemistry Webbook [192], a raw formula corresponding to no existing stable molecules was used to indicate an impossible assignment. To limit the quantity of work, we restrain to the 10 peaks with the highest intensity in each mass sub region, which are at m/z = 92, 106, 116, 128, 142, 154, 168, 180, 182 and 196. The results are shown in Table 9.3. A cell marked with a hyphen "-" corresponds to no existing species in the NIST database.

For each mass, we observe at least three possible assignments: always a hydrocarbon and a three oxygen containing species; for 1, 2 and 4 oxygen containing species, it depends. For each chemical formula, the number of isomers is important and becomes especially countless for the formulae with the highest degree of saturation, which have more aliphatic features and then more possible combinations. The electron impact mass spectra at the standard electron energy of 70 eV are often available on the NIST database. For the most unsaturated oxygen containing species, the CP was generally very simple even at the elevated 70 eV electron energy: the molecular ion dominates and the peak with the second highest intensity is generally one order of magnitude lower. On the contrary, more saturated oxygen containing species shows CP with much more fragmentation in their CP, like MMA for instance. The base peak is often not the

molecular ion peak. This is due to their aliphatic feature which promotes fragmentation [186]. Indeed, the production of a fragment requires a single bond cleavage for aliphatic molecules, against two for cyclic molecules.

Thereby, we face here the possibility of multiple assignments for the dominating peaks in the high mass region of the MMA PMS. However, several observations at this stage can clear the situation. On Figure 9.4c with masses above 90 amu, the 10 dominating peaks have mass difference between them of 12 or 14 amu, once of 10 and of 16. Their intensities tend to decrease as their mass increases. These two observations are in favor of a production path based on the repeated action of intermediates containing 1 carbon atom with small H content, like the methylene radical (H_2C:). It is very similar to the chemistry we detected for the unsaturated hydrocarbon plasma in chapter 7. For concision, this hypothesis will be referred as "repeated methylene addition".

The "repeated methylene addition" leads to a vertical progression between the species shown in Table 9.3: the addition of a methylene does not induce the addition of an oxygen atom. So we will now discuss the probability of applying this mechanism for each column of the table:

- For species containing a single O atom, a vertical progression is not likely because assignments are missing at m/z = 106, 116 and 128.
- In the case of molecules with two oxygen atoms, the progression would be more likely but should start with a saturated version of the monomer, the methyl isobutyrate $C_5H_{10}O_2$ with a mass of 102 amu, to reach the $C_6H_{12}O_2$ species. This molecule was detected ex-situ from the condensed product of MMA plasma on a nitrogen trap [11].
- A three oxygen species progression is possible. However the only referred isomer of $C_3H_8O_3$ (92 amu) is glycerin, which has three alcohol functions. It is then not likely to be produced in the large amount suggested by the high intensity of the corresponding peak at 92 amu. The reason is that the starting compound is MMA, which has an ester function and a methoxy termination -OCH_3.
- The progression with four oxygen atoms is not likely with missing assignments at 92, 106 and 128 amu.
- Finally, we observed that hydrocarbon progression is likely, considering the always possible assignments, which are all highly unsaturated and are most probably polycyclic aromatic hydrocarbons (PAH).

To end with the species progression via the repeated addition of intermediates, we must temper these considerations by the fact that oxygen addition could occur at some stages.

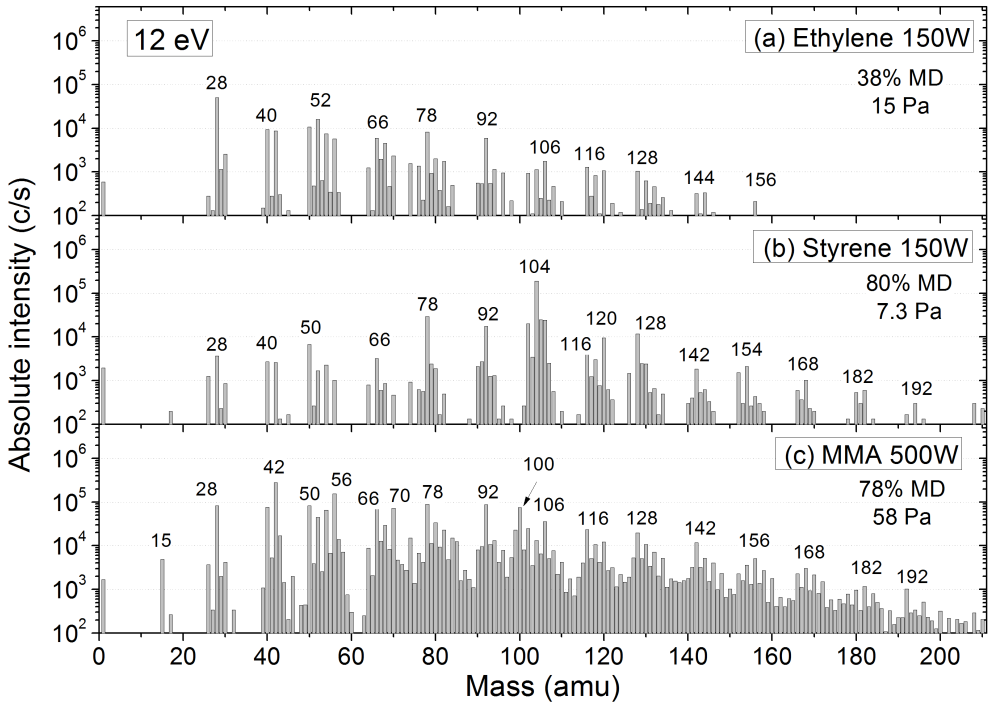

Figure 9.5: Mass spectra at 12 eV of: (a) ethylene plasma at 15 0W, (b) styrene plasma at 150 W and (c) MMA plasma at 500 W. Otherwise plasma conditions are kept constant: 6.7 Pa, 28 sccm and CW.

9.3.4 Comparison with the hydrocarbon plasmas

Another important observation will help us to conclude for the species assignment Table 9.3. It comes from the comparison of MMA plasma to the styrene and the ethylene plasma. The PMS of ethylene, styrene and MMA are shown on Figure 9.5a, b and c respectively. The electron energy is 12 eV, because no spectra were acquired at lower energy for ethylene and styrene. Absolute intensities cannot be compared as the MMA spectrum was acquired with different settings. However, it is striking to see that **the three spectra have many dominating peaks with the same m/z ratio** in each mass sub-region, from m/z = 78 to 192, to which we can add the peak at 66 amu. This is a strong indication that the dominating peaks in the MMA PMS are mainly due to hydrocarbons.

A second feature of MMA PMS when compared to styrene and ethylene PMS is the number of **satellite peaks** between each dominating peaks. From 64 to 200 amu, in the MMA PMS, the signal is always above 100 c/s, on the contrary of styrene and ethylene. On one hand, this may indicate contribution from oxygen containing species, either unsaturated and cyclic with almost single peaks CP, or more saturated and aliphatic ones with probably more complex CP. On the

other hand, the higher relative hydrogen content of MMA (H/C ratio = 8/5), when compared to the styrene plasma, may lead to a larger production of hydrogenated species.

At this stage, no other conclusions can be drawn for high mass species. The CP study of several oxygen containing aliphatic species at 10.5 and 12 eV would bring useful information. In addition, an oxygen atom balance could allow one to infer if heavy species are likely to contain oxygen. The balance could be evaluated by the partial pressure quantification of small species containing oxygen (like CO, CO_2, CH_2O and DMK), by the estimation of the pumping speed and by the measure of oxygen deposition on the reactor walls. Quantification of hydrogen in the discharge could also help. A large production would effectively dismiss the most saturated assignments.

9.4 Appearance energy in MMA plasma

Like for the styrene study, the measurement of AE can help to further confirm or ruled out peaks as being due to neutral species in the plasma. Firstly, the AE of the CP peaks of MMA will be discussed. Then, in the continuity of the previous section, we will focus first on the high-mass peaks above 90 amu, before dealing with the peaks from the low-mass region, below 90 amu. The AEs of Argon, O_2, CO and CO_2 were measured before and after all the AEs measurement. They match the theoretical IE within a precision of ± 0.1 eV. Therefore, no electron energy correction of the measured AE is required with the used settings.

9.4.1 MMA vapor

Figure 9.6 exhibits the electron energy spectrum (EES) of several important peaks in the CP of MMA at 10.5 and 12 eV. The AE of the molecular ion (m/z = 100) is equal to 9.7 eV, which is the IE of MMA. Clearly the two fragment ions at m/z = 70 and 82 have AE below the IE. Due to the fact that the molecular ion production always anticipated the production of its fragment ions (see chapter on electron impact ionization, Section 3.2), the AEs of the fragment ions are always higher than the IE, as far as we could observe in the literature. Therefore, the two problematic ions are set aside as originating from MMA, at the lowest electron energies. Indeed, they both reveal secondary AE: the m/z = 82 peak at around 10.3 eV and the m/z = 70 peak at about 12 eV. These AE seems more likely for fragment ions produced by decomposition of the molecular ion.

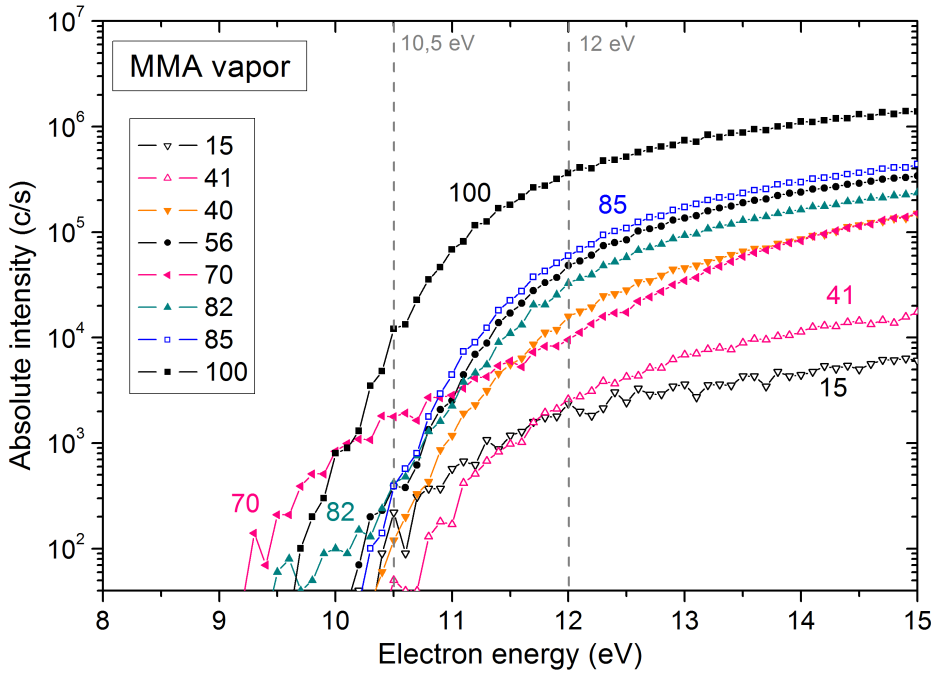

Figure 9.6: EES of several important peaks in the CP of MMA vapor. Open symbol are odd-mass fragment ions, while solid symbol for even-mass fragment ions.

These two peaks set aside, we see that the "AE criterion for molecular ion" that we established in Section 7.3.2 do not applied to an aliphatic oxygen containing and lightly unsaturated species like MMA. Indeed, the two even mass fragment ions at m/z = 40 and 56 have AEs at 10.4 and 10.2 eV, respectively. This is only 0.7 and 0.5 eV above the IE of MMA (9.7 eV). The species identification will then be less strongly supported, than in the case of the highly unsaturated hydrocarbons.

9.4.2 High-mass region AE of MMA plasma spectrum

The high-mass peaks of the MMA PMS are listed by increasing mass in Table 9.4. The peaks marked by a "+" sign in the second column are peaks which dominates in their mass sub-region. Their measured AEs during MMA plasma at 500 W are shown in the third column. Those marked by a star "*" are small signals, which most probably undergoes the important AE over-estimation of small signals shown in the experimental setup chapter (Section 5.3.8). The peak at m/z = 122 is marked by a double star, as it was the only to have its AE measured at 250 W, because of its higher intensity at that power. The fourth column includes the measured AE during styrene plasma, for comparison. The next column is the difference between the MMA AE and the styrene AE.

m/z ratio	**Major peaks**	**AE MMA 500W** eV	**AE styrene 150W** (eV)	**Difference of AE** (eV)
102		9.7	8.8	0.9
104		9.2	8.2	1.0
106	+	9.5	8.3	1.2
108		9.0	8.6	0.4
110		9.7*	9.1	0.6
116	+	9.3	8.5	0.8
118		-	8.3	
120		-	8.3	
122		8.7**	-	
124		-	-	
128	+	9.1	8.3	0.8
130		9.1	8.5	0.6
132		9.3	8.8	0.5
134		9.1	8.9	0.2
136		9.5	-	
142	+	9.2	8.4	0.8
144		9.5	8.5	1.0
146		9.2	9.0	0.2
148		9.4	-	
150		9.5*	-	
152		9.3	8.3	1.0
154	+	9.0	8.4	0.6
156	+	9.3	8.5	0.8
158		9.2	-	
160		9.4	-	
162		9.7*	-	
164		9.8*	-	
166	+	9.1	8.4	0.7
168	+	9.1	8.5	0.6
170	+	9.0	-	
172		-	-	
174		-	-	
176		-	-	
178		9.6*	8.7	0.9
180	+	9.4*	8.4	1.0
182	+	-	8.5	
190		9.8*	-	
192		-	9.0	
196	+	-	-	

Table 9.4: List of high-mass species observed from the PMS at 10.5 and 12 eV during MMA plasma. Measured AEs during MMA plasma at 500 W, 6.7 Pa, 28 sccm and CW. Measured AEs during styrene plasma at 150 W, 6.7 Pa, 28 sccm and CW (from Section 7.4.1). The styrene results required AE correction of 0.6 eV, while the results from the present section necessitated no correction.

A first observation is that AEs during MMA plasma are all below 10 eV and that 21 of the 30 measured AEs are below 9.5 eV. This supports that these peaks are being due to real neutral closed-shell species produced in the plasma and especially if further measurements proved these are predominantly unsaturated hydrocarbon species, as the similarity of PMS between styrene and MMA suggests it. The 8 AEs that are missing in the table and marked by a hyphen have simply not been measured by lack of time. However, we consider they are serious candidates for neutral species and require AE confirmation.

A second observation is the systematic higher values of MMA plasma AEs compared to the styrene plasma AEs. In contrast with the previous observations, this would indicate that styrene plasma species are not the same as the MMA plasma species.

Without considering the multiplicity of assignments for each m/z ratio and the multiplicity of isomers for each assignment, **30 species are then detected in the high-mass region**. Two of them can correspond to already observed species by ex-situ GC/MS [168]: Methyl Isobutyrate (MIB), $C_5H_{10}O_2$, with 102 amu, and Methyl Isopentanoate (MIP), $C_6H_{12}O_2$, with m/z = 116. However no assignment of them was reported by Threshold Ionization Mass Spectrometry (TIMS). The IE of MIB is 10.0 eV and does not match well the measured AE of 9.7 eV at m/z = 102. No IE could be found for MIP. To conclude for the high-mass region, **28 new species** are thus reported.

9.4.3 Hidden secondary appearance energy

Before dealing with the low-mass region, one observation requires attention. Figure 9.7 shows the electron energy spectrum (EES) at m/z = 82 during MMA plasma at 250 W. As the MMA CP contributes to this peak, the same spectrum during the MMA vapor at 6.7 Pa was added. However the signal was reduced by the value of the MMA MD at 250 W, which is 50%. Finally the difference spectrum is shown. This difference spectrum contains all the contribution to the 82 amu peak from species other than MMA.

What is important to observe is the fact that, at first glance, no secondary AE had been detected for the EES during the plasma. The subtraction of the MMA contribution shows a secondary AE around 10.7 eV. This is 0.6 eV above the AE at m/z = 2 due to MMA at 10.1 eV. This is due to the fact that a secondary signal requires to reach an intensity at least one order of magnitude below the primary signal to show visible effect with the logarithmic scale. Moreover it is important to note that the MMA AE is hidden despite its EES exceeds the one of the

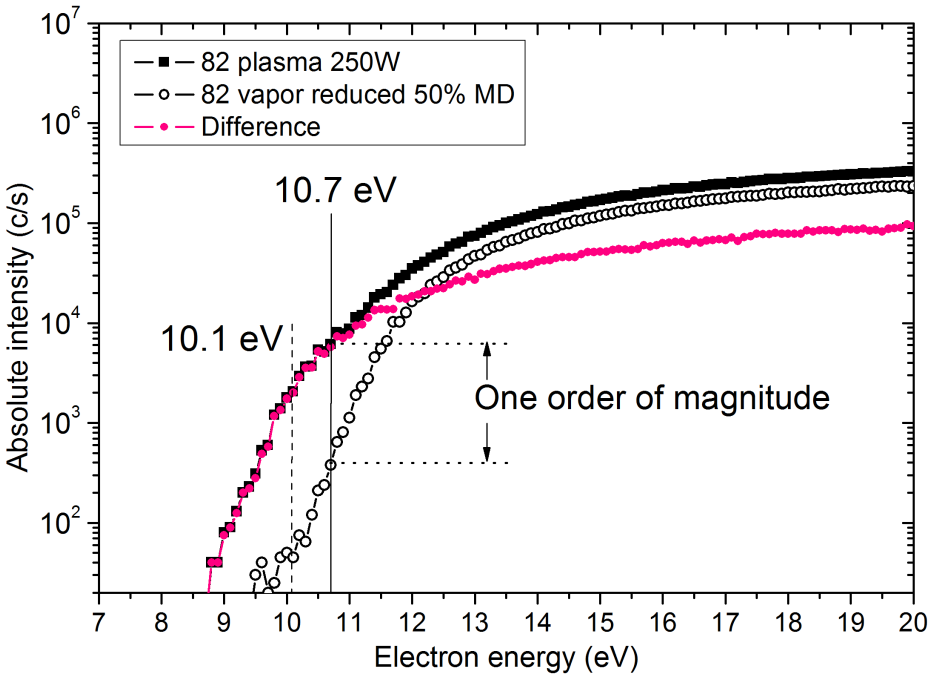

Figure 9.7: Electron energy spectra at m/z = 82 during: MMA plasma (6.7 Pa, 28 sccm, 250 W, CW), MMA vapor at 6.7 Pa diminished of 50% to take MD of MMA plasma into account, and difference of the two spectra.

difference EES above 12 eV. It is also hidden despite the fact it explains 70% of the signal as soon as at 14 eV.

All these observations show that identification of secondary AE is delicate and is subject to over-estimation. This over-estimation is similar to the "competitive shift" (Section 3.4.1), except it is not the competition between two decomposition channels of the same parent ion. Moreover, very large signal can be hidden. Most probably, secondary AE detection would be enhanced by a weaker primary signal. A better detection would also be expected if the secondary AE occurs at a position on the EES of the primary signal with lower slope.

9.4.4 Low-mass region of MMA plasma spectrum

The AE study in the low-mass region is restrained to 10 peaks at the following m/z ratios: 28, 30, 40, 42, 50, 56, 66, 70, 78 and 92. They were chosen because they dominate their mass sub-region in the MMA PMS at 12 eV. Five other peaks were added because they can be assigned to species reported in the literature which have IE above 11 eV (Section 4.2.3). These are at m/z = 2, 16, 26, 32 and 44. They can correspond to H_2, CH_4, C_2H_2/CO, O_2 or CO_2, whose IE are 15.4 eV, 12.5 eV, 11.4/14.0 eV, 12.1 eV and 13.8 eV respectively.

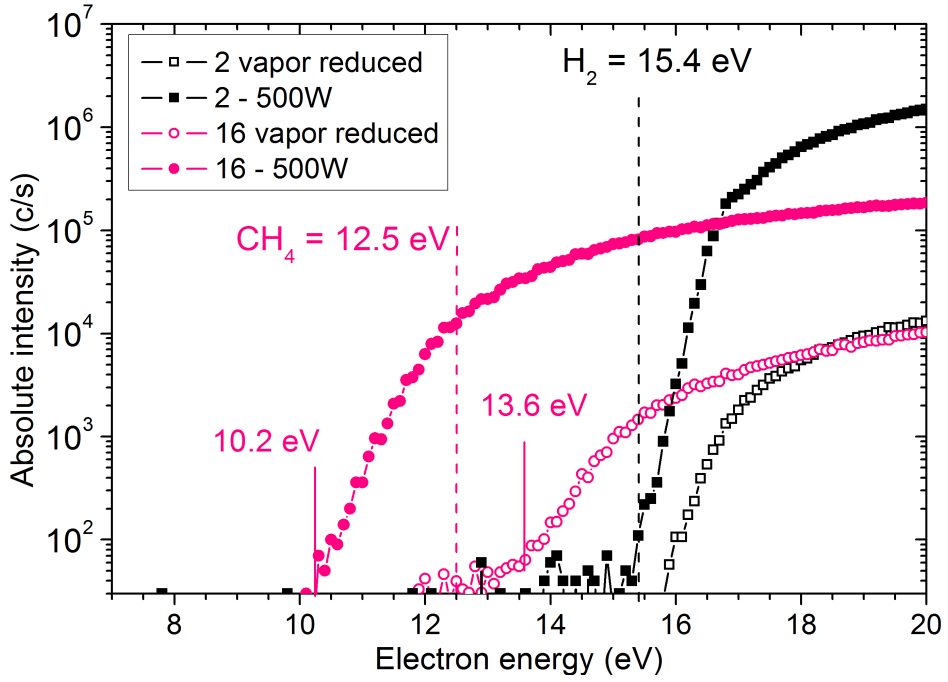

Figure 9.8: Electron energy spectra without and with plasma of the peaks at m/z = 2 and 16 and (b) m/z = 26 and 28. The "vapor reduced" values correspond to the vapor intensity reduced of 78% because of the monomer depletion was 78% at 500 W.

The EES during the MMA vapor will be systematically compared to the one during the MMA plasma in the following figures. For the plasma EES, the signal is shown during the MMA plasma either at 250 W or 500 W. The choice of power for each species was made on the base of the observation of the highest intensity at 12 eV or 16 eV (depending on the IE of the assignable species). In a previous section, we observed that the MMA MD was of 50% at 250 W and of 78% at 500 W. Therefore, to better compare the EES without and with plasma, all the MMA vapor signals shown are reduced with the corresponding MD. We also remind the lecturer that the discharge pressure is 30 Pa at 250 W and 58 Pa at 500 W.

On Figure 9.8, the EES comparison of the ion signals at m/z = 2 and 16 are shown. The only assignable ion at **m/z = 2** is H_2^+. The MMA contribution to this peak is very low, with intensity 2 order of magnitude below the one during plasma. Other species, rather saturated, containing methyl function for instance, can also contribute to this signal. However they are not expected to contribute much more than MMA as this later has already two methyl functions. As in addition the AE matches well the IE of H_2 shown on the figure at 15.4 eV, it is concluded that the signal at m/z = 2 is due to hydrogen existing in the discharge. It can also be supposed that the major part of the signal at 20 eV is due to **hydrogen** and that this electron energy could be used to quantify its partial pressure.

On the same figure, the plasma EES at **m/z = 16** shows an apparent single AE at 10.3 eV. Contribution to this signal can come from species containing methyl functions. Either rearrangement can occur to produce CH_4^+ ions, or the ^{13}C contribution of CH_3^+ can give signal at m/z = 16. However those two kinds of contribution are generally small. On one hand, it is due to the low stability of the radical CH_4^+ ion when compared to the closed-shell CH_3^+ ion. On the other hand, the ^{13}C abundance is small, with 1.1% of ^{12}C. A second contribution to the m/z = 16 peak can be from the oxygen ion O^+, produced by oxygen containing species, like water, O_2, CO, CO_2, MMA, DMK... Contributions from MMA and residual water (which was high during the measurements) are visible on the figure and cannot account for the EES during plasma. At 20 eV its intensity is 20 times below the plasma signal. Contributions from 10 Pa of O_2, CO or CO_2 were evaluated but the AEs of their m/z = 16 signal were all between 14 and 15 eV. Furthermore their signals were small with a maximum of 7 kc/s at 20 eV, far below the 200 kc/s measured during MMA plasma. Many other species could contribute but could not be evaluated. However, three considerations lead us to conclude to important **production of methane**: (i) the large intensity of the plasma signal, (ii) the possibility of a hidden secondary AE, even for a large contribution, shown in the previous section, (iii) the fact that methane production is very likely from MMA which contains two methyl functions, and (iv) the fact that the only assignable closed-shell species is CH_4. Quantification of its partial pressure would be recommended 4 eV above its IE, at about 16 eV.

On Figure 9.9, the same comparison of EES is shown for the ion signals at m/z = 26 and 28. For the first, the assignment to the ion $C_2H_2^+$ is the only possibility. The AE during plasma fits very well the IE of **acetylene**, C_2H_2, at 11.4 eV. A quantification of its partial pressure around 13 eV would reduce CP overlapping, due to the secondary AE observed at 13.7 eV.

On the same figure, the signal at m/z = 28 can be assigned to two different ions: $C_2H_4^+$ and CO^+. The primary AE at 10.7 eV is reasonably close to the IE of **ethylene**, C_2H_4, at 10.5 eV. Two secondary AEs are observed: one around 14.0 eV and a second less detectable around 15 eV. This latter can reasonably indicate production of **carbon monoxide**, CO, with its IE at 14.0 eV, considering the over-estimation of secondary AE seen in the previous section (unfortunately the m/z = 28 EES of the MMA vapor is missing). Quantification of those two possible products would preferably be done in two steps: firstly quantify C_2H_4 with a measure around 13 eV, and secondly quantify CO at 20 eV after removing the known contribution of C_2H_4 at this electron energy. However other contribution could infer at 20 eV, from CO_2 for instance. But its signal at 10 Pa with the same settings gave intensity below 10^4 c/s at 20 eV. It is below the already minor contribution of 2.10^4 c/s due to MMA at the same energy.

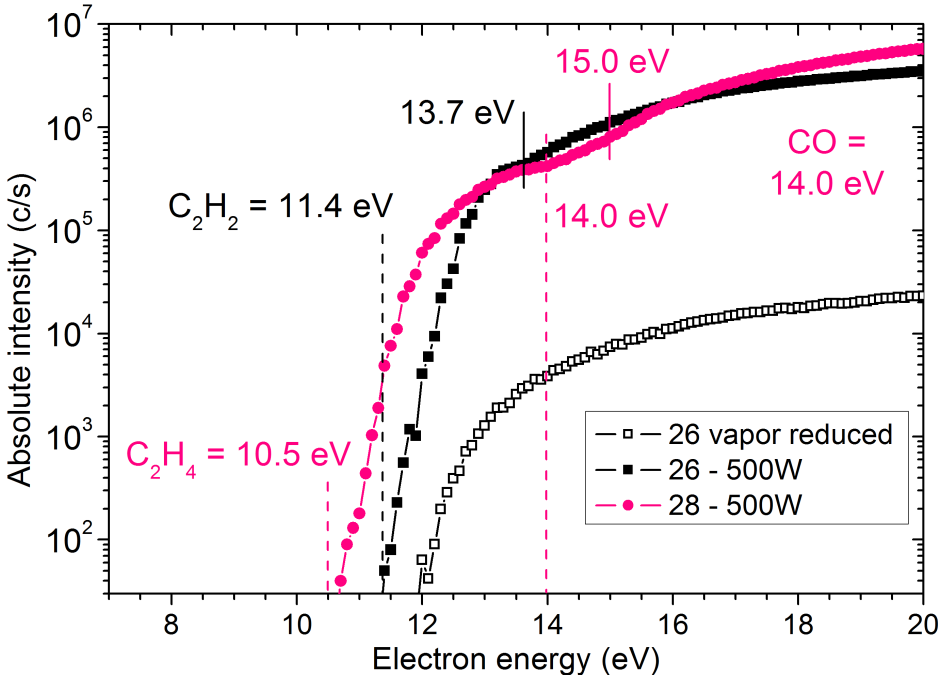

Figure 9.9: Electron energy spectra without and with plasma of the peaks at m/z = 26 and 28. The "vapor reduced" values correspond to the vapor intensity reduced of 78% because of the monomer depletion was 78% at 500 W.

The same investigation was performed on the other selected peaks. To avoid a too developed analysis, a **summary of the results** is shown through Table 9.5. The second, third and fourth columns respectively contain the AE measured in the MMA vapor, the MMA plasma at 250 W and the MMA plasma at 500 W. The AEs marked with a star means that the corresponding signal is small and that the AE over-estimation is likely. Several AEs measured for the same m/z ratio are separated by a slash. A cell with a hyphen means that no AE was measured. The three last columns of Table 9.5 show the possible assignment for every m/z ratio. They are ordered by their oxygen content: either zero, one or two oxygen atom(s). Between brackets are the values of their IE reported in the literature [13] or in the NIST Chemistry Webbook database [192]. When several isomers exist for one raw formula, the different IEs were separated by a coma. When several and rather different IE values are reported in the database for a single isomer, the energy interval is indicated by two values separated by a hyphen. A cell with a hyphen means that no assignment exists in the NIST database.

Among the possible assignments of Table 9.5, the most probable one(s) for each m/z ratio is(are) written in bold characters. The methodology followed to establish the most likely character of a species takes the several considerations already used previously and summed up here:

m/z ratio	Measured Appearance Energy (eV)			Possible assignment (IE in eV)		
	MMA Vapor	MMA 250W	MMA 500W	No oxygen	1 Oxygen	2 Oxygen
2	15.3	-	15.5 / 17.3	**H_2** (15.4)	-	-
16	10.9* / 13.6	-	10.3	**CH_4** (12.5)	-	-
26	11.9	-	11.4 / 13.7	**C_2H_2** (11.4)	-	-
28	Missing	-	10.7 / 13.9 / 15	**C_2H_4** (10.5)	**CO** (14.0)	-
30	10.1 / 11.5	9.8 / 10.9 / 11.5	-	**C_2H_6** (11.5)	**CH_2O** (10.9)	-
32	11.5*	11.1	-	-	**CH_4O (10.8)**	**O_2 (12.1)**
40	10.2	10.0	-	**C_3H_4** (9.7)	-	-
42	10.0 / 13.9	9.7	-	**C_3H_6** (9.7)	**C_2H_2O** (9.6)	-
44	10.9 / 14.5	-	10.8 / 14.6 / 15.8	**C_3H_8** (11.0)	C_2H_4O (9.3,10.2)	**CO_2** (13.8)
50	11.0	-	10.4 / 13.5	**C_4H_2** (10.1)	-	-
56	10.1	9.4	-	**C_4H_8** (9.1,9.2,9.6)	C_3H_4O (9.0, 10.1)	-
66	-	9.2	-	**C_5H_6** (9.0-10.1)	C_4H_2O (10.1)	-
70	9.1 / 11.8	8.5	-	**C_5H_{10}** (8.7,9.1,9.5,10.4)	**C_4H_6O** (**8.4**,8.7,9.2,9.6,9.7)	-
78	11.1*	-	9.4	**C_6H_6** (8.9,**9.25**,10.0)	-	-
92	-	-	9.3 / 10.4	**C_7H_8** (8.3,8.8,**9.8**)	**C_6H_4O ?** (9.0-9.1)	-

Table 9.5: List of peaks observed in the MMA PMS at 250 W and 500 W with electron energy of 10.5, 12, 16 and 20 eV. Plasma conditions were 6.7 Pa, 28 sccm and CW. AE of the corresponding peak in MMA vapor, MMA plasma at 250 W and MMA plasma at 500 W. Possible assignments of the peak with the corresponding IE added in brackets. All conventions are in the text.

- A matching between measured AE and theoretical IE, taking into account over-estimation of secondary AEs and of weak signals.
- Single possible assignment, like for C_3H_4, C_4H_2, and C_6H_6, combined with a large intensity.
- The possibility of hidden AE for species already observed in the literature with other techniques than MS, like CH_4 or CH_2O.

We will end this section with several relevant points.

- At m/z = 44, C_3H_8 could be quantified at 14 eV and the CO_2 at 20 eV after removing the C_3H_8 contribution at that energy.
- The best isomer assignment for the peak with m/z = 78 is benzene with its IE of 9.25 eV.
- At m/z = 92, the best matches are C_6H_4O for the primary measured AE and an aliphatic isomer of C_7H_8, 1,6-Heptadiyne with IE of 9.8 eV, for the secondary AE of 10.4 eV. The yet expected toluene does not match with its IE of 8.8 eV. However, very few data are available for C_6H4_O, indicating it is not a very stable compound. Further verifications are required.

Finally, from the 15 selected peaks, **22 neutral closed-shell species are then assignable in the low-mass region**. When comparing to the literature, this is the first report on species identification by TIMS. Indeed none of the MS studies reported or even suggested Threshold Ionization measurement to justify their assignments. Therefore, restraining to detection techniques which differ from MS, 12 already observed species are confirmed: H_2, C_2H_2 and DMK with strong clues; CH_4, C_2H_4, C_3H_4, C_3H_6, CH_2O, CO and CO_2 with rather good certainty; and O_2 and CH_4O with lighter clues. Therefore, potentially 1**0 new species have been detected in the low mass-region**.

9.5 Addidional remarks for the species identification

Strong indications show significant **production of diacetylene** C_4H_2 with m/z = 50 in MMA plasma. It is the main product of the plasma of acetylene, which is expected to be produced as well in large amount in the MMA plasma due to the high intensity peak at m/z = 26. The acetylene chemistry can then be expected with formation of C_6H_2 with m/z = 74 (Section 7.4.3). This latter species is effectively observed with distinct intensity in the 500 W MMA PMS (Figure 9.4.

Benzene is most probably produced in the MMA plasma and with a significant partial pressure due to the high intensity of the peak at m/z = 78. Benzene plasma chemistry produces dominating peaks at m/z = 92, 102, 116, 128 and 154. Therefore it favors hydrocarbon assignment for those peaks in the MMA plasma (Section 7.4.2).

The large production of ethylene (m/z = 28) hints as well the possible contribution of its own plasma chemistry. Its PMS were characterized by broader distribution of peaks, like the C_4 series of peaks at m/z = 50-52-54-56, the C_5 series at m/z = 64-66-68 or the C_6 series at m/z = 74-76-78-80-82 (Section 7.4.4).

The three previous observations support the **hydrocarbon assignment** in the high-mass region. However, their systematically higher AEs when compared to the ones of styrene plasma let linger some interrogations (Table 9.4). From the NIST database, it can be seen that aliphatic isomers generally have higher IE than their cyclic counterparts. This may be an explanation. Another would be the assignment of the observed peaks by oxygen containing species. The question is opened.

Definitely, partial pressure quantification could be performed for the MMA plasma. A special attention to the oxygen containing species could bring some light on the high-mass assignment.

This would pass by evaluating the number of oxygen atoms contained in small species like CO_2, CO, CH_2O, O_2 and DMK. Taking into account the change of the pumping speed, a conservation law of the oxygen atom from the initial MMA to the small oxygen containing species that are produced could indicate if producing many high-mass species containing oxygen is probable or not. The loss of oxygen from the gas-phase to the plasma deposited film could be neglected in a first step, due to the weak deposition on the wall of plasma PMMA (not discussed here).

Finally, the assignment of the high mass peaks in the MMA PMS to hydrocarbons is supported by works in the field of flames and combustion [222]. In the case of methyl ester (to which MMA belongs) no formation of heavy species containing several oxygen atoms seems to be reported [222].

9.6 Conclusions

The present chapter investigated the identification of neutral closed shell effluents of MMA discharge by mass spectrometry (MS). It proved to be more delicate than in the case of unsaturated hydrocarbons. Due to its aliphatic structure, MMA is effectively subject to higher fragmentation even at low electron energy. However, the methodology developed for species identification in unsaturated hydrocarbon plasma was successfully applied to MMA discharge, with some adjustments, like secondary hidden appearance energies.

- Quantitatively, 52 species (30 in the high mass region and 22 in the low mass region) are detected with different levels of certainty. Among them, **38 neutrals have never been reported in the literature**: 28 in the high mass region and 10 in the low mass region.
- Qualitatively, the dominant detected effluents with masses higher then MMA are most likely **hydrocarbon species, containing no oxygen atoms**. Recombinations with radicals containing oxygen seem therefore unlikely. In addition, the detection in significant amount of acetylene, ethylene and benzene in the MMA discharge, suggests the possible action of their own plasma chemistry, highlighted in the chapters 7 and 8.

Finally, thanks to the numerous measured electron energy spectra, recommendations have been made to carry out the partial pressure quantification of the MMA discharge, for instance at which energies the mass spectrum should be acquired to deal with CP overlapping (Section 9.4.4). MMA containing oxygen, these recommandations could be useful for other oxygen containing monomers.

Chapter 10

MMA plasma: film characterization and discharge pressure

The present chapter will deal with the investigation of the plasma polymerization of methyl methacrylate (MMA) in our setup. The results are interesting as they are significantly different from the styrene case and will bring additional comprehension of the flow process.

10.1 Plasma conditions

The conditions used are presented in Table 10.1. The series "A" is the main one, from which the species identification was operated in the previous chapter (Chapter 9). It was made recently (2013) with an optimal protocol and was chemically characterized with the new ESCALAB XPS spectrometer (Section 10.3).

In contrast, samples of the series B-C-D were made in 2009 within the framework of the master thesis of Ivan Ducarme in the laboratory. The older SSX XPS spectrometer was used at

Series	**Convector "pressure"** (Pa)	**Initial pressure** (Pa)	**Flow** (sccm)	**Duty cycle** (10 Hz)	**W/F range** (10^2 eV/MMA)	**Deposition time** (min)	**Pump valve** (turn)
A	-	6.7	28	-	0.5 - 2.1	5	2 + 5/16
B	4	1.1	0.5	50%	12 - 27	16	1 + 0/16
C	25	5.7	6.4	50%	1.0 - 2.3	16	1 + 0/16
D	32	8.0	10.0	50%	0.6 - 1.4	16	1 + 0/16

Table 10.1: Conditions used for the plasma polymerization of MMA.

that time and the sample charging could not always be totally canceled. Moreover the protocol was still under investigation.

- The flow was not known but the pump valve opening was already noted, which allowed to measure the used flow years after. This explains that they were studied at constant pump valve opening, with thus an increasing flow for increasing initial pressure.
- At that time, the Convector pressure gauge was used which gives pressure with large errors and with correction factors depending on the used gas. It is due to its design, based on the heat loss of a filament in contact of the gas. The wrong "Convector pressure" is indicated in the second column of Table 10.1, to allow comparison with the master thesis of Ivan Ducarme. Concerning the measured discharge pressures, unfortunately, it was not possible to correct them into absolute pressures, without doing the experiments once again. Indeed, the plasma is a mixture of several gases and each of them has its own correction factors.
- The range of the mean delivered energy by monomer molecule was calculated (6th column). It shows the very hard conditions of the B series, well above 1000 eV/MMA. The A, C and D series have very similar W/F. It must be noted that series B-C-D are pulsed at a frequency of 10 Hz and a duty cycle of 50%.

10.2 Deposition rate of pPMMA

10.2.1 Power variation

The deposition rate (DR) was measured by profilometry (using the scotch tape technique) and is shown on Figure 10.1a. The error bars were calculated by estimating a constant error of 3 nm on all the measured thicknesses and are therefore smaller for longer deposition duration.

Compared to styrene (20 to 700 nm/min when increasing power from 90 to 240W), the DR is low for MMA. Except for the B series and the highest power of the A series, the DR is below 5 nm/min and is not markedly affected by an increase of power. In contrast, the most energetic B series (very low flow and very low pressure) shows a strong dependence with increasing power. The DR of the highest power of A series (at 400 W) more than doubled when compared to the one at 300 W.

On Figure 10.1b, the DR is this time plotted in function of the specific energy, W/F (mean delivered energy per molecule). The B series is far on the right, out of the shown range, because its smallest W/F is equal to 1.2 keV/MMA. This second result may show that a sufficiently

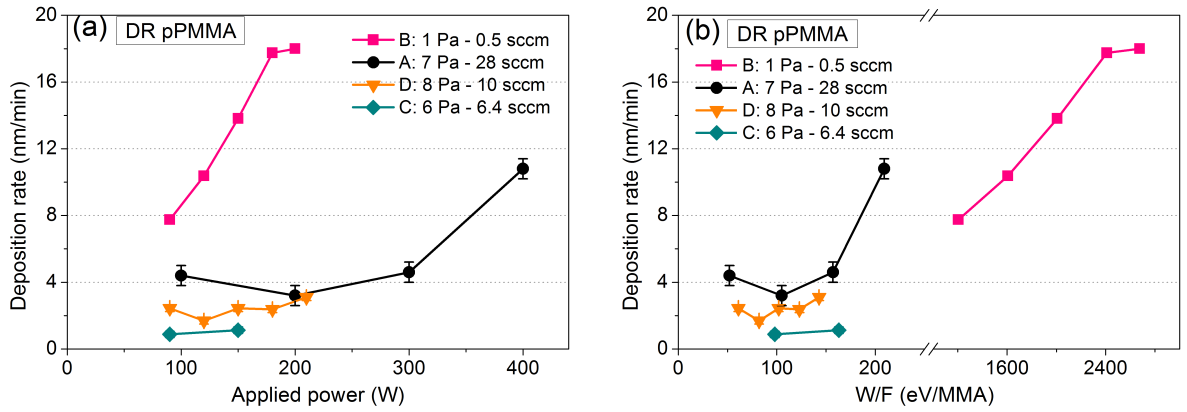

Figure 10.1: Deposition rate of pPMMA at substrate holder location in function of: (a) increasing power. (b) increasing W/F ratio.

high W/F is needed to start a DR increase for a given pressure-flow condition. Otherwise no significant increase of the DR can be obtained.

Two reasons can be proposed for this observation.

- The first is an expansion of the glow volume, progressively reaching the substrate holder at a sufficiently high W/F for a given pressure. It would applied for all the W/F range of the energetic B series: its very low initial pressure (1 Pa) allows a large glow volume. It could also apply for the highest W/F of the A series, however as we will see, the discharge pressure reaches 50 Pa for this condition (see Section 10.4.1). A progressive reduction of the distance "substrate holder - quartz window" at a given W/F and pressure condition could test this hypothesis.
- The second explanation may be the need of a sufficiently high partial pressure of a decomposition product of the initial monomer. Activated MMA (excited or dehydrogenized) could be a bad deposition precursor: due to its methyl function, steric effect could limit its sticking coefficient on the surface.

However, the substrate holder location may not be the best place to investigate the deposition rate. Other places like the quartz window or the side wall could show different evolution. In addition, the film density (or the mass deposition rate) still needs to be measured.

10.2.2 Time variation

An interesting observation was made when plotting the deposition rate for a given power with increasing time of deposition (Figure 10.2). The deposition rate is increasing linearly with the

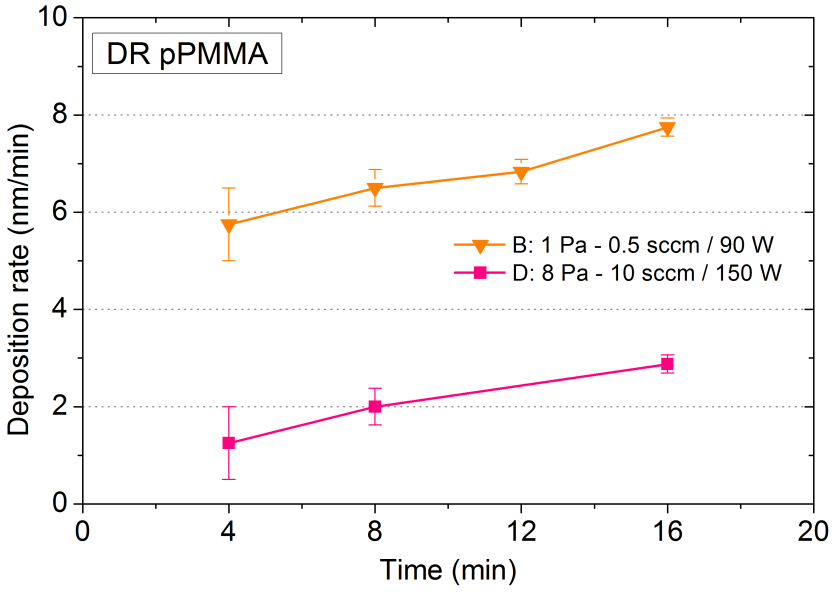

Figure 10.2: Deposition rate at substrate holder location in function of deposition duration.

deposition time. To our view, an effect on this timescale must originate from heating effect. As the deposition rate generally decreases with increasing the substrate temperature [53, 77], it is not expected to be due to the substrate heating. Thus a possible heating of the quartz window is considered. It may decrease the deposition rate of the film-forming species at that location and lead to an enrichment of these species in the gas phase, leading to higher deposition rate at remote locations. Another possibility is an initial different growth rate on the pristine substrate, than on already deposited pPMMA. However this seems unlikely for the deposited thickness of the B series, from 22 to 125 nm, and as a film growth by island seems not likely by plasma polymerization

10.3 Chemical characterization of pPMMA by XPS

Regarding the methodology, the spectra of the B-C-D series samples were acquired at one point, while three different points were characterized for each sample of series A. The data shown for the latter are the mean values of the three acquisitions and the error bars were estimated by taking the largest difference from the mean value: with a minimum of 0.5% for the atomic concentration and 1% for the components of high resolution spectra.

The general survey XPS spectra only revealed presence of carbon and oxygen atoms in plasma deposited PMMA. The oxygen content for increasing power is plotted on Figure 10.3. The experimental value of conventional PMMA from Louette *et al.* is indicated at 27% [159].

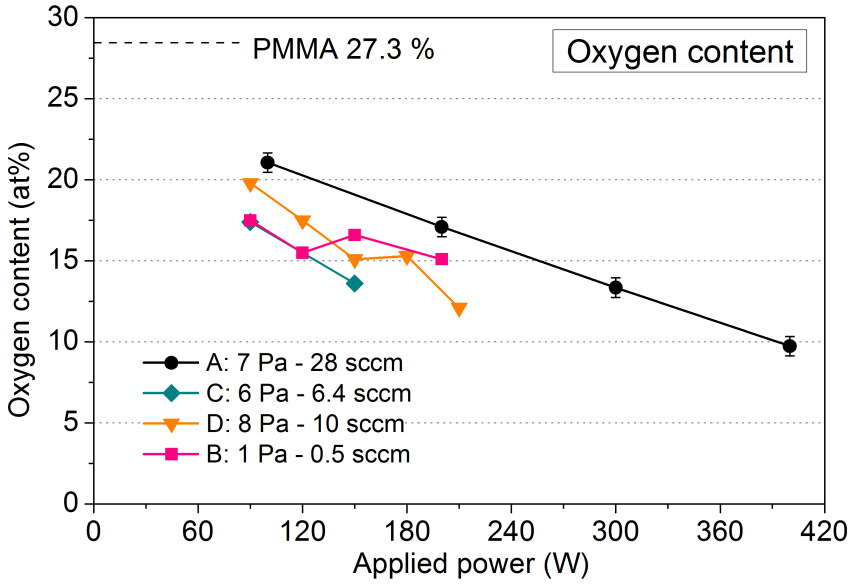

Figure 10.3: Oxygen content evolution with power, as measured from the low resolution survey XPS spectrum on pPMMA samples.

The general trend is a loss of oxygen for increasing power. The A series shows a convincing linear decrease and thus a potential control of the oxygen retention from 75 to 35%.

As described in Section 4.2.2 (page 65), four carbon environments exist in the structure of conventional PMMA: C-C, β shifted C-CO2, C-O-CO and O-C=O (written COO and denoting the ester functionality). Their respective chemical shifts relative to the C-C component are indicated in Table 10.2. Due to fragmentation in the discharge, mainly two new oxygen functionalities can be incorporated in pPMMA (indicated as "new" in Table 10.2):

- The mechanism n°1 described in Figure 4.4 (page 70) is assuming a loss of the methoxy end from the side ester functionality. This mechanism leaves in the polymer an isolated carbonyl functionality, C=O, with a chemical shift of 2.9 eV [137] , just between the one of the COO and the C-O-CO components. However, this also corresponds to the chemical shift of the ether functionality, O-C-O, which is possibly incorporated in the film.
- The inclusion of simple C-O bond is also possible, for instance from grafting of a methoxy radical OCH_3. The C-O chemical shift is then equal to 1.4 eV [137].

The six possible binding energy (BE) positions are indicated on Figure 10.4a, on the four high resolution spectra of pPMMA of the A series. With increasing power, the loss of the ester (COO) component is clear. The loss of the C-O-C=O component can also be seen. Regarding the potential appearance of C=O or C-O components, they cannot be visually stated. In the

Component	Chemical shift (eV)	
C-C	0.0	
C-COO	≈ 0.7	
C-O	≈ 1.4	New
C-O-CO	≈ 1.8	
C=O / O-C-O	≈ 2.9	New
COO	≈ 4.0	

Table 10.2: Chemical shifts relative to the C-C binding energy of the different carbon environments present in pPMMA [137].

literature, only a C=O component is generally added, as mentioned in Section 4.2.2 (page 65). This may be due to a more clearly separated BE (from the COO and the C-O-C=O components) than the C-O component whose BE (≈1.4 eV) is very close to the one of C-O-C=O (≈1.8 eV). Therefore, we decided to decompose the C1s high resolution spectra with the four components of cPMMA and add the one of C=O. However, a potential contribution from C-O to the C-O-C=O component cannot be excluded. The C-COO component was constrained to be equal to the one of the COO component. A result of decomposition is shown for the spectrum with the highest functional retention of series A (100 W) on Figure 10.4b.

The component COO is a measure of the **ester content** and is plotted in function of power on Figure 10.5 (missing data from the B and C series are due to sample charging). The experimental value of conventional PMMA from Louette *et al.* is indicated at 18% [159]. The general trend is an almost linear loss of the ester content with power, allowing a functional tuning on the base of power.

The difficult establishment of the C=O component from the B-C-D series did not allow the same comparison. However, the content in oxygen, ester, C-O-C=O and C=O are altogether shown on Figure 10.6 for the A series. The linear fits are added to more clearly show the relative trends. With increasing power, **atomic oxygen is decreasing as all oxygen functional group contents**. The new component C=O reaches a very limited incorporation of 2% at the lowest power, well below the maximal value of 7% reported in the literature (see Section 4.2.2 [164]). The slopes of the two components of cPMMA (ester - COO and C-O-C=O) are similar, but the values of C-O-C=O are systematically 5% higher. This may be due to the incorporation of C-O, which can contribute to the C-O-C=O component due to their very close BEs.

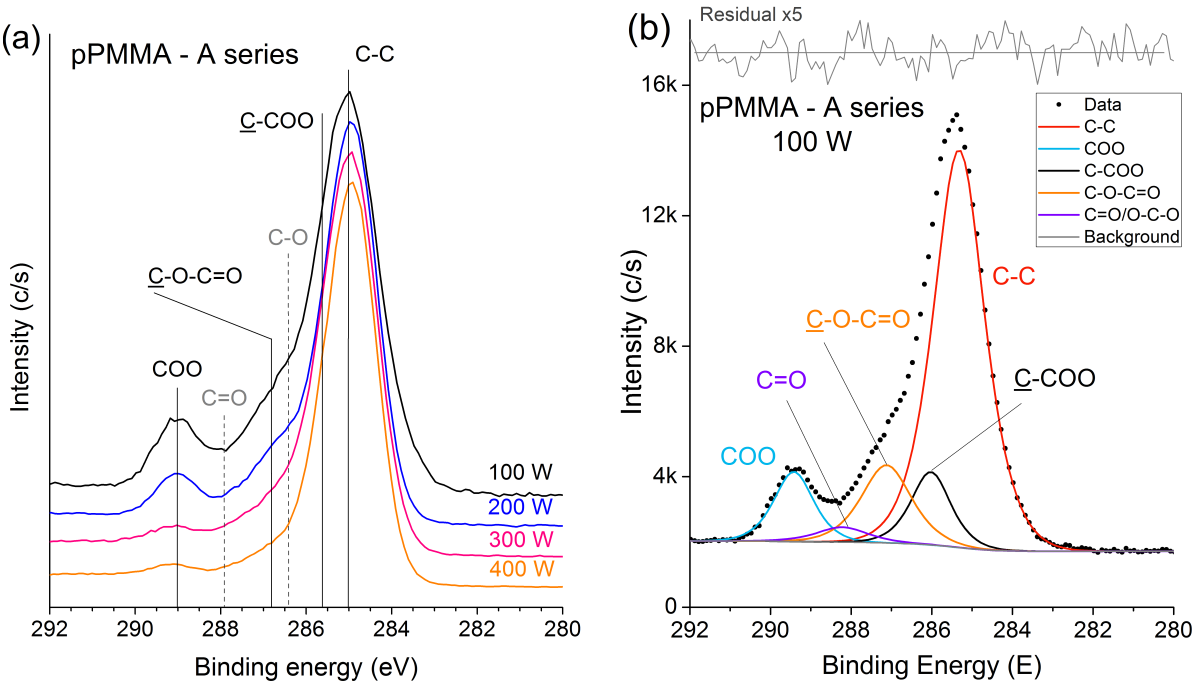

Figure 10.4: (a) Comparison of the four high resolution spectra of C1s of the A series, with location of the six components mentioned in Table 10.2. (b) Decomposition of the C1s high resolution spectrum of the pPMMA sample deposited at 100 W of the A series.

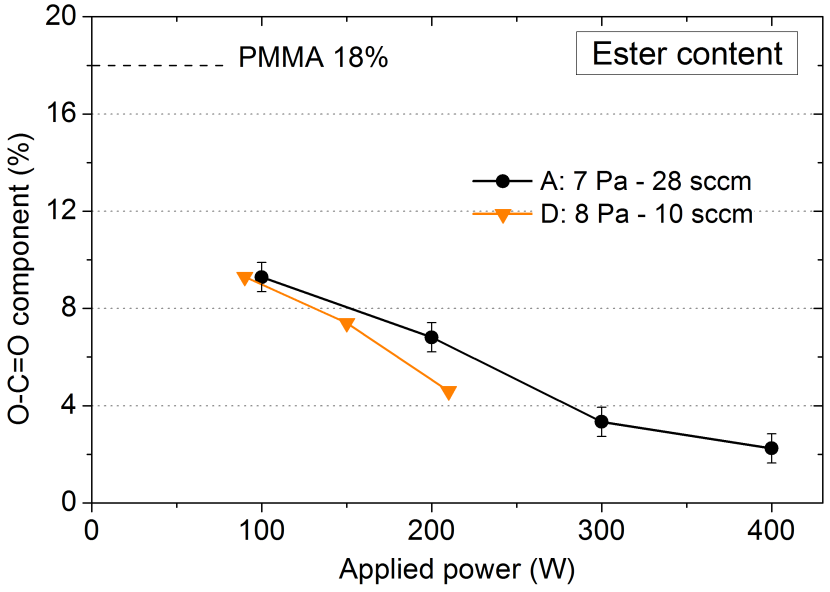

Figure 10.5: Evolution of the ester content for increasing power.

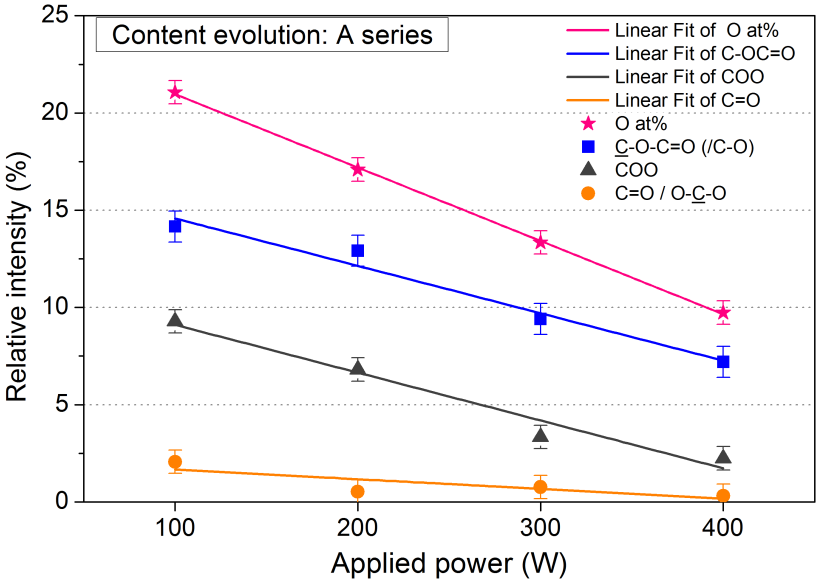

Figure 10.6: Evolution of content in oxygen, C-O-C=O(/CO), ester (COO) and ether/carbonyl (O-C-O/C=O in the deposited pPMMA.

The full-width at half maximum (FWHM) of the fitted components are large with values from 1.2 to 1.6 eV, consistent with a larger chemical diversity in carbon environment in pPMMA than in cPMMA, as reported in the literature (Section 4.2.2). The FWHMs also tend to increase with increasing power, showing an increase in the chemical diversity.

No precise structure exists for the plasma polymer and cross-linking is likely to increase with power, leading to change in the carbon environment distribution without modifying the stoechiometry. Hence it is delicate to assume more than a general loss of oxygen and oxygen functionality with increasing power. In the low pressure literature, no studies on the variation of power have been found for pPMMA, as Ward *et al.* varied the W/F ratio by increasing the MMA flow [164]. On the other hand, one study at atmospheric pressure reports increasing loss of oxygen and ester functionality for increasing power [223].

10.4 Discharge pressure in MMA plasma

A full section dedicated on the discharge pressure in MMA plasma may seem surprising. However, comparing the MMA partial pressure measured by mass spectrometry to the remaining pressure of its decomposition products will show an impossible decomposition scheme of MMA (Section 10.4.1). This brought us to investigate the different pumping rates of pure gases (Section 10.4.2) and of gas mixtures (Section 10.4.3). Finally, the results of these measurements

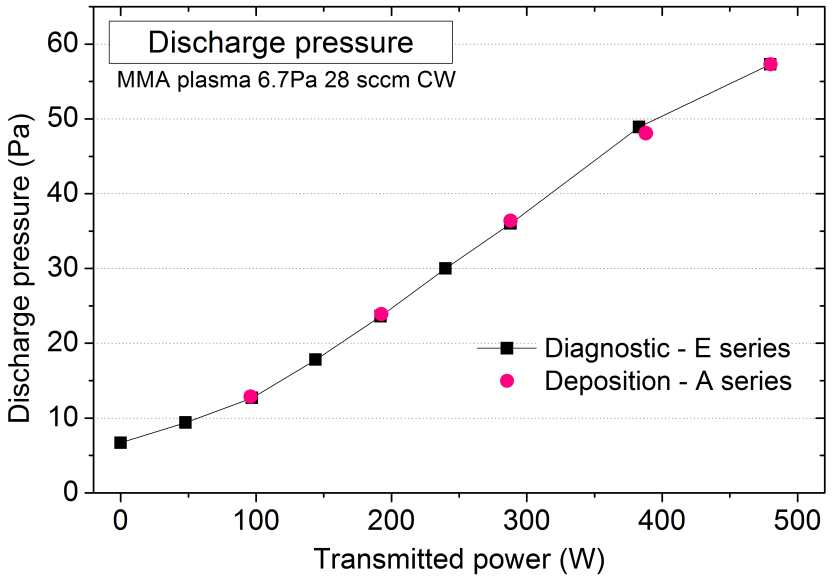

Figure 10.7: Discharge pressure in MMA plasma at initial pressure of 6.7 Pa, 28 sccm and CW conditions. Error with baratron® pressure gauge is below 1%.

revealed important consequences on the possibility of pumping rate prediction (Section 10.4.4) and led us to correct the impossible decomposition scheme initially found for MMA.

10.4.1 Discharge pressure compared to the monomer depletion

Two series of diagnostics were made at two weeks of interval. One is the A series whose DR rate and XPS charaterization has been described in the two previous sections. The other is the E series, made with the exact same conditions than the A one but with more different investigated power values. Their discharge pressures at plasma equilibrium are shown on Figure 10.7. Comparison between them shows a high reproducibility. The pressure is observed to be always higher than before plasma ignition and increases with power, as reported for closed systems (with no continuous injection of monomer) [113, 146, 169]. In our flow system, the increase shows a linear dependence with the power between 100 and 400 W. Below 100 W and above 400 W, the slope has smaller values.

For each power, a mass spectrum was recorded just before and another during the MMA plasma at pressure equilibrium, after 1 minute. The MS intensity of the molecular ion of MMA (m/z = 100) could then be used as conversion factor to quantify the remaining partial pressure of MMA during the discharge. Instead of presenting the partial pressure, the **monomer depletion** (MD = (I_{gas}-I_{pla})/I_{gas}) was calculated for the same two sets of experiments and is shown on Figure 10.8. Again the reproducibility is high between the two series. The MD increases with

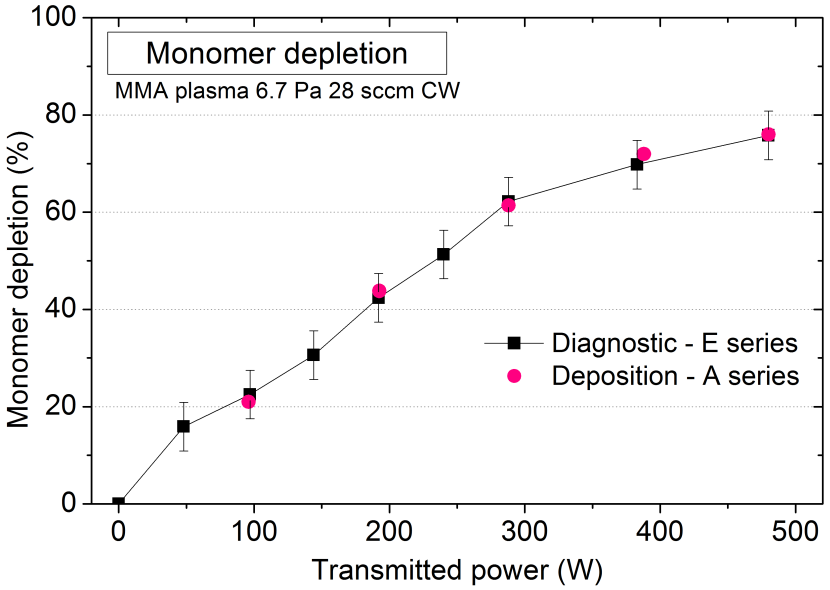

Figure 10.8: Monomer depletion in MMA plasma at 6.7 Pa, 28 sccm and CW conditions. The relative errors are estimated to be of 5%, based on the observed drift of the mass spectrometer intensities (Section 5.3.7).

the power, as already reported in MMA flow system [4]. The increase is linear up to 300 W, then shows a reduced slopes.

Compared to styrene which reaches 99% of MD at 185 W under the same flow and initial pressure conditions, MMA only reaches 76% of MD at 500 W of applied power. The total bond energy is roughly 74 eV for styrene and 59 eV for MMA (see Section 2.4.1). Hence MMA may seem easier to fragment. However, discharge pressure is 1.8 Pa at 185 W for styrene and 58 Pa at 500 W for MMA. The significant amount of decomposition products in MMA discharge, like hydrogen, CO or CO_2 ([169]), may altogether play the roles we highlighted for hydrogen in the previous chapter in Section 8.4.4: electron cooling and power dissipation.

Assuming the same pumping rate before and after plasma ignition, it is interesting to evaluate the number of moles of the MMA **fragmentation products** compared to the amount of moles of **consumed MMA**. The pressure of consumed MMA is simply the difference between the initial pressure and the remaining pressure of MMA during the plasma. The latter is the only partial pressure that could be measured by using the "conversion factor" of MMA from the MMA vapor mass spectrum, taken just before the plasma ignition. As mentioned in chapter on the partial pressure quantification (Section 8.2.2), in that case, the pressure error is expected to be less than 5% (Section 5.3.7). Regarding the pressure of the MMA plasma products ("product pressure"), it is calculated by subtracting the total pressure by the remaining MMA pressure in

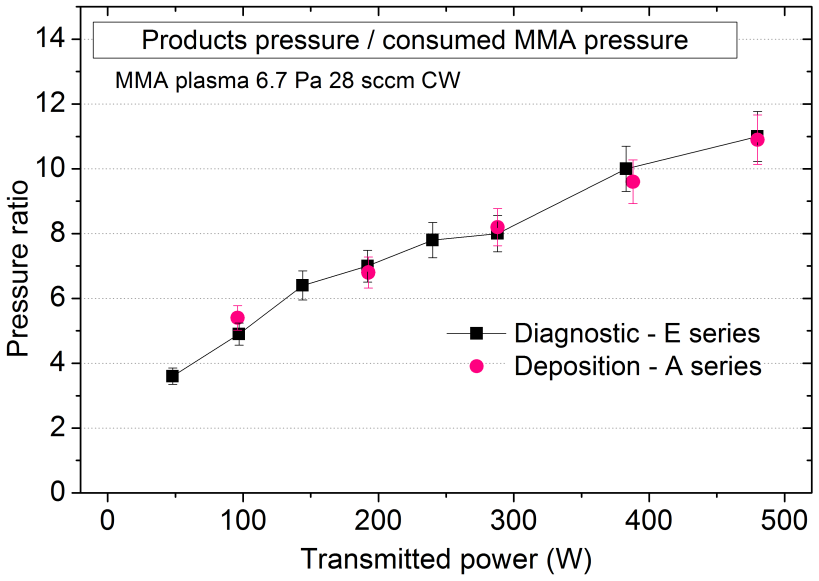

Figure 10.9: Ratio of the product pressure to the consumed MMA pressure. The relative errors are 5% for the monomer pressure (e_1), then 5% for the product pressure (e_2) and thus 7% on the pressure ratio (e_r) according to the exact calculation of the relative error of a ratio: $e_r = (e_1^2 + e_2^2)^{1/2}$.

MMA decomposition	product / consumed MMA
Naive result	11
Maximal theoretically possible	6
Already reported (Pan *et al.* [169])	3.3

Table 10.3: Decomposition scheme of MMA and ratio of the products pressure over the consumed MMA pressure.

the discharge. The ratio of the product pressure to the consumed MMA pressure is shown on Figure 10.9. As simple interpretation, at 50 W, 1 mole of consumed MMA produces 3.5 moles of gas products. At 500 W, it provides 11 moles of gas products.

This latter figure seems unlikely. Indeed, an advanced decomposition of MMA, $C_5H_8O_2$, could reasonably lead to production of: 2 CO + 2 H_2 + 1 C_3H_4. The latter species, propadiene, can react with another propadiene and form: 2 $C_3H_4 \rightarrow$ 2 C_2H_2 + 1 H_2. Hence as a limit case of full decomposition in stable products without any deposition, 1 mole of MMA can decompose into 6 moles of products: 1 $C_5H_8O_2 \rightarrow$ 2 CO + 2.5 H_2 + 1.5 C_2H_2. The maximal pressure ratio should then be equal to 6, as reported in Table 10.3.

This latter ratio can be compared to the one in the closed system of Pan *et al.* [169]. Starting from a initial pressure of 40 Pa at a power of 100 W, the final pressure increases of a factor 3.3,

reaching around 133 Pa (without any MMA remaining). So the theoretical limit case of MMA decomposition seems too idealized even for closed system, which should reasonably reach a higher degree of fragmentation of the MMA than in flow system.

The pressure ratio of "only" 3.3 obtained by Pan *et al.* [169] can be explained by a deposition on the electrode, but also by their gas composition. The partial pressures of eight gas products were measured by Fourier Transform Infrared Spectrometry (FTIR). By decreasing importance, the final composition at 100 W is: 40% of CO, 10% of CO_2, 7.5% of C_2H_2, 3.7% of CH_4, 1.6% of C_2H_4 and the other four products are estimated to contribute to less than 2% (DMK, CH_2O, CH_4O and MMA). The remaining 35% of unknown pressure can reasonably be attributed to H_2 which cannot be detected by IR (or to errors). Thereby, we can note that, even in a closed system, the final composition contains CO_2 and CH_4, which do not correspond to an optimal decomposition of MMA, producing a maximal pressure.

10.4.2 Pumping rate of single gases

The question is opened: Why did we find a pressure ratio as large as 11? The answer lies in a change of the pumping rate. The six gases observed with the highest partial pressure in the Pan *et al.* study has been injected pure in our reactor: CO, CH_4, H_2, CO_2, C_2H_2 and MMA [169]. The equilibrium pressure was measured when varying the flow, using the same valve opening as that used for the MMA discharge (2.31 turns).

The results are shown on Figure 10.10. It clearly reveals that the three discharge products H_2, CO and CH_4 are much less well pumped, than MMA, CO_2 and C_2H_2. This is a simple expression of their boiling temperature; which is -253°C, -191°C and -164°C for H_2, CO and CH_4 respectively. It is too low to condense on the nitrogen trap, as the nitrogen boiling temperature is -196°C. On the contrary, C_2H_2 and CO_2 have much higher boiling temperatures, -81°C and -59°C respectively, and MMA is liquid at room temperature. Concerning the differences of the pressure curve of the three less well pumped gases, it is due to pump efficiency difference of the primary pump. It is known that H_2 is better pumped by a primary pump than heavier gas [80] (p280). This is the opposite than for turbo-molecular pump and is caused by the higher collision rate of the hydrogen molecules on the "virtual surface" of the entrance pump pipe.

For each pressure curve, it is worth noting that the pressure is not linearly related to the flow, but rather shows a slight decrease of slope. This is simply due to the increase of the pumping rate at higher pressure, as seen in the chapter on pressure quantification (Section 8.1.1). The power dependence of Yasuda and Hirotsu, $p = a F^b$, again best fits the data, but in this case

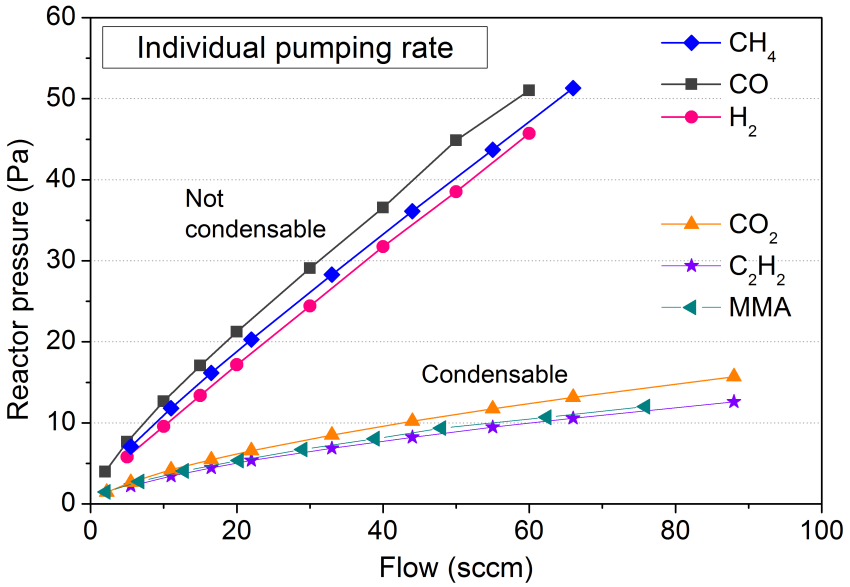

Figure 10.10: Reactor pressure at V_P = 2.31 turns (2+5/16) depending on the injected flow and on the gas, for MMA and five of its discharge products which are H_2, CH_4, C_2H_2, CO and CO_2.

using a nitrogen trap in addition of the primary pump [80, 215]. The factor b is once again below 1 with values of around 0.82 for non condensable gases and 0.62 for condensable ones (for V_P = 2+5/16).

10.4.3 Pumping rate of gas mixture

As H_2, CO and CH_4 account for 82.5% of the final discharge pressure in the closed system of Pan *et al.*, we can expect an important contribution from those three non-condensable gases at our highest power. But to which extent inefficiently pumped gases affect the overall pumping rate of the process? Are the individual pumping rates conserved when the gases are mixed?

To answer these questions, the reactor pressure was measured when a mixture of CO and CO_2 is injected. On Figure 10.11, three series were carried out at constant contribution to the total flow: a first with 25% of CO flow to the total flow, a second with 50% of CO flow and a last one with 75%. Series with 100% of CO and 0% of CO (100% of CO_2) were added for comparison. Each series has slopes which slightly decreases with the total flow increase, like for the individual gas measurement on the previous figure. The weak number of data did not allow good fits, but the obtained power coefficients (b) have been added on the figure for indication. It is also interesting to note that the series have pressure curves which are regularly spaced.

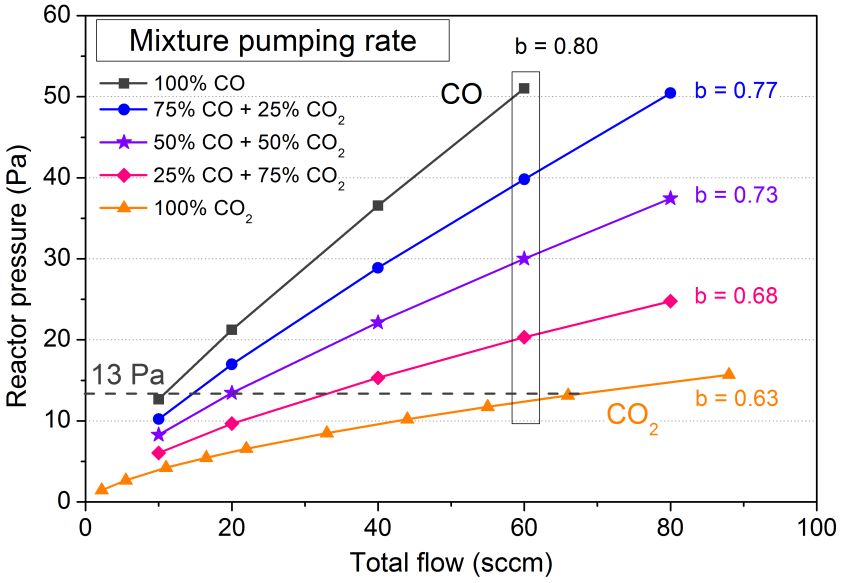

Figure 10.11: Reactor pressure at V_P = 2.31 turns (2+5/16) depending on the injected total flow for five series of CO and CO_2 mixtures.

To evaluate the vertical regularity between the curves, the **total pressure was measured at a constant flow** of 60 sccm, while varying the gas composition. It corresponds to the range of data in the rectangle drawn on Figure 10.11. The result is shown on Figure 10.12. The pressure variation is almost linear (shown by the dash line), except at the lowest CO contribution.

To evaluate the horizontal variation of the pumping rate curves, the **total flow was measured while maintaining the pressure constant** at 13 Pa, for different gas composition. It corresponds to the range of data along the horizontal dash line of Figure 10.11. The result, shown on Figure 10.13, reveals a clear non linear dependence. Several functions were tested to fit the data and the best result was obtained for an exponential dependence, as shown on the figure.

Measure of the partial pressures at constant flow

To understand the linear vertical variation of the total pressure with the gas composition, we measured the partial pressures by MS in the case of the total flow of 60 sccm. To this aim, pure CO and pure CO_2 were alternatively injected at 10 Pa in the reactor for calibration, by measuring their cracking patterns and their absolute intensities at 20 eV. The absolute intensity of their respective molecular ion at m/z = 28 for CO and 44 for CO_2 was divided by the 10 Pa pressure to establish the "conversion factor". The cracking pattern (CP) of CO_2 has a peak at m/z = 28, interfering with the molecular ion peak of CO. However, at the electron energy used

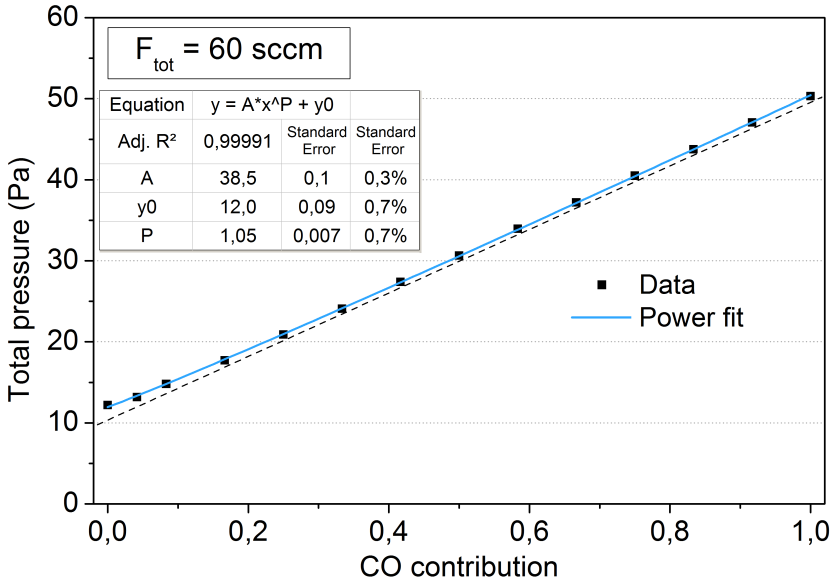

Figure 10.12: Evolution of the total pressure at constant total flow while varying the gas composition.

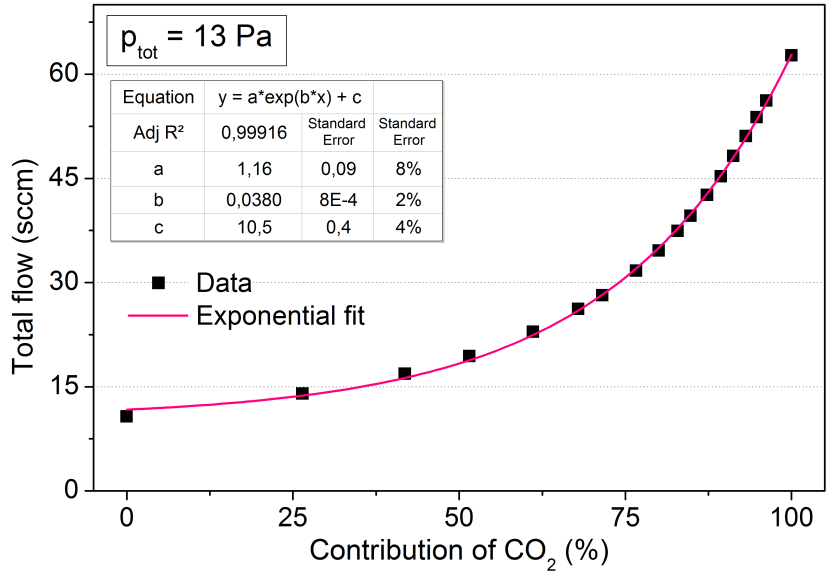

Figure 10.13: Evolution of the total flow at constant total pressure while varying the gas composition.

of 20 eV, the contribution is less than 1% of the CO intensity for the same pressure of 10 Pa. The conversion factors were measured once before the mixing of the gases and once after. Their values were stable within 4%. The mean factor was used for the calculation. Then the mass spectra were recorded for the three gas mixtures, keeping the total flow at 60 sccm. The partial pressures were calculated by dividing the measured absolute intensities by their corresponding

CO / CO_2 flow (sccm)	15/45	30/30	45/30
CO relative pressure	30%	53%	74%
CO pressure (Pa)	6.1	16.5	29.4
CO_2 pressure (Pa)	14.3	14.3	10.0
Summed pressure (Pa)	20.4	30.7	39.3
Measured pressure (Pa)	20.2	30.0	38.6
Relative difference	0.7%	2.6%	1.7%

Table 10.4: For three gas mixtures of CO and CO_2 with total flow of 60 sccm: relative pressure of CO, measured partial pressures of CO and CO_2 , the sum of the two measured pressures, the total measured pressure in the reactor and the relative difference of the two latters.

conversion factor. The obtained values are shown in Table 10.4. The sum of the two partial pressures matches well with the total measured pressure (relative difference below 3%). It shows once again the quantitativeness of the procedure.

Finally, the relative pressure of CO to the summed pressure is shown on Figure 10.14. The x axis is the relative flow of CO to the total injected flow. The errors are estimated to be reasonably around 5% of the measured partial pressures (Section [215]). The figure reveals that the relative pressure of CO is equal to its relative flow. The following equation can then be written, with the factor C_i we will called the "contribution" of the gas i:

$$\frac{F_i}{F_{tot}} = \frac{p_i}{p_{tot}} = C_i \tag{10.1}$$

This result is surprising. CO is around four times less well pumped than CO_2, when injected pure at the same flow. Therefore, when injecting 30 sccm of CO and 30 sccm of CO_2 altogether, it would have been anticipated that the partial pressure of CO would be much higher than the partial pressure of CO_2. It is not the case. The two gases contribute equally to the total pressure. Hence the gas mixture seems to behave as a gas with a unique molecule pumped at an unique rate. The best explanation for this aspect is that the flow is in viscous regime. A high rate of collisions between the molecules of the two gases would induce a friction between them and an effect of "dragging".

The flow regimes are determined by the Knudsen number, K, defined as the ratio of the mean free path, λ, to the diameter of the pipe through which the gas flows, d. If K<0.01, the gas flow is said to be in viscous regime, above 1 the flow is molecular and in between lies the transition regime, in which the flow is viscous or molecular depending on the exact geometry.

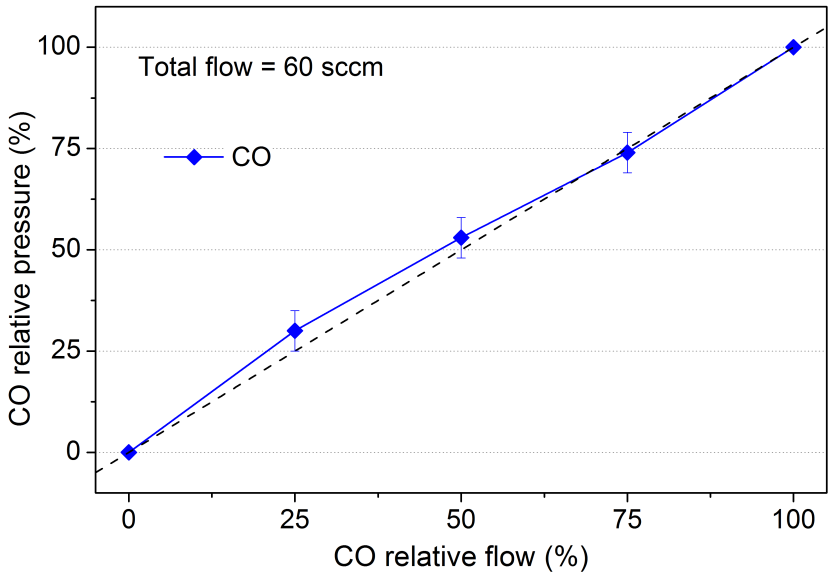

Figure 10.14: Relative pressure of CO to the summed pressure as a function of the relative CO flow to the total flow of 60 sccm.

Pressure (Pa)	λ (N_2) (cm)	K (chamber)	K (tube)
1	0.7	0.02	0.1
10	0.07	0.002	0.01
100	0.007	0.0002	0.001

Table 10.5: Evaluation of the Knudsen number, $K = \lambda/d$, for different pressures in the chamber (30 cm diameter) or in the pumping tube (5 cm diameter).

Table 10.5 shows the evaluation of K for nitrogen (classical radius of 1.8 Å to evaluate the mean free path with Equation 1.5, page 16) at different pressures operated in our reactor. The range of pressure investigated mainly lies in the viscous flow regime (Knudsen number K<0.01) or in the transition regime (0.01<K<1) for the lowest pressures.

10.4.4 Consequences of the single pumping rate of gas mixture

The single pumping rate of all the different molecules in a mixture has important consequences. To establish them, we will consider that the complex plasma composition can be simplified as follows. The plasma is composed of only two gases: one condensable, gas A, and one not condensable, gas B. This can be assumed as all the condensable gases have very close pumping rate curves, as well as all the non-condensable gases have similar curves between them (see Figure 10.10).

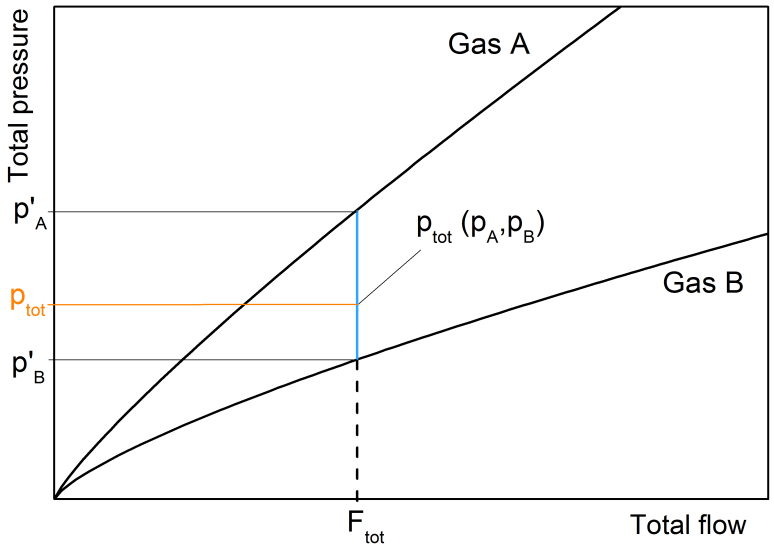

Figure 10.15: Pressure curves or pumping curves of gas A and B. For a known total flow F_{tot}, the total pressure p_{tot} varies between p'_A and p'_B, depending on the gas composition.

Prediction of pressures

The two gases, A and B, are injected at known values of flow, F_A and F_B, respectively. The total flow is then known, being $F_{tot} = F_A + F_B$. The calculated relative flows thus give the contribution C_A ($=F_A/F_{tot}$) and C_B ($=F_B/F_{tot}$). In addition, their pressure curves depending on the injected flow have been measured and are schematically shown on Figure 10.15 (page 211).

(1) **The total pressure can be predicted**. The total pressure variation occurs between two limit pressures shown on Figure 10.15: p'_A which is the pressure obtained when only gas A is injected at F_{tot}, and p'_B which is the pressure obtained at the same flow but for a pure injection of gas B. The linear variation of p_{tot} between these two pressures (see Figure 10.12) can be then expressed as follows, in function of the gas B contribution:

$$p_{tot}(C_B) = p'_A + (p'_B - p'_A)C_B \tag{10.2}$$

It is the equation of a straight line, where the slope is given by $\Delta p/1 = (p'_B - p'_A)/1$. When $C_B = 0\%$, the total pressure equals p'_A and on the contrary, when C_B is equal to 100%, $p_{tot} = p'_B$. In this expression, all the values are known, enabling to calculate p_{tot}.

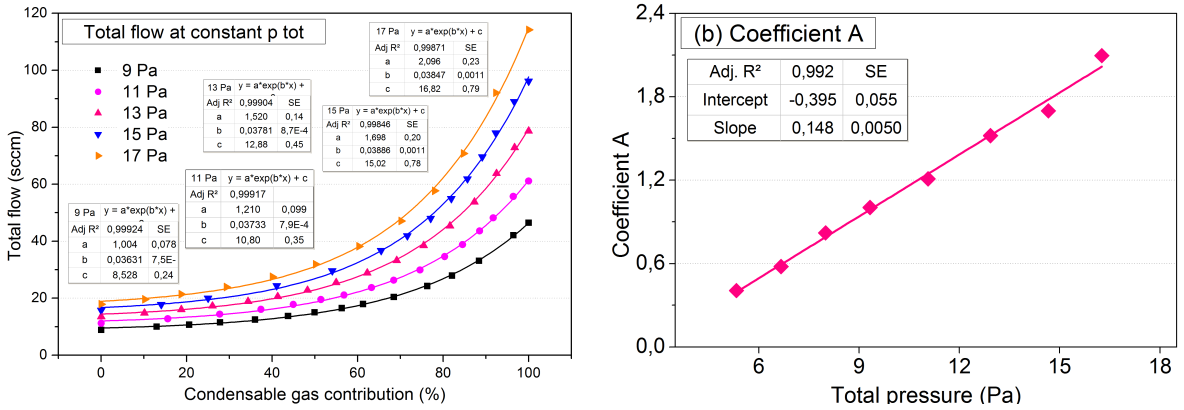

Figure 10.16: (a) Exponential fits of the total flow in function of the gas composition at five constant total pressures. (b) Variation of the A coefficient of the exponential fits with the total pressure.

(2) **The partial pressures can be predicted**. From Equation 10.1, the contribution of gas B can be changed into p_B/p_{tot}. Once the total pressure has been calculated, the only unknown in the equation is p_B, which isolated gives:

$$p_B = \frac{p_{tot}^2 - p'_A p_{tot}}{p'_B - p'_A} \tag{10.3}$$

A similar formula for p_A can be found.

Estimation of injection flows

Now we consider the situation where two gases are injected with unknown flows. However, the total pressure is measured by the gauge, as well as the partial pressures by a quantitative technique such as mass spectrometry.

This time, the prediction of the **total flow** is more complex because the total flow does not vary linearly with the gas composition at a constant total pressure (see Figure 10.13). Therefore, this non-linear variation was measured for eight different constant total pressures. Figure 10.16a shows the plots fitted with exponential functions, written as: $A \cdot \exp(B \cdot x) + C$. As the curves are regularly spaced, the three coefficient factors were plotted to check their evolution, as shown on Figure 10.16b, 10.17a and 10.17b. The three coefficient turned out to vary linearly with the total pressure! The result for the coefficient B is the less convincing on Figure 10.17a but as the relative variation is actually small, we will assume this linear variation.

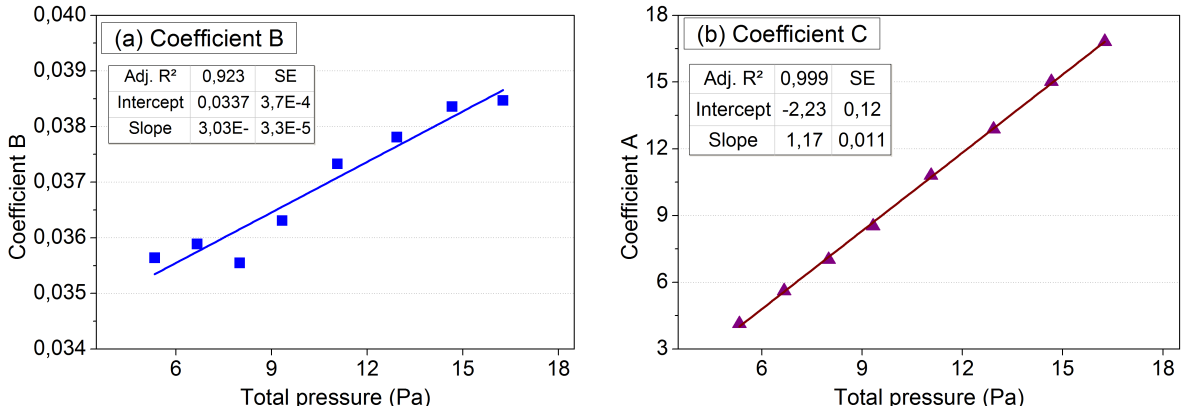

Figure 10.17: (a) Variation of the B coefficient of the exponential fits with the total pressure. (b) Variation of the C coefficient of the exponential fits with the total pressure.

This is very fortunate because one measure of the exponential fit at one high constant total pressure, p_1, and another at one low constant total pressure, p_2, allows to interpolate very simply the coefficients for all the total pressure in between. As a result, the **total flow can be predicted** at any total measured pressure between p_1 and p_2 if the gas composition is known (if the partial pressures are known). In addition, once the total flow is known, the **partial flows** are easily obtained through the contribution: $F_i = C_i \cdot F_{tot}$ (Equation 10.1).

Power dependence between the pressure discharge and the monomer flow

The single pumping rate of the gas mixture also justifies a posteriori a second empirical observation of Yasuda and Hirotsu [6]. During plasma, the discharge pressure (and no more the initial one) and the monomer flow are also empirically related by a power dependence: $F = a\ p^b$.

The present results can not only give a justification for this observation, but in addition correct it, as it is suspected to be not general, as explained hereafter.

- Yasuda and Hirostu established this power dependence during discharge of acetylene and ethylene plasma [7] (p283-284).
- We observed that for constant gas composition (25% CO and 75% CO2 for instance), the slope of the pressure curve was diminishing like for a single gas. Actually, these pressure curves at constant mixture composition can effectively be fitted by a power dependence.
- We therefore expect, but without experimental verification, that for a linear change of composition with the total flow, a power dependence could be established as well.

- However, for a non-linear change of composition with the total flow, we expect that the power dependence would not stand anymore.
- From our partial pressure quantification in acetylene and ethylene discharge in chapter 8 (see section 8.4.3), we observed an almost linear production of hydrogen with the applied power, as long as the power stays below the critical power. This means as long as the discharge stays in the energy-deficient plasma polymerization domain. To change the domain, it is necessary to vary the W/FM factor, i.e. either change the power W or the monomer flow F. In our case, the power was varied, in the case of Yasuda and Hirotsu, it is the flow.
- Hydrogen is the only significant gas product which does not condense on a nitrogen trap, among the products of acetylene and ethylene discharges (methane contribution is negligible).

From all these considerations, we expect that if the acetylene and ethylene discharges were driven out from the energy-deficient regime, the production of hydrogen would not be linear anymore and the gas composition between condensable gases and not condensable gases would not linearly vary anymore. As a consequence, we predict that the power dependence would fail to relate monomer flow and discharge pressure. However, now this prediction has to be verified experimentally.

10.4.5 Consequence on adding a second gas

In Section 8.1.1, the partial pressures were studied when two gases are injected in the reactor. The increase of the pumping rate when a second gas is added in the reactor reduces the partial pressure of the first injected gas. This was explained by the better pumping rate at higher total pressure (the non-linear power dependence between flow and pressure). However, this was observed in the case of two gases with similar pumping rate.

Now, in the case of two gases with very different pumping rate, it is demonstrated that it **depends on the order of injection**. This has been investigated for simultaneous injection of hydrogen (H_2 - condensable) and ethylene (C_2H_4 - non-condensable):

(1) **The non-condensable gas is injected first**. Figure 10.18a shows the partial pressure evolutions (measured by MS) of hydrogen and ethylene. H_2 is injected at a constant flow of 12 sccm and ethylene with increasing flow. The x axis is the total flow. The above mentioned assumption holds: the injection of a second condensable gas (ethylene) decreases the partial pressure of the first one (hydrogen).

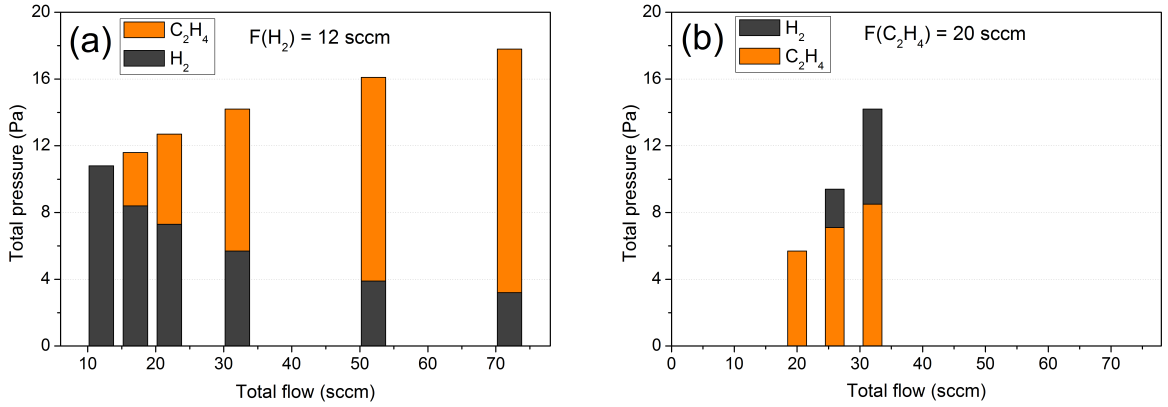

Figure 10.18: Evolution of total pressure and partial pressure of hydrogen and ethylene for: (a) constant injection flow of hydrogen (non-condensable) and (b) constant injection flow of ethylene (condensable).

(2) **The condensable gas is injected first**. The opposite situation is plotted on Figure 10.18b: ethylene is injected at a constant flow of 20 sccm and hydrogen is added. Clearly, the assumption must be reversed: the addition of the second non-condensable gas (H_2) increases the partial pressure of the first one (C_2H_4). The cause of this effect is the overall pumping rate decrease when a non-condensable gas is added, which is higher than the increase of pumping effect due to the higher total pressure.

10.4.6 Consequence on the monomer depletion and the products pressure

We can now find a reason why the ratio of the product pressure to the consumed MMA pressure reached a value of 11 at the highest power. In the MMA plasma at the highest power, a large part of the pressure can be reasonably assumed to be due to species with pumping rate 4 times below the MMA pumping rate (85% of pressure due to non-condensable gases in the closed system of Pan *et al.* [169]). With the single pumping rate of gas mixture we observed, it is thus reasonable to consider that the pumping rate of the overall MMA discharge is reduced by an approximate factor of 3, if those slowly pumped species dominates the discharge.

This variable pumping rate is a problem. Indeed, the same injection flow of a species will provide a different pressure in the reactor if the pumping rate is different. Therefore measuring the pressure is not a reliable way to measure the injection flow of a species. Applied to plasma, measuring the partial pressure does not give access to the average production rate of a species.

Discussion (MMA plasma at 500 W)	Discharge pressure (Pa)	Monomer depletion	Depleted MMA (Pa)	Products pressure (Pa)	Products/ depleted ratio
Naive	58	78%	5.2	56.5	11
Variable rate	19	93%	6.2	18.8	3.0

Table 10.6: Naive discussion is without taking care of the change of the pumping rate. The variable rate discussion does integrate this effect. The MMA pressure before discharge is 6.7 Pa.

Implicitely, we have here distinguish the rate of injection, F_{IN}, from the pumping rate, S_{OUT}. Both are equal at equilibrium, meaning when the reactor pressure is constant:

$$F_{IN} + S_{OUT} = \frac{dN}{dt} = 0 \tag{10.4}$$

where N is the number of molecules in the reactor. This number is constant when $F_{IN} = S_{OUT}$ and evolves if not.

All the discussion now is about establishing the pressures if the pumping rate, S_{OUT}, had not changed. Said in other words, we want to **remove the effect of the variable pumping rate**. In that case, the pressures are directly related to the injection flow, F_{IN}, and we will call them the "significant pressures" to distinguish them from the measured pressures. For the sake of simplicity, we will also assume that the total pressure is linear with the injected flow, meaning that there is no increase of the pumping rate at higher pressure. Strictly, this is not true as we observed a power dependence of the total pressure with the injected flow (see Figure 10.10 on page 206).

For the MMA plasma at 500 W, we said it was reasonable to consider that the pumping rate is divided by a factor of 3, compared to the pumping rate before plasma. The measured pressures must then be divided by 3 to obtained the "significant pressures". We apply now this hypothesis for the results at the power of 500 W and will compare it to our initial naive discussion made without caring about the pumping rate (Section 10.4.1). The main conclusions are summed up in Table 10.6, where the new discussion is referred as "variable rate" and is developed hereafter.

The "significant" discharge pressure is a third of the measured one: 58 Pa / 3 = 19 Pa. The measured pressure of the MMA remaining in the discharge is obtained thanks to the MD of 78%: (100%-78%) $\cdot$ 6.7 Pa = 1.5 Pa, because the initial MMA pressure is 6.7 Pa. The "significant" MMA remaining pressure is also a third of this value: 1.5 Pa /3 = 0.5 Pa. Thereby, the pressure

of the depleted MMA is not anymore 6.7-1.5 = 5.2 Pa, but instead 6.7-0.5 = 6.2 Pa. Thus, the monomer depletion is actually higher than the 78% of the "naive" discussion: it is rather 6.2 Pa/6.7 Pa = 93%.

Regarding the "significant" product pressures, it has changed from (58-1.5) = 56.5 Pa to (58-1.5)/3 = 18.8 Pa. Thus, the ratio of the product pressure to the depleted MMA pressure now equals to: 18.8 Pa / 6.2 Pa = 3.0, instead of 11 for the naive discussion. It is physically acceptable as our full decomposition scheme with no deposition gives a factor of 6 and as Pan *et al.* observed a final factor of 3.3 in their closed system (see Table 10.3, page 204).

Therefore the effect of the pumping rate is of uttermost importance to carry out the "correct" quantification in flow plasma system. It is not enough to measure the partial pressures: **the total pumping rate and the partial pumping rates must be measured to access to the partial injection flows equal to the average production rates**. Concerning the monomer depletion, the change of pumping rate has a significant effect. Corrections should then be made in the previous chapter on the quantification in hydrocarbon plasmas: the actual depletion must be higher than presented when large production of hydrogen is observed in the discharge.

To summarize, the measurements of partial pressures when mixing two gases revealed two effects:

- at constant composition, the pumping rate moderately increases with the pressure;
- at constant total flow, the pumping rate strongly increases with a more condensable composition of the gas mixture.

10.5 Conclusions

The present chapter investigated the surface characterization of pPMMA thin films and the discharge pressure during MMA plasma.

Regarding the **film characterization**, the deposition rate of MMA is low at the substrate holder location and moderate W/F values. Moreover it stays rather constant for increasing power, up to a threshold value of W/F regarding the A series. In contrast, at very high W/F values and low initial pressure (1 Pa), the DR showed a linear variation with power and then saturation. The measure of the light emission would be welcomed to investigate these observations. Especially, the very large increase of the MMA discharge pressure could contribute to discuss its unanswered interaction with the E/H transition, for plasma polymerizing system. Indeed, the increase of the discharge pressure is very impressive for MMA (58 Pa at 500 W),

even when compared to ethylene (16 Pa at 400 W). In addition, the results may also show that working at a low pressure expands the plasma up to the substrate holder.

The chemical composition of the pPMMA film shows a regular if not linear decrease of the oxygen content and of the oxygen functionalities. No modification of this linear decrease of composition have been detected for the main series (the A series) at the highest power, for which the DR rate increases notably.

Regarding the **plasma characterization**, the naive analysis of the discharge pressure and the monomer depletion of the MMA plasma led us to estimate a too large amount of gas products in regards of the MMA injection. The study of the pumping rate of gases known to be produced in MMA discharge allowed one to explain the observed discharge pressures within a physically possible decomposition scheme of MMA. The nitrogen cold trap effectively leads to large discrepancies of the pumping rate depending on the nature of the gases: some gases condense on the nitrogen trap, others don't. However, on the contrary of our initial intuition, a gas mixture in our range of pressure revealed a unique pumping rate for every gas composing the mixture, whatever if they are easily or slowly pumped out, when injected alone in the reactor. Thereby a slowly pumped gas, like CO, CH_4 or H_2, decreases the pumping rate of an easily exhausted gas like MMA. This effect can be explained by our range of pressure, corresponding to a viscous regime of gas flow.

In addition, the pumping rate investigation allowed to establish a method to predict the total pressure and the partial pressure for known flows of injected gases. The reverse prediction has been successfully adressed too. The total flow and the partial flow can be predicted if the total and the partial pressures are known. It is of uttermost importance for plasma polymerization processes using cold trap, since it allows to **quantify the production rates of the plasma effluents**.

Finally, at the present state of the work, no correlation have been proposed between the film characterization and the discharge pressure. However the data are available to discuss the relative variation of species in the gas-phase like CO_2 or CO. As they tend to increase with the increase of power, explanation of the oxygen loss with power could be discussed. However, it may rather be worth to endeavor the partial pressure quantification to allow a more complete discussion. The tracking of the mass but also of the oxygen atoms could be very interesting for MMA. Being an oxygen containing monomer, it opens the doors towards others, largely used for thin film depositions.

Chapter 11

Conclusions and perspectives

It is now time to draw the general conclusions of the present work, which investigated the plasma polymerization of two model compounds: styrene and methyl methacrylate (MMA). The results regarded physical aspects of the process like the exhaust gas rate, the achievement of an E/H transition and full glow regime or the physical effects of hydrogen on the plasma flow. Moreover, general trends in the plasma chemistry of unsaturated hydrocarbons and oxygen-containing monomers have been established. Throughout the work, a complete quantification method using Mass Spectrometry has been developped, regarding not only the partial pressures but also the total production rates of the plasma effluents.

Consequence of the pumping rate on the quantification of reactions

Two significant effects were observed when continuously injecting two gases in a pumped vacuum system. First, it regards two gases with the same pumping rate. The partial pressure of a gas injected at constant flow is reduced when a second gas is injected, despite the first gas flow is maintained constant. This was explained by the higher exhaust rate of the pump at higher pressure. Second, it concerns two gases with very different pumping rate, due to a different ability to condense on a cold trap. Injected at the same flow, the best pumped gas has not a lower pressure than the least pumped. Instead, both gases have equal partial pressures, which means that all molecules in the gas mixture are exhausted with a single pumping rate. As a result of their initially very different pumping rates, adding a non-condensable gas to a condensable one can increase the partial pressure of the condensable, cancelling the first above mentioned effect.

The present work succeeds to predict the total pressure and the partial pressures when the input and the output flow of species are known. More importantly, the total input flow and the partial input flows can also be predicted when the total pressure, the partial pressures and the pumping rate of the single gases have been measured. In addition, the current work predicts a correction of the power dependence between the monomer flow and the discharge pressure observed by Yasuda & Hirotsu in 1978 [215].

These results have considerable consequences to quantify the gas-phase reactions in plasma of flow system. The measure of the partial pressure by Mass Spectrometry (MS) is indeed not enough to determine the number of reaction per unit of time. The knowledge of the partial pumping rates of the different effluents gives direct access to their average rate of production in the plasma.

Planar inductively-coupled geometry, E/H transition and full glow

The deposition rate (DR) of styrene plasma at the sample position showed a sudden and large increase above a critical applied power. It was correlated with a sharp drop of the total discharge pressure and the occurrence of a E-to-H transition. The latter is an abrupt increase of both the coupling efficiency and the electron density, increasing greatly the activation by electrons in the plasma. The gas phase quantification showed that hydrogen was responsible for more than 80% of the remaining small pressure. The absence of hydrocarbons in the plasma-phase was successfully explained by their complete deposition on the reactor wall.

The burst of deposition can be explained either by the E-to-H transition or by the pressure drop, initiated by the achievement of a full glow regime. This means the plasma has reached its maximal volume, as established by Yasuda for other geometries (CCP and helical ICP) [70]. In our case, below the critical power, the reduced plasma volume allows an important by-pass of the monomer flow. The plasma being far from the walls, the process results in a limited wall deposition. It is supported by a small mean free path in these conditions (2 mm). Above the critical power, the plasma volume is so large that the monomer flow cannot by-pass it anymore. The plasma volume contacts the walls and the sample holder, which markedly increases the deposition. This is consistent with the well-established correlation between the glow region of a plasma (region emitting light) and the deposition region ([70] on page 222 or [177]). Especially very close to the injection ring, the deposition is such that it is reasonable to expect a deviation of the monomer flow, by a collective diffusion towards the wall (suction). This view is supported by the fact that the styrene dehydrogenation and thus its fragmentation are lowered at these

high power conditions than at moderate ones. It is thought that the plasma intensity is much lower at the side-walls, that the deposition can then occur there in a gentle way and that the species does not reach anymore the center of the reactor where the plasma intensity is much higher.

Maybe more than in other geometries, our planar inductively coupled reactor offers a more abrupt increase of surface able to collect radicals when the plasma reaches its full glow condition. Indeed, the progressive increase of the plasma volume in helical geometries for increasing power is accompanied by a regular increase of the contact region between the plasma and the reactor walls. In our planar geometry, the increase of the plasma volume does not significantly increase the surface between the walls and the plasma, as long as the plasma volume gently spread in the vacuum. But when the power has sufficiently increased for the plasma to contact the side-wall, the deposition is suddenly enhanced and the pressure may drop.

The pressure drop includes a hydrogen partial pressure drop, meaning that the monomers dissociate much less. The deposition then does not require an intense activation/dissociation. However, this is not supported by the aromaticity measured by XPS, which was the least retained above the critical power. As it was at the sample holder position, the author proposed a characterization of the aromaticity retention of benzene and styrene plasma deposition on the side wall and compared it to the one at the sample holder. It would allow one to verify the assumption that soft dissociation is sufficient to ensure a high deposition rate at the reactor walls.

The question to know if the E/H transition initiate the pressure drop or if it is the reverse has been opened. Further investigations should bring original contributions to this emerging field in polymerizing flow system [178, 179].

The roles of hydrogen and non-polymerizing gases

Having studied the plasma polymerization of acetylene, ethylene and other hydrocarbons, Kobayashi *et al.* observed that addition of hydrogen in the discharge reduces the deposition rate [55]. Hydrogen was then assumed to scavenge the polymerizing precursor. However, beside that effect, the evolution of the hydrogen partial pressure in the styrene and ethylene discharges led us to propose three other roles for hydrogen. To our sense, they explain as well the deposition rate reduction when it is present in large amount:

(1) The "electron cooler" role: increasing the total pressure without participating to the polymerization, hydrogen induces a lower electron mean free path and then a decrease of the electron temperature, resulting in a lower activation of the polymerizing species.
(2) The "power dissipator" role: electronically excited by the inelastic electron impact in the discharge, the hydrogen molecules deexcite radiatively and an important part of the produced photons are lost.
(3) The "pumping rate modifier" the produced hydrogen increases the total pressure and therefore the pumping rate, but being a non-condensable gas on cold trap it also lowers the pumping rate at the same time. This latter effect being much stronger, the pumping rate significantly diminishes. As a single pumping rate has been observed for all the species, all the other process effluents have an increase of their partial pressures, enhancing the pressure increase.

This is supported by the ethylene discharge which produces the largest amount of hydrogen and is the less depleted. The low depletion is supposed to indicate as well a low deposition. The possible roles of hydrogen are transposable to other non-polymerizing gases. This is supported by the MMA discharge, which shows large increase of the discharge pressure, but limited monomer depletion, although its aliphatic feature makes it much easier to dissociate than benzene.

Finally, the question has been raised concerning that these hydrogen effects could be at the basis of the monomer classification established by Yasuda.

A chemistry based on small and unsaturated carbon containing intermediates

The sets of species identified in the plasmas of styrene, benzene, ethylene and acetylene were very similar [224]. The dominating species were separated by the same mass interval corresponding to CH_2 and had decreasing partial pressures with increasing mass. The repeated addition of small carbon compounds with low H content is assumed to explain these observations. In the gas-phase the recombination between large radicals is then not favored (at some exceptions like for benzene, with the phenyl radical). These assumptions agree well with the Rapid Step-Growth Polymerization mechanism proposed by Yasuda.

The observed molecules are the ones which survives the plasma and the deposition process: they are stable closed shell species. However, it is expected that their formation occurs through the same intermediates that the ones proceeding to the plasma polymer formation on the reactor walls.

Interestingly, several observations indicate the same dominating species in the discharge of MMA, which is a monomer containing two oxygen atoms. Supported by results in combustion flame of hydrocarbons

Partial pressures quantification and species identification

The present work leads to a partial pressure quantification method which revealed excellent agreement between the estimated pressures and the total discharge pressure. The pressure quantification in unsaturated hydrocarbon plasmas was eased by their high stability in their ionized state. The lower ion stability of MMA and aliphatic compounds indicates a more difficult quantification, but the present work suggested ways to deal with it: acquire mass spectra at several low electron energies, carefully chosen to minimize peak overlapping or to allow sequential pressure quantification. Finally, a thorough analysis of the mass spectra acquired at low electron energy has been combined with the systematic measurement of the appearance energy of observed ions. For unsaturated hydrocarbons, this method proved to be efficient to detect numerous species, which help to determine a part of the plasma chemistry. For the oxygen-containing MMA, it reveals to be heavier but fruitful.

Perspectives

Throughout the bibliographic work and the present research, several questions were raised about plasma polymerization but were left unanswered. They are schematically represented on Figure 11.1.

The question of the deposition which includes the sticking coefficients is to our eyes very important. Without this step, there is no plasma polymer, but it seems rather difficult to investigate. The substrate temperature is apparently a central point to approach this issue as high substrate temperatures exclude any polymer formation [53]. The exposition of the glow region to the surface seems also an important feature, as suggested by the pressure drops of the present study.

Being at the center of the Rapid Step-Growth Polymerization mechanism of Yasuda to explain the very fast kinetic of plasma polymer formation, the diradicals seem largely unaddressed in the literature. Though, their formation may be not unlikely: only 2.0 eV is required to isomerize acetylene into $H_2C{=}C{:}$ [14], $^{\bullet}C_2{}^{\bullet}$ has been observed in our discharge by OES [117] and has been integrated in a model of formation of diamond thin films by plasma [219], and methylene $^{\bullet}CH_2{}^{\bullet}$

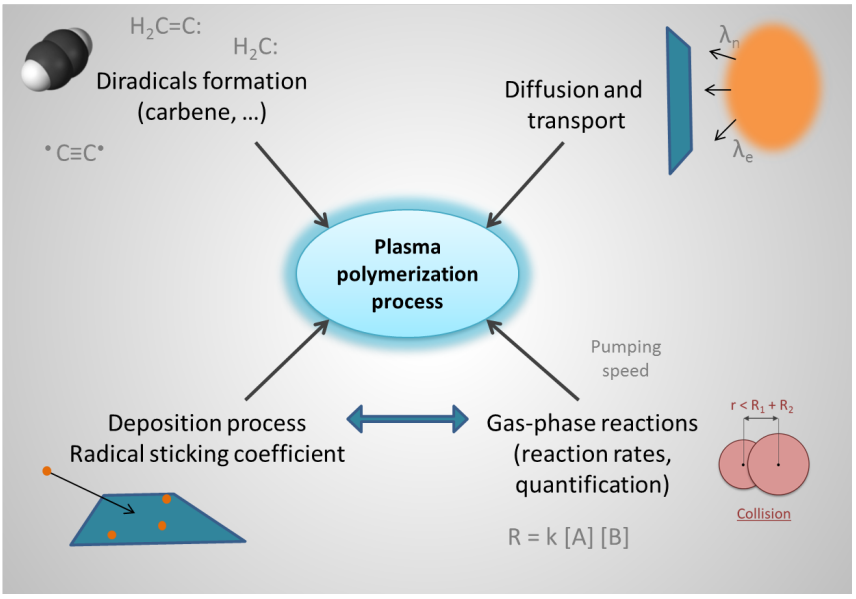

Figure 11.1: Schematic representation of the questions regarding plasma polymerization which would be investigated by the present author, in continuation of the present work.

seems the most probable intermediates of reaction of plasma polymerization in the present work. The study of their sticking coefficient would be very interesting, as from steric considerations they are much more likely to react when colliding with a surface.

Another issue is the combination of the glow volume, the pressure and the proximity of a surface to allow the deposition. To our eyes, it can be seen in the ability of the reactive species to spread out from the glow or the plasma region. It is therefore highly related to the mean free path, but also to the process of diffusion. Yasuda devoted a small part of his book to diffusion and this increases our feeling to investigate this issue [221] (p15). Surprisingly, the author just found right now a paper of 2007, co-signed by Yasuda, addressing the question for methane plasma [225].

Finally, at the end of the present work, the laboratory is now at hand to attempt quantification of the partial flows and not only of the partial pressures. This expertise could allow one to estimate properly if not measure some production of plasma effluents in flow system. The author believes that this would be better investigated at first for monomers like MMA which leads to low deposition. Indeed little concern about deposition would simplify the study. Furthermore, this kind of study should be better carried out in a reactor designed for it. Helical ICP reactor offers almost no by-passing possibilities, simplifying as well the investigation.

Appendices

Contents

Appendix A

E/H transition and discharge pressure in acetylene and ethylene plasma

(The present appendix has not been reviewed by all Jury members)

Complementary measurements of light emission from acetylene and ethylene plasma have been performed. The objective is to discuss the simultaneous occurrence of an E/H transition along with a drop of the discharge pressure, observed for styrene (Section 6.4 and 6.5.1). Acetylene was chosen as it also shows a pressure drop at a critical power, like styrene, and ethylene because it does not (Section 8.4.1 at page 158). The plasma conditions are exactly the same as the ones used in chapter 8 on pressure quantification (see Table 8.4 on page 149).

The total light emission was measured as explained in Section 6.4, on page 100. The result is shown for ethylene and acetylene on Figure A.1a and A.1b respectively. No abrupt increase of the light emission occurs for ethylene, while an increase by a factor of 4 occurs for acetylene from 144 to 150 W of delivered power. An hysteresis behavior has been detected for acetylene: the transition power is not the same if increasing or decreasing the applied power [226].

The discharge pressures have been measured once again and are shown for ethylene and acetylene on Figure A.2a and A.2b respectively. It globally follows the ones reported on Figure 8.8 on page 159. However, for ethylene we observe a slightly decreasing pressure above 175 W. For acetylene, powers up to 230 W have been delivered and reveal a slightly decreasing discharge pressure above the critical power.

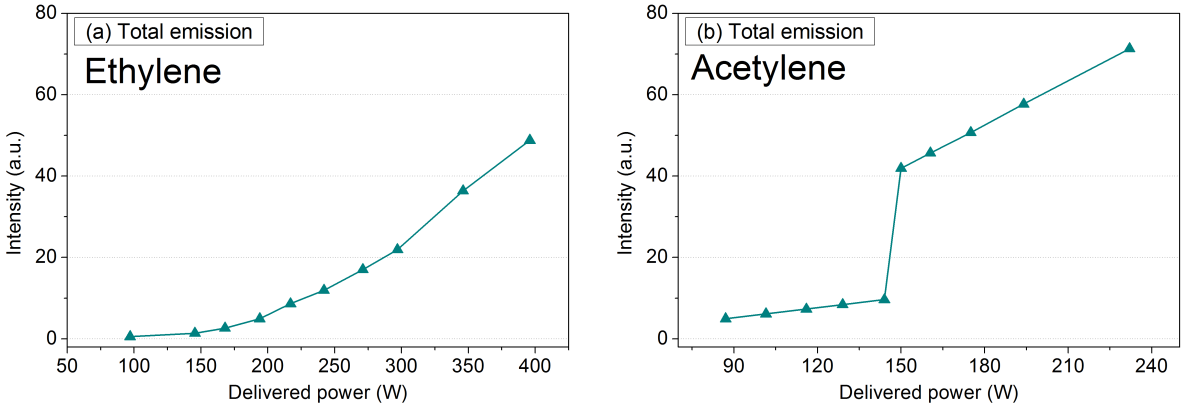

Figure A.1: Total light emission of (a) ethylene plasma and (b) acetylene plasma. Conditions are in Table 8.4.

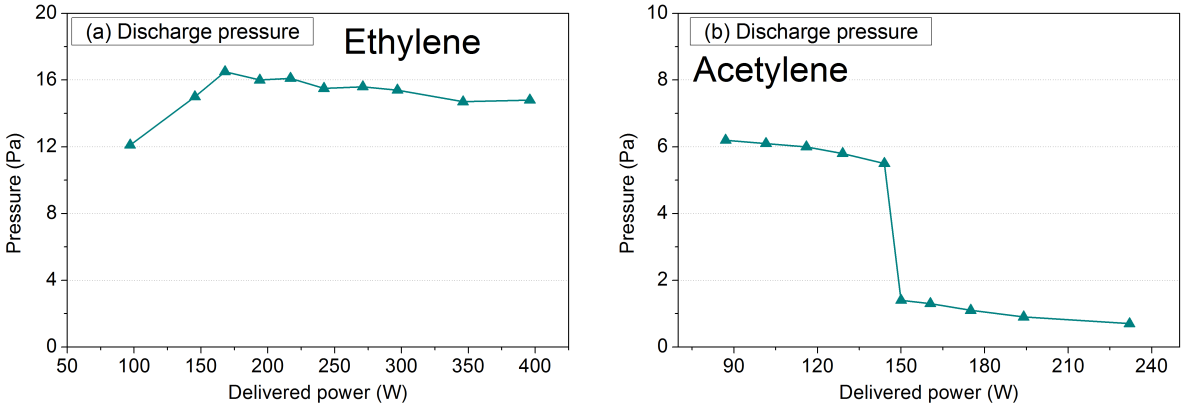

Figure A.2: Discharge pressure of (a) ethylene plasma and (b) acetylene plasma. Conditions in Table 8.4

Discussion

The critical power of pressure drop of acetylene at 150 W thus corresponds to a E/H transition. No E/H transition is observed for ethylene in the range of power investigated. Higher powers could be interesting to apply.

To our view, these observations strengthen our assumption that the discharge pressure affects the occurrence of a E/H transition (Section 6.7.1 & 8.6). The difference of gas composition may also explain the observations as ethylene plasma contains much more hydrogen than the acetylene plasma. Indeed the gas composition has been shown to affect the E/H transition [180].

Appendix B

Pressure quantification at variable initial pressure

(The present appendix has not been reviewed by all Jury members)

The variation of the initial pressure has been investigated while keeping the flow and the power constant for styrene plasma, and thus the specific energy parameter W/F (Section 2.4.1). The objective was to establish the pressure effect on the partial pressures of the monomer and its plasma effluents. Especially, the presented measurements aim at explaining the reason why ethylene is much less depleted at high power than styrene, benzene and acetylene, as observed in Figure 8.10 (page 161). It has been proposed in Section 8.4.5 that an increase of the discharge pressure softens the plasma conditions (page 165). It corresponds to the "electron cooling" effect due to hydrogen production (Section 8.4.4 on page 163).

To settle the monomer flow at a desired value, the pumping valve can be used as described in Section 5.2.2 (page 78). The required valve openings to obtain a constant styrene flow of 28 sccm at different equilibrium pressure in the reactor are indicated in Table B.1. The other conditions were kept constant: 135 W of applied power and continuous wave conditions.

Initial pressure (Pa)	5.4	6.7	8.5	10.5	12.6	15.9
Pumping valve opening (turn)	3+8/16	2+0/16	1+/16	1+4/16	1+2/16	1+0/16

Table B.1: Equilibrium pressures of styrene vapor in the reactor and their corresponding pump valve openings to obtain a flow of 28 sccm.

The measured pressures are indicated in Figure B.1. Once again, the agreement is excellent between the pressure measured by the gauge and the one obtained by MS by adding all the measured partial pressures. A second result is the markedly changing styrene pressure. It shows that varying the initial pressure affects strongly the styrene depletion in the discharge. At higher pressure, the styrene is much less depleted (15%) than at the lowest pressure (60%). The effluent production seems also lower at higher pressure, while the exact production rates have not been measured (see Appendix on pumping rate quantification). The dashed line is simply an indicative linear dependence between the discharge and the initial pressure, with an offset of -2 Pa.

To our view, the observations show that a higher total pressure in the discharge markedly softens the plasma intensity and leads to a lower monomer consumption and fragmentation. This may further support the assumption that the E/H transition is affected by the discharge pressure, made in Section 8.6 and further discussed in Appendix A on light emission in the ethylene plasma. Indeed, ethylene monomer is the only one among the hydrocarbon monomers to combine the following features: a large production of hydrogen with increasing power, accompanied by a large increase of the total discharge pressure; no observation of an E/H transition. Therefore, we think that the increase of discharge pressure of the ethylene plasma is the cause for its absence of E/H transition.

The effect of the discharge pressure on the plasma intensity could be due to a change in the plasma volume and/or a change in the electron density. It should be further investigated by measuring the total optical emission.

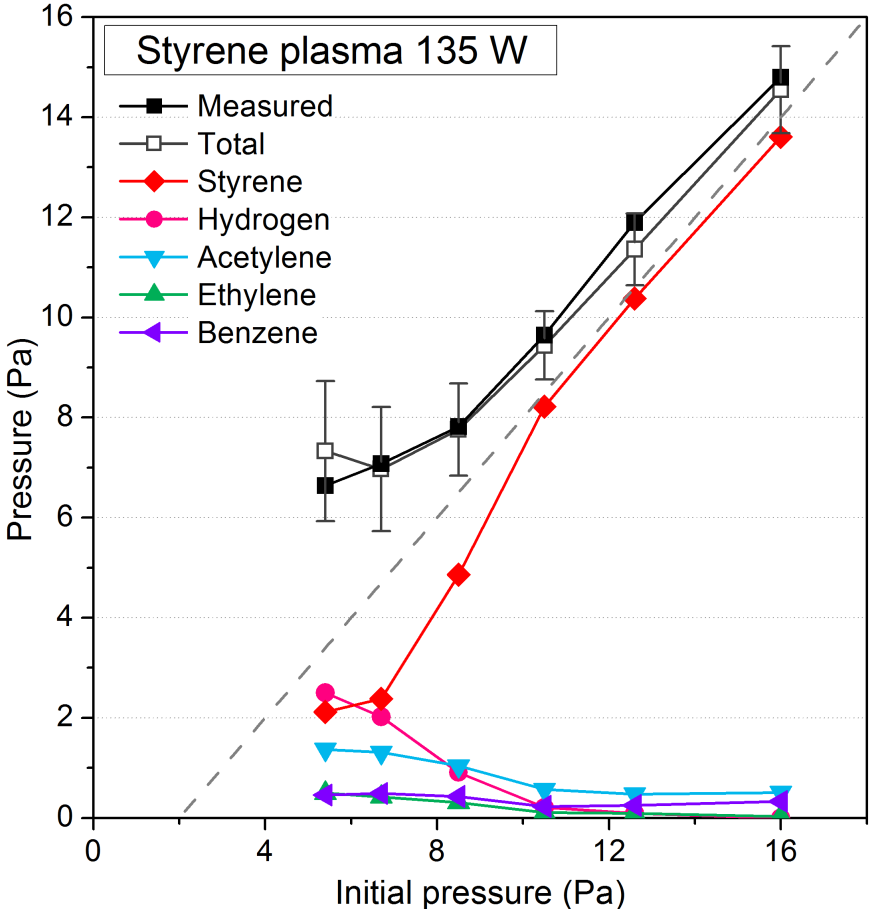

Figure B.1: Discharge, total and partials pressures in styrene plasma at 28 sccm, 135 W and CW conditions.

Appendix C

Production rate of effluents in styrene plasma

(The present appendix has not been reviewed by all Jury members)

In Section 10.4.4, a methodology has been described to quantify the pumping rate of the stable effluents of the plasma polymerization process using a cold trap. At the pressure equilibrium, these rates are equal to the production rates of the effluent in the plasma region. The current Appendix presents the results when applying this methodology to the styrene plasma. The data have been calculated on the basis of the partial pressures presented in Section 8.3.1.

Figure C.1a shows the calculated production rates and the total one, which is the sum of the partial ones. Regarding the styrene monomer, the term "survival rate" should better be used, being not produced in the plasma. The measured partial pressures in the same conditions are reminded on Figure C.1b.

A first observation is that the total production rate is decreasing. The only reason for the total pressure increase from 120 to 180 W is thus the production of hydrogen in the styrene plasma which reduces the total pumping rate, as shown in Section 10.4.5. To better visualize it, we divided the total pumping rate by the total discharge pressure. The ratio values are shown on Figure C.2 and constitute a pumping efficiency indicator: it is the number of sccm evacuated per Pa of pressure in the reactor. A clear decrease of this efficiency is observed with almost a factor of 4 between 30 W and 165 W where the discharge pressure is the highest.

A second observation is that the effluent production rate is much more modest than the one that could be inferred on the basis of the pressure. It is especially visible for hydrogen which reaches 4.7 Pa at the most, which constitutes 70% of the initial monomer pressure, while the

maximal production rate is of 6 sccm which is equal to 21% of the initial monomer injection rate.

Regarding the error bars shown on the total pumping rate curve of Figure C.1a, they have been estimated if the measured partial pressures were accurate for each pumping rate curve and were added to give the total pumping rate error.

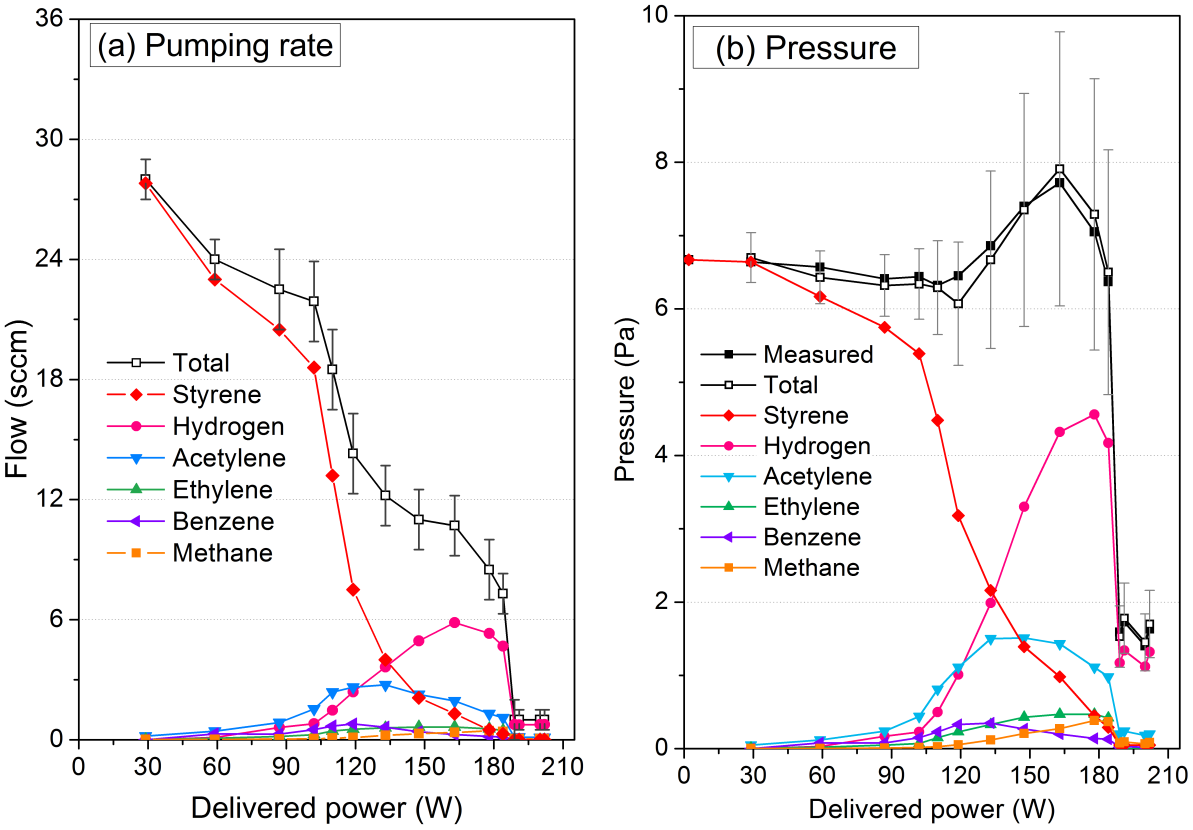

Figure C.1: Styrene plasma at 6.7 Pa of initial pressure, 28 sccm and CW conditions: (a) Partial and total pumping rates and (b) reminder of the discharge, total and partial pressures from Section 8.3.1.

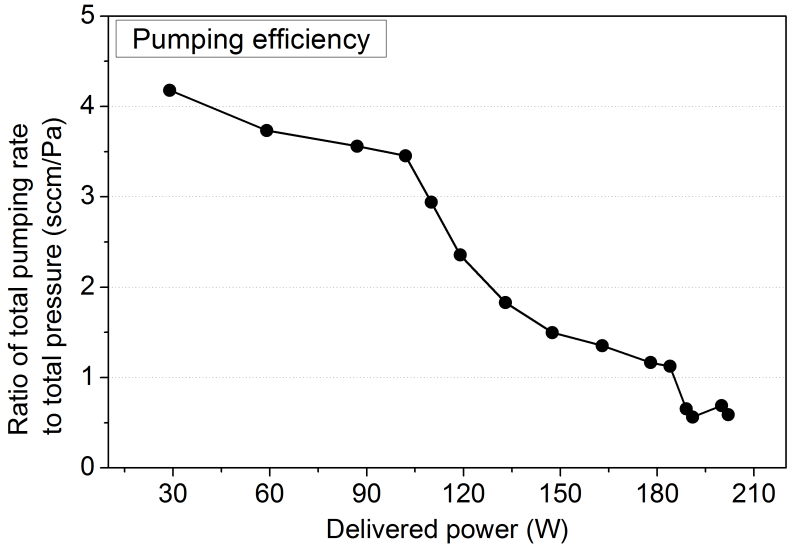

Figure C.2: Ratio of the total pumping rate to the total discharge pressure measuring the pumping efficiency during the styrene plasma.

Appendix D

Additional styrene literature

(The present appendix has not been reviewed by all Jury members)

To ease the reading, the complete table of styrene plasma polymerization articles was left for the current appendix. Moreover, a detailed discussion of SIMS literature on plasma polymerized styrene is added: initially planned to be included in the manuscript, SIMS measurements were finally set aside to focus on the most original results.

D.1 Complete list of articles on styrene plasma polymerization

Table D.1 shows the 45 peer-reviewed articles found on plasma polymerization of styrene. The main conclusions drawn from the table are discussed in Section 4.1.1. Among the "Techniques" columns, the two first are plasma diagnostics (MS and OES), the four next columns are surface characterizations (IR, XPS, SIMS/ToF-SIMS and DR) and the last column contains several other surface characterization techniques. The following columns regard the used gases (gas / comment), the type of reactor, the frequency of the applied field, the frequency of pulsation, and finally the pressure, the power and the flow used.

The different acronyms are the following: ESR = Electron Spin Resonance, TGA = Thermal Gravimetric Analysis, SEM = Scanning Electron Microscopy, kyn = kynetic study (Arrhenius-like plot), NMR = Nuclear Magnetic Resonance, GC = Gas Chromatography, MWDistr. = Molecular Weight Distrihution, UPS = Ultraviolet Photoelectron Spectroscopy, SFM = Scanning Force Microscopy, Grid = Powered grid to measure ion energy, WCA = Water Contact Angle, Resist = Electrical resistance, PyGC = Pyrolysis Gas Chromatography, NEXAFS = Near-Edge X-Ray Absorption Fine Structure, AFM = Atomic Force Microscopy,

ARXPS = Angle-Resolved X-Ray Photoelectron Spectroscopy, EDX = Energy-dispersive X-ray spectroscopy.

Date	Author & ref	Techniques						Content	Type	Freq (Hz)	Puls (Hz)	(Pa)	(W)	(sccm)
1960	Goodman [227]		IR			Solubility		St & 17 mono	DC-AC			0.1	-	-
1966	Jesch [119]		IR					St & 5 mono		20k		133	2.5-5	closed
1966	Williams [21]		IR		DR			St & 11 mono		10k		/	/	-
1968	Denaro [47]		IR		DR	Radical				2M		25-250	10-75	-
1971	Yasuda [52]				DR			St, St+gas	IC			2.7-8	10-150	0.06-0.7
1971	Morita [228]					ESR		St & 2 mono	-	5k		67	-	-
1972	Thompson [120]		IR	SIMS		TGA,SEM,kyn			IC			-	8-36	0.2
1973	Takeda [109]				DR					1M		67	-	-
1976	Takeda [229]					Dielec cst				1M		67	-	-
1979	Sawa [230]					Opt microsc		Breakdown		/		67	-	-
1979	Tsuneto [132]				DR							6-80	-	-
1981	Takeda [231]					SEM,humidity				1M		54	-	-
1984	Prohaska [121]		IR	XPS		ellipsometry			IC		0.1-100k	7-13	50	5-?
1985	Yasuda [53]				DR			Substrate T		10k		-	15	1
1987	Ferreiro [111]	MS						St, water				4.5	1.3	1.6
1991	Ozden [113]	MS	IR					St, St+MMA				200	10-50	closed
1991	Ozden [112]		IR			NMR		St, St+MMA				-	20	closed
1992	Morita [133]		IR		DR	GC,MWDistr.		St+carrier				25-80	20-35	0.4-1
1993	Potter [126]			XPS				UV degrad	IC			<133	10	3
1995	Leggett [127]			XPS	ToFS							24-40	10-50	-
1995	Schelz [232]			UPS		PES,SFM		UV-PS				7-100	20-100	-
1997	Geckeler [110]					Biocompatib.		St+Ar				500	400	-
1996	Miura [233]					CO_2 solubil.				-		100	80	-
1995	Chen [114]	OES	IR	XPS						10M		/	/	/
1996	Chen [115]	MS	IR		DR					10M		5-9	20-50	20
1998	Chen [122]		IR	XPS		Grid				10M		45-120	5-30	12-28
1999	Chen [116]	MS OES			DR					10M		3-9	20-50	20
1998	Beck [62]	MS	IR	XPS				st, PA	IC			1	1-10	1
1997	Kurosawa [234]					Biocompatib.		St & 18 mono				40-80	30-250	-
1999	Kurosawa [235]					WCA		St & 2 mono				50-150	100-200	-
2000	Kurosawa [134]				DR			St & 6 mono				100	100	-
2003	Kurosawa [123]		IR		DR	Resist						100	100	-
2004	Zhang [124]		IR		DR			St, MA	IC			8	30	-
2004	Kim [104]		IR			PyGC		St+CH_4/Ar				27	35	1-10
2001	Retzko [59]		IR	XPS		NEXAFS		St & 3 mono			1k	8	30-150	20?
2004	Oran [131]			ToFS				air exposure			1k	5-15	10-60	-
2004	Swaraj [128]			XPS		NEXAFS		ex-situ			1k	5-15	5-60	-
2007	Luo [125]		IR	XPS		Microsc		St+CO_2				-	85	-
2006	Haidopoul. [135]		IR	XPS	ToF	SEM,AFM			CC-IC			10	10-30	-
2007	Haidopoul. [129]			XPS	DR	SEM			IC		10	13-66	120-200	-
2008	Haidopoul. [130]			XPS		ARXPS		O_2 treatment	IC			10?	30	-
2010	Choudhury [106]		IR			SEM,EDX		St+Ar				7-16	40-150	-
2011	Li [117]	OES	IR	XPS	ToFS			St, St+MMA	IC		10	7	120	-
2013	Li [118]	OES		XPS	ToFS			St, St+3mono	IC		10	7	120	-
2012	Fahmy [236]				DR							10	50	36

Table D.1: List of peer-reviewed articles on characterization of low-pressure styrene plasma and/or styrene plasma deposited films at low pressure. A hyphen "-" is indicated when the author did not mention the conditions and a slash "/ " means that the experimental setup does not allow to establish the corresponding quantity. A blank cell means: a reactor of type CC, a frequency of 13.56 MHz and continuous-wave plasma for the "puls" column.

D.2 SIMS literature on plasma PS

Table D.2 summarizes the main conclusions of the ten SIMS articles which will be discussed in detail in the present section. Four reports were selected because they studied conventional PS, deuterium- and methyl substituted conventional PS and conventional PS modified by plasma. The six remaining papers are the only ones found on Static SIMS studies made on styrene plasma deposited films.

Date	Author & ref	Type of PS	Indicators & information	Other techniques / comment
1992	Legget [237]	Conventional	Tandem MS → ion structures Ion formation processes are complex	
1991	Chilkoti [238]	Methyl substituated & deuterated PS	H-scrambling Ion formation processes are complex	XPS
1994	Petrat [138, 239]	Conv. modified by plasmas O_2-N_2-Ar	Integrity: $91^+/55^+$ Atmospheric O uptake: $C_2H_3O^+/C_3H_5^+$ Plasma O uptake: $COH^+/C_3H_3^+$	XPS
1970 - 1972	Thompson [120]	Plasma Conventional	Plasma: C_3 - C_5 - C_7 peaks (+) Conventional: C_2 - C_4 peaks (+) → possible crosslinking on the α carbon	XRD, IR, TGA, TDA
1995	Legget [127]	Plasma Conventional	Aromaticity: 91^+, 77^+ Integrity: 115^+, 105^+, 103^+ Crosslink: small ions total I(+), $105^+/103^+$ Unsaturation: six M/M+2 ratios (+)	Methyl substitution discussion
2004	Oran [131]	Plasma Conventional	Aromaticity: 91^+, 77^+, $105^+/103^+$ Integrity: 115^+, 117^+, 105^+, 103^+ Unsaturation: five M/M+2 ratios (+) Branching/crosslink: total yield (+) Crosslinking: $91^+/105^+$ Oxygen uptake: peaks, $(O^-+OH^-)/CH^-$	XPS
2006	Haidopou. [135]	Plasma Conventional	Characteristic peaks Aromaticity 91^+ Branching $\Sigma C_4H_x^+$ Molecular weight: total (+) ion yield Oxygen uptake: $(O^-+OH^-)/CH^-$	IR, XPS
2011 - 2013	Li [117, 118]	Plasma Plasma copolymer	Characteristic peaks presence Plasma PS in copol: 77^+, 91^+, 105^+	IR, XPS, OES

Table D.2: Bibliographic summary for SIMS characterization of conventional PS, plasma modified conventional PS and plasma deposited styrene films.

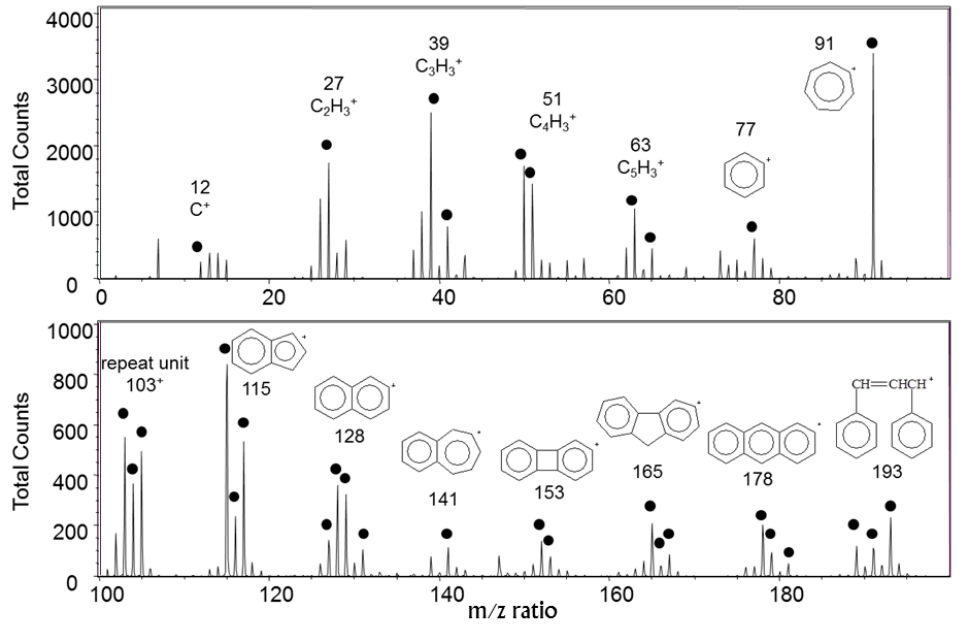

Figure D.1: Characteristic SIMS spectrum of conventional PS in the positive polarity [240].

D.2.1 Conventional PS

Figure D.1 shows the positive characteristic spectrum of PS with molecular weight of 10 kg/mol, obtained from the SIMS spectra library of the IONTOF software [240]. A series of characteristic peaks is generally identified, marked with a bold point in the spectrum, in accordance with reference [241]. The shown ion structures follows the conclusions of Legget *et al.* [237]. The objective of the section is to summarize each paper for future work in the laboratory.

The Static-SIMS (SSIMS) literature on conventional PS reveals two interesting studies. The first investigates and determines the structure of several large characteristic ions of PS by tandem MS [237]. Their main conclusion is that the ion formation is complex because of significant rearrangement. The combined measure of the neutral lost fragments and of the daughter ions of every ion observed in the spectrum lead to establish schemes of their decomposition. It also showed their usually high stability, often benefiting from aromatic stabilization. This observation also suggests that their fragmentation generally occurs before their surface emission. In the second work, deuterated and methyl substituated PS were characterized by SSIMS [238]. For the deuterated PS, a significant H scrambling is observed in the formation of the characteristic ions of PS. From the methyl substituated PS, the $105^+/103^+$ ratio increases above the value of 1 on the contrary of the usual PS, and is accompanied by a decrease of the 91^+ peak, an increase at 128^+–131^+ and a new positive characteristic peaks at m/z = 119^+.

D.2.2 Plasma PS

The five reports on plasma PS will now be discussed. The three first works includes a comparison to conventional PS produced in their own lab.

Thompson *et al.* used a Nuclide HT90 spectrometer of unknown specifications which gives rather intense peaks in the low-mass region [120].

- Their conventional PS has a 20,000 molecular weight. The plasma PS was deposited with hard conditions during a very long period of 12h. Their monomer flow of 0.061 g/h corresponds to a very low flow of 0.2 sccm with the styrene molecular mass of 104 g/mol. With an intermediate power of 22 W, this correspond to a very high W/FM of 1.4 $.10^9$ J/kg = 1531 eV/styrene.
- Only below 110 amu of the positive polarity are reported and normalized to the most abundant one, which was the tropilium peak at m/z = 91 for both conventional and plasma PS.
- The main observation is that C_2H_x and C_4H_x fragments are more intense for conventional PS and the C_3H_x, C_5H_x and C_7H_x for plasma PS. The main proposed explanation for this is a possible extensive crosslinking of the plasma PS.

Legget *et al.* used a quadrupolar SIMS instrument which gives a much higher intensity in the low mass region [127, 237].

- The conventional PS is of unknown molecular weight, spin cast with 1% weight/volume solution in toluene. For the plasma PS, there is no clear mention on the styrene flow value. The reactor is described in another work [242], where the pressure is said to be measured by a capacitance gauge and the pressure maintained constant with an automatic butterfly valve. If not controlled, the flow can thus be expected to have varied, as shown in the present work when the pumping valve opening is changed (Section 5.2.3). The power used is sometimes missing for some presented results, but was kept between 10 and 50 W. A large air leak with significant incorporation of nitrogen in the plasma deposited films is reported. All plasma films were aged 24h in atmosphere, except stated otherwise.
- All SIMS spectra were acquired in the positive polarity with no normalization.
  - A conservation of the aromatic signals in the plasma PS is detected, as indicated by strong peaks at m/z = 91 and 77. The peaks at 51, 63 and 65 observed for many aromatic compounds are left aside in the analysis as they are daughter ions and because they can be concealed with smaller non aromatic ions.

  - Characteristic peaks of conventional PS were also observed at m/z = 115, 105 and 103 for plasma PS. They indicate a rather good integrity of the pPS in regard to the conventional PS.
  - For plasma PS, higher intensities were observed in the low-mass region. It can be due either to air contamination or to crosslinking.
  - The 105/103 ratio was below 1 for conventional PS and above 1 for plasma.
  - Six ratios are chosen being indicative for unsaturation of the plasma deposited films: 102/103, 126/128, 139/141, 150/152, 163/165 and 176/178. Unsaturation is much higher for the plasma deposited films, but it decreases with the exposure time to atmosphere. This latter observation is favoring the scenario of crosslinking, by the suggested reaction of trapped radicals with double C=C bonds.

- A large discussion is dedicated to the **105/103 ratio**.
  - The ratio is below 1 for their conventional PS (around 0.6) and in the cited literature. [In the IONTOF Spectra library [240], this ratio ranges from 0.53 to 1.06 for PS with molecular weight from 1k to 100k]. For the plasma PS, the ratio was around 0.8 when the so called "fresh " sample was directly transferred from reactor to SIMS spectrometer with a quick exposure to air. With 24h of air exposure, this ratio increased to 3.5 as we could estimate from their shown spectra. In between, they notice little change from fresh to 6h samples, then a markedly change from 6h to 12h.
  - To explain the inversion of the 105/103 ratio, the methyl substituted polystyrenes are considered, which show 105/103 above 1 in the literature. The authors checked it by characterizing their own spectra of poly(2-methylstyrene) and poly(α-methylstyrene). These two polymers have characteristic peaks at m/z = 119, 129 and 143. As the plasma PS has too low intensity for these three peaks, the methyl substitution trail is finally excluded.
  - Their conclusion for the 105/103 ratio inversion is crosslinking, according to several observations. Firstly, the oxygen uptake as measured by XPS occurred very rapidly, as soon as after 1h exposure to air. Secondly, Jesch *et al.* observed a crosslinking after 12h for its plasma deposited film of benzene by IR measurement [119]. As the ratio inversion occurred at least after 6h, they concluded that the inversion cannot be due to an effect of the oxygen uptake. They strengthen this affirmation by the observation of crosslinking by Prohaska for which plasma PS shows IR spectrum similar to crosslinked PS [121].

  - Our position with regards to their conclusions is the following. As soon as 1968, Denaro reported an increase in insolubility and of weight of its plasma PS with exposure to air [47]. Thanks to their IR measurement, they observed an oxygen uptake with appearance of OH and C=O bands. They proposed a mechanism in two steps for this oxidation. Firstly a reaction of atmospheric oxygen with the trapped radicals of their plasma deposited film, with the formation of peroxy radicals, also reported by Retzko *et al.* [59]. In a second step, they suggest these radicals have sufficient mobility to lead to crosslinking reactions. Therefore, we think that, for a sufficiently slow kinetic, this second step can explain that the observed crosslinking is retarded compared to the oxygen uptake.

The third and extensive SIMS work on plasma PS has been carried out by Oran *et al.* [131], during a thesis work [142]. It investigated the aging to atmospheric air by comparing in-situ to ex-situ films. They used a TOF-SIMS IV spectrometer.

- The conventional PS was spin-coated with a polystyrene oligomer powder of 3400 g/mol diluted by 3% weight concentration in toluene. The plasma styrene was deposited with unknown monomer flow rate. The W/FM parameter is then not estimable. However, the effective power was varied from 1 to 60 W thanks to the combined power and duty cycle variation.
- The difference degree of the plasma PS from the conventional PS is discussed on the basis of several indicators, some inspired from Legget:
  - **Aromaticity** through presence or absence of the aromatic peaks at m/z = 77 and 91. From Petrat *et al.* [138], they used the ratio $91^+/55^+$ as a measure of aromaticity. The 91^+ ion ($C_7H_7^+$) is characteristic of aromatic polymers and the 55^+ ion (C_4H_7+) is characteristic for many aliphatic polymers.
  - **Integrity** of the styrene unit via presence or absence of characteristic peaks of PS at m/z = 115^+, 117^+, 103^+ and 105^+, and others at higher masses as well.
  - **Unsaturation** via the $126^+/128^+$, $139^+/141^+$, $150^+/152^+$, $163^+/165^+$ and $176^+/178^+$ ratios, but not the $102^+/103^+$.
  - The **branching and/or crosslinking** of the films is evaluated via the total ion yield. Another crosslinking indicator was the $91^+/105^+$ ratio. It was chosen because the peak 91^+ is the most intense one of conventional PS and 105^+ the one of plasma PS (see below). Moreover, according to them, Legget *et al.* delivered sufficient proof to the link between crosslinking and the 105^+ ion.

  - The **oxygen uptake** with atmosphere exposition was firstly checked through observation of oxygen containing peaks either in the positive and the negative polarity. Then the ratio $(O^- + OH^-)/CH^-$ is used to evaluate the degree of oxygen uptake. This indicator was effectively correlated to the O/C ratio from XPS by Briggs *et al.* with R^2=0.85 for the above mentioned polyethylene oxidized by many different techniques [241]. Chilkoti *et al.* observed the same correlation [243]. Otherwise no consistent correlation between oxygen containing peaks and oxygen functional groups exists, as stated by Briggs *et al.* [241].

- The plasma PS deposited in the mildest conditions (10 W, 10% duty cycle) was structurally very close to the conventional PS. The aromatic peaks and the styrene characteristic peaks were presents. The unsaturation ratios were very similar and the aromatic ratio $91^+/55^+$ was almost the same. The same sample aged 1 night under vacuum did not significantly change. The major difference was observed with the m/z = 105^+ peak which shows the highest intensity.
- The plasma deposited PS obtained from the most energetic conditions (60 W, continuous-wave, so 60 times more energetic than the mildest) was very different. The $91^+/55^+$ ratio decreases of around 60% and the total ion yield of 63% comparing to the mildest one. On the other hand, the unsaturation ratios did not significantly change except the $150^+/152^+$ ratio.
- From the plasma power and the duty cycle variation, a decrease of the aromaticity and an increase of branching/crosslinking is observed with an increasing effective power.
- In-situ samples revealed already small amount of oxygen by XPS and SIMS. The anti-polymerizing additive in liquid styrene is suggested as a cause.
- The oxygen uptake were found to:
  - increase with exposure time to atmosphere
  - increase with effective power, so with duty cycle and power, for the same exposure time
  - be faster within the first hour of exposure to air and then slows down progressively.

Haidopoulos *et al.* compared plasma polymerized styrene films deposited either in a capacitive reactor or in an inductive reactor [135]. Using a TOF-SIMS IV, the 25 keV Ga^+ primary ion dose was kept below 10^{13} ions/cm^2, which is quite high. In both geometries, the pPS films were optimized to be as close as possible to conventional spin coated PS (300 kg/mol, 0.57% w in toluene). W/FM parameter cannot be compared because of missing styrene flow. When

comparing both pPS films to the conventional one, all characteristic PS peak were detected. The 105^+ signal is by far the strongest. No variation of the normalized 91^+ was observed indicating no aromaticity change relatively to conventional PS. The decrease of the $\Sigma C_4H_x^+$ signal suggested an increase in the branching of the pPS. The increase of the total ion yield supported the hypothesize of the presence of light oligomers at the extreme surface of the pPS. The increase of the $(O^-+OH^-)/CH^-$ ratio with aging linked to the oxygen uptake was four times higher for the inductive pPS after one week than for the capacitive one.

Li *et al.* reported briefly on positive SSIMS of PS and PMMA plasma homopolymers and plasma copolymers in our laboratory [117]. The ToF-SIMS IV spectrometer is used but analysis conditions are not reported. The flow is unspecified and the W/FM not estimable. The m/z = 105 peak dominates largely the spectrum, which is consistent with Oran, Legget and Haidopoulos. Many PS characteristic peaks are detected.

D.2.3 Conventional PS modified by plasma

A last interesting work is the SIMS part of the already mentioned work of Petrat *et al.* on conventional PS modified by plasma of nitrogen, argon and oxygen [138]. They used a TOF-SIMS apparatus, with 10 keV Ar^+ primary ion and a constant ion dose of $2\ .10^{11}$ ions/cm^2, well below the static limit.

- Aromaticity was evaluated by the $91^+/55^+$ ratio. It was shown this indicator decreased much more than the XPS aromaticity indicator and quickly stabilized with the time of plasma treatment. The difference is supposed to be due on the difference of sampling depth of around 10 nm for XPS and 1 nm for SIMS.
- Two different SIMS indicators were found to describe two different kind of oxygen incorporation in the plasma treated films. The first indicator is the $C_2H_3O^+/C_3H_5^+$ ratio and is linked to the oxygen amount which incorporates in the film with exposure to air. Indeed, it was observed to be equal to zero for oxygen treated PS with no exposure to air, whilst XPS showed around 7% of incorporated oxygen in the film. With increasing exposure time to atmosphere, this ratio increased, which is consistent with the moderate increase of the oxygen content observed by XPS. The second indicator is the $COH^+/C_3H_5^+$ ratio and is expected to be characteristic of the oxygen which incorporates in the film during the plasma treatment. This latter was indeed observed to be non-zero for in-situ PS treated by oxygen and to markedly decrease with exposure time to air. The same trends were observed for these two indicators with argon treated PS.

Appendix E

Publications derived from the thesis

Published articles

(1) X. Gillon & L. Houssiau: *Plasma polymerization chemistry of unsaturated hydrocarbons: neutral species identification by mass spectrometry* – Plasma Sources Science and Technology **23** (2014) 045010-14p – DOI: 10.1088/0963-0252/23/4/045010 [224]

(2) Z. Li, X. Gillon, M. Diallo, J.-J. Pireaux & L. Houssiau: *Synthesis of copolymer films by RF plasma: Correlation between plasma chemistry and film characteristics* – IEEE Transactions on Plasma Science **41** (2013) 518-527 – DOI: 10.1109/TPS.2012.2234763 [118]

(3) Z. Li, X. Gillon, M. Diallo, L. Houssiau & J.-J. Pireaux: *Styrene and methyl methacrylate copolymer synthesized by RF inductively coupled plasma* – Journal of Physics: Conference Series **275** (2011) 012020-8p – DOI: 10.1088/1742-6596/275/1/012020 [117]

Two papers are under redaction: one on partial pressure quantification in plasmas of unsaturated hydrocarbons and one on the method of partial flow quantification for system using cold trap.

Published articles not directly related to the thesis work

(4) J. Brison, N. Mine, N. Wehbe, X. Gillon, T. Tabarrant, R. Sporken & L. Houssiau: *Molecular depth profiling of model biological films using low energy monoatomic ions* – International Journal of Mass Spectrometry **321–322** (2012) 1-7 – DOI: 10.1016/j.ijms.2012.04.001

(5) A. Felten, X. Gillon, M. Gulas, J.-J. Pireaux, X. Ke, G. Van Tendeloo, C. Bittencourt, E. Najafi & A. P. Hitchcock: *Measuring Point Defect Density in Individual Carbon Nanotubes Using Polarization-Dependent X-ray Microscopy* – ACS Nano **4** (2010) 4431-4436 – DOI: 10.1021/nn1002248

Proceedings

(A) Z. Li, X. Gillon, L. Houssiau & J.-J. Pireaux: *Plasma polymerization: chemical analysis of the plasma gas phase* – 20^{th} International Symposium on Plasma Chemistry (ISPC 20), Philadelphia (USA) **2011**

(B) Z. Li, X. Gillon, M. Diallo, L. Houssiau & J.-J. Pireaux: *Plasma diagnostic and analysis for the styrene polymerization by low pressure inductively-coupled plasma* – 19^{th} International Symposium on Plasma Chemistry (ISPC 19), Bochum (Germany) **2009**

Posters

(a) X. Gillon & L. Houssiau: *Identification and Quantification of Neutral Species in Styrene Plasma by Mass Spectrometry* – XXII Europhysics Conference on Atomic and Molecular Physics of Ionized Gases (ESCAMPIG XXII), Greifswald (Germany) **2014**

(b) X. Gillon, Z. Li, J.-J. Pireaux & L. Houssiau: *Gas Quantification in Organic Plasma by Mass Spectrometry* – 20^{th} International Symposium on Plasma Chemistry (ISPC 20), Philadelphia (USA) **2011**

(c) X. Gillon, Z. Li, I. Ducarme, N. Mine, J.-J. Pireaux, L. Houssiau: *Plasma polymerization: correlation between internal plasma parameters and film characteristics* – 19^{th} International Symposium on Plasma Chemistry (ISPC 19), Bochum (Germany) **2009**

(d) X. Gillon, Z. Li, I. Ducarme, N. Mine, J.-J. Pireaux & L. Houssiau: *Plasma polymer thin films by low-pressure RF inductively coupled discharge* – European Conference on Nano-Films, Liège (Belgium) **2009**

(e) X. Gillon, N. Mine, J.-J. Pireaux & L. Houssiau: *Plasma polymerization mechanisms study: From the gas phase to the surface* – Wintershool on Organics Electronics: The Role of Interfaces, Donnersbac (Austria) **2008**

Bibliography

[1] A R Denaro, P A Owens and A Crawshaw: *Glow discharge polymerization–styrene* - European Polymer Journal **4** (1968) 93–106.

[2] H Yasuda and C E Lamaze: *Polymerization of styrene in an electrodeless glow discharge* - Journal of Applied Polymer Science **15** (1971) 2277–2292.

[3] A R Westwood: *Glow discharge polymerization - I. Rates and mechanisms of polymer formation* - European Polymer Journal **7** (April 1971) 363–375. (DOI: 10.1016/0014-3057(71)90007-3)

[4] David K Lam, Raymond F Baddour and Arnold F Stancell: *A Mechanisms and Kinetics Study of Polymeric Thin-Film Deposition in Glow Discharge* - Journal of Macromolecular Science: Part A - Chemistry **10** (March 1976) 421–450. (DOI: 10.1080/00222337608061191)

[5] Bilge Özden (Orhan), Jale HacaloÇ§lu and Güneri Akovali: *A mass spectrometric study on plasma reactions of styrene and methyl methacrylate* - European Polymer Journal **27** (1991) 1405–1410. (DOI: 10.1016/0014-3057(91)90243-H)

[6] A J Beck, F R Jones and R D Short: *Mass spectrometric study of the radiofrequency-induced plasma polymerisation of styrene and propenoic acid* - J. Chem. Soc. Faraday Trans. **94** (1998) 559–565.

[7] Zhiling Li, Xavier Gillon, Marwane Diallo, Laurent Houssiau and Jean-Jacques Pireaux: *Styrene and methyl methacrylate copolymer synthesized by RF inductively coupled plasma* - Journal of Physics: Conference Series **275** (2011) 12020. (DOI: 10.1088/1742-6596/275/1/012020)

[8] L M Ferreiro, D W Ernie and J F Evans: *Mass spectrometric and ion energy diagnostics in the study of plasma etching and polymerization* - Journal of Vacuum Science & Technology A **5** (1987) 2280. (DOI: 10.1116/1.574435)

[9] M Chen and T C Yang: *Diagnostic analysis of styrene plasma polymerization* - Journal of Polymer Science Part a-Polymer Chemistry **37** (1999) 325–330.

[10] Zhiling Li, X Gillon, E M Diallo, J.-J. Pireaux and L Houssiau. *Synthesis of Copolymer Films by RF Plasma: Correlation Between Plasma Chemistry and Film Characteristics*, (2013).

[11] X Gillon and L Houssiau: *Plasma polymerization chemistry of unsaturated hydrocarbons: neutral species identification by mass spectrometry* - Plasma Sources Science & Technology **23** (2014) 045010. (DOI: 10.1088/0963-0252/23/4/045010)

[12] Damien Thiry, Nikolay Britun, Stephanos Konstantinidis, Jean-Pierre Dauchot, Laurent Denis and Rony Snyders: *Altering the sulfur content in the propanethiol plasma polymers using the capacitive-to-inductive mode transition in inductively coupled plasma discharge* - Applied Physics Letters **100** (2012) 071604. (DOI: 10.1063/1.3686902)

[13] H K Yasuda. *Operational Parameters of Plasma Polymerization.* In *Plasma Polymerization*, chapter 9, pages 277–332. Academic Press, Orlando, third edition, (1985).

[14] Irving Langmuir: *Oscillations in Ionized Gases* - Proceedings of the National Academy of Sciences **14** (August 1928) 627–637.

[15] Alexandre Fridman, *Plasma chemistry.* Cambridge University Press, New York, (2008).

[16] H K Yasuda, *Plasma Polymerization.* Academic Press, London, third edition, (1985).

[17] R Sorrentino and G Bianchi, *Microwave and RF Engineering.* John Wiley & Sons, (2010).

[18] F S Denes and S Manolache: *Macromolecular plasma-chemistry: an emerging field of polymer science* - Progress in Polymer Science **29** (2004) 815–885.

[19] Michael A. Lieberman and Alan J. Lichtenberg, *Principles of Plasma Discharges and Materials Processing.* John Wiley & Sons, Inc., 2nd edition, (2005).

[20] Michael A. Lieberman and Alan J. Lichtenberg. *Inductive Discharges.* In *Principles of Plasma Discharges and Materials Processing*, chapter 12, pages 461–534. John Wiley & Sons, Inc., 2nd edition, (2005).

[21] U Kortshagen, N D Gibson and J E Lawler: *On the E - H mode transition in RF inductive discharges* - Journal of Physics D: Applied Physics **29** (1996) 1224.

[22] Achim von Keudell and Jan Benedikt: *A Physicist's Perspective on "Views on Macroscopic Kinetics of Plasma Polymerisation"* - Plasma Processes and Polymers **7** (May 2010) 376–379. (DOI: 10.1002/ppap.201000011)

[23] R O Dendy, *Plasma Dynamics.* Oxford University Press, (1990).

[24] D Hastings and H Garrett, *Spacecraft-Environment Interactions*, Cambridge Atmospheric and Space Science Series. Cambridge University Press, (2004).

[25] B P Pandey and S V Vladimirov: *A simple formula for the wall potential in the plasma sheath* - EPL (Europhysics Letters) **94** (2011) 55002.

[26] Fred Warren McLafferty, *Interpretation of mass spectra.* University Science Books, Mill Valley, 3rd edition, (1980).

[27] Kent M Ervin, Scott Gronert, S E Barlow, Mary K Gilles, Alex G Harrison, Veronica M Bierbaum, Charles H DePuy, W C Lineberger and G Barney Ellison: *Bond strengths of ethylene and acetylene* - Journal of the American Chemical Society **112** (July 1990) 5750–5759. (DOI: 10.1021/ja00171a013)

[28] Www.lxcat.net. *Hayashi database*, (2014).

[29] Http://www.bolsig.laplace.univ-tlse.fr/. *BOLsig+ website*, (2014).

[30] Karl T Compton and Irving Langmuir: *Electrical Discharges in Gases. Part I. Survey of Fundamental Processes* - Reviews of Modern Physics **2** (April 1930) 123–242.

[31] Irving Langmuir and Karl T Compton: *Electrical Discharges in Gases Part II. Fundamental Phenomena in Electrical Discharges* - Reviews of Modern Physics **3** (April 1931) 191–257. (DOI: 10.1103/RevModPhys.3.191)

[32] E G Linder and A P Davis: *Reactions of Hydrocarbons in the Glow Discharge* - The Journal of Physical Chemistry **35** (January 1930) 3649–3672. (DOI: 10.1021/j150330a017)

[33] H Biederman and Y Osada, *Plasma Polymerization Processes*, ISBN 3. Elsevier, (1992).

[34] T Williams and M W Hayes: *Polymerization in a Glow Discharge* - Nature **209** (February 1966) 769–773.

[35] Arthur Bradley and John P Hammes: *Electrical Properties of Thin Organic Films* - Journal of The Electrochemical Society **110** (January 1963) 15–22. (DOI: 10.1149/1.2425663)

[36] H Yasuda: *Glow discharge polymerization* - Journal of Polymer Science: Macromolecular Reviews **16** (January 1981) 199–293. (DOI: 10.1002/pol.1981.230160104)

[37] Alexis T. Bell. *The Mechanism and kinetics of plasma polymerization.* In Stanislav Veprek and Mundiyath Venugopalan, editors, *Plasma Chemistry III SE - 2*, ISBN 94 of *Topics in Current Chemistry*, pages 43–68. Springer Berlin Heidelberg, (1980).

[38] N Inagaki, *Plasma Surface Modification and Plasma Polymerization.* Technomic Publishing Company, (1996).

[39] H Biederman, *Plasma Polymer Films.* Imperial College Press, London, (2004).

[40] Jason David Whittle, David A Steele and Robert D Short: *Reconciling the Physical and Chemical Environments of Plasma: A Commentary on "Mechanisms of Plasma Polymerisation - Reviewed from a Chemical Point of View"* - Plasma Processes and Polymers **9** (September 2012) 840–843. (DOI: 10.1002/ppap.201100193)

[41] J Benedikt: *Plasma-chemical reactions: low pressure acetylene plasmas* - Journal of Physics D: Applied Physics **43** (February 2010) 43001. (DOI: 10.1088/0022-3727/43/4/043001)

[42] D Hegemann, U Schütz and A Fischer: *Macroscopic plasma-chemical approach to plasma polymerization of HMDSO and CH4* - Surface and Coatings Technology **200** (October 2005) 458–462. (DOI: 10.1016/j.surfcoat.2005.02.194)

[43] Jörg Friedrich: *Mechanisms of Plasma Polymerization - Reviewed from a Chemical Point of View* - Plasma Processes and Polymers **8** (September 2011) 783–802. (DOI: 10.1002/ppap.201100038)

[44] M Bauer, T Schwarz-Selinger, W Jacob and A von Keudell: *Growth precursors for a-C:H film deposition in pulsed inductively coupled methane plasmas* - Journal of Applied Physics **98** (2005) 073302. (DOI: 10.1063/1.2061890)

[45] Robert D Short and David A Steele: *Testing the Hypothesis: Comments on Plasma Polymerisation of Acrylic Acid Revisited* - Plasma Processes and Polymers **7** (May 2010) 366–370. (DOI: 10.1002/ppap.200900101)

[46] Dirk Hegemann, David A Steele and Robert D Short: *Joint Commentary to the Debate* - Plasma Processes and Polymers **7** (May 2010) 365. (DOI: 10.1002/ppap.201000039)

[47] Karen K Gleason: *A Chemical Engineering Perspective on "Views on Macroscopic Kinetics of Plasma Polymerisation"* - Plasma Processes and Polymers **7** (May 2010) 380–381. (DOI: 10.1002/ppap.201000012)

[48] Mauritius C M (Richard) van de Sanden: *Views on Macroscopic Kinetics of Plasma Polymerization: Acrylic Acid Revisited* - Plasma Processes and Polymers **7** (November 2010) 887–888. (DOI: 10.1002/ppap.201000034)

[49] Hynek Biederman and OndÅ™ej Kylián: *Some Remarks to Macroscopic Kinetics of Plasma Polymerization* - Plasma Processes and Polymers **8** (June 2011) 475–477. (DOI: 10.1002/ppap.201000188)

[50] Jan Trieschmann and Dirk Hegemann: *Plasma polymerization at different positions in an asymmetric ethylene discharge* - Journal of Physics D: Applied Physics **44** (2011) 475201.

[51] A von Keudell, I Kim, A Consoli, M Schulze, A Yanguas-Gil and J Benedikt: *The search for growth precursors in reactive plasmas: from nanoparticles to microplasmas* - Plasma Sources Science and Technology **16** (2007) S94.

[52] Kathleen De Bleecker, Annemie Bogaerts and Wim Goedheer: *Detailed modeling of hydrocarbon nanoparticle nucleation in acetylene discharges* - Physical Review E **73** (February 2006) 26405.

[53] M Mao, J Benedikt, A Consoli and A Bogaerts: *New pathways for nanoparticle formation in acetylene dusty plasmas: a modelling investigation and comparison with experiments* - J. Phys. D: Appl. Phys. **41** (2008) 225201.

[54] E Neyts, A Bogaerts, R Gijbels, J Benedikta and M C M van de Sanden: *Molecular dynamics simulation of the impact behaviour of various hydrocarbon species on DLC* - Nuclear Instruments and Methods in Physics Research Section B: Beam Interactions with Materials and Atoms **228** (2005) 315–318.

[55] George Odian, *Principles of Polymerization*. John Wiley & Sons, Inc., Staten Island, fourth edi edition, (2004).

[56] M Szwarc: *'Living' Polymers* - Nature **178** (November 1956) 1168–1169.

[57] Krzysztof Matyjaszewski and Jianhui Xia: *Atom Transfer Radical Polymerization* - Chemical Reviews **101** (September 2001) 2921–2990. (DOI: 10.1021/cr940534g)

[58] Tuyu Xie, Kim B McAuley, James C C Hsu and David W Bacon: *Gas Phase Ethylene Polymerization: Production Processes, Polymer Properties, and Reactor Modeling* - Industrial & Engineering Chemistry Research **33** (March 1994) 449–479. (DOI: 10.1021/ie00027a001)

[59] H.-U. Poll, M Arzt and K.-H. Wickleder: *Reaction kinetics in the polymerization of thin films on the electrodes of a glow-discharge gap* - European Polymer Journal **12** (1976) 505–512. (DOI: /10.1016/0014-3057(76)90006-9)

[60] H Carchano: *Gas-discharge polymerization* - The Journal of Chemical Physics **61** (November 1974) 3634–3643.

[61] J M Tibbitt, R Jensen, A T Bell and M Shen: *A Model for the Kinetics of Plasma Polymerization* - Macromolecules **10** (May 1977) 647–653. (DOI: 10.1021/ma60057a029)

[62] H Yasuda and C R Wang: *Plasma polymerization investigated by the substrate temperature dependence* - Journal of Polymer Science: Polymer Chemistry Edition **23** (January 1985) 87–106. (DOI: 10.1002/pol.1985.170230110)

[63] A R Denaro, P A Owens and A Crawshaw: *Glow discharge polymerizationâ€"III. Allyl alcohol and crotyl alcohol* - European Polymer Journal **6** (March 1970) 487–497. (DOI: 10.1016/0014-3057(70)90107-2)

[64] H Kobayashi, M Shen and A T Bell: *Plasma Polymerization of Saturated and Unsaturated Hydrocarbons* - Macromolecules **7** (1974) 277–283.

[65] H Kobayashi, M Shen and A T Bell: *The Role of Halogens in the Plasma Polymerization of Hydrocarbons* - Journal of Macromolecular Science: Part A - Chemistry **8** (December 1974) 1345–1360. (DOI: 10.1080/00222337408068636)

[66] H Kobayashi, M Shen and A T Bell: *Effects of Reaction Conditions on the Plasma Polymerization of Ethylene* - Journal of Macromolecular Science: Part A - Chemistry **8** (1974) 373–391.

[67] H Yasuda and T Hsu: *Plasma polymerization investigated by the comparison of hydrocarbons and perfluorocarbons* - Surface Science **76** (1978) 232–241.

[68] I Retzko, J F Friedrich, A Lippitz and W E S Unger: *Chemical analysis of plasma-polymerized films: The application of X-ray photoelectron spectroscopy (XPS), X-ray absorption spectroscopy (NEXAFS) and fourier transform infrared spectroscopy (FTIR)* - Journal of Electron Spectroscopy and Related Phenomena **121** (2001) 111–129.

[69] J Friedrich, I Retzko, G Kuhn, W Unger and A Lippitz: *Plasma polymers with chemically defined structures in contact with metals* - Surface and Coatings Technology **142-144** (2001) 460–467.

[70] L O'Toole, A J Beck, A P Ameen, F J Jones and R D Short: *Radiofrequency-induced plasma polymerisation of propenoic acid and propanoic acid* - J. Chem. Soc. Faraday Trans. **91** (1995) 3907–3912.

[71] H Yasuda and C E Lamaze: *Polymerization in an electrodeless glow discharge. II. Olefinic monomers* - Journal of Applied Polymer Science **17** (May 1973) 1519–1531. (DOI: 10.1002/app.1973.070170517)

[72] Hiroaki Kobayashi, Alexis T Bell and Mitchel Shen: *Formation of an amorphous powder during the polymerization of ethylene in a radio-frequency discharge* - Journal of Applied Polymer Science **17** (1973) 885–892.

[73] S Morita, A T Bell and M Shen: *The effect of frequency on the plasma polymerization of ethane* - Journal of Polymer Science: Polymer Chemistry Edition **17** (September 1979) 2775–2782. (DOI: 10.1002/pol.1979.170170914)

[74] Lloyd C Brown and Alexis T Bell: *Kinetics of the Oxidation of Carbon Monoxide and the Decomposition of Carbon Dioxide in a Radiofrequency Electric Discharge. II. Theoretical Interpretation* - Industrial & Engineering Chemistry Fundamentals **13** (August 1974) 210–218. (DOI: 10.1021/i160051a009)

[75] Anna Maria Coclite and Karen K Gleason: *Initiated PECVD of Organosilicon Coatings: A New Strategy to Enhance Monomer Structure Retention* - Plasma Processes and Polymers **9** (April 2012) 425–434. (DOI: 10.1002/ppap.201100167)

[76] H K Yasuda. *Fundamental Aspects of Polymerization.* In *Plasma Polymerization*, chapter 5, pages 44–72. Academic Press, Orlando, third edition, (1985).

[77] A. D. McNaught and A. Wilkinson, editors: *Compendium of Chemical Terminology (the "Gold Book").* On-line corrected version (2006), 2nd edition, (1997).

[78] H K Yasuda. *Kinetic and Mechanistic Aspects of Polymer Deposition in Plasma Polymerization.* In *Plasma Polymerization*, chapter 8, pages 196–276. Academic Press, Orlando, third edition, (1985).

[79] H K Yasuda. *Kinetic and Mechanistic Aspects of Plasma Polymerization.* In *Plasma Polymerization*, chapter 6, pages 73–177. Academic Press, Orlando, third edition, (1985).

[80] Dirk Hegemann: *Macroscopic investigation of reaction rates yielding plasma polymer deposition* - Journal of Physics D: Applied Physics **46** (2013) 205204.

[81] H Yasuda and Toshihiro Hirotsu: *Critical evaluation of conditions of plasma polymerization* - Journal of Polymer Science: Polymer Chemistry Edition **16** (April 1978) 743–759. (DOI: 10.1002/pol.1978.170160403)

[82] J Hopwood: *Planar RF induction plasma coupling efficiency* - Plasma Sources Sci. Technol. **3** (1994) 460–464.

[83] D Hegemann: *Influence of pressure on an asymmetric, radio frequency discharge with methane* - Thin Solid Films **515** (December 2006) 2173–2178. (DOI: 10.1016/j.tsf.2006.06.020)

[84] A H M Smets, W M M Kessels and M C M van de Sanden: *Temperature dependence of the surface roughness evolution during hydrogenated amorphous silicon film growth* - Applied Physics Letters **82** (2003) 865–867.

[85] T. B. Casserly and K. K. Gleason: *Effect of Substrate Temperature on the Plasma Polymerization of Poly(methyl methacrylate)* - Chemical Vapor Deposition **12** (January 2006) 59–66. (DOI: 10.1002/cvde.200506409)

[86] Dirk Hegemann, Urs Schütz and Enrico Körner: *Macroscopic Approach to Plasma Polymerization Using the Concept of Energy Density* - Plasma Processes and Polymers **8** (August 2011) 689–694. (DOI: 10.1002/ppap.201000211)

[87] H K Yasuda. *Competitive Ablation - Polymer Formation.* In *Plasma Polymerization*, chapter 7, pages 178–195. Academic Press, Orlando, third edition, (1985).

[88] Y. S. Yeh, I. NI. Shyy and H Yasuda: *No Title* - J. Appl. Polym. Sci., Appl. Polym. Symp. **42** (1988) 1–25.

[89] Soo Young Park, Nakjoong Kim, Un Young Kim, Sung Il Hong and Hiroyuki Sasabe: *Plasma Polymerization of Hexamethyldisilazane* - Polym J **22** (March 1990) 242–249.

[90] Dirk Hegemann, Mohammad Mokbul Hossain, Enrico Körner and Dawn J Balazs: *Macroscopic Description of Plasma Polymerization* - Plasma Processes and Polymers **4** (April 2007) 229–238. (DOI: 10.1002/ppap.200600169)

[91] R Liepins and K Sakaoku: *Submicron polymer powder in electrodeless radio frequency-induced plasma-initiated polymerization* - Journal of Applied Polymer Science **16** (October 1972) 2633–2645. (DOI: 10.1002/app.1972.070161016)

[92] H Yasuda, M O Bumgarner and J J Hillman: *Polymerization of organic compounds in an electrodeless glow discharge. IV. Hydrocarbons in a closed system* - Journal of Applied Polymer Science **19** (February 1975) 531–543. (DOI: 10.1002/app.1975.070190216)

[93] H Yasuda and C E Lamaze: *Polymerization in an electrodeless glow discharge. III. Organic compounds without olefinic doublebond* - Journal of Applied Polymer Science **17** (May 1973) 1533–1544. (DOI: 10.1002/app.1973.070170518)

[94] Edmond de Hoffmann and Vincent Stroobant, *Mass Spectrometry: Principles and Apllications.* Wiley, third edition, (2007).

[95] Gregory H Wannier: *The Threshold Law for Single Ionization of Atoms or Ions by Electrons* - Physical Review **90** (June 1953) 817–825.

[96] H Klar: *Threshold fragmentation of atomic and molecular systems by charged particle impact* - Zeitschrift für Physik A Atoms and Nuclei **307** (1982) 75–81. (DOI: 10.1007/BF01416074)

[97] T Fiegele, G Hanel, I Torres, M Lezius and T D Märk: *Threshold electron impact ionization of carbon tetrafluoride, trifluoromethane, methane and propane* - Journal of Physics B: Atomic, Molecular and Optical Physics **33** (2000) 4263.

[98] J W Otvos and D P Stevenson: *Cross-sections of Molecules for Ionization by Electrons* - Journal of the American Chemical Society **78** (February 1956) 546–551. (DOI: 10.1021/ja01584a009)

[99] B L Schram, M J van der Wiel, F J de Heer and H R Moustafa: *Absolute Gross Ionization Cross Sections for Electrons (0.6-12 keV) in Hydrocarbons* - The Journal of Chemical Physics **44** (1966) 49.

[100] J Edwards and S J Rose: *Ionization time scales in hot dense plasma* - Journal of Physics B: Atomic, Molecular and Optical Physics **26** (1993) L523.

[101] A H Zewail: *Femtochemistry. Past, present, and future* - Pure Appl. Chem. **72** (2000) 2219–2231.

[102] S E Van Bramer, *An Introduction to Mass Spectrometry (course).* Widener University, (1997).

[103] J Benedikt, A Hecimovic, D Ellerweg and A Von Keudell: *Quadrupole mass spectrometry of reactive plasmas* - Journal of Physics D: Applied Physics **45** (2012) 403001. (DOI: 10.1088/0022-3727/45/40/403001)

[104] H M Rosenstock, M B Wallenstein, A L Wahrhaftig and Henry Eyring: *Absolute Rate Theory for Isolated Systems and the Mass Spectra of Polyatomic Molecules* - Proceedings of the National Academy of Sciences **38** (August 1952) 667–678.

[105] R A Marcus: *Unimolecular Dissociations and Free Radical Recombination Reactions* - The Journal of Chemical Physics **20** (1952) 359.

[106] P. J. Robinson and K. A. Holbrook, *Unimolecular reactions*, ISBN 6. Wiley-Interscience, London, (September 1972).

[107] P F Bente, F W McLafferty, D J McAdoo and C Lifshitz: *Internal energy of product ions formed in mass spectral reactions. Degrees of freedom effect* - The Journal of Physical Chemistry **79** (March 1975) 713–721. (DOI: 10.1021/j100574a011)

[108] Fred W McLafferty, Timothy Wachs, Chava Lifshitz, Giuseppe Innorta and Philip Irving: *Substituent effects in unimolecular ion decompositions. XV. Mechanistic interpretations and the quasi-equilibrium theory* - Journal of the American Chemical Society **92** (November 1970) 6867–6880. (DOI: 10.1021/ja00726a025)

[109] S Matt, O Echt, R Wörgötter, V Grill, P Scheier, C Lifshitz and T D Märk: *Appearance and ionization energies of multiply-charged C70 parent ions produced by electron impact ionization* - Chemical Physics Letters **264** (January 1997) 149–156. (DOI: 10.1016/S0009-2614(96)01303-6)

[110] M Stano, S Matejcik, J D Skalny and T D Märk: *Electron impact ionization of CH4 : ionization energies and temperature effects* - Journal of Physics B: Atomic, Molecular and Optical Physics **36** (2003) 261.

[111] J.-T. Kim, K.-B. Lim and D.-C. Lee: *The influence of CH4 carrier gas in plasma polymerized styrene films* - Surface and Coatings Technology **182** (2004) 1–6.

[112] B J Kinzig and R R Smardzewski: *Plasma-polymerized thin coatings from methyl-methacrylate, styrene and tetrafluoroethylene* - Surface Technology **14** (September 1981) 3–16. (DOI: 10.1016/0376-4583(81)90003-0)

[113] A J Choudhury, H Kakati, A R Pal, D S Patil and Joyanti Chutia: *Synthesis and characterization of plasma polymerized styrene films by rf discharge* - Journal of Physics: Conference Series **208** (2010) 1–9.

[114] Young-Do Son, Myung-Whan Hwang, Jae-Sung Lim and Paik-Kyun Shin: *Fabrication and Characterization of Gate Insulator Thin Films prepared by Plasma Polymerization* - Journal of the Korean Institute of Illuminating and Electrical Installation Engineers **12** (2011) 48–53. (DOI: 10.5207/JIEIE.2011.25.12.048)

[115] Hee-Sung Kim, Boong-Joo Lee, Paik-Kyun Shin and Shizuyasu Ochiai: *Floating-gate type organic memory device with organic insulator film of plasma polymerized styrene* - Japanese Journal of Applied Physics **53** (2014) 31602.

[116] Shinichi Takeda and Yukio Saito: *Growth Rate of Polystyrene Films Formed by Electrodeless R-F Excitation* - Japanese Journal of Applied Physics **12** (1973) 749.

[117] K E Geckeler, R Gebhardt and H Grünwald: *Surface Modification of Polyethylene by Plasma Grafting with Styrene for Enhanced Biocompatibility* - Naturwissenschaften **84** (1997) 150–151. (DOI: 10.1007/s001140050367)

[118] B O Ozden and G Akovali: *Plasma Polymerization and Copolymerization of Styrene and Methylmethacrylate .1. Plasma Initiated Polymerization Studies* - Polymer Bulletin **26** (1991) 409–416.

[119] M Chen, T C Yang and Z Ma: *Investigation on RF styrene plasma by emission spectroscopy* - IEEE Transactions on Plasma Science **23** (1995) 151–155.

[120] M Chen, T C Yang and X Zhou: *Zone-resolved mass spectroscopic study on RF plasma polymerization of styrene* - Journal of Polymer Science Part B: Polymer Physics **34** (1996) 113–120.

[121] K Jesch, J E Bloor and P L Kronick: *Structure and physical properties of glow discharge polymers. I. Polymers from hydrocarbons* - Journal of Polymer Science Part A-1: Polymer Chemistry **4** (June 1966) 1487–1497. (DOI: 10.1002/pol.1966.150040613)

[122] L F Thompson and K G Mayhan: *The plasma polymerization of vinyl monomers. II. A detailed study of the plasma polymerization of styrene* - J. Appl. Polym. Sci. **16** (1972) 2317–2341.

[123] G W Prohaska, E D Johnson and J F Evans: *Preparation and characterization of plasma-polymerized styrene thin films* - Journal of Polymer Science: Polymer Chemistry Edition **22** (1984) 2953–2972.

[124] M Chen, T.-C. Yang and Z.-G. Ma: *Plasma polymerization of styrene with controlled particle energy* - J Polym Sci A: Polym Chem **36** (1998) 1265–1270.

[125] Shigeru Kurosawa, Hideyuki Miura, Mitsuhiro Tozuka, Shoichiro Yamahira, Hidenobu Aizawa, Kongkiat Kongswan, Mutsuo Matsunaga, Kazunori Yamada and Mitsuo Hirata: *Conventional Measurement Method of Film Resistance of Plasma-Polymerized Thin Films Using a High-Resistance Meter* - Journal of Photopolymer Science and Technology **16** (2003) 43–48.

[126] C Zhang, J Wyatt, S P Russell and D H Weinkauf: *Methanol vapor sorption in plasma polymerized thin films* - Polymer **45** (October 2004) 7655–7663. (DOI: 10.1016/j.polymer.2004.08.055)

[127] H L Luo, J Sheng and Y Z Wan: *Plasma polymerization of styrene with carbon dioxide under glow discharge conditions* - Applied Surface Science **253** (2007) 5203–5207.

[128] W Potter, A J Ward and R D Short: *The stability of plasma polymers: Part I, A preliminary XPS study of the photostability of plasma polymerised styrene and methyl methacrylate* - Polymer Degradation and Stability **43** (1994) 385–391. (DOI: 10.1016/0141-3910(94)90010-8)

[129] G J Leggett, B D Ratner and J C Vickerman: *Characterization of plasma-deposited styrene films by XPS and static SIMS* - Surface and Interface Analysis **23** (1995) 22–28.

[130] S Swaraj, U Oran, A Lippitz, R D Schulze, J F Friedrich and W E S Unger: *Surface analysis of plasma-deposited polymer films, 2 - Analysis of post-plasma air reacted plasma polymerized styrene by X-ray photoelectron spectroscopy and X-ray absorption spectroscopy* - Plasma Processes and Polymers **1** (2004) 134–140.

[131] M Haidopoulos: *Morphology of polystyrene films deposited by RF plasma* - Journal of Microscopy **228** (2007) 227–239.

[132] Marie Haïdopoulos, Matthieu Horgnies, Frédéric Mirabella and Jean-Jacques Pireaux: *Angle-Resolved XPS Study of Plasma-Deposited Polystyrene Films after Oxygen Plasma Treatment* - Plasma Processes and Polymers **5** (2008) 67–75.

[133] Umut Oran, Sufal Swaraj, Jörg F Friedrich and Wolfgang E S Unger: *Surface Analysis of Plasma-Deposited Polymer Films, 1* - Plasma Processes and Polymers **1** (September 2004) 123–133. (DOI: 10.1002/ppap.200400002)

[134] K Tsuneto and I Taniguchi. *The Formation Mechanism of Styrene Polymer Film by Glow Discharge Direct Method.* In *Plasma Polymerization*, ISBN 108 of *ACS Symposium Series*, pages 4–65. American Chemical Society, (September 1979).

[135] Shinzo Morita and Sang Hyun Park: *Plasma polymerization model in gas-flow type reactor* - Applied Surface Science **60-61** (1992) 338–341. (DOI: 10.1016/0169-4332(92)90440-9)

[136] S Kurosawa, T Hirokawa, K Kashima, H Aizawa, D.-S. Han, Y Yoshimi, Y Okada, K Yase, J Miyake, M Yoshimoto and J Hilborn: *Detection of deposition rate of plasma-polymerized films by quartz crystal microbalance* - Thin Solid Films **374** (2000) 262–267.

[137] M Haidopoulos, J Larrieu, M Horgnies, L Houssiau and J J Pireaux: *A comparative study between inductively and capacitively coupled plasma deposited polystyrene films: chemical and morphological characterizations* - Surface and Interface Analysis **38** (2006) 1266–1275.

[138] G Beamson, D T Clark, J Kendrick and D Briggs: *Observation of vibrational asymmetry in the high resolution monochromatized XPS of hydrocarbon polymers* - Journal of Electron Spectroscopy and Related Phenomena **57** (September 1991) 79–90. (DOI: 10.1016/0368-2048(91)85015-L)

[139] G Beamson and D Briggs, *High Resolution XPS of Organic Polymers: the Scienta ESCA300 Database.* Wiley, Chichester, (1992).

[140] F M Petrat, D Wolany, B C Schwede, L Wiedmann and A Benninghoven: *Comparative in situ ToF-SIMS/XPS study of polystyrene modified by argon, oxygen and nitrogen plasmas* - Surface and Interface Analysis **21** (June 1994) 402–406. (DOI: 10.1002/sia.740210614)

[141] Sufal Swaraj. *Surface Chemical Characterization of Plasma-Chemically Deposited Polymer Films by X-ray Photoelectron Spectroscopy and Near-Edge X-ray Absorption Fine Structure.* PhD thesis, Freie Universität Berlin, (2005).

[142] D T Clark and A Dilks: *ESCA studies of polymers. VII. Shake-up phenomena in some alkane-styrene copolymers* - Journal of Polymer Science: Polymer Chemistry Edition **14** (March 1976) 533–542. (DOI: 10.1002/pol.1976.170140302)

[143] Erika E Johnston and Buddy D Ratner: *Surface characterization of plasma deposited organic thin films* - Journal of Electron Spectroscopy and Related Phenomena **81** (September 1996) 303–317. (DOI: 10.1016/0368-2048(95)02666-5)

[144] Umut Oran. *Surface Chemical Characterization of Plasma-Chemically Deposited Polymer Films by Time of Flight Static Secondary Ion Mass Spectrometry.* PhD thesis, Freie Universität Berlin, (2005).

[145] J S Brinen, S Greenhouse and L Pinatti: *ESCA and SIMS studies of plasma treatments of intraocular lenses* - Surface and Interface Analysis **17** (February 1991) 63–70. (DOI: 10.1002/sia.740170202)

[146] Gábor Harsányi: *Polymeric sensing films: new horizons in sensorics?* - Materials Chemistry and Physics **43** (March 1996) 199–203. (DOI: 10.1016/0254-0584(95)01629-9)

[147] Alistair M Leeson, Morgan R Alexander, Robert D Short, D Briggs and M J Hearn: *Secondary Ion Mass Spectrometry of Polymers: a ToF SIMS Study of Monodispersed PMMA Standards* - Surface and Interface Analysis **25** (April 1997) 261–274. (DOI: 10.1002/(SICI)1096-9918(199704)25)

[148] Michael Zeuner and Jürgen Meichsner: *Ion kinetic aspects of plasma chemical deposition of PMMA (Polymethylmethacrylate) films* - Vacuum **46** (January 1995) 27–31. (DOI: 10.1016/0042-207X(93)E0003-4)

[149] Wei Ao, Jae-Sung Lim and Paik-Kyun Shin: *Preparation and Characterization of Plasma Polymerized Methyl Methacrylate Thin Films as Gate Dielectric for Organic Thin Film Transistor* - Journal of Electrical Engineering and Technology **6** (2011) 836. (DOI: 10.1063/1.2093940)

[150] J A Tobin and D D Denton: *Effects of deposition parameters on the refractive index in plasma polymerized methyl methacrylate thin films* - Applied Physics Letters **60** (1992). (DOI: 10.1063/1.106920)

[151] J A Tobin. *No Title.* PhD thesis, University of Wisconsin-Madison, (1994).

[152] Guifang Li, Jeffrey A Tobin and Denice D Denton: *Photoluminescence of plasma polymerized methyl methacrylate films* - Applied Physics Letters **62** (1993). (DOI: 10.1063/1.108645)

[153] Shinzo Morita, Junji Tamano, Shuzo Hattori and Masayuki Ieda: *Plasma polymerized methyl-methacrylate as an electron-beam resist* - Journal of Applied Physics **51** (1980). (DOI: 10.1063/1.328170)

[154] Jae-Sung Lim, Paik-Kyun Shin, Boong-Joo Lee and Sunwoo Lee: *Plasma polymerized methyl methacrylate gate dielectric for organic thin-film transistors* - Organic Electronics **11** (May 2010) 951–954. (DOI: 10.1016/j.orgel.2010.02.005)

[155] Se-Hyun Lee, Boong-Joo Lee, Young-Taek Lim, Jae-Sung Lim, Sunwoo Lee, Shizuyasu Ochiai, Jun-Sin Yi and Paik-Kyun Shin: *Process Condition Considered Preparation and Characterization of Plasma Polymerized Methyl Methacrylate Thin Films for Organic Thin Film Transistor Application* - Japanese Journal of Applied Physics **51** (2012) 21602.

[156] Andrew R K Ralston, Jeffrey A Tobin, Sateesh S Bajikar and Denice D Denton: *Comparative performance of linear, cross-linked, and plasma-deposited PMMA capacitive humidity sensors* - Sensors and Actuators B: Chemical **22** (November 1994) 139–147. (DOI: 10.1016/0925-4005(94)87013-6)

[157] S Kurosawa, B Atthoff, H Aizawa and J Hilborn: *Detection of deposition rate of plasma-polymerized acrylate and methacrylate derivatives using quartz crystal microbalance* - Thin Solid Films **457** (2004) 26–33.

[158] M G Neira-Velazquez, L F Ramos-de Valle, H E Hernandez-Hernandez and I Zapata-Gonzalez: *Surface modification of carbon nanofibers (CNFs) by plasma polymerization of methylmethacrylate and its effect on the properties of PMMA/CNF nanocomposites* - e-Polymers **162** (2008) 1–11.

[159] C Zhang, J Wyatt and D H Weinkauf: *Carbon dioxide sorption in conventional and plasma polymerized methyl methacrylate thin films* - Polymer **45** (2004) 7665–7671.

[160] N De Geyter, R Morent, S Van Vlierberghe, M Frère-Trentesaux, P Dubruel and E Payen: *Effect of electrode geometry on the uniformity of plasma-polymerized methyl methacrylate coatings* - Journal of Polymer Science Part A: Polymer Chemistry **70** (April 2011) 293–299. (DOI: 10.1016/j.porgcoat.2010.11.009)

[161] Pierre Louette, Frederic Bodino and Jean-Jacques Pireaux: *Poly(methyl methacrylate) (PMMA) XPS Reference Core Level and Energy Loss Spectra* - Surface Science Spectra **12** (2005). (DOI: 10.1116/11.20050914)

[162] L O'Toole, R D Short, A P Ameen and F R Jones: *Mass spectrometry of and deposition-rate measurements from radiofrequency-induced plasmas of methyl isoburate, methyl methacrylate and n-buthyl methacrylate* - J. Chem. Soc. Faraday Trans. **91** (1995) 1363–1370.

[163] Y Vickie Pan, Ernesto Z Barrios and Denice D Denton: *In situ FTIR investigation of MMA plasmas, plasma-polymerized films, and reaction mechanisms* - Journal of Polymer Science Part A: Polymer Chemistry **36** (March 1998) 587–602. (DOI: 10.1002/(SICI)1099-0518(199803)36:4<587::AID-POLA8>3.0.CO;2-M)

[164] Guifang Li, Jeffrey A Tobin and Denice D Denton: *Morphology of plasma polymerized methyl methacrylate films* - Applied Physics Letters **64** (1994). (DOI: 10.1063/1.111103)

[165] A J Ward and R D Short: *A time-of-flight secondary ion mass spectrometry and X-ray photoelectron spectroscopy investigation of the structure of plasma polymers prepared from the methacrylate series of monomers* - Polymer **34** (1993) 4179–4185.

[166] A J Ward and A D Short: *A t.o.f.s.i.m.s. and x.p.s. investigation of the structure of plasma polymers prepared from the methacrylate series of monomers. II: The influence of the W/F parameter on structural and functional group retention* - Polymer **36** (1995) 3439–3450.

[167] O W Webster, W R Hertler, D Y Sogah, W B Farnhara and T V Rajanbabu: *Synthesis of Reactive-Ended Acrylic Polymers by Group Transfer Polymerization: Initiation with Silyl Ketene Acetals* - Journal of Macromolecular Science: Part A - Chemistry **21** (July 1984) 943–960. (DOI: 10.1080/00222338408056584)

[168] A J Ward. *No Title.* PhD thesis, University of Sheffield, (1994).

[169] Masakazu Tatsumi, Minoru Okashita, Takanobu Matsunaga, Kazuhito Ashida and Seika Yamamoto: *Initiation of Methyl Methacrylate Polymerization by the Products of Plasma Reactiont* - NIPPON KAGAKU KAISHI **1989** (1989) 1909–1918. (DOI: 10.1246/nikkashi.1989.1909)

[170] Ferencz Denes, A.Majid Sarmadi, Cornelis E C A Hop and Raymond A Young. *Plasma polymerization of methyl methacrylate.* In *Journal of Applied Polymer Science: Applied Polymer Symposium*, number 54, pages 55–75, (1994).

[171] Y Vickie Pan and Denice D Denton: *Plasma dissociation reaction kinetics. I. Methyl methacrylate* - Journal of Applied Polymer Science **73** (July 1999) 1–16. (DOI: 10.1002/(SICI)1097-4628(19990705)73:1<1::AID-APP1>3.0.CO;2-4)

[172] JE PlasmaConsult Gmbh, *ICP-P200 User's Manual.* JE PlasmaConsult GmbH, (2004).

[173] J Hopwood: *Review of inductively coupled plasmas for plasma processing* - Plasma Sources Sci. Technol. **1** (1992) 109–116.

[174] *Email correspondance with company (2013).*

[175] Fabian Renaux. *Alternative plasma à la "chromatation".* PhD thesis, Université de Mons-Hainaut, (2006).

[176] D Briggs and J Grant. *Perspectives on XPS and AES.* In D Briggs and J Grant, editors, *Surface Analysis by Auger and X-Ray Photoelectron Spectroscopy*, chapter 1, pages 1 – 30. IM Publication and SurfaceSpectra Limited, first edit edition, (2003).

[177] A W Drummond. *XPS: Instrumentation and Performance.* In D Briggs and J Grant, editors, *Surface Analysis by Auger and X-Ray Photoelectron Spectroscopy*, chapter 5, pages 117–144. IM Publication and SurfaceSpectra Limited, first edit edition, (2003).

[178] D Briggs. *XPS: Basic Principles, Spectral Features and Qualitative Analysis.* In D Briggs and J Grant, editors, *Surface Analysis by Auger and X-Ray Photoelectron Spectroscopy*, chapter 2, pages 31–56. IM Publication and SurfaceSpectra Limited, first edit edition, (2003).

[179] H Yasuda, N Morosoff, E S Brandt and C N Reilley: *Plasma polymerization of tetrafluoroethylene. I. Inductive radio frequency discharge* - Journal of Applied Polymer Science **23** (February 1979) 1003–1011. (DOI: 10.1002/app.1979.070230405)

[180] Damien Thiry, Nikolay Britun, Stephanos Konstantinidis, Jean-Pierre Dauchot, Maxime Guillaume, Jérôme Cornil and Rony Snyders: *Experimental and Theoretical Study of the Effect of the Inductive-to-Capacitive Transition in Propanethiol Plasma Polymer Chemistry* - The Journal of Physical Chemistry C **117** (April 2013) 9843–9851. (DOI: 10.1021/jp400829z)

[181] Seongsoo Jang and Wonjong Lee: *Pressure and input power dependence of Ar/N2/H2 inductively coupled plasma systems* - Journal of Vacuum Science & Technology A **19** (2001) 2335.

[182] Young Wook Lee, Hye Lan Lee and T H Chung: *E-H mode transition in low-pressure inductively coupled nitrogen-argon and oxygen-argon plasmas* - Journal of Applied Physics **109** (2011) 113302. (DOI: 10.1063/1.3587156)

[183] *Email correspondance with author (2014).*

[184] *Molecular Sieves.* http://chem.chem.rochester.edu/ nvd/molecularsieves.html.

[185] A Dilks and E Kay: *Plasma polymerization of ethylene and the series of fluoroethylenes: plasma effluent mass spectrometry and ESCA studies* - Macromolecules **14** (May 1981) 855–862. (DOI: 10.1021/ma50004a074)

[186] Jan Benedikt, Sumit Agarwal, Dimitri Eijkman, Wouter Vandamme, Mariadriana Creatore and M C M van de Sanden: *Threshold ionization mass spectrometry of reactive species in remote Ar/C2H2 expanding thermal plasma* - Journal of Vacuum Science & Technology A **23** (2005) 1400. (DOI: 10.1116/1.2006138)

[187] S E Van Bramer and M V Johnston: *10.5-eV photoionization mass spectrometry of aliphatic compounds* - Journal of the American Society for Mass Spectrometry **1** (November 1990) 419–426. (DOI: 10.1016/1044-0305(90)85024-G)

[188] P. H. Dawson, *Quadrupole Mass spectrometry and Its Applications.* Elsevier, (1976).

[189] James R Doyle: *Chemical kinetics in low pressure acetylene radio frequency glow discharges* - Journal of Applied Physics **82** (1997) 4763. (DOI: 10.1063/1.366333)

[190] Shun-I Shih, Ta-Chang Lin and Minliang Shih: *Decomposition of benzene in the RF plasma environment: Part I. Formation of gaseous products and carbon depositions* - Journal of Hazardous Materials **116** (December 2004) 239–248. (DOI: 10.1016/j.jhazmat.2004.09.006)

[191] V Rouessac, S Roualdes and J Durand: *In-situ Mass Spectrometry analyses of the fragmentation of linear and cyclic siloxanes in a glow discharge compared with ex-situ FTIR analyses of the deposits* - Chemical Vapor Deposition **8** (2002) 155–161.

[192] Felix Güthe, Hongbin Ding, Thomas Pino and John P Maier: *Diagnosis of a benzene discharge with a mass-selective spectroscopic technique* - Chemical Physics **269** (July 2001) 347–355. (DOI: 10.1016/S0301-0104(01)00319-6)

[193] P. J. Linstrom and W. G. Mallard, editors: *NIST Chemistry WebBook, NIST Standard Reference Database number 69.* National Institute of Standards and Technology, Gaithersburg, US, (2014).

[194] Roland Weisbeck: *Synthese von Diphenyl aus Benzol im kalten Plasma elektrischer Entladungen* - Chemie Ingenieur Technik **43** (June 1971) 721–726. (DOI: 10.1002/cite.330431206)

[195] M Duval and A Théorêt: *A Comparative Study of Microwave and Radiofrequency Plasma Polymerization of Benzene* - Journal of The Electrochemical Society **122** (April 1975) 581–585. (DOI: 10.1149/1.2134265)

[196] G Smolinsky and M J Vasile: *The radiofrequency discharge chemistry of benzene and mixtures with helium, argon, or xenon* - International Journal of Mass Spectrometry and Ion Physics **24** (July 1977) 311–322. (DOI: 10.1016/0020-7381(77)80038-7)

[197] Shun-I Shih, Ta-Chang Lin and Minliang Shih: *Decomposition of benzene in the RF plasma environment: Part II. Formation of polycyclic aromatic hydrocarbons* - Journal of Hazardous Materials **117** (January 2005) 149–159. (DOI: 10.1016/j.jhazmat.2004.09.030)

[198] Michael Frenklach and Hai Wang: *Detailed modeling of soot particle nucleation and growth* - Symposium (International) on Combustion **23** (1991) 1559–1566. (DOI: 10.1016/S0082-0784(06)80426-1)

[199] Masahiro Niinomi and Kenji Yanagihara. *Plasma Diagnostics of Polymerizing Benzene Plasma.* In *Plasma Polymerization*, ISBN 108 of *ACS Symposium Series*, chapter Chapter 6, pages 6–87. American Chemical Society, (September 1979).

[200] J Benedikt, A Consoli, M Schulze and A von Keudell: *Time-Resolved Molecular Beam Mass Spectrometry of the Initial Stage of Particle Formation in an Ar/He/C2H2 Plasma* - The Journal of Physical Chemistry A **111** (2007) 10453–10459. (DOI: 10.1021/jp072892w)

[201] M J Vasile and G Smolinsky: *The chemistry of radiofrequency discharges: Acetylene and mixtures of acetylene with helium, argon and xenon* - International Journal of Mass Spectrometry and Ion Physics **24** (May 1977) 11–23. (DOI: 10.1016/0020-7381(77)83002-7)

[202] I Platzner and P Marcus: *Condensation reactions in a microwave-induced acetylene plasma* - International Journal of Mass Spectrometry and Ion Physics **41** (February 1982) 241–250. (DOI: 10.1016/0020-7381(82)80079-X)

[203] A Consoli, J Benedikt and A von Keudell: *Initial Polymerization Reactions in Particle-Forming Ar/He/C2H2 Plasmas Studied via Quantitative Mass Spectrometry* - The Journal of Physical Chemistry A **112** (2008) 11319–11329.

[204] A Consoli, J Benedikt and A von Keudell: *The role of C2H4 for the acetylene chemistry in particle forming Ar/He/C2H2 plasmas studied via quantitative mass spectrometry* - Plasma Sources Science and Technology **18** (2009) 34004.

[205] Ch. Deschenaux, A Affolter, D Magni, Ch. Hollenstein and P Fayet: *Investigations of CH4 , C2H2 and C2H4 dusty RF plasmas by means of FTIR absorption spectroscopy and mass spectrometry* - J. Phys. D: Appl. Phys. **32** (1999) 1876.

[206] Valérie De Vriendt, Fabrizio Maseri, Aurélien Nonet and Stéphane Lucas: *Study of Nanoparticles Formation in a Pulsed Magnetron Discharge in Acetylene* - Plasma Processes and Polymers **6** (June 2009) S6–S10. (DOI: 10.1002/ppap.200930105)

[207] S Stoykov, C Eggs and U Kortshagen: *Plasma chemistry and growth of nanosized particles in a C 2 H 2 RF discharge* - Journal of Physics D: Applied Physics **34** (2001) 2160.

[208] J Benedikt, D C Schram and M C van de Sanden: *Detailed TIMS study of Ar/C2H2 expanding thermal plasma: identification of a-C:H film growth precursors* - J Phys Chem A **109** (2005) 10153–10167.

[209] H Richter and J B Howard: *Formation of polycyclic aromatic hydrocarbons and their growth to sootâ€"a review of chemical reaction pathways* - Progress in Energy and Combustion Science **26** (August 2000) 565–608. (DOI: 10.1016/S0360-1285(00)00009-5)

[210] H Bockhorn, F Fetting and H W Wenz: *Investigation of the Formation of High Molecular Hydrocarbons and Soot in Premixed Hydrocarbon-Oxygen Flames* - Berichte der Bunsengesellschaft für physikalische Chemie **87** (November 1983) 1067–1073. (DOI: 10.1002/bbpc.19830871121)

[211] Michael Frenklach and Jürgen Warnatz: *Detailed Modeling of PAH Profiles in a Sooting Low-Pressure Acetylene Flame* - Combustion Science and Technology **51** (February 1987) 265–283. (DOI: 10.1080/00102208708960325)

[212] Jens Olaf P Pedersen, Brian J Opansky and Stephen R Leone: *Laboratory studies of low-temperature reactions of ethynyl with acetylene and implications for atmospheric models of Titan* - The Journal of Physical Chemistry **97** (July 1993) 6822–6829. (DOI: 10.1021/j100128a013)

[213] Michael Frenklach: *Reaction mechanism of soot formation in flames* - Physical Chemistry Chemical Physics **4** (2002) 2028–2037. (DOI: 10.1039/B110045A)

[214] G Smolinsky and M J Vasile: *The chemistry of the ethylene radiofrequency discharge* - International Journal of Mass Spectrometry and Ion Physics **22** (November 1976) 171–183. (DOI: 10.1016/0020-7381(76)80117-9)

[215] G Le Dû, N Celini, F Bergaya and F Poncin-Epaillard: *RF plasma-polymerization of acetylene: Correlation between plasma diagnostics* - Surface and Coatings Technology **201** (2007) 5815–5821.

[216] H Yasuda and Toshihiro Hirotsu: *Polymerization of organic compounds in an electrodeless glow discharge. XI. Pressure in glow discharge* - Journal of Applied Polymer Science **22** (May 1978) 1195–1205. (DOI: 10.1002/app.1978.070220504)

[217] Allan H Laufer and Askar Fahr: *Reactions and Kinetics of Unsaturated C2 Hydrocarbon Radicals* - Chemical Reviews **104** (April 2004) 2813–2832. (DOI: 10.1021/cr030039x)

[218] George Vacek, J Russell Thomas, Bradley J DeLeeuw, Yukio Yamaguchi and Henry F Schaefer: *Isomerization reactions on the lowest potential energy hypersurface of triplet vinylidene and triplet acetylene* - The Journal of Chemical Physics **98** (1993) 4766. (DOI: 10.1063/1.464980)

[219] Michael A. Lieberman and Alan J. Lichtenberg. *Molecular Collisions.* In *Principles of Plasma Discharges and Materials Processing*, chapter 8, pages 235–284. 2nd, 2nd edition, (2005).

[220] F. J. Gordillo-Vázquez and J. M. Albella: *Influence of the pressure and power on the non-equilibrium plasma chemistry of C2 , C2H, C2H2 , CH3 and CH4 affecting the synthesis of nanodiamond thin films from C2H2 (1%)/H2 /Ar-rich plasmas* - Plasma Sources Science and Technology **13** (2004) 50.

[221] Michael A. Lieberman and Alan J. Lichtenberg. *Chemical Kinetics and Surface Processes.* In *Principles of Plasma Discharges and Materials Processing*, chapter 9, pages 285–326. 2nd edition, (2005).

[222] H K Yasuda. *Fundamental Aspects of Gas-Phase Reactions.* In *Plasma Polymerization*, chapter 3, pages 11–18. Academic Press, Orlando, third edition, (1985).

[223] Nils Hansen, Terrill A Cool, Phillip R Westmoreland and Katharina Kohse-Höinghaus: *Recent contributions of flame-sampling molecular-beam mass spectrometry to a fundamental understanding of combustion chemistry* - Progress in Energy and Combustion Science **35** (April 2009) 168–191. (DOI: /10.1016/j.pecs.2008.10.001)

[224] N De Geyter, R Morent, S Van Vlierberghe, P Dubruel, C Leys, L Gengembre, E Schacht and E Payen: *Deposition of polymethyl methacrylate on polypropylene substrates using an atmospheric pressure dielectric barrier discharge* - Progress in Organic Coatings **64** (2009) 230–237.

[225] L Ledernez, Hirotsugu K Yasuda, F Olcaytug, F Gemetz and G Urban: *Pressure Dependence of Plasma Polymerization of Methane at Constant W/FM* - Plasma Processes and Polymers **4** (2007) S794–S796.

[226] M M Turner and M A Lieberman: *Hysteresis and the E-to-H transition in radiofrequency inductive discharges* - Plasma Sources Science and Technology **8** (1999) 313. (DOI: 10.1088/0963-0252/8/2/312)

[227] Jerome Goodman: *The formation of thin polymer films in the gas discharge* - Journal of Polymer Science **44** (June 1960) 551–552. (DOI: 10.1002/pol.1960.1204414428)

[228] Shinzo Morita, Teruyoshi Mizutani and Masayuki Ieda: *Electron Spin Resonance in Thin Polymer Films Formed in a Glow Discharge* - Japanese Journal of Applied Physics **10** (1971) 1275.

[229] Shinichi Takeda: *Dielectric properties of polystyrene thin films formed by rf electrodeless excitation* - Journal of Applied Physics **47** (1976).

[230] G Sawa, K Arakawa, M Nagao and M Ieda: *Conditions for complete self-healing breakdown in glow discharge polymerized styrene films* - Thin Solid Films **59** (1979) 131–141.

[231] Shinnichi Takeda: *Capacitive Humidity Element Using Polystyrene Thin Films Formed by Plasma Polymerization* - Japanese Journal of Applied Physics **20** (1981) 1219.

[232] S Schelz, N Schühler, T Richmond and P Oelhafen: *Surface study of plasma- and UV-polymeryzed films using scanning force microscopy and in-situ photoelectron spectroscopy* - Thin Solid Films **266** (1995) 133–139.

[233] Kei-ichi Miura, Katsuto Otake, Shigeru Kurosawa, Takeshi Sako, Tsutomu Sugeta, Takashi Nakane, Masahito Sato, Tomoya Tsuji, Toshihiko Hiaki and Masaru Hongo: *Solubility and adsorption of high pressure carbon dioxide to poly(styrene)* - Fluid Phase Equilibria **144** (February 1998) 181–189. (DOI: 10.1016/S0378-3812(97)00256-2)

[234] S Kurosawa, N Kamo, N Minoura and M Muratsugu: *Dose response in solid-phase radioimmunoassay to human IgG on plasma-polymerized films coated with F(ab')2 anti-human IgG antibody* - Materials science & engineering C **4** (1997) 291–296.

[235] S Kurosawa, K Kobayashi, H Aizawa, Y Yoshimi and M Yoshimoto: *Behavior of Contact Angle on Glass Plates Coated with Plasma- Polymerized Styrene, Allylamine and Acrylic Acid* - J. Photpolym. Sci. Technol. **12** (1999) 63–67.

[236] Alaa Fahmy, Renate Mix, Andreas Schönhals and Jörg Friedrich: *Surface and Bulk Structure of Thin Spin Coated and Plasma-Polymerized Polystyrene Films* - Plasma Chemistry and Plasma Processing **32** (2012) 767–780. (DOI: 10.1007/s11090-012-9372-1)

[237] Graham J Leggett, John C Vickerman, David Briggs and Martin J Hearn: *Surface studies by static secondary ion mass spectrometry: cluster ion formation studied by tandem mass-spectrometric techniques* - Journal of the Chemical Society, Faraday Transactions **88** (1992) 297–309. (DOI: 10.1039/FT9928800297)

[238] Ashutosh Chilkoti, David G Castner and Buddy D Ratner: *Static Secondary Ion Mass Spectrometry and X-Ray Photoelectron Spectroscopy of Deuterium- and Methyl-Substituted Polystyrene* - Applied Spectroscopy **45** (1991) 209–217.

[239] F M Petrat, D Wolany, B C Schwede, L Wiedmann and A Benninghoven: *In situ ToF-SIMS/XPS investigation of nitrogen plasma-modified polystyrene surfaces* - Surface and Interface Analysis **21** (May 1994) 274–282. (DOI: 10.1002/sia.740210503)

[240] IONTOF. *Spectra Library*, (2010).

[241] D Briggs. *Interpretation of Spectra.* In J C Vickerman and D Briggs, editors, *ToF-SIMS: Surface Analysis by Mass Spectrometry*, chapter 16, pages 447–474. IM Publication and SurfaceSpectra Limited, (2001).

[242] Joseph A Chinn, Thomas A Horbett, Buddy D Ratner, Michael B Schway, Yasmeen Haque and Stephen D Hauschka: *Enhancement of serum fibronectin adsorption and the clonal plating efficiencies of Swiss mouse 3T3 fibroblast and MM14 mouse myoblast cells on polymer substrates modified by radiofrequency plasma deposition* - Journal of Colloid and Interface Science **127** (January 1989) 67–87. (DOI: 10.1016/0021-9797(89)90008-8)

[243] Ashutosh Chilkoti, Buddy D Ratner and David Briggs: *Analysis of polymer surfaces by SIMS: Part 15. Oxygen-functionalized aliphatic homopolymers* - Surface and Interface Analysis **18** (August 1992) 604–618. (DOI: 10.1002/sia.740180807)